Differentiation of Human Pluripotent Stem Cells into Inner Ear Cells

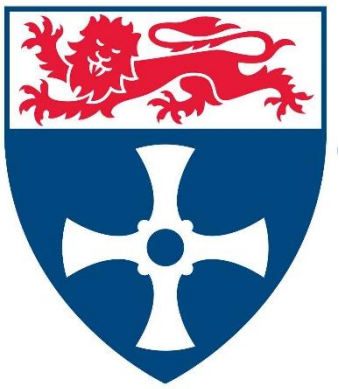

Minjin Jeong

Doctor of Philosophy

Institute of Genetic Medicine

Newcastle University

June 2017

Abstract

Hearing loss is among the most common of sensory impairments and there are over 500 million deaf individuals in the world. Currently, most treatment strategies depend on acoustic amplification or cochlear implantation in severe cases. These electronic devices can give help to those with hearing loss, but they are not perfect cures for deafness. Over the last decade, stem cell technology has received a great attention as a possible and powerful treatment for a number of diseases. The induction of human inner ear tissue from pluripotent stem cells would be applicable not only to modelling of sensorineural hearing loss disease but also for the generation of clinically useful sensory cells.

In this study, we have developed a method for differentiating human pluripotent stem cells to inner ear cells. Using a three-dimensional culture system, we modulated TGF, BMP, and FGF signalling to generate otic vesicle-like structures alongside neural progenitor cells from stem cell embryoid bodies (EBs). Over 3 months, the vesicles developed into EBs that give rise to sensory hair cells bearing stereocilia bundles that are innervated by possible sensory neurons. Additionally, using FM1-43FX we detected hair-cell-like cells and possible sensory neurons that have active mechanotransduction ion channels. We also showed that derived neurons exhibit electrophysiological properties similar to primary auditory neurons of the rat cochlea. Finally, we demonstrated how these otic EBs are structurally and biochemically similar to developing human cochlear and vestibular organs. We believe that this study would facilitate the study of human inner ear development and also could benefit a broad range of individuals suffering from sensorineural hearing loss.

Acknowledgments

I would like to take this opportunity to thank all those who offered me a great help and support during the duration of my Ph.D. in Newcastle.

First and foremost, I would like to thank my supervisors Professor Lyle Armstrong and Professor Majlinda Lako. Their expert guidance and supervision were essential to the completion of this thesis. Thanks also for proof reading through this thesis. Especially thanks to Lyle for being patient when talking with me and respecting my opinions about the experiments all the time. It meant a lot to me and was the number one reason finishing Ph.D. on time.

I want to thank all the colleagues in the Institute of Genetic Medicine, especially stem cell group for their kindness help and friendship. I would like to thank Taty Anna Kamarudin for being a great friend and colleague. Special thanks must go to Min Yu, who was taking care of me like mom. Professor Susan Lindsay and Dr. Heiko Peters who provided a great help, encouragements, and criticism required to improve my work during each annual assessment. Thanks to Lisa Hodgson for the induction of microscopes and cryostat. I would also like to thank the EM group for TEM images and Professor Corne Kros and Molly O'Reilly for the electrophysiology experiments.

I would like to thank my previous supervisor Professor Bert Binas and Dr. Gun-Sik Cho who led the way to the science world. Big thanks to my best friend Hyunsook Kwon who offered me a great support and encouragement in all difficult times. She has been always sticking by my side. I would also like to thank Dongjun Han for his helpful scientific advice and encouragement. In the end, I would like express appreciation to all members of my family, particularly my parents who have always believed and encouraged me for each new challenge I have taken in my life. Thanks to my adorable two younger brothers Sunwoo and Doyun. It is difficult to imagine my life without them. Thank you all with the bottom of my heart and soul.

Table of Contents

Abstract ..... **i**

Acknowledgments ..... **ii**

Table of Contents ..... **v**

List of Figures ..... **x**

List of Tables ..... **xiii**

Abbreviations ..... **xiv**

Chapter 1. Introduction **2**

1.1 Development and regeneration of the inner ear 2

1.1.1 Development of the inner ear in the vertebrates 2

1.1.1.1 Formation of the otic placode 4

1.1.1.2 Formation of the otocyst 7

1.1.1.3 Regional morphogenesis of the otocyst 10

1.1.2 Development of human inner ear 13

1.1.2.1 Development of vestibular hair cells and vestibular auditory neurogenesis 16

1.1.2.2 Development of cochlear hair cells and auditory neurogenesis 20

1.1.3 Inner ear cell regeneration 24

1.2 The hearing process and causes of hearing loss 28

1.2.1 How hearing works in human? 28

1.2.2 Hearing loss 33

1.3 Reconstitution of inner ear development from human pluripotent stem cells *in vitro* 35

1.3.1 Human pluripotent stem cells (hPSCs) 35

1.3.1.1 Human embryonic stem cells (hESCs) 35

1.3.1.2 Human Induced pluripotent stem cells (hiPSCs) 37

1.3.2 Definitive ectoderm 39
1.3.3 Non-neural Ectoderm 42
1.3.4 Pre-placodal Region (PPR) 44
1.3.5. Otic induction 45

1.4 Types of cell culture methods and conditions 46
1.4.1 Types of cell culture methods 46
1.4.1.1 2D monolayer methods 46
1.4.1.2 3D EB methods 48
1.4.1.3 Combination of both 3D and 2D methods 49
1.4.2 Basic materials for cell culture 50

1.5 Differentiation protocols of human pluripotent stem cells into inner ear cells 52
1.5.1. Generation of mouse inner ear sensory epithelia from pluripotent stem cells in 3D culture 52
1.5.2. Restoration of auditory evoked responses by human ES-cell-derived otic progenitors 54
1.5.3 Inner ear hair-cell-like cells from human embryonic stem cells 56
1.5.4 Induction of differentiation of human embryonic stem cells into functional hair-cell-like cells in the absence of stromal cells 57

1.6 Project aims 59

Chapter 2. Materials and methods 63

2.1 Cell culture 63
2.1.1 Mouse embryonic fibroblasts (MEFs) culture 63
2.1.2 Freezing and thawing of MEFs 64
2.1.3 Mitotic inactivation of MEFs 64
2.1.4 Maintenance and passage of hESC and hiPSC on MEFs 65
2.1.5 Feeder-free hESC and hiPSC culture 65

2.2 Differentiation protocols 67
2.2.1 Differentiation protocol adapted from generation of inner ear sensory epithelia from mESCs in 3D culture (Koehler et al., 2013) 68
2.2.2 2-mercaptoethanol high concentration protocol 69
2.2.3 2-mercaptoethanol low concentration protocol 70

2.2.4 KOSR high concentration protocol 71

2.3 Reverse transcription polymerase chain reaction (RT-PCR) 72
2.3.1 RNA isolation 72
2.3.2 cDNA synthesis 72
2.3.3 Real-time quantitative polymerase chain reaction (qRT-PCR) 73

2.4 Immunohistochemistry 75

2.5 Dye permeation experiment 77
2.5.1 Basic concepts of FM1-43 77
2.5.2 FM1-43FX labelling protocol 78

2.6 Electron microscopy 80
2.6.1 Basic concepts of Electron Microscopy 80
2.6.2 Transmission electron microscopy (TEM) protocol 80

2.7 Flow cytometry 81

2.8 Electrophysiological recordings 82
2.8.1 Basic concepts of patch clamp techniques 82
2.8.2 Electrophysiology recording protocol 83

Chapter 3. Differentiation of hESCs to otic lineages 85

3.1 Differentiation of hESCs to inner ear cells using the mouse protocol 86
3.1.1 A timeline of mouse protocol 86
3.1.2 Analysis of differentiated hESCs under the mouse differentiation conditions 86
3.1.3 Conclusions 90

3.2 Differentiation of hESCs to inner ear cells using media with a high concentration of 2-mercaptoethanol 91
3.2.1. A timeline of high concentration of 2-mercaptoethanol protocol 91
3.2.2 Analysis of differentiated hESCs under the high concentration of 2-mercaptoethanol condition 91
3.2.3 Conclusions 99

3.3 Differentiation of hESCs to inner ear cells using media with a low concentration of 2-mercaptoethanol 100

3.3.1. hESC differentiation protocol under low 2-mercaptoethanol concentration 100
3.3.2. EB formation (d0 – d8) 100
3.3.3. Prosensory vesicle formation (d8 – d20) 102
3.3.4. Prosensory otic vesicles (d36) 106
3.3.5. Induction of early hair cells / supporting cells and auditory neurons (d60) . 109
3.3.6. Maturation of hair cells / supporting cells (d90) 115
3.3.7 Conclusions 118

3.4 Differentiation of hESCs to inner ear cells using media with a high concentration of KOSR 119
3.4.1. A timeline of high concentration of KOSR protocol 119
3.4.2. Analysis of differentiated hESCs under the high concentration of KOSR condition 119
3.4.3 Conclusions 126

Chapter 4. Differentiation of hiPSCs to otic lineages 128

4.1 Differentiation of hiPSCs to inner ear cells using media with a low concentration of 2-mercaptoethanol 129
4.1.1 EB formation (d0 – d8) 129
4.1.2 Prosensory vesicle formation (d8 – d20) 129
4.1.3 Prosensory otic vesicles (d36) 133
4.1.4 Induction of early hair cells and auditory neurons (d60) 136
4.1.5 Induction of matured hair cells / supporting cells (d90) 140

4.2 Conclusions 143

Chapter 5. TEM analysis and functional tests during otic lineage differentiation 145

5.1 Differentiation of hESCs to inner ear cells using media with a low concentration of 2-mercaptoethanol 145
5.1.1. TEM analysis 145
5.1.2. FM1-43FX uptake assay 149
5.1.3. Electrophysiological recordings 151
5.1.4 Conclusions 153

5.2 Differentiation of hiPSCs to inner ear cells using media with a low concentration of 2-mercaptoethanol 154
5.2.1. TEM analysis.....154
5.2.2. FM1-43FX uptake assay 160
5.2.3. Electrophysiological recordings.....162
5.2.4 Conclusions.....163

Chapter 6. Discussion.....165

6.1 Summary of findings.....165

6.2 Importance of derivation of inner ear tissue from hPSCs 167

6.3 Ways to identify hair cell types *in vitro*.....170

6.4 Limitations of the study and future directions 172

References.....175

List of Figures

Figure 1 | Summary of inner ear early development in a vertebrate.....3
Figure 2 | Simple two-step model for the induction of the otic placode. 4
Figure 3 | Model of inner ear induction.....6
Figure 4 | Morphogenesis of the inner ear. 7
Figure 5 | Model showing control of Phase 1 and Phase 2 otic invagination.....9
Figure 6 | Development and specification of the prosensory domain (PD) and the organ of Corti (OC) in mouse. 11
Figure 7 | Formation of the otic vesicles from thickened otic placodes in human.....14
Figure 8 | Development of the human inner ear. 15
Figure 9 | Vestibular hair cells from human semicircular canal organs. 16
Figure 10 | Afferent nerve ending development and synaptogenesis in the vestibular epithelium of human fetuses.....19
Figure 11 | Structure of stereocilia bundles in developing fetal cochlea.....22
Figure 12 | Anatomy of the adult' human ear. 28
Figure 13 | Mechanoelectrical transduction mediated by hair cells. 31
Figure 14 | Central auditory pathways.....32
Figure 15 | Cleavage, the blastula stage, and gastrulation 36
Figure 16 | Three techniques to generate pluripotent stem cells.....38
Figure 17 | Derivation of definitive ectoderm-like cells from hESCs. 41
Figure 18 | Models for the role of BMP in ectodermal patterning. 43
Figure 19 | Differentiation culture formats. 47
Figure 20 | Overt morphological changes of human EBs occur in serum-free media. 49
Figure 21 | Schematic drawing of the 30-day guidance protocol.....53
Figure 22 | FM1-43 rapidly fills the cytoplasm of mouse hair cells, entering from the tops and progressing to the bases of cells. 78
Figure 23 | The patch-clamp recording 82
Figure 24 | Otic lineage guidance of hESCs using the mouse differentiation conditions published by Koehler et al (Koehler et al., 2013).....86
Figure 25 | Morphological changes during differentiation of hESCs under the mouse differentiation condition. 89

Figure 26 │ Otic lineage guidance of hESCs under the high concentration of 2-mercaptoethanol condition. 91
Figure 27 │ The inner ear cell induction of hESCs derived EBs under the high concentration of 2-mercaptoethanol condition. 93
Figure 28 │ qRT-PCR analysis.....95
Figure 29 │ Immunohistological analysis on day 32 under the high concentration of 2-mercaptoethanol condition. 96
Figure 30 │ Morphological changes in the various concentration of 2-mercaptoethanol condition. 98
Figure 31 │ Otic lineage guidance of hESCs under the low concentration of 2-mercaptoethanol condition. 100
Figure 32 │ Overview of otic vesicle formation and marker genes. 102
Figure 33 │ Morphological changes during differentiation of hESCs. 103
Figure 34 │ Immunohistological analysis in the formation of possible otic vesicles (d20). 105
Figure 35 │ Overview of prosensory otic vesicles and marker genes. 106
Figure 36 │Size of vesicles during differentiation of hESCs. 107
Figure 37 │ Immunohistological analysis in the prosensory otic vesicle-like structures (d36). 108
Figure 38 │ Overview of matured prosensory otic vesicles and neuronal structures. 109
Figure 39 │ Immunohistological analysis of the possible matured otic vesicles (d60). 112
Figure 40 │ Immunohistological analysis in the possible auditory neurons (d60). ...114
Figure 41 │ Overview of matured otic vesicles containing hair cells and supporting cells 115
Figure 42 │ Immunohistological analysis to identify cell types (d90). 117
Figure 43 │ Otic lineage guidance of hESCs under the high concentration of KOSR condition. 119
Figure 44 │ The inner ear cell induction of hESCs derived EBs. 121
Figure 45│Size of vesicles during differentiation of hESCs under the high concentration of KOSR condition. 122
Figure 46 │ Immunohistological analysis in the prosensory otic vesicle-like structures (d36). 123

Figure 47 | Immunohistological analysis in possible otic vesicles and neuronal structures (d60). 124
Figure 48 | Morphological changes during differentiation of hiPSCs. 130
Figure 49 | Immunohistological analysis in the formation of otic vesicle-like structures (d20). 132
Figure 50 | Size of vesicles during differentiation 134
Figure 51 | Immunohistological analysis in the prosensory otic vesicle-like structures (d36). 135
Figure 52 | Immunohistological analysis of the possible matured otic vesicles (d60). 137
Figure 53 | Immunohistological analysis in the possible neurons (d60). 139
Figure 54 | Immunohistological analysis to identify cell types (d90). 142
Figure 55 | TEM images of possible microvilli or cilia (d36). 147
Figure 56 | TEM images of possible stereocilia bundles (d60). 148
Figure 57 | Functional properties of hESCs-derived hair cells and neuronal cells using a FM1-43FX uptake assay. 150
Figure 58 | Isolated possible otocysts and neuronal cells from EBs and electrophysiological recordings. 152
Figure 59 | TEM images of possible stereocilia bundles (d60). 156
Figure 60 | TEM images of possible stereocilia bundles (d90). 159
Figure 61 | Functional properties of hiPSCs-derived hair cells and neuronal cells using a FM1-43FX uptake assay. 161
Figure 62 | Possible hair cells and neuronal cells after sorting flow cytometry. 163
Figure 63 | Overview of an *in vitro* otic differentiation 165

List of Tables

Table 1 | Specific aims for each differentiation stage 61
Table 2 | Composition of the differentiation medium on day 0. 68
Table 3 | Composition of the differentiation medium on day 0. 69
Table 4 | Composition of the differentiation medium on day 0. 70
Table 5 | Composition of the differentiation medium on day 0. 71
Table 6 | GoScript Reverse Transcription System reverse transcription reaction mix components. 73
Table 7 | qRT-PCR reaction components. 73
Table 8 | List of primers used in this study. 74
Table 9 | List of antibodies used in this study 76
Table 10 | Defining different hair cell types by morphology and protein markers. 170

Abbreviations

2D	Two Dimensional
3D	Three Dimensional
AC	Anterior Crista ampullaris
ASC	Anterior Semicircular Canal
ATOH1	Atonal bHLH Transcription Factor 1
BME	2-mercaptoethanol
BMP	Bone Morphogenetic Protein
CB2	Calbindin2
CGRP	Calcitonin Gene Related Peptid
CNS	Central Nervous System
Dl1	Delta1
DMEM	Dulbecco’s Modified Eagle’s Medium
DNA	Deoxyribonucleic Acid
DV	Dorsal-Ventral
EBs	Embryoid Bodies
EC	Embryonal Carcinoma
ECM	Extracellular Matrix
EDTA	Ethylene Diaminetetraacetic Acid
EGF	Epidermal Growth Factor
EM	Electron Microscopy
EpiSCs	Epiblast Stem Cells
ES	Embryonic Stem

ESCs	Embryonic Stem Cells
FBS	Fetal Bovine Serum
FGF2	Fibroblast Growth Factor 2
FITC	Fluorescein Isothiocyanate
GAPDH	Glyeraldehyde-3-Phosphate Dehydrogenase
GER	Greater Epithelial Ridge
GMEM	Glasgow's Minimal Essential Medium
GS	Glutamine Synthetase
hESCs	Human Embryonic Stem Cells
hiPSCs	Human Induced pluripotent stem cells
hPSCs	Human Pluripotent Stem Cells
KO-DMEM	Knockout-Dulbecco’s Modified Eagle’s Medium
KOSR	Knockout Serum Replacement
HIER	Heat Induced Epitope Retrieval
I_{Ca}	Ca^{2+} current
ICM	Inner Cell Mass
IHCs	Inner Hair Cells
I_K	Outward Delayed Rectifier K^+ currents
I_{K1}	K^+ current
I_{Kv}	Delayed Rectifying K^+ Current
I_{Na}	Na^+ current
IPC	Inner Pillar Cell
iPSCs	Induced Pluripotent Stem Cells
IV	Invitrogen

I-V	Current-Voltage
IVF	In Vitro Fertilization
Jag1	Jagged1
LC	Lateral Crista ampullaris
LDN	LDN-193189
LER	Lesser Epithelial Ridge
LSC	Lateral Semicircular Canal
mESCs	Mouse Embryonic Stem Cells
MEFs	Mouse Embryonic Fibroblasts
MEM NEAA	Minimum Essential Medium Non-Essential Amino Acids
MLC	Myosin Light Chain
RNA	Ribonucleic Acid
MYO7A	Myosin 7A
n	Number
NC	Neural Crest
NE	Neuro-ectoderm
NEAA	Nonessential Amino Acids
NFM	Neurofilament
nGFP	Enhanced Green Fluorescent Protein
Ngn1	Neurogenin1
NT	Nuclear Transfer
OC	Organ of Corti
OCM	Oncomodulin
OEPD	Otic Epibranchial Progenitor Region

OEPs	Otic Epithelial Progenitor Cells
OHC	Outer Hair Cell
ONPs	Otic Neural Progenitor Cells
OPC	Outer Pillar Cell
OTOP1	Otopetrin1
PBS	Phosphate Buffered Saline
PC	Posterior Crista ampullaris
PD	Prosensory Domain
PFA	Paraformaldehyde
PGCs	Peripheral Glial Cells
PIER	Proteolytic Induced Epitope Retrieval
PKCα	Protein Kinase C Alpha
PLCγ	Phospholipase C Gamma
PI	Propidium iodide
PPE	Preplacodal Ectoderm
PPR	Pre-Placodal Region
P/S	Penicillin/ Streptomycin
PSCs	Pluripotent Stem Cells
PSC	Posterior Semicircular Canal
PV	Parvalbumin
qRT-PCR	Quantitative Reverse Transcription Polymerase Chain Reaction
RA	Retinoic Acid
RNA	Ribonucleic Acid
Rock-I	Rho-associated protein kinase inhibitor

RP	Retinitis Pigmentosa
rpm	Revolutions Per Minute
SB	SB-431542
sb	Synaptic Bodies
SCNT	Somatic Cell Nuclear Transfer
SEM	Scanning Electron Microscope
SGCs	Satellite Glial Cells
SGNs	Spiral Ganglion Neurons
SHH	Sonic Hedgehog
SM	Saccular Macula
SP	Sodium Pyruvate
SS	Somatic Stage
SSEA	Stage Specific Embryonic Antigen
SY	Synaptophysin
TEM	Transmission Electron Micrograph
TGF-β	Transforming Growth Factor-β
TUBB3	β-III-tubulin
UM	Utricular Macula
USH	Usher Syndrome
VGNs	Vestibular Ganglion Neurons
WG	Weeks Gestation

Chapter 1

Introduction

Chapter 1. Introduction

1.1 Development and regeneration of the inner ear

The development of the inner ear has been studied actively for more than 100 years. In the early 20th century, the majority of studies relied on morphological or histological identification of ear tissue using chick, amphibian and fish model systems. In the late 20th century, the availability of genetic markers for inner ear cell types has prompted new studies of inner ear induction. In this section, development of the inner ear of the vertebrates is reviewed together with the process of otogenesis in human.

1.1.1 Development of the inner ear in the vertebrates

The ear can be divided into three parts, the external, middle, and inner ear, each of which has distinct embryonic origins (Fekete, 1999). The external and middle ears develop from the first and second pharyngeal arches and the intervening pharyngeal cleft, membrane, and pouch (Fekete, 1999). In contrast, the inner ear develops from the surface ectodermal otic placode that appears on either side of the neural tube (Alvarez et al., 1989).

The early development of the inner ear occurs in three phases (Figure 1). The first phase, the formation of the otic placode, occurs as a result of inductive interactions with surrounding tissues (Ohyama et al., 2007). The second phase involves the morphogenesis of the otic placode to form the otocyst, a spherical vesicle that gives rise to both a dorsal vestibular region and a ventral cochlear region (Ladher, 2016, Sai and Ladher, 2015). The final phase of early development of the inner ear consists of the regional patterning of the otocyst, which comprises formation of the anteroposterior, dorsoventral, and mediolateral axes and localized morphogenesis along these axes, resulting in the complex three-dimensional (3D) morphology (Basch et al., 2016, Wu and Kelley, 2012, Nakajima, 2015, Whitfield, 2015).

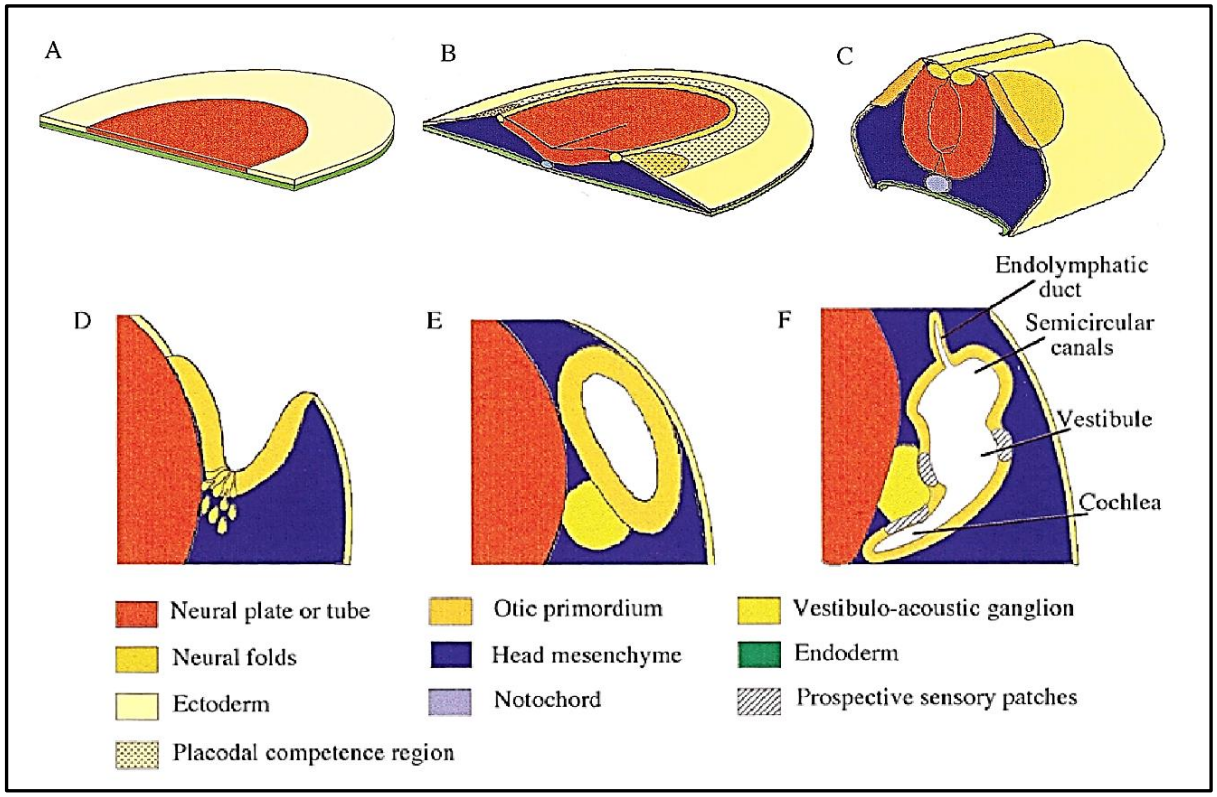

Figure 1 | Summary of inner ear early development in a vertebrate.

A, B, 3D representations of anterior halves of early embryos, sectioned at the prospective otic area to show the disposition of embryonic layers. C, A transverse segment of the head region at the otic placode level. D, E, and F, Transverse sections at the otic level. Stages: (A) Pregastrula. (B) Head fold, the prospective otic placode is indicated in orange and the prospective multiplacodal ectoderm stripe is stippled. (C) Otic placode. (D) Otic cup, neuroblast appears delaminating from the otic epithelium. (E) Otic vesicle. (F) Otocyst differentiation, the primordia of the different anatomical regions is indicated. Figure adapted from (Torres and Giraldez, 1998).

1.1.1.1 Formation of the otic placode

All craniofacial sensory organs including the inner ear derive from a common region of the ectoderm in early development (Ohyama et al., 2007). The formation of the otic placode is the earliest morphologically visible event after the events of gastrulation have laid down the body plan of the vertebrate embryo (Ohyama et al., 2007). The induction of the otic placode occurs in a two-stage process (Figure 2). The first step is the formation of a pre-placodal region which is competent to form all the craniofacial sensory placodes (Ohyama et al., 2007). The second step is the pre-otic field within the pre-placodal domain which further divides into the otic placode and surrounding non-otic epidermis (Ohyama et al., 2007).

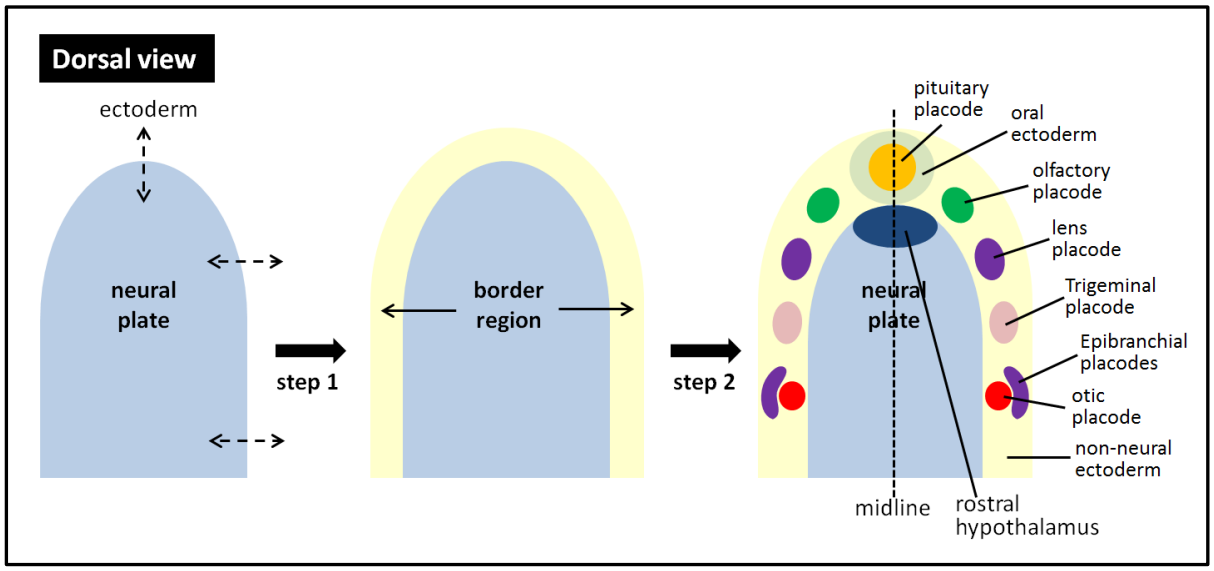

Figure 2 | Simple two-step model for the induction of the otic placode.

(Step 1) Neural plate-ectoderm interactions lead to the establishment of a border region marked by genes such as *Six4, Dlx5, Dlx6, ERN1, BMP4*, and *Msx1* (Kelley, 2005). (Step 2) Within this region, local signals from the mesoderm and hindbrain, which may include fibroblast growth factor (FGF) family members, act to specify the otic placode (Suga et al., 2011).

All craniofacial sensory organs (ear, nose, lens, trigeminal and epibranchial ganglia and lateral line) arise from a pre-placodal domain located at the periphery of the neural plate (Figure 2) (Baker and Bronner-Fraser, 2001, Brugmann and Moody, 2005). Morphological studies have shown the presence of a thickened continuous band of ectoderm running along the boundary of the anterior neural plate (Orahilly and Muller, 1985, Braun, 1996, Miyake et al., 1997). It can be characterized by a number of genes belonging to the *Dlx, Six, Eya, Iro, BMP*, and *Msx* families (Glavic et al., 2004a, Ohyama and Groves, 2004, Streit, 2004, Brown et al., 2005). Loss and gain of function of some of these genes result in widening or reduction respectively of the pre-placodal region (Brugmann et al., 2004, Glavic et al., 2004a, Litsiou et al., 2005). This morphological change becomes restricted to the different placodes and individual placodes are then induced by local specific signals as they differentiate (Baker and Bronner-Fraser, 2001, Brugmann and Moody, 2005).

It is necessary to summarize the genes involved in the otic placode, in order to study which tissues are destined to give rise to the otic placode and when the induction starts and finishes. Over the last two decades, a variety of molecular markers have been identified that label the otic placode prior to invagination (Kozlowski et al., 1997). The earliest marker reported so far is the transcription factor *Pax8* (Pfeffer et al., 1998, Heller and Brandli, 1999). The second earliest molecular marker known is *Pax2* (Nornes et al., 1990, Krauss et al., 1991). Some transcription factors (*EyaI, GATA3, Nkx5.1, Gbx2, Sox3, Sox9*) and signalling molecules (BMP7 and FGFs) appear to be expressed in the otic placode prior to invagination (George et al., 1994, Rinkwitzbrandt et al., 1995, Wright et al., 1995, Penzel et al., 1997, Shamim and Mason, 1998, Sahly et al., 1999, Sheng and Stern, 1999, Solloway and Robertson, 1999, Wood and Episkopou, 1999, Xu et al., 1999, Groves and Bronner-Fraser, 2000, Liu and Joyner, 2001, Sanchez-Calderon et al., 2002). The cells destined to give rise to the otic placode are less likely to be a physically discrete population instead; the cells committed to the otic placode intermingle with cells destined to form other tissues. During chick gastrulation, otic placode precursors appear to be mixed with cells that are competent to give rise to the central nervous systems, neural crest, epibranchial placodes, and epidermis (Streit, 2002). Similar results have also been obtained in zebrafish (Kozlowski et al., 1997).

There are two main candidates for tissues capable of inducing the otic placode; the hindbrain which lies adjacent to the otic placode, and the cranial paraxial mesoderm, which comes to lie under the otic placode (Figure 3). Over the last 90 years, many studies have shown that FGF signalling from the hindbrain and cranial paraxial mesoderm is necessary for otic placode induction, although their specific roles appear to vary from one species to another (Zhang et al., 1998, Gritsman et al., 1999, Phillips et al., 2001, Leger and Brand, 2002, Kil et al., 2005, Waskiewicz et al., 2002, Kwak et al., 2002, Maroon et al., 2002). The otic–epibranchial progenitor region (OEPD) is a common progenitor domain for otic and epibranchial placodes. For the refinement of the OEPD into distinct otic and epibranchial region, the activity of Wnt and its downstream signalling mediators is required (Ohyama et al., 2006, Freter et al., 2008).

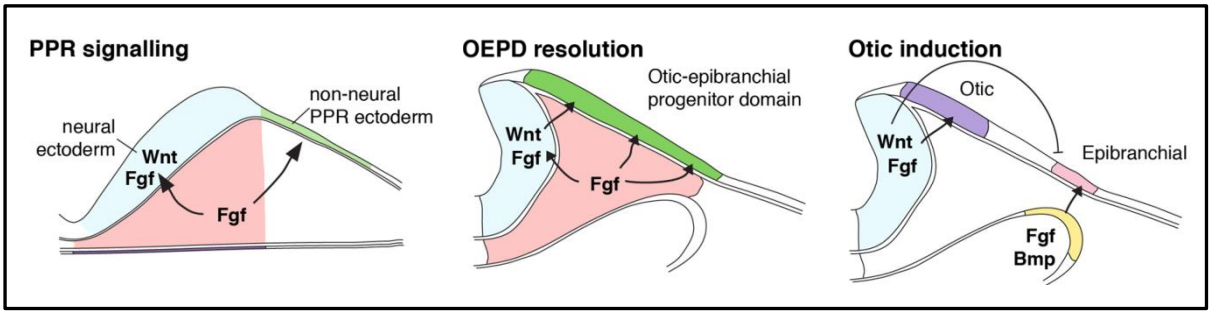

Figure 3 | Model of inner ear induction.

Schematic diagram summarizing the induction of the inner ear, synthesizing data from zebrafish, chick, and mouse. At early neurulation stages, mesodermal source (pink) of FGF signals overlying pre-placodal ectoderm to adopt an otic-epibranchial placode (OEPD) fate. Mesodermal FGF also signals neural ectoderm to express FGF and Wnt signals. At later neurulation stages, soon after the neural tube has closed, Wnt then acts on OEPD to specify the inner ear from within the OEPD. Figure adapted from (Sai and Ladher, 2015).

1.1.1.2 Formation of the otocyst

The otic placode is a surface structure, while the inner ear is internalised and is embedded within the cranial mesenchyme. As development progress, the otic placode undergoes dramatic morphogenesis involving thickening (Figure 4A), invagination (Figure 4B, C), and closure (Figure 4D) (Ladher, 2016, Sai and Ladher, 2015). The superficially located structure is internalised, and forms a spherical cyst embedded within the mesenchyme of the head (Ladher, 2016, Sai and Ladher, 2015).

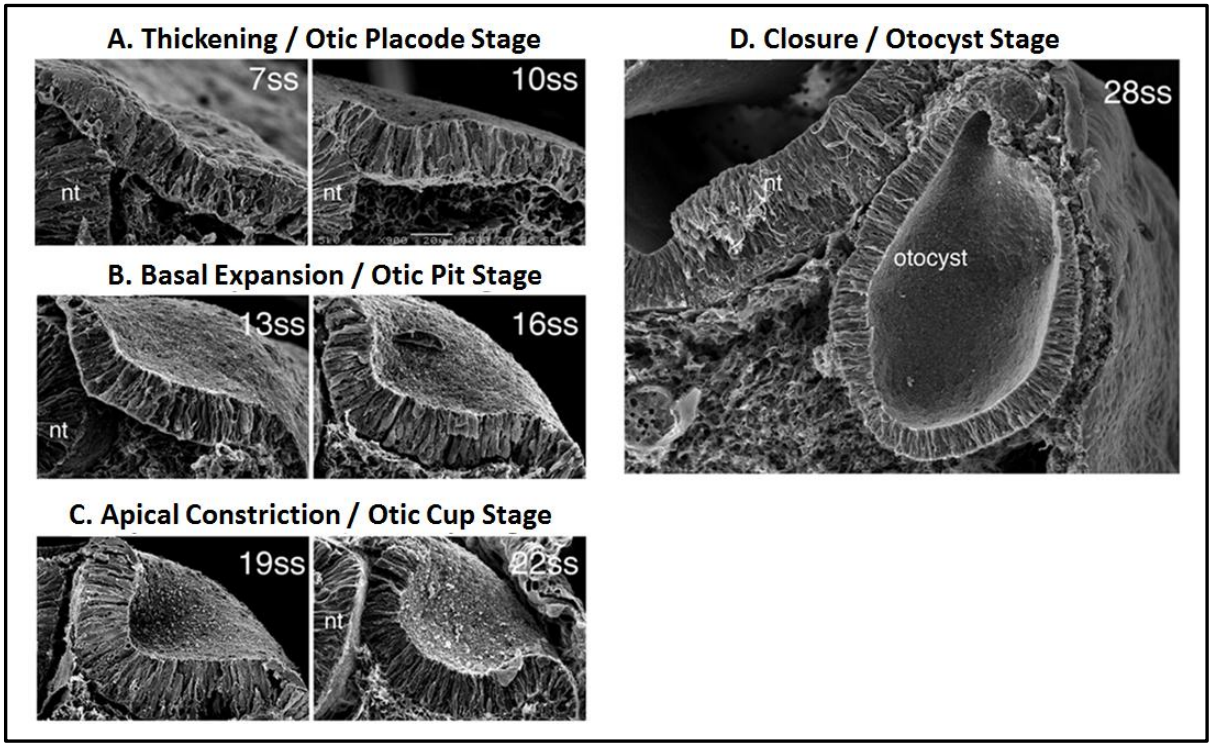

Figure 4 | Morphogenesis of the inner ear.

Scanning electron microscopy (SEM) images show the development of chick otocysts. By the 7th somatic stage (ss), the otic placode has segregated from the OEPD. At around 10ss of development, the placode begins to invaginate such that at 13ss and 16ss the basal part of the placode expands and forms the otic pit. After 16ss and until closure, the apical constriction is the main process driving invagination and the otic placode at these stages progressively deepens form the otic cup. With

the closure, the final form of the otocyst is apparent. Modified from (Sai and Ladher, 2015).

Epithelial thickening is a prerequisite of the mode of division in the otic placode because it divides using intra-kinetic nuclear migration a process involving smooth migration of nuclei from apical to basal and back during the G1 and G2 phases of the cell cycle, respectively (Spear and Erickson, 2012). It is suggested that this morphology has arisen to maximize the density of generative cells per unit area of the apical surface (Fish et al., 2008). The process of thickening of the otic placode converts the cuboidal epithelium of the non-neural ectoderm into columnar morphology just prior to invagination and columnar to the pseudo-stratified epithelia of the organ precursor during further thickening (Sai and Ladher, 2015, Meier, 1978a, Meier, 1978b).

Soon after thickening the basal face of the otic placode expands followed by an apical constriction in both mouse and chick (Figure 5) (Sai et al., 2014). In some teleosts such as zebrafish, however, the placode does not invaginate but rather forms a thickened ball that becomes hollow by cavitation (Haddon and Lewis, 1996). During the basal expansion, F-actin is located on the apical side of the placode and active myosin-II basally (Figure 5A) (Sai and Ladher, 2015). FGF signals originating from the mesoderm, in contact with the basal side of the placode, activate myosin light chain in the basal region (Sai et al., 2014). During the phase of apical constriction, the co-localization of activated myosin-II and F-actin provides a contractile force to constrict the apical junctional region of the cells resulting in driving the otic placode deeper into the mesenchyme of the head (Figure 5B) (Sai et al., 2014).

The final act of internalization of the otic placode is the closure of the otocyst with the two edges fusing, segregating the otic vesicle from the surface ectoderm. This process is not well understood in otic development, but parallels can be drawn with wound healing and neural tube closure (Colas and Schoenwolf, 2001, Martin and Parkhurst, 2004). In the case of neural tube closure, it is initiated by the non-neural ectoderm itself, with the action of filopodial likened to a zippering effect (Ray and Niswander, 2012). These act to bring the epithelium into close juxtaposition allowing selective adhesive junctions to be established that bring together opposite

edges of the two ectodermal regions (Pyrgaki et al., 2010). Thus the selective expression of cell adhesion molecules leads to the closure and segregation of ectodermal lineages (Pyrgaki et al., 2010). This process may also function in otic vesicle fusion.

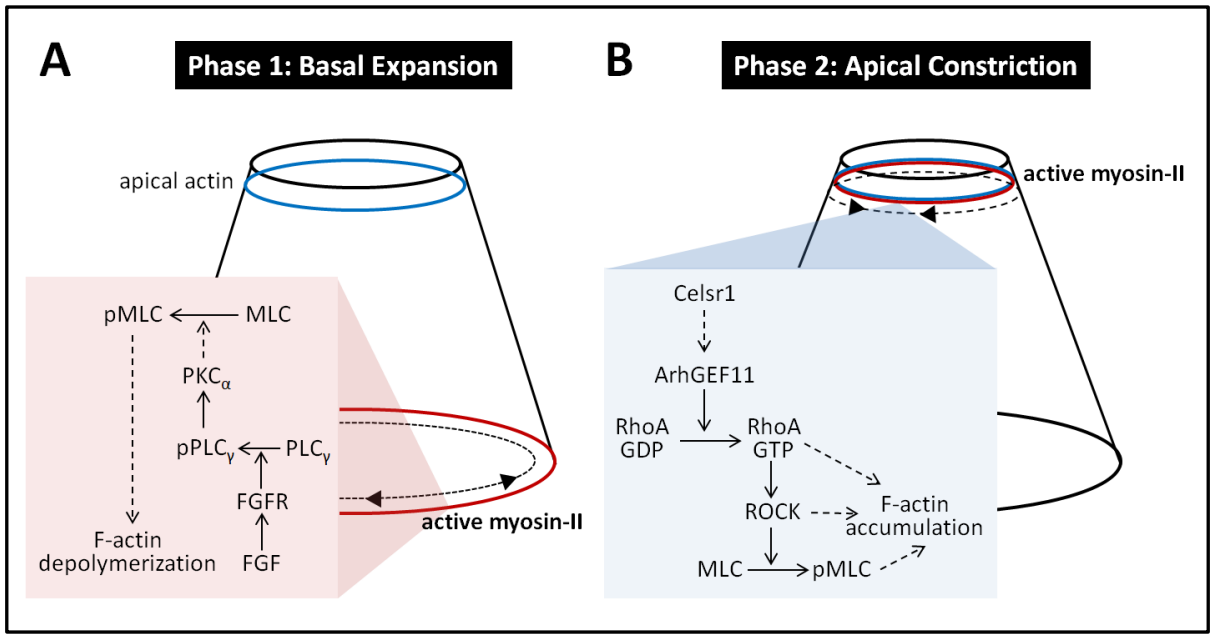

Figure 5 | Model showing control of Phase 1 and Phase 2 otic invagination.

A, Diagram indicating a cell undergoing basal expansion showing the active myosin–II in basal side of the cells (red). The apical junctional region is devoid of active myosin-II. Myosin-II is activated by the basal FGF, triggering a cascade via phospholipase C gamma (PLCγ) and protein kinase C alpha (PKCα) which results in the phosphorylation of myosin light chain (MLC). B, Diagram shows the apical constriction by the co-localization of actin and active myosin-II in the apical junctional region. RhoA is activated through the activity of ArhGEF11, downstream of apically located Celsr1. RhoA triggers to the activation of ROCK, which in turn phosphorylates MLC. RhoA, ROCK, and pMLC lead to apical F-actin accumulation in the apical region. Modified from (Sai et al., 2014).

1.1.1.3 Regional morphogenesis of the otocyst

After the development of the otic vesicle is completed, establishing the dorsal-ventral (DV) patterning is necessary to further generate the complex inner ear morphology consisting of the dorsal vestibular labyrinth (dorsal bulge) and ventral cochlea (ventral bulge). At this time, the floor plate in the hindbrain and notochord secrete sonic hedgehog (Shh) to establish the DV axis (Bok et al., 2005). The endolymphatic duct emerges from the dorsal-medial surface of the otic vesicle and two distinct pouches, the dorsal pouch and lateral pouch, subsequently develop from the dorsal bulge (Figure 6A) (Martin and Swanson, 1993). The dorsal pouch gives rise to two superior (vertical) ducts, the anterior and posterior semicircular ducts, while the lateral pouch gives rise to the lateral (horizontal) semicircular duct (Martin and Swanson, 1993). FGF, retinoic acid (RA), and Wnt signalling play an important role in the development of the vestibular system (Maier and Whitfield, 2014, Rakowiecki and Epstein, 2013). For example, Wnt/β-catenin signalling promotes the expression of BMP4/FGF10 in the cristae, which then stimulate the expression of BMP2 in the prospective semicircular duct epithelium (Chang et al., 2004, Chang et al., 2008, Gerlach et al., 2000). BMP2 induces the expression of Dlx5 in the perimeter rim of the pouch (future semicircular duct) to inhibit Netrin1 expression, thereby maintaining the epithelial structure of the semicircular duct (Chang et al., 2004, Chang et al., 2008, Rakowiecki and Epstein, 2013).

At the onset of cochlear formation, the cochlear bud grows out from the posteromedial ventral region of the otic vesicle to form the cochlear duct. In mouse, the cochlear duct continues to elongate and coil in an anterior-medial direction until it reaches its full one and three-quarters turns (Figure 6A) (Wu and Kelley, 2012). From E12.5 onward, the asymmetrical distribution of patterning signals is translated into three distinct regions in the medial thickened cochlea epithelium; Kölliker's organ which is one of the earliest visible epithelial structures of the developing cochlea and is the source of the sensory cells (neural side of the cochlear duct) (Dayaratne et al., 2014), the prosensory auditory domain, and the outer sulcus (Figure 6B). Initially, the sensory competent region of the cochlea expresses Sox2 and Jag1 (Figure 6C) (Ohyama et al., 2010). A gradient of BMP4 from the outer epithelial sulcus region refines the prosensory region as development proceeds (Figure 6C) (Ohyama et al., 2010). Then FGF signalling pathway is required for further differentiation of the

auditory sensory epithelium, which consists of hair cells and supporting cells (Munnamalai et al., 2012).

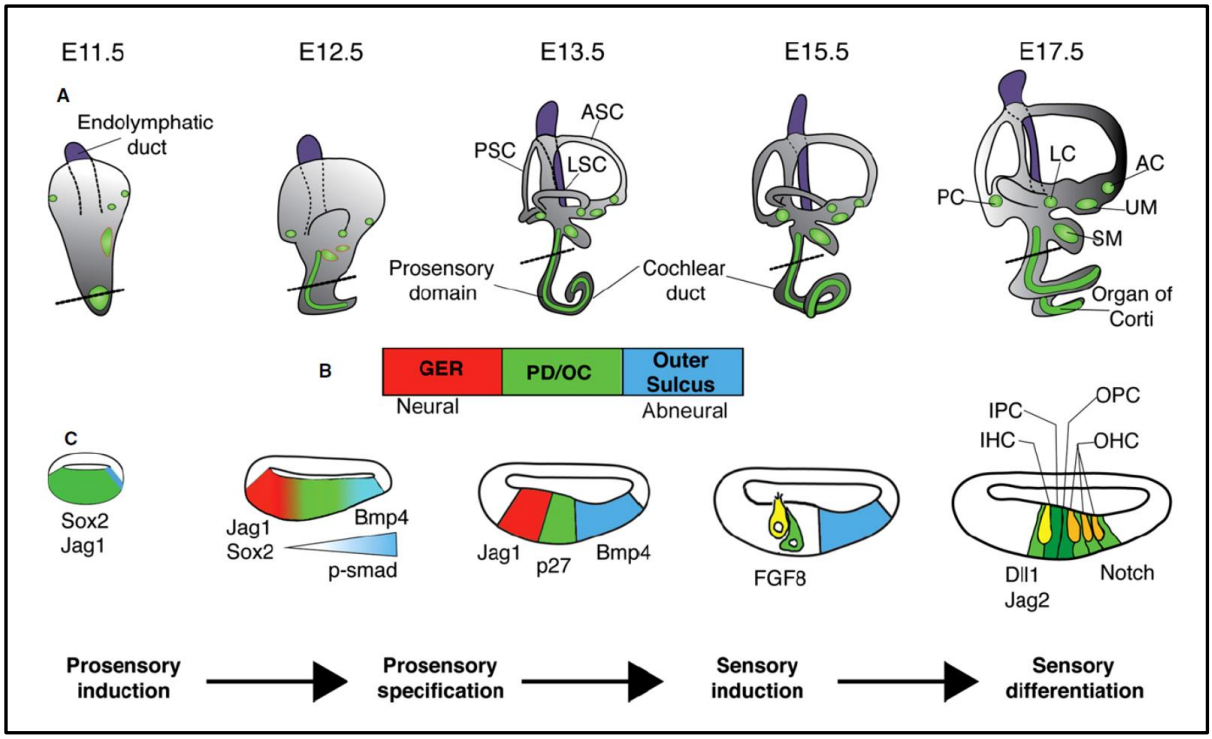

Figure 6 | Development and specification of the prosensory domain (PD) and the organ of Corti (OC) in mouse.

A, Time course of inner ear development in mouse. Between E11.5 and E17.5, the cochlear duct elongates from the ventral wall of the otocyst. By E15.5, the plates in the vestibular portion undergo extensive morphogenesis and thus the vestibular labyrinth and its associated sensory organs have developed, while the OC continues to differentiate. B, The bar indicates the orientation of the cochlear sections shown in C. The PD, which gives rise to the OC, is located between non-sensory tissues. On the neural side, the PD is flanked by the greater epithelial ridge (GER; red) and on the abneural side by the cells that will give rise to the outer sulcus (blue). C, Schematic diagrams of cochlear sections at the stage of the lines shown in A. AC, anterior crista ampullaris; ASC, anterior semicircular canal; IPC, inner pillar cell; LC, lateral crista ampullaris; LSC, lateral semicircular canal; OPC, outer pillar cell; PC, posterior crista ampullaris; PSC, posterior semicircular canal; SM, saccular macula; UM, utricular macula. Figure adapted from (Basch et al., 2016).

The otic vesicle is the origin of nearly all the cell types in the inner ear, including the afferent neurons of the VIIth cranial ganglion, which innervate the auditory and vestibular sensory hair cells (Maier et al., 2014). Neural cells and sensory cells develop from a population of common neurosensory progenitors, which is located in the anteromedial region of the otic vesicle and express Sox2 (Sapede et al., 2012). At the onset of neural determination, Sox2 initiates the expression of Neurogenin1 (Ngn1), which then suppresses Sox2 and upregulates the expression of NeuroD (Evsen et al., 2013). Neural progenitor cells also express the Notch ligand, Delta1 (Dl1), which activates Notch signalling in the neighbouring cells to inhibit a neural fate, resulting in the preservation of undifferentiated sensory progenitors by lateral inhibition (Jeon et al., 2011). Once the prosensory domains are established, the Notch ligand, Jagged1 (Jag1), acts to maintain these prosensory cells by lateral induction (Pan et al., 2013, Petrovic et al., 2014). A key gene for the hair cell development is atonal bHLH transcription factor 1 (*Atoh1)*, which is known to be both necessary and sufficient for hair cell specification and differentiation (Petrovic et al., 2014, Neves et al., 2012, Ahmed et al., 2012, Cai and Groves, 2015). In prospective hair cells, *Atoh1* induces expression of Dl1, which binds to the Notch receptors of neighbouring cells to maintain Sox2 positive supporting cells by inhibition (Petrovic et al., 2014, Neves et al., 2012, Ahmed et al., 2012, Cai and Groves, 2015). After the specification of hair cell development, hair cells begin to be oriented as a set of three rows of outer hair cells (OHCs) and a single row of inner hair cells (IHCs) in the cochlea (Nakajima, 2015). The OHCs mechanically amplify low-level vibration by changing the cell length (Brownell et al., 1985). The IHCs convert the sound vibrations in the fluids of the cochlea into electrical signals that are then relayed via the auditory nerve to the brain (Dallos et al., 1972).

1.1.2 Development of human inner ear

Development of the human inner ear begins from an otocyst forming as an invagination of ectodermal cells at four weeks gestation (4 WG) (Figure 7A) (Bruska et al., 2009, Streeter, 1905). At this stage, the otic vesicle has two pouches; dorsal and ventral (Figure 8A). The dorsal pouch will form the primordial endolymphatic duct and the ventral pouch becomes the cochlea (Bruska et al., 2009, Streeter, 1905). Between 4 and 5 WG, the dorsal pouch enlarges into a triangular shaped mass that will form the basis of all three semicircular canals (Figure 8A, B) (Streeter, 1905). At the same stage of development the vestibule, which will contain the future utricle and saccule, also enlarges (Streeter, 1905). By 10 WG, a partition forms between the utricle and saccule (Figure 8E, F, and G) (Streeter, 1905). The all three semicircular canals (anterior, posterior, and horizontal semicircular canals) are complete at this stage, although they have not reached a mature size (Jeffery and Spoor, 2004).

The cochlea elongates as a tubular structure from the ventral pouch (Figure 8A, B, C, D). It attains one complete revolution at 8 WG and two revolutions by 10 WG (Figure 8E, F, G) (Kim et al., 2011, Yasuda et al., 2007). The ductus reunions separate the vestibular organs from the cochlea by 10 WG (Streeter, 1905). The OC, which is the sensitive element containing hair cells and is situated on the basilar membrane, originates from the region between the GER and lesser epithelial ridge (LER) at 9 – 10 WG (Lavigne-Rebillard and Bagger-Sjoback, 1992). At this stage of development the tectorial membrane, located above the OC and composed of collagen fibers, is formed (Richardson et al., 2008, Lavigne-Rebillard and Pujol, 1987). Another gross morphological change is the formation of the perilymphatic spaces between 11 – 12 WG. The development of the scala vestibuli and scala tympani occurs by vacuolization of mesenchymal tissue surrounding the cochlear duct. By 16 – 17 WG, these perilymphatic spaces have elongated along the length of the cochlear duct so that they are close to mature size (Kim et al., 2011). Between 17 and 19 WG, cochlea radius has ceased to change and its size is comparable to adult (Jeffery and Spoor, 2004). The last half turn of the cochlear spiral (a total of two and one-half turns) is completed by 25 WG (Kim et al., 2011, Yasuda et al., 2007).

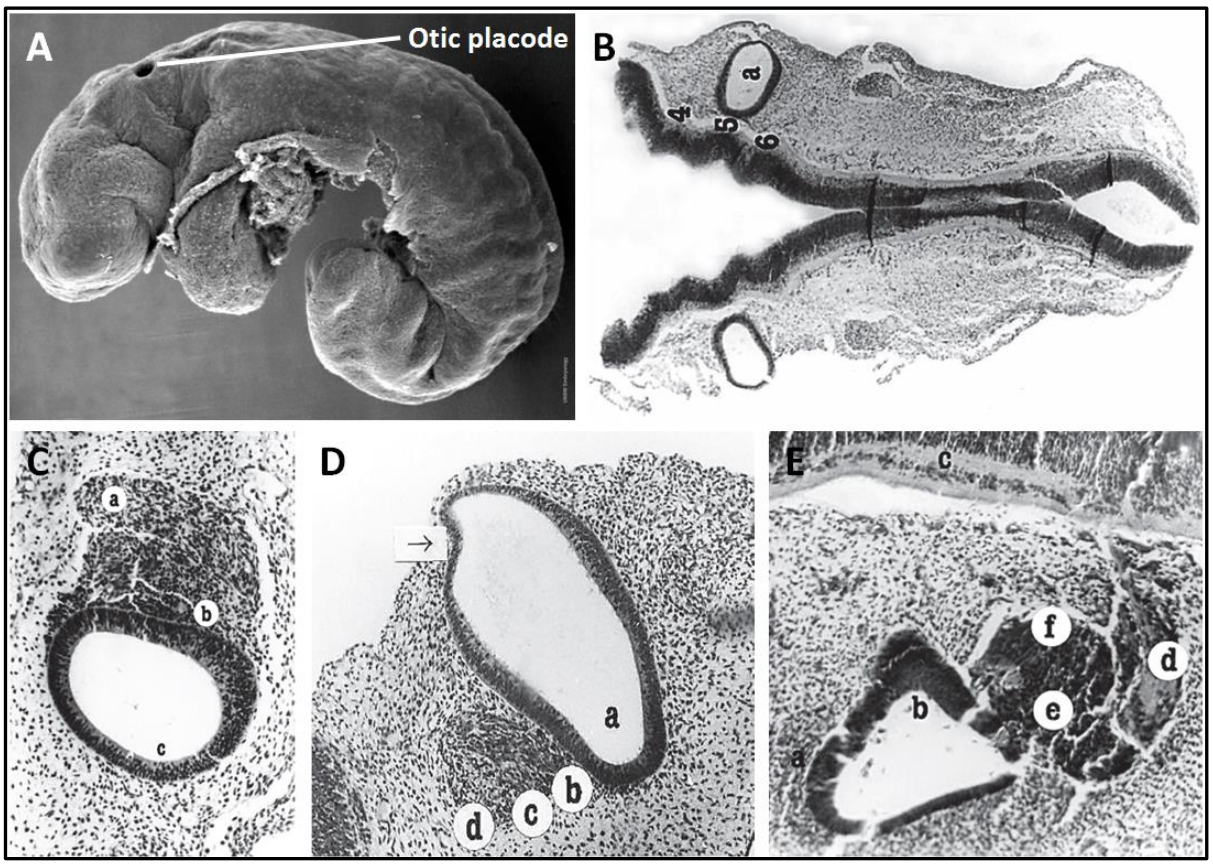

Figure 7 | Formation of the otic vesicles from thickened otic placodes in human.

A, A human embryo at 4 WG. B, A horizontal section of the brain in human embryo at 5 WG (32 postovulatory days). H + E, X 40; a - otic vesicle; 4, 5, 6 - rhombomeres. C, A horizontal section of a human embryo at 5 WG (32 postovulatory days). H + E, X 200; a - geniculate ganglion, b - vestibulocochlear ganglion, c - otic vesicle. D, Sagittal section of a human embryo at 5 WG (33 postovulatory days). H + E, X 100; a - otic vesicle, b - vestibular ganglion, c - cochlear ganglion, d - geniculate ganglion, arrow points endolymphatic duct. E, Sagittal section of a human embryo at 6 WG (36 postovulatory days). H + E, X 150; a - capsule of otic vesicle, b - otic vesicle, c - common afferent tract, d - geniculate ganglion, e - cochlear ganglion, f - vestibular ganglion. Modified from (Bruska et al., 2009) and (https://embryology.med.unsw.edu.au/embryology/index.php /Carnegie_stage_11).

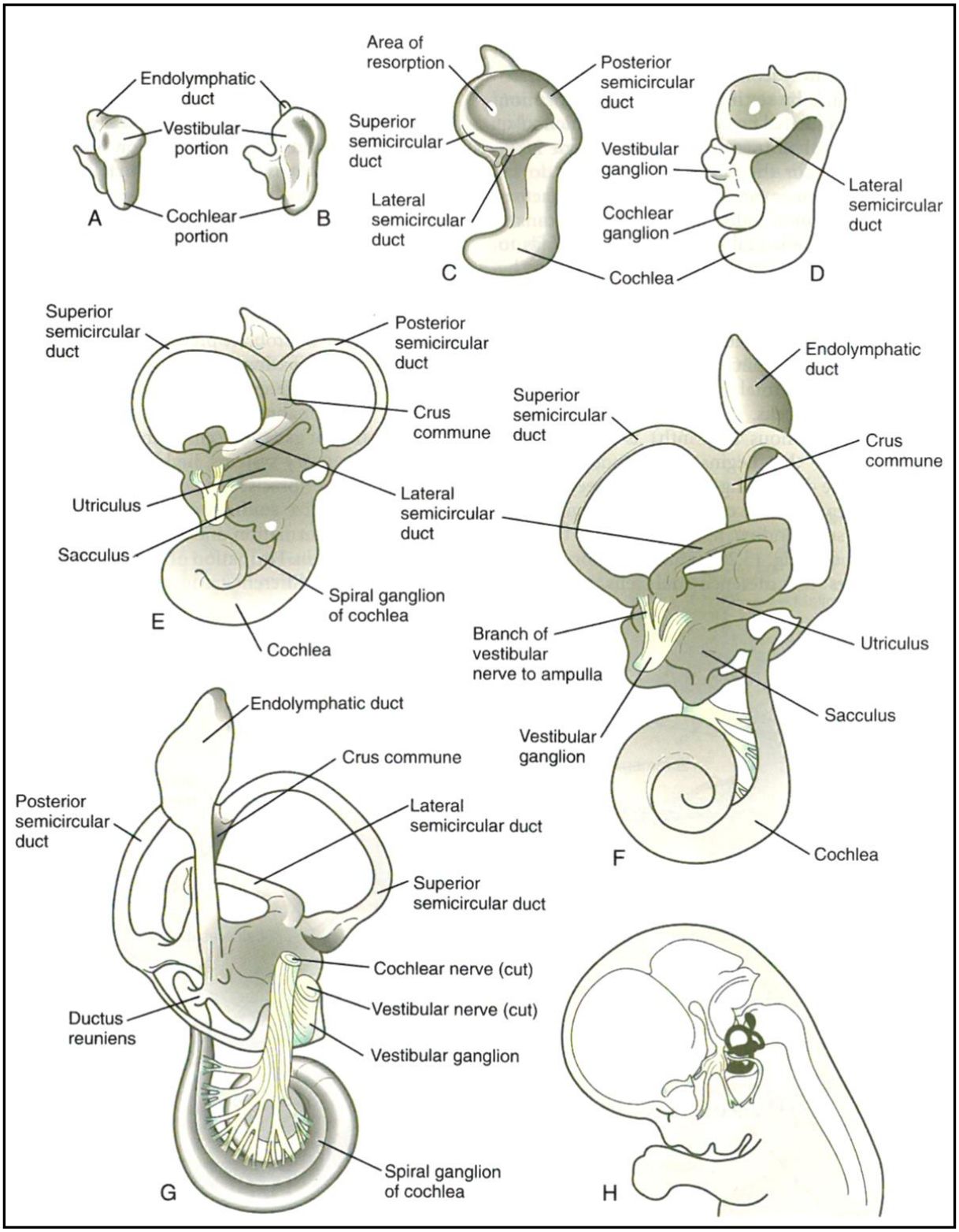

Figure 8 | Development of the human inner ear.

A, At 28 days. B, At 33 days. C, At 38 days. D, At 41 days. E, At 50 days. F, At 56 days, lateral view. G, At 56 days, medial view. H, Central reference drawing at 56 days. Figure adapted from (Carlson, 2014).

1.1.2.1 Development of vestibular hair cells and vestibular auditory neurogenesis

In vestibular organs (three cristae, a utricular macula, and a saccular macula) there are two types of vestibular hair cells: type I and type II. These hair cells convert mechanical movement especially angular and linear accelerations into electrical signals. Type I hair cells are amphora-shaped with variability in the length of the constricted neck (Figure 9A), and type II hair cells are more cylindrical in shape (Figure 9B) (Oghalai et al., 1998). In addition to their clear morphological differences, there is a distinct way that afferent nerve terminals contact each hair cell type. Type I hair cells are only contacted by afferent calyx nerve terminals that engulf the entire cell body and form tight junctions that ring the apical surface of the cell and efferent neurons form bouton terminals on the calyx endings around type I cells. On the other hand, type II hair cells are contacted by bouton afferent and efferent nerve terminals (Lysakowski and Goldberg, 1997, Lim and Brichta, 2016). Both types of hair cells are distributed throughout the vestibular organs, with a higher proportion of type I hair cells localized to the central zones (Lim and Brichta, 2016).

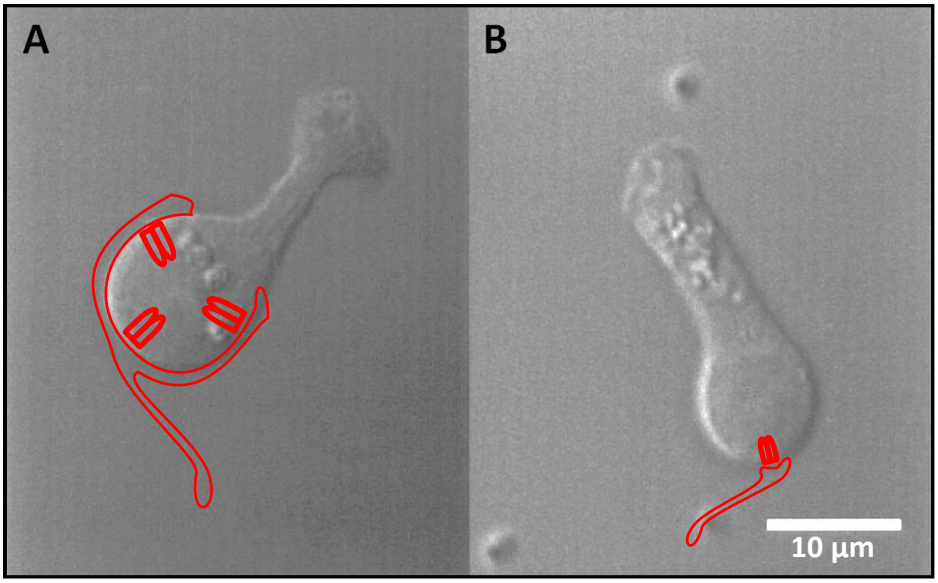

Figure 9 | Vestibular hair cells from human semicircular canal organs.

A, Type I hair cells have a constricted neck and contacted by afferent calyx nerve terminals. B, type II cells have a more cylindrical shape and are contacted by bouton nerve terminals. Figures adapted from (Oghalai et al., 1998).

In mature vestibular hair cells, numerous actin-filled stereocilia project from the apical surface, in a staircase arrangement, from the shortest at one end to the longest stereocilium at the other (Lim and Brichta, 2016). The longest stereocilium is closest to a single microtubule-based cilium, the kinocilium (Falk et al., 2015). The kinocilium comprises nine peripheral doublet microtubules that encircle two central single tubules (9 × 2 + 2 structure) (Falk et al., 2015). The kinocilium does not exhibit mechanosensitivity but the position of the kinocilium coincides with a directional sensitivity of the vestibular hair cells (Colclasure and Holt, 2003, Hudspeth and Jacobs, 1979). Bending the stereocilia toward the kinocilium depolarizes the cell and results in increased afferent activity and bending the stereocilia away from the kinocilium hyperpolarizes the cell and results in a decrease in afferent activity (Colclasure and Holt, 2003). Afferent innervation requires specialized organelles such as the synaptic ribbons expressed in both the presynaptic hair cell and the postsynaptic afferent terminal for synaptic transmission (Moser et al., 2006). Ribbons tether a monolayer of synaptic vesicles, with a high packing density (Lenzi et al., 1999). A fraction of these ribbon-associated vesicles “docks” onto the presynaptic membrane (Spicer et al., 1999). Shape, size, and a number of the ribbons differ between species as well as along the tonotopic axis, during development (Shnerson et al., 1981, Sobkowicz et al., 1982, Khimich et al., 2005).

In scanning and transmission electron microscope (SEM and TEM) studies, the earliest human fetal vestibular neuroepithelium is described as undifferentiated epithelial cells at 7 WG (Dechesne and Sans, 1985, Sans and Dechesne, 1985). It was shown even at this early stage, the most part of the vestibular surface is occupied by cells with one mini-kinocilium at their center and numerous microvilli on their edges (Dechesne and Sans, 1985). Between 8 and 9 WG, stereocilia cover the whole apical surface of each sensory hair cell and hair bundles are already unidirectionally polarized with the kinocilium (Sans and Dechesne, 1985, Dechesne and Sans, 1985). Between 12 and 14 WG, hair bundle length increases dramatically but the cilia are still not of adult size (Sans and Dechesne, 1985). Even these immature hair bundles appear to be of graded heights and are directionally polarized (Hoshino, 1982). From 14 WG, all hair bundles are oriented towards the striola which is a centrally positioned, crescent-shaped band in the utricle and saccule (Rosenhall, 1972). Both types of vestibular hair cells are innervated by specific afferent and

efferent systems forming a loop to and from the brainstem. The afferent nerve fibers originate from vestibular ganglion neurons (VGNs). The first studies to describe the vestibular ganglion are from human embryos at 5 WG (33 postovulatory days) (Bruska et al., 2009). At this stage of development, the otic vesicle lies adjacent to rhombomere 5 of the developing brain and the vestibular ganglion is closely attached to the otic vesicle (Figure 7D) (Bruska et al., 2009). At 6 WG (36 postovulatory days), the centrally directed nerve fibers from the VGNs extend to the brainstem (Bruska et al., 2009). The first evidence of afferent nerve terminals at the bottom as well as in the upper part of the vestibular epithelium occurs at 7 WG (Sans and Dechesne, 1987). At this stage, numerous afferent endings touch the cell membrane but no synaptic differentiation can be detected. At 8 WG, the first synaptic contacts are established (Figure 10A) (Dechesne and Sans, 1985). The presynaptic densities and synaptic bodies are present at the basolateral surface in vestibular hair cells while postsynaptic densities also appear in afferent terminals (Dechesne and Sans, 1985). In more mature synapses aged between 9 and 12 WG, the length of synaptic bars become taller and the number of microvesicles surrounding them also increase (Figure 10B, C, D) (Sans and Dechesne, 1987). In addition to afferent innervation, TEM studies also indicate that efferent fibers make contact with calyx terminals early in fetal development at 11 WG (Sans and Dechesne, 1987). The efferent terminals make direct contact with type II hair cells and afferent axon fibers; however, it is not known when these efferent contacts occur during human development (Lysakowski and Goldberg, 1997).

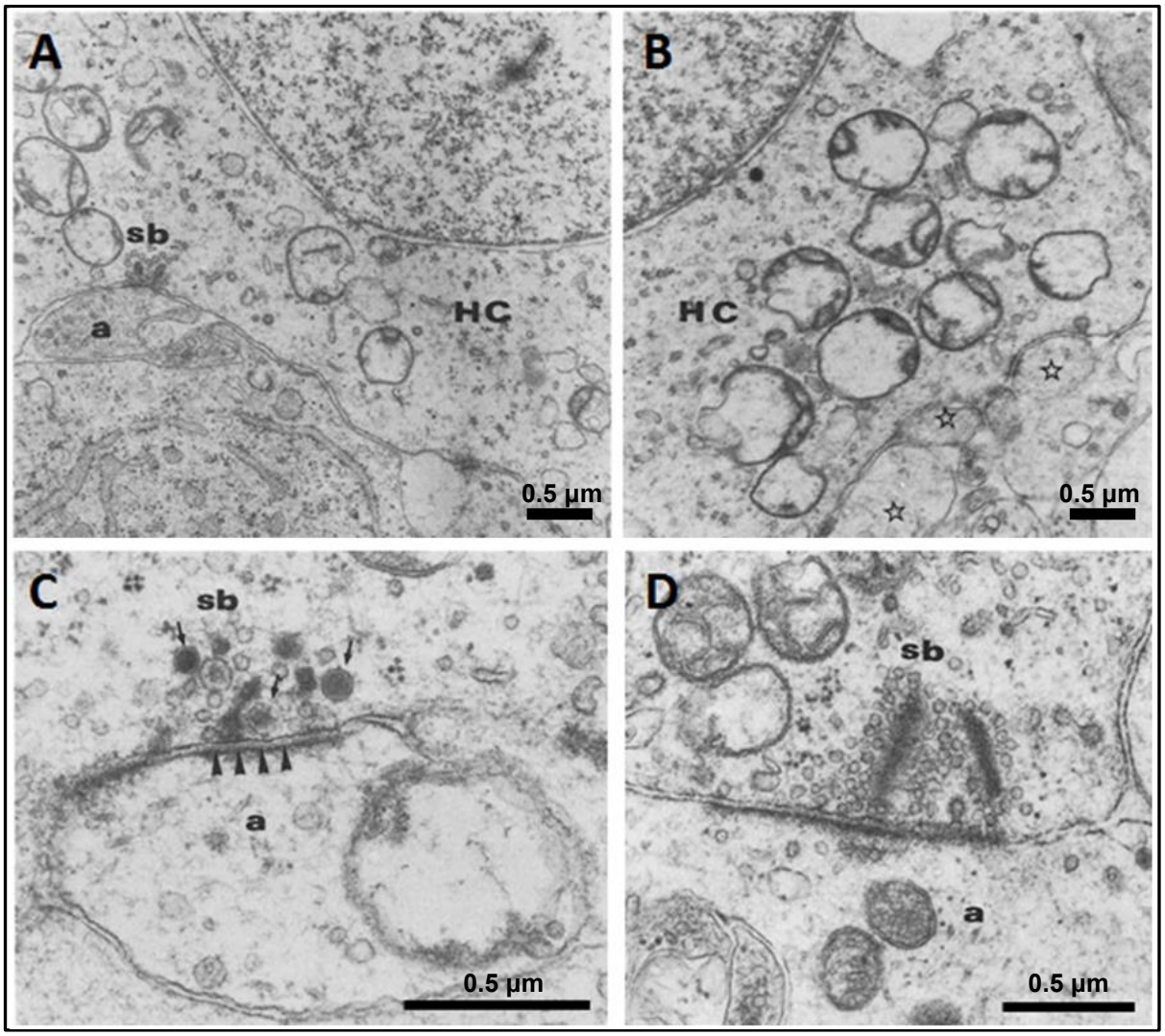

Figure 10 | Afferent nerve ending development and synaptogenesis in the vestibular epithelium of human fetuses.

A, A primitive synapse is formed between a hair cell and an afferent nerve ending (a) at 8 WG. Two small synaptic bodies (sb) are located in front of the afferent terminal. B, Numerous afferent fibers (stars) of various sizes contact the hair cell membrane between 8 and 9 WG. C, The dense bar contacting the cell membrane is surrounded by microvesicles and dense core vesicles (arrows) at 10 WG. The synapse is asymmetric with a postsynaptic densification (arrowheads) on the afferent ending (a). D, The length of the dense bars and the number of microvesicles has increased at 12 WG. Modified from (Sans and Dechesne, 1987).

The stages of fetal development at which vestibular hair cells acquire type I and II hair cell morphological and physiological characteristics are currently unknown. Recent preliminary functional data suggests the acquisition of voltage-gated conductances in fetal vestibular hair cells and primary afferent calyx terminals between 11 and 18 WG. During early fetal development (11 – 14 WG), type II hair cells express whole-cell conductances that are qualitatively similar but quantitatively smaller than those responses evoked from the mature hair cells (Lim et al., 2014). As development progressed (15 – 18 WG), peak outward conductances increase in magnitude with age, but still do not reach amplitudes observed in adult human vestibular hair cells (Oghalai et al., 1998). Mature type I hair cells uniquely express a low-voltage activating conductance, $G_{K,L}$ (Lim et al., 2014). A similar current is first observed at 15 WG but remains relatively small, even at 18 WG. The presence of a "collapsing" tail current indicates a maturing type I hair cell phenotype and suggests the presence of a surrounding calyx afferent terminal. At 15 WG, calyx afferent terminals exhibit a single action potential during depolarizing steps (Lim et al., 2014). Together, these data suggest a time point that vestibular hair cells become differentiated enough to begin expression of physiological characteristics observed in mature vestibular hair cells.

1.1.2.2 Development of cochlear hair cells and auditory neurogenesis

Hair cells in the auditory system are slightly different from those in the vestibular system. The hair cells of the OC are arranged in a single row of IHCs and typically three rows of OHCs along the length of the basilar membrane. This organization is arranged in a tonotopic gradient and auditory hair cells are the mechanoreceptors that convert sound into electrical energy. In the mature adult cochlea, IHCs have a rectilinear arrangement of hair bundles and OHCs have 'V' or 'W' shaped hair bundles with a staircase arrangement in the height of stereocilia (Comis et al., 1990). IHCs and OHCs are innervated by type I and type II spiral ganglion neurons (SGNs), respectively (Meyer et al., 2009a, Zhang and Coate, 2016). Each IHC is innervated by several afferent fibres that terminate in small rounded boutons, but each afferent fibre innervates only one IHC (Zhang and Coate,

2016). These afferent fibres are responsible for sending auditory information transduced by the inner ear to the central nervous system (CNS) (Zhang and Coate, 2016). Conversely, OHCs mostly receive efferent innervation, the role of which is to modulate the electromechanical amplification of the cochlear partition (Zhang and Coate, 2016).

The earliest observation of developing auditory hair cells is described as nascent hair cells that have a well-defined cuticular plate and stereocilia between 11 and 12 WG (Sanchez Fernandez et al., 1983). At 12 WG TEM studies suggest that the differentiating cochlea epithelium form a single row of IHCs along all sections from the base to the apex of the cochlea, while three or sometimes four rows of OHCs are only observed in basal regions (Pujol and Lavigne-Rebillard, 1985). At this stage, IHCs first differentiate their stereocilia so that they are clearly distinguished from microvilli of surrounding cells (Pujol and Lavigne-Rebillard, 1985). This is very slow when compared to the vestibular epithelium where the growth of the stereocilia has been observed as early as 7 to 8 WG. At 14 WG, typically three rows of OHCs are observed at the mid-turn region of the cochlea and both IHCs and OHCs show clusters of stereocilia (Igarashi, 1980a). Hair bundles of IHCs have a “U” shaped configuration with shorter medial stereocilia and longer lateral stereocilia, and a centrally located kinocilium (Figure 11A, B). This cilium is thick at its root and becomes thinner towards the tip. Unlike the adult case, the space between the stereocilia is not so wide (Igarashi, 1980a). In contrast, hair bundles of OHCs consist of short cilia converging at the tips with flower buds like arrangement (Figure 11C). At this stage of development, stereocilia are connected to each other with fine thread-like structures. At 22 WG, the patterns of hair bundles are closely similar as those of the adult with the exception of the presence of a short kinocilium on the OHCs and a slim kinocilium on the IHCs (Figure 11D, E) (Igarashi, 1980a). With age, this kinocilium decrease in size and disappear by 28 WG (Fujimoto et al., 1981).

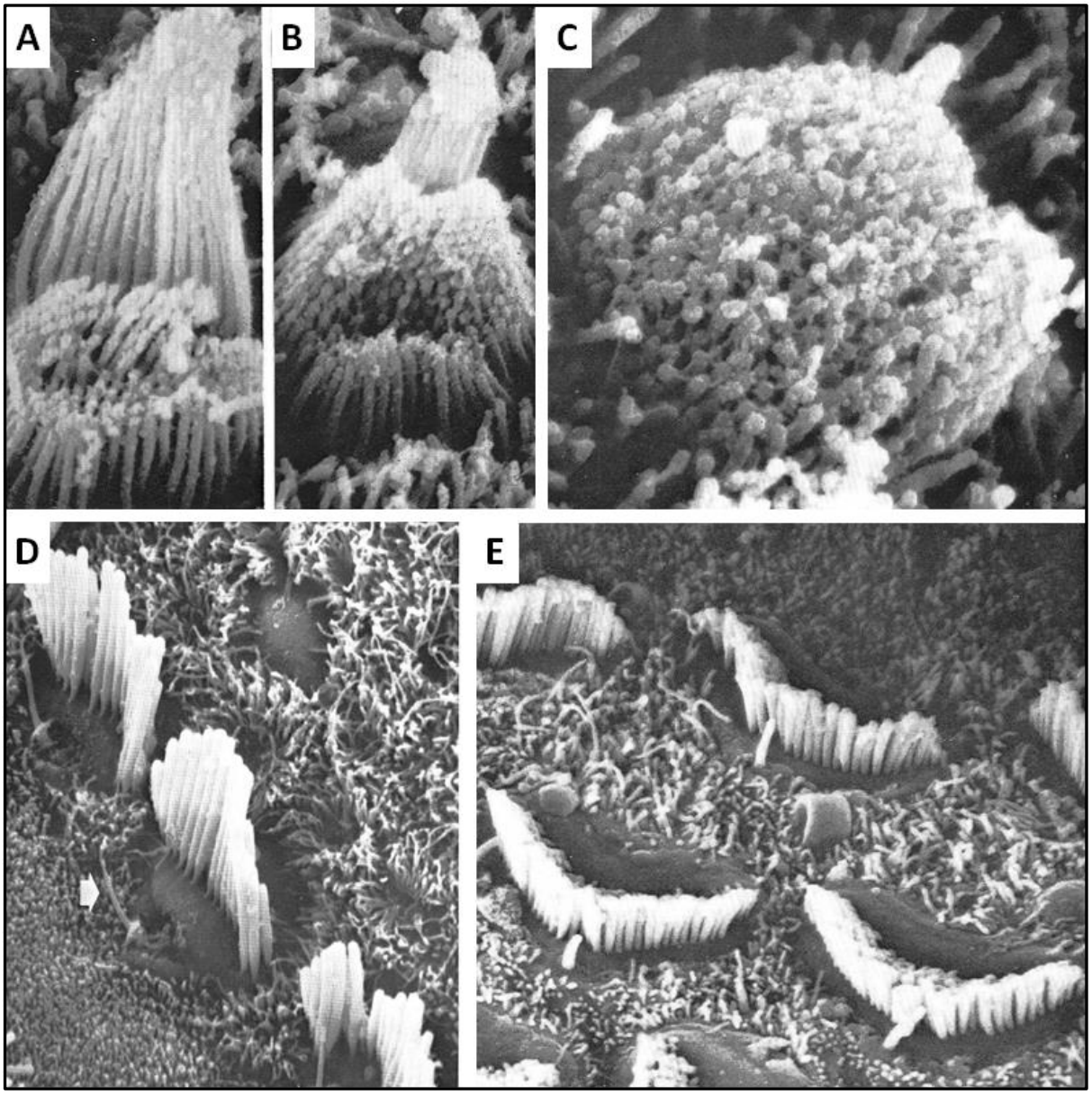

Figure 11 | Structure of stereocilia bundles in developing fetal cochlea.

A, A 14-week 6-day old fetus. Laterally located stereocilia of the IHC are remarkably taller than medially arranged ones. ×24,000. B, A 14-week 6-day old fetus. The pattern of IHC bundles is somewhat different from one seen in A, but basic arrangement seems same. ×19,000. C, A 14-week 6-day old fetus. The hairs consist of short stereocilia converging at the tips. ×39,000. D, A 22-week 2-day old fetus. IHCs have well-developed stereocilia and very slim kinocilium is noted lateral to stereocilia in each IHCs (arrows). E, A 22-week 2-day old fetus. OHCs take W shape of stereocilia bundles and have short kinocilia. ×10,000. Modified from (Igarashi, 1980b).

The emergence of SGN nerve innervation and synapses is a critical feature of auditory hair cell development and maturation. The penetration of afferent nerve fibers into an undifferentiated OC's primordium occurs very early, as soon as the 9 WG, prior to the cytodifferentiation of sensory hair cells (Pujol and Lavigne-Rebillard, 1985). By 10 WG the first row of hair cells destined to be the IHCs contact with many nerve fibers (Pujol and Lavigne-Rebillard, 1985). Auditory hair cells, like vestibular hair cells, have specialized ribbon synapses, for the release of glutamate neurotransmitter. Presynaptic specializations are first observed at 11 - 12 WG as synaptic ribbons or asymmetric thickenings at the junctions between afferent dendrites and IHCs or OHCs (Pujol and Lavigne-Rebillard, 1985, Pujol and Lavigne-Rebillard, 1995). At this stage of development, the first appearance of the efferent fibers beneath IHCs are also observed, while no efferent connections are made with OHCs (Pujol and Lavigne-Rebillard, 1985). At 14 WG, the number of synaptic contacts with IHCs increases, also multiple synaptic ribbons are observed between OHCs and afferent nerve terminals (Lavigne-Rebillard and Pujol, 1988). The OHCs are still exclusively innervated by afferent nerve endings. (Lavigne-Rebillard and Pujol, 1988, Pujol and Lavigne-Rebillard, 1995). It is not until 20 – 22 WG that the base of OHCs is innervated by efferent nerve, forming axo-somatic synapses (Lavigne-Rebillard and Pujol, 1988, Pujol and Lavigne-Rebillard, 1995).

1.1.3 Inner ear cell regeneration

During recent decades the regeneration of the inner ear to facilitate the development of therapeutic strategies to repair damaged hair cells has been the subject of intense research. Numerous studies have reported that the avian cochlea (the basilar papilla) is able to regenerate lost hair cells and auditory function can fully recover (Corwin and Cotanche, 1988, Cruz et al., 1987, Ryals and Rubel, 1988). For example, the chick cochlear hair cell regeneration after noise-induced hearing loss was first reported in 1987 (Cotanche, 1987). After 48 hours of recovery, new hair cells were identifiable in the region of hair cell loss and with time microvilli appeared on the apical surface of the epithelial tissue (Cotanche, 1987). During regeneration in the avian cochlea, the supporting cells served as the source of regenerated hair cells via mitotic regeneration or via direct phenotypic conversion of a supporting cell into a hair cell without undergoing mitosis (Stone and Cotanche, 2007).

In mammals, however, auditory hair cells are unable to regenerate, and damage to these cells results in a permanent hearing loss. These highly specialized hair cells are derived from prosensory cells, which have lost their capacity to divide by expressing cell cyclin-dependent kinase inhibitor $p27^{Kip1}$ and begin to express *Atoh1* in response to a variety of signals (Bermingham et al., 1999, Chen et al., 2002). Nevertheless, a few studies have reported that some hair cell populations in mouse utricle are able to regenerate after injury, but only at very early stages of development (Kawamoto et al., 2009). In addition, a previous study has demonstrated that post-mitotic supporting cells purified from the postnatal mouse cochlea retained the ability to divide and transdifferentiate into new hair cells in culture (White et al., 2006). These results helped to reveal that age-dependent changes in supporting cell proliferative capacity are due in part to changes in the ability to downregulate $p27^{Kip1}$ (White et al., 2006). Despite extensive work, it is still not clear whether the inability of mammalian hair cell regeneration is caused by an intrinsic inability of supporting cells to divide and differentiate or by an absence of proper regenerative signals.

The Notch pathway plays critical roles in cochlear development. Many studies have shown that Notch signalling is necessary and sufficient for specifying prosensory cells (Brooker et al., 2006, Munnamalai et al., 2012). After the initiation of

hair cell differentiation, differentiating hair cells express Notch ligands whose activate Notch signalling in neighbouring supporting cells (Atkinson et al., 2015). The importance of Notch signalling in the regenerative process has been underlined by a comprehensive analysis of the hair cell regeneration. For example, Notch target genes were upregulated in damaged avian cochlea and utricle, as well as in injured zebrafish lateral line (Daudet et al., 2009, Ku et al., 2014, Ma et al., 2008, Stone and Rubel, 1999). Moreover, upregulation of Notch target genes in the damaged mammalian cochlea and utricle was also observed though the regenerative capacities of both organs were low (Batts et al., 2009, Korrapati et al., 2013, Lin et al., 2011, Mizutari et al., 2013, Wang et al., 2010).

As discussed previously, the role of FGF signalling is important for hair cell development as well as hair cell regeneration. Ku and colleagues found that expression of *Fgf20* and *Fgfr3* decrease when chicken utricle supporting cells proliferate to regenerate (Ku et al., 2014). A decrease in *Fgfr3* expression has also been observed after damage in the chicken cochlea and in the zebrafish lateral line (Bermingham-McDonogh et al., 2001, Jiang et al., 2014), while *Fgfr3* upregulation occurs in the mammalian cochlea after injury (Pirvola et al., 1995). Additional work is still needed to verify whether this difference in FGF receptor expression accounts for their contrasting proliferative capacities.

The Wnt signalling pathway is involved in prosensory cell specification and hair cell differentiation (Groves and Fekete, 2012, Munnamalai and Fekete, 2013a). The role of Wnt signalling during hair cell regeneration has also been closely examined in recent years. Activation of Wnt/β-catenin has been shown to stimulate the degree of regeneration after damage in the zebrafish lateral line (Head et al., 2013, Jacques et al., 2014). Similarly, recent studies of the damaged neonatal mouse utricle revealed that Wnt/β-catenin activation enhances the mitotic activity of supporting cells and thus hair cell regeneration *in vivo* (Wang et al., 2015). However, the responsiveness to β-catenin overexpression was not seen in supporting cells of the adult mouse cochlea (Shi et al., 2013). This could be due to decreased expression of the Wnt target gene Lgr5 in the adult, and it will be useful to determine whether the Wnt pathway could lead to regeneration after damage in mammals (Shi et al., 2013).

The Shh signalling pathway is one of the key signal transduction mechanisms are involved in the development of hair cells. Despite great efforts to elucidate the roles of Shh signalling during the inner ear development, its roles during hair cell regeneration remain largely unknown. One study has demonstrated that Shh treatment of neonatal rat cochleae damaged by neomycin induces cell cycle re-entry and renews proliferation of supporting cells (Lu et al., 2013).

Several studies have demonstrated that the EGF/EGFR signalling pathway could be involved in the regeneration of the mammalian inner ear. It has been shown that EGF is a mitosis-promoting factor for otic progenitors, which contribute to hair cell proliferation and regeneration in rat utricles after aminoglycoside ototoxic damage (Zine and de Ribaupierre, 1998). The EGFR pathway is also a crucial pathway in hair cell regeneration (White et al., 2012). White et al. demonstrated that the conserved mechanism involving EGFR signalling governs proliferation of auditory supporting cells in birds and mammals. In addition, they showed that EGFR signalling in mouse supporting cells is required for the down-regulation of the p27Kip1 to enable cell cycle re-entry (White et al., 2012).

To summarize, a major difference between the regenerating cochlea in non-mammals and the non-regenerating mammalian counterpart is the proliferate ability of the supporting cells. The avian cochlear supporting cells are the precursors of regenerated hair cells and regenerative proliferation of supporting cells is triggered by signals that act locally within the damaged epithelium (Warchol and Corwin, 1996). Similarly, in the zebrafish lateral line system, damaged hair cells lead to the reappearance of new hair cells within 24 hours from non-dividing precursors under conditions that damage only differentiated hair cells, whereas harsher conditions are followed by a longer recovery period with extensive cell division (Hernandez et al., 2007). In contrast, no mitotic response or hair cell regeneration is observed in the damaged adult cochlea (Chai et al., 2011). The second distinction relates to the timing of mitosis and hair cell formation. During mammalian cochlear development, the timing of mitotic termination in prosensory cells and differentiation of hair cells differ dramatically depending on the location of the cochlea. The prosensory cells in the apical turn of the cochlea first stop dividing and the last adopt a hair cell fate because hair cell maturation starts from basal to apex (Atkinson et al., 2015). Conversely, mitotic regeneration from supporting cells in non-mammals occurs much

more simultaneously (Atkinson et al., 2015). These differential responses to damage are suggested to be one of the reasons why the mammalian auditory hair cells are unable to regenerate.

1.2 The hearing process and causes of hearing loss

1.2.1 How hearing works in human?

The ear is divided into three distinct anatomical compartments, the outer, the middle and the inner ear (Figure 12A). The outer ear is the most external part of the ear. It includes the pinna, the ear canal, and the outer layer of the tympanic membrane. The middle ear is an air-filled cavity, including three bones (ossicles): the malleus, incus, and stapes. It also connects to the upper throat via the Eustachian tube. The inner ear is split anatomically into bony and membranous labyrinths. This contains the sensory organs for balance and motion, namely the vestibules of the ear (utricle and saccule), and the semicircular canals. The inner ear also contains the sensory organ for hearing, the cochlea (Drake et al., 2005).

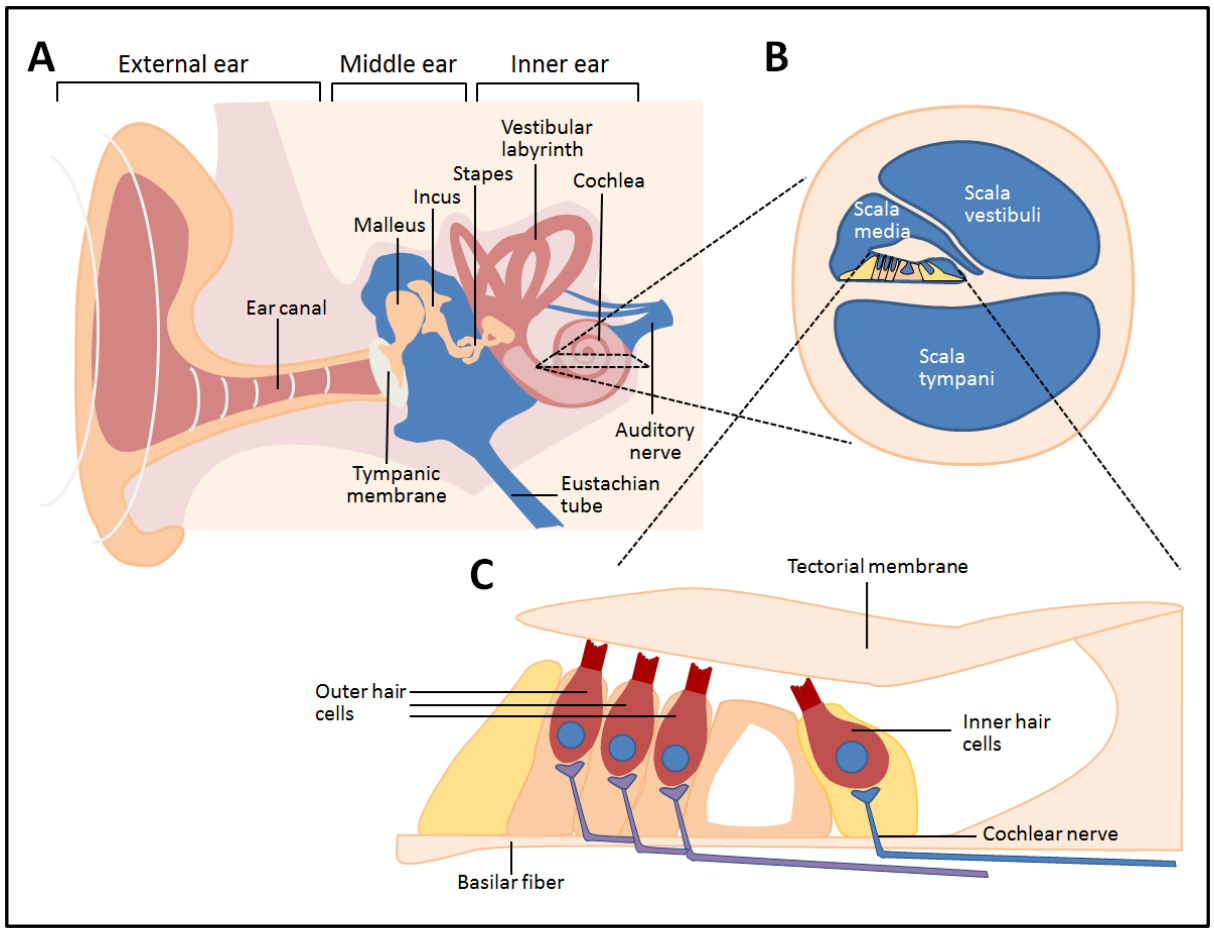

Figure 12 | Anatomy of the adult' human ear.

A, Sound waves captured by the pinna pass through the ear canal reaching the tympanic membrane causing it to vibrate. The middle ear conducts the mechanical energy of the sound vibration and sends it to the inner ear. B, A cross section of the cochlea reveals its associated fluid field compartments. C, The organ of Corti resides within the scala media along the cochlea from base to apex. Complex innervations at the basal region of the sensory hair cells propagate the electrical signal through the auditory nerve into the brain.

The pinna, the outer part of the ear, plays a role to catch the sound waves. Its curved structures help to determine the direction of a sound. Once the sound waves travel into the ear canal, they vibrate the tympanic membrane. It is a very sensitive thin, cone-shaped piece of skin, about 10 millimeters wide. The malleus is connected to the center of the tympanic membrane. When the tympanic membrane vibrates, it moves the malleus from side to side. The other end of the malleus is connected to the incus, which is attached to the stapes. The other end of the stapes rests against the cochlea, through the oval window (Figure 12B). When air-pressure waves hit the tympanic membrane, the ossicles move and amplify the force so that the faceplate of the stapes creates waves in the inner ear fluid to represent the air-pressure fluctuation of the sound wave. The cochlea is a frequency analyser located in the inner ear. It contains two curved fluid-filled ducts called the scala vestibuli and the scala tympani. The basilar membrane, the middle membrane of the cochlea, is a rigid surface that extends across the length of the cochlea. When the stapes moves in and out, it pushes and pulls on the part of the basilar membrane. This force starts a wave moving along the surface of the membrane until the wave reaches the fibres of the basilar membrane with the same resonant frequency. When a specific wave frequency resonates perfectly with the fibres, the wave's energy is suddenly released. This energy is strong enough to move the OC hair cells (Figure 12C). The OC is a structure containing thousands of hair cells and lies on the surface of the basilar membrane. Hearing relies on the faithful synaptic coding of mechanical input by the auditory hair cells of the inner ear. During sound stimulation, the mechanical deflection of hair bundle towards its taller stereocilia stretches the tip links that

connect adjacent stereocilia (Gillespie and Muller, 2009). These axial filaments, which join all the bundles along with their length, ensure that the bundle moves as a unit (Gillespie and Muller, 2009). The tension in the tip links is then transmitted to mechanosensitive ion channels located at the tips of the stereocilia, increasing their probability of opening and allowing the flow of a K^+ current (Figure 13) (Gillespie and Muller, 2009). This inward transducer current causes hair cell depolarization, which opens voltage-gated Ca^{2+} channels in the cell soma, allowing calcium entry and release of neurotransmitter onto the afferent nerve endings (Gillespie and Muller, 2009). The cochlear nerve sends impulses on to the cerebral cortex through central auditory pathways (Guyton and Hall, 2006) (Figure 14).

The axons in the cochlear nerve project to dorsal and ventral cochlear nuclei in the rostral medulla which is a group neuron located close to the midline of the brain (Popper and Fay, 1992). Axons of the second-order neurons emerging from the dorsal cochlear nucleus (dorsal acoustic stria) and axons of both dorsal and ventral cochlear nuclei (intermediate acoustic stria) cross to the mid-pons and synapse on neurons in the inferior colliculus located in the caudal midbrain (Guyton and Hall, 2006). Axons emerging from the ventral cochlear nucleus form the ventral acoustic stria, which crosses to the contralateral side in the mid-pons and synapse in the superior olivary complex (Guyton and Hall, 2006). This nuclear complex is a collection of brainstem nuclei that can discriminate the differences in the intensity of sound to each ear or the differences in the time of arrival of the sound (Guyton and Hall, 2006). Neural impulses are transmitted from the superior olivary complex to the inferior colliculus through the lateral lemniscus (Guyton and Hall, 2006). The dorsal part of the inferior colliculus receives projections from neurons responding to low frequencies of sound, while the ventral part receives projections from those neurons responding to high frequencies of sound (Guyton and Hall, 2006). The auditory information is then relayed by the inferior colliculus to the medial geniculate nucleus of the thalamus which processes precise intensity, frequency, and binaural properties of the sound (Guyton and Hall, 2006). The axons of these neurons, in turn, project to the primary auditory cortex to process auditory information (Popper and Fay, 1992).

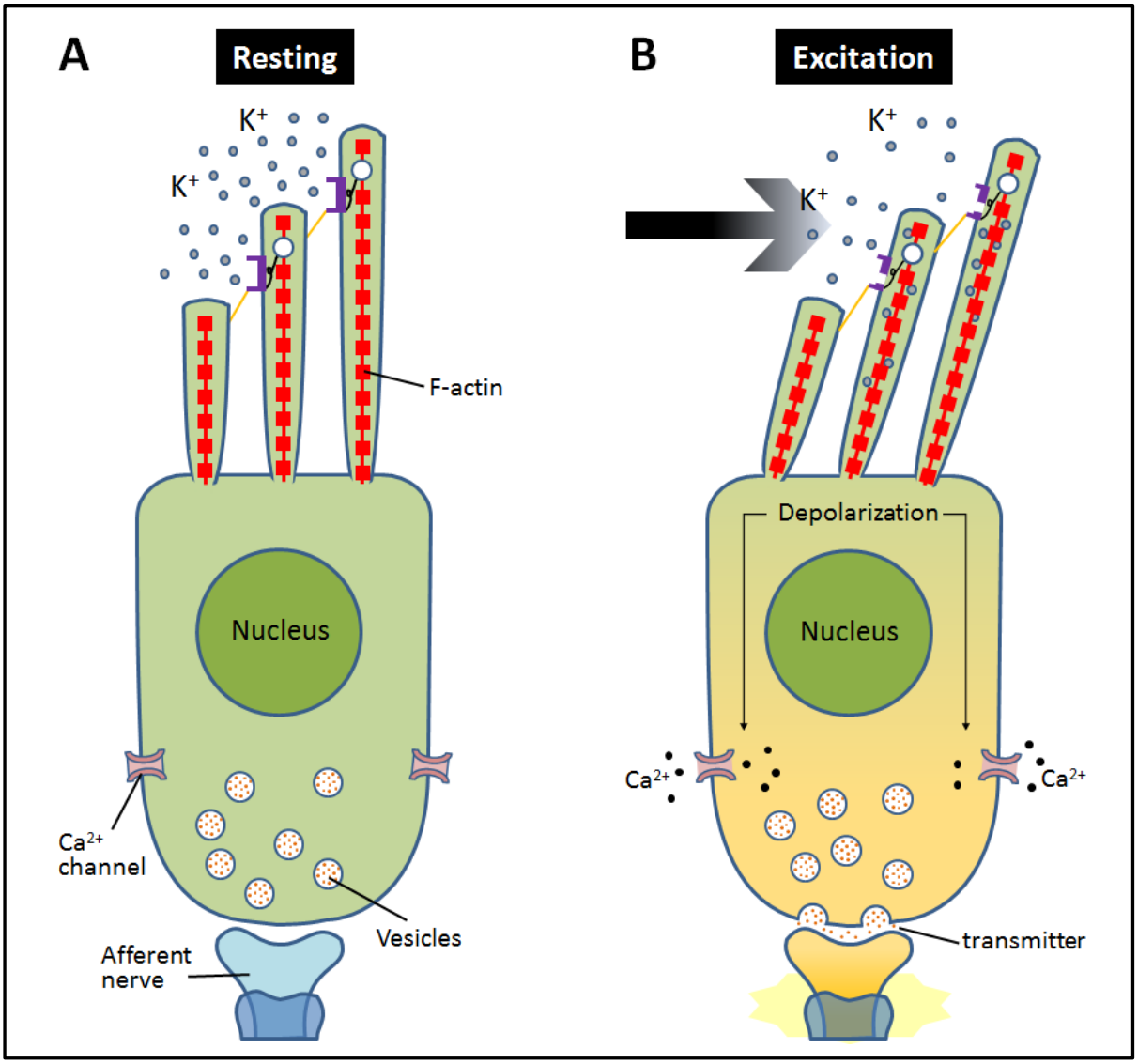

Figure 13 | Mechanoelectrical transduction mediated by hair cells.

Deflections that tilt the bundle toward the tallest stereocilia induce mechanosensitive ion channels to open near the tips of the stereocilia, allowing K^+ ions to flow into the hair cell. The resulting depolarization of the hair cell opens voltage-gated Ca^{2+} channels, allowing calcium entry and release of neurotransmitter onto the afferent nerve terminals.

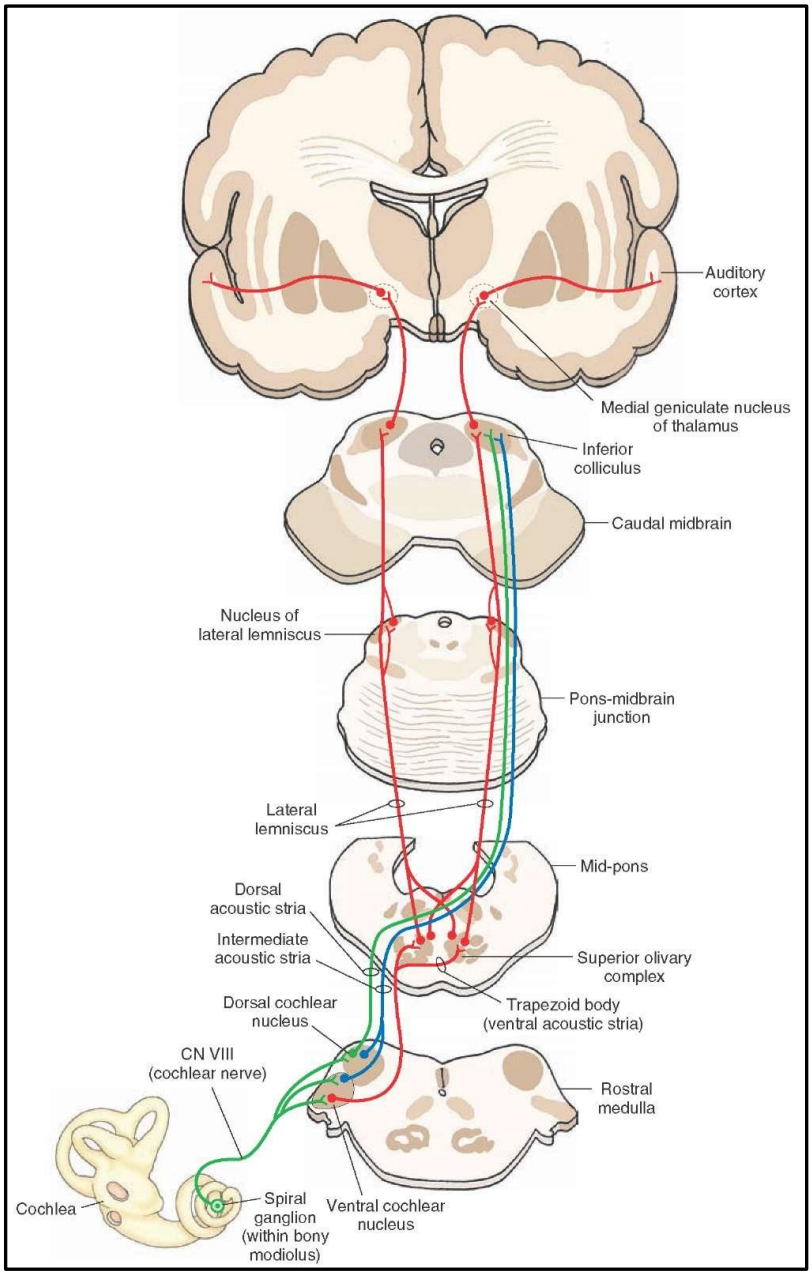

Figure 14 | Central auditory pathways

Most of the axons of the cochlear nucleus cells cross over to the opposite side of the brain. Both crossed and uncrossed fibres from the cochlear nuclei synapse in the superior olivary complex which is the first place in the ascending pathway to receive information from both ears. Neural impulses are transmitted from the superior olivary complex to the inferior colliculus through the lateral lemniscus, from there to the medial geniculate nucleus and finally to the auditory cortex. Figures adapted from (http://what-when-how.com/neuroscience/auditory-and-vestibular-systems-sensory-system-part-2/).

1.2.2 Hearing loss

Hearing loss occurs in more than 1 in 1000 live births and places a significant burden on health-care and special education systems (Schoenwolf et al., 2015). The prevalence of individuals who have a partial hearing loss or who are deaf rises to 1 in 500 by adulthood (Schoenwolf et al., 2015). About half of all hearing loss has genetic causes, with the other half attributed to environmental factors (Schoenwolf et al., 2015). The latter include in utero viral infections, neonatal exposure to aminoglycoside antibiotics, and postnatal exposure to loud noise. There are three main types of hearing loss, conductive, sensorineural hearing loss and a combination of the two called mixed hearing loss (Elzouki, 2011).

A conductive hearing impairment is the blockage of the middle ear which prevents the conduction of sounds to the inner ear, the cochlea. This can be due to external ear canal malformation, dysfunction of the eardrum or malfunction of the bones of the middle ear (Riss et al., 2014). The conductive hearing loss is treatable with middle ear implants or bone conduction implants (Riss et al., 2014).

A sensorineural hearing loss can arise from defects in the inner ear, vestibulocochlear nerve, or auditory regions of the brain. Many genes affect the morphogenesis of the hair cell bundle and, when mutated, result in hearing loss or vestibular dysfunction (Frolenkov et al., 2004). These include genes that encode stereocilia cytoskeletal components such as *ACTG1, ESPIN, HDIA1, USH1C, USH1G, WRHN*, intracellular motors that control actin assembly such as *MYO6, MYO7A, MYO15A*, and cell adhesion components such as *CDH23, PCDH15* (Frolenkov et al., 2004). The sensitivity of stereocilia to gene mutations is illustrated by Usher syndrome (USH), an autosomal recessive genetic disease, characterized by hearing loss and vision disorder called retinitis pigmentosa (RP) (Mathur and Yang, 2015). This syndrome can be caused by mutations in one of several different genes such as *MYO7A, USH1C, CDH23, PCDH15, USH1G, CIB2, USH2A, GPR98, DFNB31, CLRN1, and PDZD7* (Mathur and Yang, 2015). The genes associated with USH are expressed in various tissues, but USH proteins are mainly localized to the hair bundle and synapse of inner ear hair cells (Keats and Corey, 1999). Also, they are localized in photoreceptor and other retinal cell types (Keats and Corey, 1999). High levels of K^+ are required for the signalling through the ion channels and

maintenance of hair cell integrity. This is regulated by recycling the K^+ that enters the activated hair cells and thus defects in K^+ recycling can result in hearing loss (Hubner and Jentsch, 2002). In addition, mutations in several connexion genes such as *GJB2, GJB3,* and *GJB6*, all of which are expressed in the gap junction system, have been identified in many patients with deafness (Hubner and Jentsch, 2002). Auditory neuropathy is classified as a defect in auditory nerve function and can be due to mutations in *SLC17A8, OTOF, DFNB59*, and *DIAPH3* (Delmaghani et al., 2006) (Manchaiah et al., 2011). *SLC17A8* is expressed in the inner hair cells and produces glutamate in synaptic vesicles (Seal and Edwards, 2006), whereas *OTOF* is necessary for synaptic vesicle production and fusion of the synaptic vesicles in the ribbon synapses (Shearer and Smith, 1993).

The mixed hearing loss is caused by a combination of conductive damage in the outer or middle ear and sensorineural damage in the inner ear or hearing/auditory nerve. Treatment options may include medication, surgery, hearing aids, a middle ear hearing implant or a bone conduction implant (Elzouki, 2011).

1.3 Reconstitution of inner ear development from human pluripotent stem cells *in vitro*

Sensory hair cells and primary afferent neurons in the human inner ear do not regenerate to any clinically relevant degree, thus damaged cells result in permanent hearing loss or balance disorders. Stem cells have been proposed as a possible source of cells to replace damaged cells. In this section, we will discuss the key developmental checkpoints leading to normal inner ear induction from human pluripotent stem cells (hPSCs).

1.3.1 Human pluripotent stem cells (hPSCs)

1.3.1.1 Human embryonic stem cells (hESCs)

During early embryonic development, the embryo undergoes gastrulation that occurs when a blastula, made up of one layer, folds inward and enlarges to create a three-layered structure known as the gastrula (Figure 15). These three germ layers are known as the ectoderm, mesoderm, and endoderm. The ectoderm subsequently divides into three parts which includes the neural crest (pigment cells, ganglia, dorsal root ganglia, Schwann cells, facial cartilage, spiral septum, and ciliary body), the neural tube (brain, spinal cord, motor neurons, retina, and posterior pituitary), and the external ectoderm (skin, epithelium, enamel, lens, cornea, apical ectodermal ridge, and sensory receptors) which is of particular interest in this project (Chandross KJ, 2001). The mesoderm gives rise to mesenchyme (connective tissue), mesothelium, non-epithelial blood cells (Kendrew and Lawrence, 1994). The endoderm is the innermost of the three germ layers and develops into the linings of two tubes within the body, the digestive tube (liver, pancreas) and the respiratory tube (trachea, bronchi, and alveoli of the lungs) (Gilbert, 2010).

Embryonic stem cells (ESCs) are derived from one of the earliest stages of embryonic development, called the blastocyst and have the ability of unlimited, undifferentiated proliferation *in vitro* (Figure 16A) (Evans and Kaufman, 1981, Martin,

1981). The essential characteristics of ESCs should include (i) derivation from the preimplantation or preimplantation embryo, (ii) indefinitely undifferentiated proliferation, and (iii) stable developmental potential to form derivatives of all three embryonic germ layers even after prolonged culture (Thomson et al., 1998, Thomson and Marshall, 1998). This last characteristic is generally referred to as pluripotency.

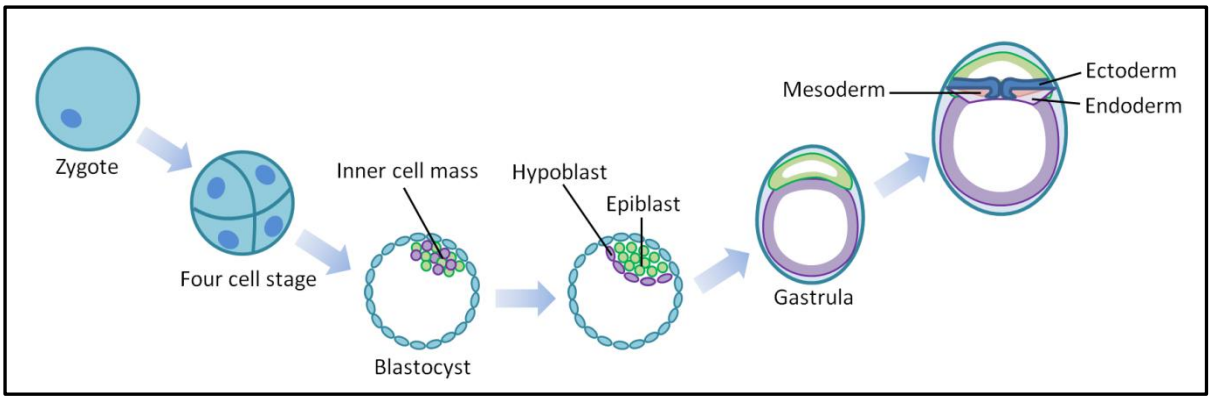

Figure 15 | Cleavage, the blastula stage, and gastrulation

The one cell embryo, or zygote, undergoes a series of cleavage divisions. In humans, blastocyst formation begins about 5 days after fertilization. The blastocyst contains an inner cell mass (ICM) which subsequently forms the embryo. At the late blastocyst stage, the ICM become rearranged into the epiblast and the hypoblast. As the 3 WG begins, the embryo enters the period of gastrulation, during which the single-layered blastula is reorganized into three germ layers: the ectoderm, the mesoderm, and the endoderm.

In 1998, hESCs were successfully derived from early human embryos by Thomson's group (Thomson et al., 1998). Surplus human embryos obtained via assisted reproductive techniques were cultured to the blastocyst stage, 14 ICM were isolated, and ES cell lines originating from five separate embryos were derived. Three cell lines (H1, H13, and H14) had a normal XY karyotype, and two cell lines (H7 and H9) had a normal XX karyotype. All the cell lines expressed high levels of telomerase activity. It suggests that their replicative life-span will exceed that of somatic cells. They also expressed cell surface markers that characterize undifferentiated nonhuman primate ES and human embryonal carcinoma (EC) cells,

including stage-specific embryonic antigen (SSEA)-3, SSEA-4, TRA-1-60, TRA-1-81, and alkaline phosphatase (Thomson et al., 1998).

1.3.1.2 Human Induced pluripotent stem cells (hiPSCs)

Until Shinya Yamanaka's team found a new way to reprogram adult cells to turn them into stem cells by being forced to express genes important for maintaining stemness (Takahashi and Yamanaka, 2006), differentiated cells could only be reprogrammed to an embryonic-like state by somatic cell nuclear transfer (SCNT) (Figure 16B) (Yamada et al., 2014) or by fusion of somatic cells with existing pluripotent cells such as ESCs (Foshay et al., 2012). The latter technique results in polyploid hybrid cells with unstable karyotype that are not suitable for transplant into humans or animals (Foshay et al., 2012). Nuclear transfer is also technically demanding, inefficient and has only been shown recently to reprogram human somatic cell nuclei to pluripotency (Yamada et al., 2014).

In 2006, Shinya Yamanaka's group demonstrated induction of pluripotent stem cells (PSCs) from mouse embryonic or adult fibroblasts by introducing four factors, Oct3/4, Sox2, c-Myc, and Klf4 under ES cell culture conditions (Figure 16C) (Takahashi and Yamanaka, 2006). Mouse iPSCs demonstrate important characteristics of PSCs, including expressing stem cell markers, forming tumors containing cells from all three germ layers, and being able to contribute to many different tissues when injected into mouse embryos at a very early stage in development (Takahashi and Yamanaka, 2006).

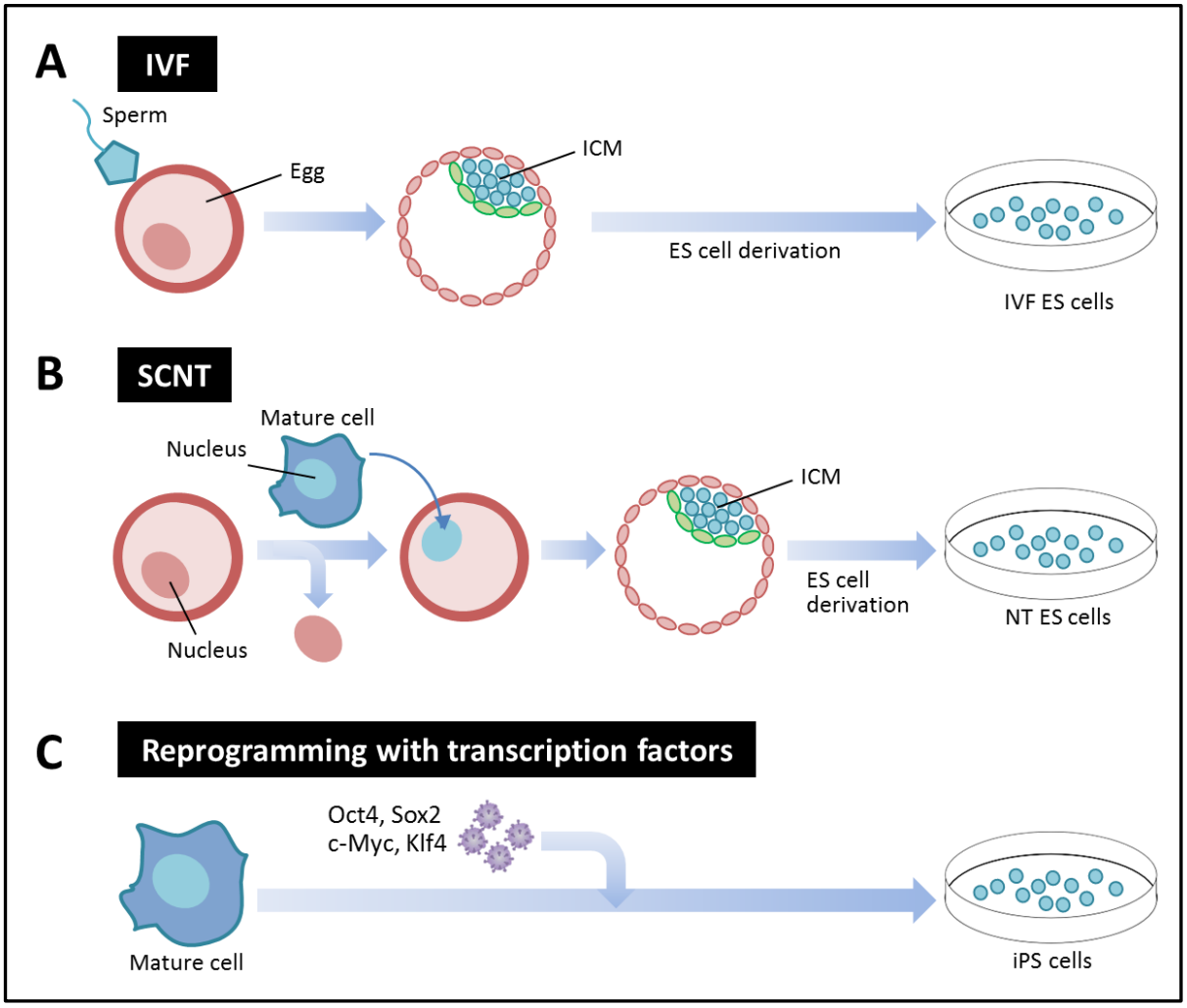

Figure 16 | Three techniques to generate pluripotent stem cells

A, Embryos derived from *in vitro* fertilization (IVF) give rise to IVF ES cells that can be extracted from the ICM (Thomson et al., 1998). B, In somatic cell nuclear transfer (SCNT), the nucleus is removed from an egg and replaced with the nucleus from a mature donor cell. As this hybrid cell develops into an embryo, pluripotent stem cells called nuclear transfer embryonic stem (NT ES) cells can be extracted from the ICM (Yamada et al., 2014). C, iPSCs are generated from differentiated cells by the addition of a transcription-factor cocktail (Takahashi and Yamanaka, 2006).

One year later, his team succeeded in generating iPSCs from differentiated human somatic cells (Takahashi et al., 2007). To induce hiPSCs, the retroviruses containing human Oct3/4, Sox2, Klf4, and c-Myc were introduced into human dermal fibroblasts which are derived from the facial dermis. 6 days after transduction, the

cells reseeded onto feeder cells and around day 25, flat and resembled hESC colonies were observed. These hiPSCs were similar to hESCs in morphology, proliferation, surface antigen, gene expression, epigenetic status of pluripotent cell-specific genes and telomerase activity (Takahashi et al., 2007).

1.3.2 Definitive ectoderm

As mentioned in the previous section, the inner ear arises from the ectoderm germ layer. At the completion of gastrulation, the cells located in a proximal and posterior direction have lost pluripotency, and have a differentiation potential limited to the ectodermal lineages (Lawson et al., 1991). This transient state of cells is known as the definitive ectoderm (Carey et al., 1995). The definitive ectoderm is a bipotent precursor of the non-neural and neural ectoderm (Hemmati-Brivanlou and Melton, 1997). Several approaches have been reported for the direction of ES cells to the neural ectoderm lineages (Li et al., 1998) (Rathjen et al., 2002), but scant attention has been paid to the formation and characterization of the definitive ectoderm. This is because neural ectoderm can be generated with relative ease in serum-free conditions or using BMP inhibitors such as Noggin, Dorsomorphin, and LDN-193189 (Wilson and Hemmati-Brivanlou, 1995). More commonly, inhibition of transforming growth factor beta (TGFβ) signalling by suppressing primed pluripotent and meso-/endodermal states using SIS3 or SB-431542 can induce ectodermal lineages (Chambers et al., 2009).

It is challenging to identify the definitive ectoderm *in vitro* due to the lack of specific marker genes or proteins. Recently, however, Harvey et al. observed a transient cell population in their mouse ESC (mESC) culture that responded to BMP4 treatment by differentiating into cells of a non-neural ectoderm fate (Harvey et al., 2010). Koehler et al. also defined mESC-derived definitive ectoderm as $Nanog^-$ (pluripotency marker), $N\text{-}cadherin^-Sox1^-$ (neural marker), $Brachyury^-$ (mesoderm marker), and $E\text{-}cadherin^+$ (definitive ectoderm and non-neural marker) cells that differentiate into non-neural ectoderm-like cells upon BMP4 treatment (Koehler et al., 2013). Similarly, in our preliminary data, we defined hESC-derived definitive

ectoderm-like cells as $OCT4^-$ (pluripotency marker), $NCAD^-$ (neural marker), $PAX6^-$ (neural marker), and $ECAD^+$ (definitive ectoderm and nonneural ectoderm marker) cells (Figure 17). During differentiation of hESCs into neuroectoderm cells, we identified an $OCT4^-PAX6^-$ and $ECAD^+$ definitive ectoderm-like epithelium in small EBs on day 7 of serum-free culture, before the expression of neuroectoderm associated proteins ($PAX6^+NCAD^+$) on day 14 (Figure 17C). Since during hESC neural differentiation, the initial neuro-ectoderm (NE) cells do not express SOX1 which is the earliest marker of NE in mouse embryos or in NE differentiation from mESCs, we used PAX6 as a neuronal marker instead of SOX1 (Li et al., 2005, Pankratz et al., 2007, Pevny et al., 1998, Suter et al., 2009, Ying et al., 2003). Pax6, a paired box transcription factor expressed in region-specific neural progenitors after neural tube closure in mouse (Schmahl et al., 1993, Walther and Gruss, 1991), is uniformly expressed in hESC-derived NE (Li et al., 2005, Pankratz et al., 2007).

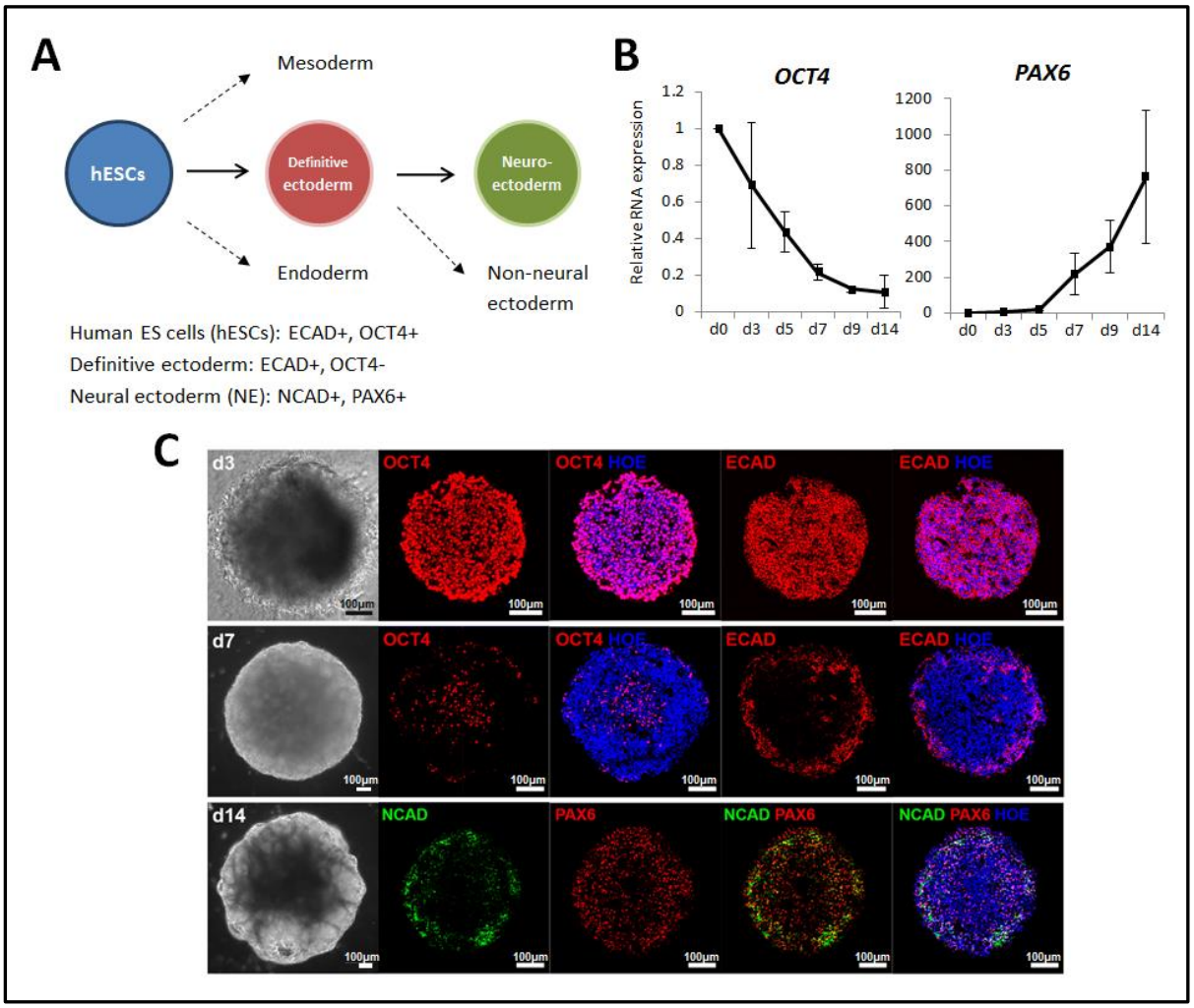

Figure 17 │Derivation of definitive ectoderm-like cells from hESCs.

A, Schematic overview of the key cell fate decisions underlying definitive ectoderm induction. The lower panel indicates makers to identify each tissue type. B, Quantitative reverse transcription polymerase chain reaction (qRT-PCR) analysis of day 0, 3, 5, 7, 9, 14 embryoid bodies (EBs) (n=3; mean ±s.e.m). C, Immunohistochemistry analysis of day 3, 7, 14 EBs. Data are representative of 8 EBs from at least 3 independent experiments (n=3).

1.3.3 Non-neural Ectoderm

The non-neural ectoderm also referred as the surface ectoderm is the next critical precursor during inner ear development. The non-neural ectoderm gives rise to both the epidermis and pre-placodal ectoderm. Studies in lower vertebrates have determined that BMP4 is an important factor in the patterning of definitive ectoderm and induces differentiation towards surface ectoderm (Hemmati-Brivanlou and Melton, 1997, Wilson and Hemmati-Brivanlou, 1995). A gradient of BMP molecules patterns the ectodermal layer with high lateral concentrations and low medial concentrations of BMP molecules demarcating regions of non-neural and neural ectoderm, respectively (Figure 18A) (Barth et al., 1999, Kishimoto et al., 1997, Neave et al., 1997, Reversade and De Robertis, 2005, Wilson et al., 1997). Moreover, BMP antagonists secreted from cells at the midline of the embryo promote pre-placodal development (Figure 18B) (Litsiou et al., 2005).

Several studies have reported non-neural induction by BMP signalling during differentiation of hESCs into keratinocytes or lens tissue (Green et al., 2003, Metallo et al., 2008, Leung et al., 2013, Yang et al., 2010). Recently, Koehler et al. emphasized the non-neural ectoderm as an essential precursor for the induction of inner ear cells from mESCs (Koehler et al., 2013). They used BMP treatment together with TGFβ inhibition to steer mESCs towards a non-neural fate and used several non-neural associated markers such as *Dlx3, E-cadherin*, and *AP2* to identify non-neural ectoderm cells (Koehler et al., 2013).

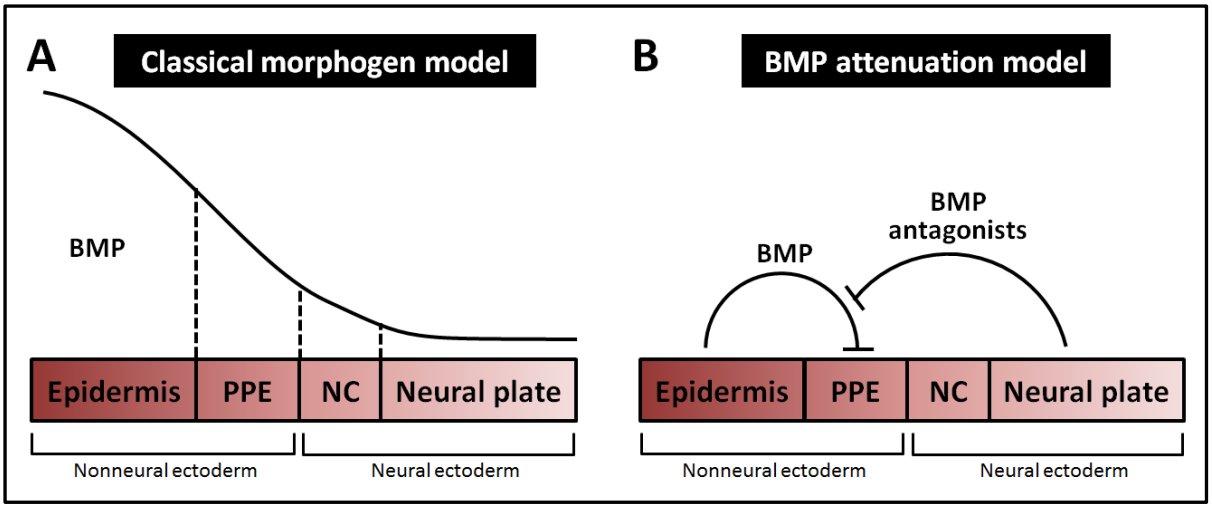

Figure 18 | Models for the role of BMP in ectodermal patterning.

A, Classical models of ectodermal patterning posit that multiple fates, including epidermal ectoderm, pre-placodal ectoderm (PPE), neural crest (NC) and neural plate are specified by readout of a BMP morphogen gradient (Glavic et al., 2004b). B, More recent studies indicate that BMP-antagonists are critical for promoting pre-placodal development (Litsiou et al., 2005).

1.3.4 Pre-placodal Region (PPR)

As mentioned above, the PPE originates from the non-neural ectoderm, which contains progenitor cells that will ultimately give rise to the otic placode (Figure 18). The PPE develops in a 'U'- shaped domain of head ectoderm at the border of neural ectoderm and surface ectoderm. These neural-epidermal boundary tissues include the neural crest precursor that lies adjacent to the neural plate and a precursor of the pre-placodal region (PPR) next to the neural crest. The PPR is established in response to signaling cues mediated by BMPs, FGFs, and Wnts and gives rise to six cranial placodes including the otic placode (Figure 2).

The PPR is defined by expression of Six1, Six4, Eya1, and Eya2 in addition to non-neural markers. Several studies in vertebrates have demonstrated that the BMP activity needed for non-neural induction must be subsequently attenuated for the PPR to develop properly (Ahrens and Schlosser, 2005, Brugmann et al., 2004, Glavic et al., 2004a, Kwon et al., 2010, Litsiou et al., 2005). Furthermore, other studies have shown that FGF signaling and the inhibition of Wnt signaling are critical for PPR induction (Litsiou et al., 2005, Kwon et al., 2010, Patthey et al., 2009). These basic developmental studies are important to recreate inner ear development with PSCs *in vitro*. The recent studies demonstrated the generation of pre-placodal cells from mESCs using treatment of BMP4 followed by BMP inhibitor LDN-193189 (Koehler et al., 2013). Leung et al. also presented a differentiation protocol that allows production of human pre-placodal cells (Leung et al., 2013). To derive pre-placodal like cells, they cultured hESCs using the neural differentiation medium without neural inducing molecules, Noggin and SB431542 (Leung et al., 2013). Unlike the mESC differentiation (Koehler et al., 2013), extra treatment of BMP4 had a negative effect on the production of pre-placodal cells in hESC culture although BMP signaling is essential for induction of pre-placodal cells. It was identified that hESCs follow their endogenous BMP differentiation pathway, by blocking BMP signaling using antagonist of BMP ligands such as NOGGIN (Leung et al., 2013). The identity of pre-placodal cells was confirmed by PPE competent genes (*TFAP2A, GATA3*, and *DLX5*), and the PPE genes (*SIX1*) (Leung et al., 2013).

1.3.5. Otic induction

Once the PPR is specified, various combinations of local signaling molecules and placode-specific transcription factors, promote the induction of individual cranial placodes (Baker and Bronner-Fraser, 2001). As mentioned in chapter 1.1.1, FGF signaling emanating from the neighboring hindbrain and the underlying mesenchyme is essential for otic placode induction. In mice, OPED is initiated by the action of localized two FGF isoforms, FGF-3 and FGF-10, in PPR. Pax2 and Pax8 are initially expressed throughout the OPED; however, the Pax2 expression is confined to the otic placode over time due to Wnt-mediated transcriptional control (Freter et al., 2008). Recently, DeJonge et al. showed that Wnt signaling plays a similar role during mouse inner ear organoid formation as it does during inner ear development in the embryo (DeJonge et al., 2016). They demonstrated that treatment with the potent Wnt agonist CHIR99021 promotes induction of otic vesicles from mESCs (DeJonge et al., 2016).

Finding the proper markers to identify otic associated cells needs careful consideration because many proteins expressed in otic lineage cells *in vivo* are not unique to the inner ear during development. For this reason, combined expression of Pax2, Pax8, E-cad, Jag1, Sox2, and Myo7a was used to preclude the mistaken identification of optic stalk or mid-hindbrain tissue for an otic tissue during mESC differentiation into inner ear cells (Koehler and Hashino, 2014). However, little is known about the molecular expression patterns and dynamics of signaling molecules during fetal development of the human inner ear. It has been only confirmed that human otic progenitors express SOX2, SOX9, SOX10, and PAX2 (Locher et al., 2013).

1.4 Types of cell culture methods and conditions

1.4.1 Types of cell culture methods

Cell fate decisions are based on components of the surrounding microenvironment, including soluble factors, substrate or extracellular matrix (ECM), cell-cell interactions, mechanical forces, and the spatial organization of the microenvironment. Depending on their spatiotemporal context, these specific microenvironmental stimuli can signal hPSCs to either self-renew or differentiate into cell types of the ectoderm, mesoderm, or endoderm. hPSCs can be induced to differentiate using a variety of methods. Simply removing PSCs from the culture conditions that maintain the stemness is enough to cause them to commit to multiple development pathways resulting in mixed populations of cell types.

There are primarily three types of culture methods for the differentiation: monolayer (two-dimensional; 2D), EB (three-dimensional; 3D), and a combination of both 3D and 2D methods. Differentiation is mostly spontaneous in structures of these types and it is difficult to predict which types of the somatic cell if any will predominate so most differentiation methods attempt to direct PSCs to differentiate down preferred developmental pathways (Amit and Itskovitz-Eldor, 2012). Typically such direction requires the addition of specific growth factors or small molecule inhibitors/activators of signal transduction systems that are active in either the PSCs themselves or in their differentiating progeny (Amit and Itskovitz-Eldor, 2012). So far, most inner ear derivation studies have mainly adopted a 2D or 3D-2D approach especially in differentiation of hPSCs (Chen et al., 2012, Ronaghi et al., 2014, Ding et al., 2016) In this section, we will discuss advantages and disadvantages of each method and also talk about which method is proper to recreate stepwise development of inner ear *in vitro*.

1.4.1.1 2D monolayer methods

In the 2D method, the cells are attached to the bottom of a culture dish. Many biological processes are based on studies of cells cultured on flat, 2D plastic or glass substrates. Generally, hPSCs are cultured as adherent cells in conditions supporting

undifferentiated growth (Thomson et al., 1998, Takahashi and Yamanaka, 2006). 2D culture systems have also been developed to induce differentiation of hESCs using either co-culture systems or completely defined systems (Baharvand et al., 2007, Shin et al., 2006). For example, Baharvand et al. demonstrated that hPSCs in monolayer culture can be rapidly and efficiently differentiated into neural derivates in the presence of small molecules or recombinant proteins resulting in >90% cells expressing neuron associated proteins (Baharvand et al., 2007). This study suggests that the 2D approach may yield a more homogeneous population of the desired cell type. This is likely because the relatively same concentration of signal transduction molecules presents on the surface of all cells. It also has been suggested that the flattening of cells can change the effective surface-to-volume ratio, such that signalling from the cell surface is better propagated into the cell (Meyers et al., 2006). However, the noticeable difference between monolayer culture and the *in vivo* scenario has been a double-edged sword. The simplicity of 2D culture has enabled reductionist approaches to analyse individual cellular phenomena but the 2D model might not faithfully follow the physiological behaviour of cells *in vivo* (Figure 19) (Baker and Chen, 2012).

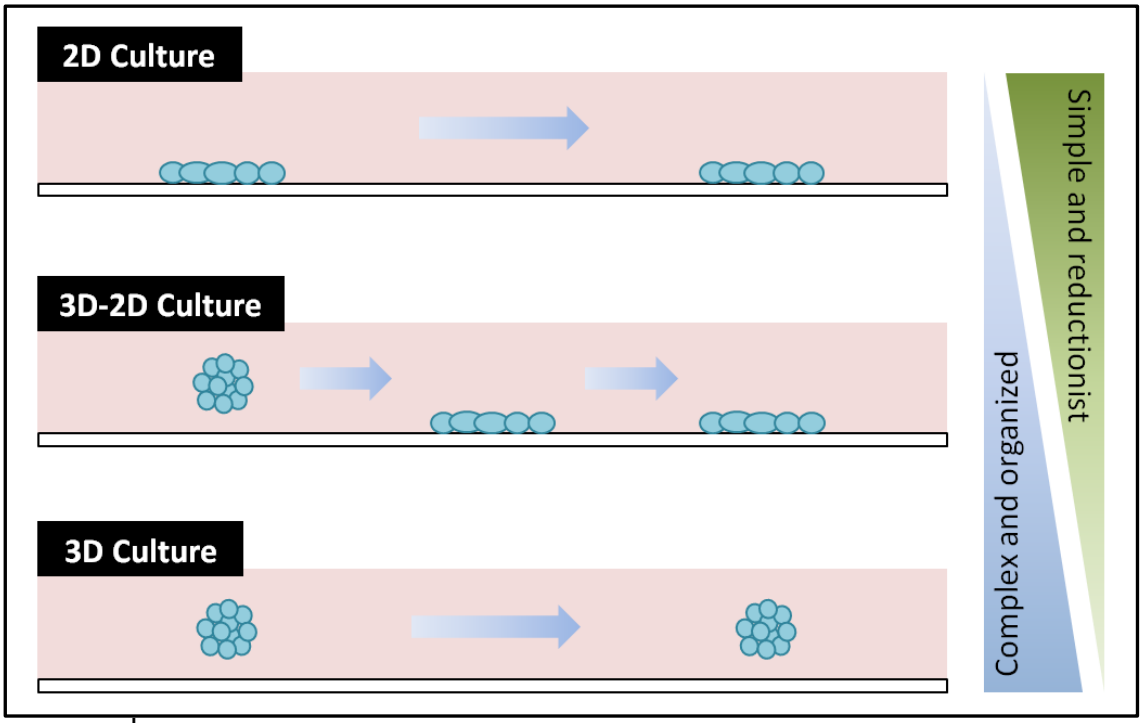

Figure 19 | Differentiation culture formats.

Illustrations of the 2D, 3D-2D, and 3D culture formats.

One of the most striking disparities between 2D and 3D is the dissimilarity in cell morphology. Cells cultured in the 2D system are mostly flat and spread freely in the horizontal plane but have minor support for spreading in the vertical dimension, so they mainly have a forced apical-basal polarity (Baker and Chen, 2012). This polarity is might relevant for epithelial cells that connect to one another via their lateral membranes but is unnatural for most of the other cells (Mseka et al., 2007). These changes in cell geometry and organization can directly affect cell function (Mseka et al., 2007).

1.4.1.2 3D EB methods

In vivo, cells are intimately connected to surrounding cells through intercellular signalling and closely regulated by interactions with multiple ECM components. More recently the biology field has come to appreciate this dissimilarity between flat surfaces of 2D systems and topographically complex of 3D systems (Figure 19). This has been motivated for the development of *in vitro* 3D biomimetic environments.

When hPSCs are transferred from an environment supporting self-renewal to tissue culture-treated low attachment plates comprising suspension culture, they spontaneously form cell aggregates known as EBs. Compared to 2D culture, 3D approach using EBs demonstrate less homogeneous differentiation (Doetschman et al., 1985, Itskovitz-Eldor et al., 2000). This is likely because cells may receive varying levels of signalling cues depending on their spatial location within the EB and the diffusion properties of a particular molecule or protein (Kinney et al., 2011). Nonetheless, several 3D culture methods have been developed that lead to the relatively efficient differentiation of PSCs. Our preliminary data show that 3D culture methods can be used to induce definitive ectoderm-like cells on the surface of the EBs (Figure 20). Of particular note is the serum-free culture of EBs with quick aggregation also known as SFEBq method developed by Yoshiki Sasai‘s team (Eiraku et al., 2008). They demonstrated that this method can be used to generate a nearly 90% pure population of neural ectoderm cells, which can give rise to forebrain, midbrain, and retinal tissue (Sasai et al., 2012, Eiraku et al., 2008, Muguruma et al., 2010). A major advantage of SFEBq culture is that 3D culture conditions facilitate the formation of 3D neural networks characteristic of the cytoarchitecture similar to *in*

vivo (Sasai et al., 2012, Eiraku et al., 2008, Muguruma et al., 2010). Moreover, 3D scaffolds have been shown to facilitate the improved development of functional network connectivity and neural synapses (Ma et al., 2004). Beyond providing appropriate physiological cues, 3D culture also enhances biological responses that might not be observable on 2D substrates such as the collective cell migration, force generation and tissue folding that occurs during gastrulation or the angiogenic sprouting of blood vessels (Baker and Chen, 2012).

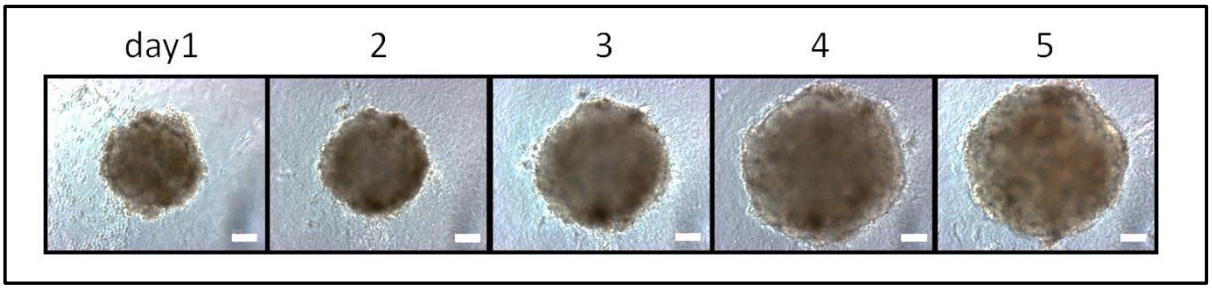

Figure 20 | Overt morphological changes of human EBs occur in serum-free media.

Data are representative of 8 EBs from at least 3 independent experiments (n=3). Scale bars present 100μm.

1.4.1.3 Combination of both 3D and 2D methods

Relatively many differentiation protocols for hPSCs rely on 3D-2D formats (Figure 19). For example, the re-plating of spontaneously differentiating EBs on an adherent substrate containing beating areas generates cells exhibiting structural and functional properties of early-stage cardiomyocytes (Kehat et al., 2001, Germanguz et al., 2011). Similar approaches have been used in the generation of hair-cell-like cells from hESCs (Ronaghi et al., 2014). The cells are cultured as EBs until a pre-placodal ectoderm stage and then plated on a flat culture dish (Ronaghi et al., 2014). One of the main reasons to take 3D-2D culture is that it makes easier to identify otic progenitor-like cells amongst a monolayer of cells. However, same as the 2D culture, 3D-2D cultures morphological properties are often lost because cells conform to the flat culture surface.

1.4.2 Basic materials for cell culture

- Lipidure coated 96 well U or V bottom plates: Lipidure coated 96 well plate designed for spheroid formation by reducing cell attachment. Spheroid cell culture is typically based on the formation of an aggregate of cells in an environment where cell-cell interactions dominate over cell-substrate interaction. This can be achieved by using U bottom low-cell-adhesion 96-well plates in mESC culture. Unlike mESCs, making EBs of hESCs is slow and often incomplete using a conventional U-bottomed well. According to Nakano et al. (2012), this problem is largely solved by using a newly designed V-bottomed 96-well plate, in which the aggregation is facilitated by the pointed bottom.
- Glasgow's Minimal Essential Medium (GMEM): GMEM is a basal medium that contains no proteins, lipids, or growth factors. It was originally developed for use with kidney cell lines, such as BHK-21.
- Knockout Serum Replacement (KOSR): KOSR is for replacing fetal bovine serum (FBS). Before the development of KOSR, FBS was the only option for nutritive supplementation of ESC media. However, it contains factors which can promote spontaneous differentiation of ES cells. Moreover, it contains many undefined and variable components, so each lot of FBS must be screened before use. KOSR has a more defined formulation compared to FBS. It has been shown to support a culture of ESCs and iPSCs on feeders, EB formation, and *in vitro* differentiation.
- Essential Medium Non-Essential Amino Acids (MEM NEAA): MEM NEAA is a growth supplement for cell culture medium used to increase cell growth and viability.
- Sodium pyruvate: Sodium pyruvate is commonly added to cell culture media as a source of energy in addition to glucose.
- Penicillin/Streptomycin (P/S): P/S is one of the antibiotics to prevent bacterial contamination of cell cultures. Penicillin acts by interfering with the turnover of the bacterial cell wall and Streptomycin acts by binding to the 30S subunit of the bacterial ribosome leading to inhibition of protein synthesis.
- 2-Mercaptoethanol (BME): BME is a potent reducing agent to prevent toxic levels of oxygen radicals.

- Rho-associated protein kinase inhibitor (Rock-I): Rock-I, Y-27632, increases the survival rate of dissociated single hESCs.
- N-2 Supplement: N2 is a serum-free supplement and is widely used for growth and expression of neuronal cells.
- Advanced Dulbecco's Modified Eagle Medium/Ham's F-12 (Advanced DMEM/F-12): Advanced DMEM/F-12 is a basal medium for mammalian cells. FBS supplementation can be reduced by 50–90% with no change in growth rate or morphology compared to another basal medium (https://www.thermofisher.com/order/catalog/product/12634010?SID=srch-srp-12634010).
- GlutaMAX: GlutaMAX is an alternative to L-glutamine with increased stability that improves cell viability and growth. In addition, it helps to minimize toxic ammonia build-up.
- Normocin: Normocin is a combination of three antibiotics to prevent mycoplasma, bacterial and fungal contaminations. It acts on mycoplasmas and both Gram+ and Gram - bacteria by blocking DNA and protein synthesis. It also eradicates yeasts and fungi by disrupting ionic exchange through the cell membrane. Normocin can be used instead of P/S containing Aminoglycosides which are toxic to inner ear hair cells.
- IWR-1: IWR-1 is a potent inhibitor of the Wnt response, blocking a cell-based Wnt/β-catenin pathway reporter response.

1.5 Differentiation protocols of human pluripotent stem cells into inner ear cells

The development of an efficient method to generate inner ear hair cells or auditory neurons *in vitro* using PSCs has been the subject of intense investigation over the past decade. However, most of the stem cell research on the inner ear has been widely carried out using mESCs rather than hESCs (Koehler et al., 2013, Li et al., 2003, Oshima et al., 2010, Ouji et al., 2012). In this section, previous attempts to derive inner ear sensory cells from PSCs will be introduced and we will also discuss how closely researchers reconstitute the normal developmental process *in vitro*. This information would be helpful for the development of a precise protocol to drive inner ear cells from hPSCs.

1.5.1. Generation of mouse inner ear sensory epithelia from pluripotent stem cells in 3D culture

A recent publication has described the use of a 3D culture system to direct mESC differentiation towards inner ear sensory epithelia (Figure 21) (Koehler et al., 2013). Unlike many other mouse inner ear cell derivation studies, this paper was the first to demonstrate the guidance of mESCs thorough each of the epithelial cell fates representing the definitive ectoderm, non-neural ectoderm, pre-placodal epithelium, otic prosensory vesicles and sensory epithelia vesicles containing functional mechanosensitive hair cells. During the first 8 days of *in vitro* differentiation, they attempted to generate pre-placodal ectoderm cells using a treatment of BMP4 and SB-431542, followed by FGF-2 and LDN-193189. They discovered that the surface epithelium of each EB thickened like placodes *in vivo*. A vital component of this protocol was adding growth factor reduced Matrigel into the serum-free medium. Laminin and entactin proteins in the Matrigel have been shown to promote the development of epithelium on the surface of EBs (Eiraku et al., 2011, Nasu et al., 2012). In this way, the epithelial cells differentiated from mESCs shared a nearly similar morphology with the equivalent cells in the developing mouse embryo.

Subsequently, EBs were transferred to a serum-free floating culture to allow self-guided differentiation instead of exogenous signaling cues to direct differentiation. Further characterization revealed that mESC derived sensory epithelia vesicles contained functional type II vestibular hair cells based on co-expression of Myo7a/Brna3c/Pax2/Calretinin, stereocilia bundle structures, FM1-43FX (hereafter FM1) dye uptake assay, and electrophysiological recordings. Even though they showed mESC-derived vesicles in their culture represent the utricle or saccule, further research will be needed to elucidate the mechanisms leading to only type II vestibular cells among four different types of hair cells.

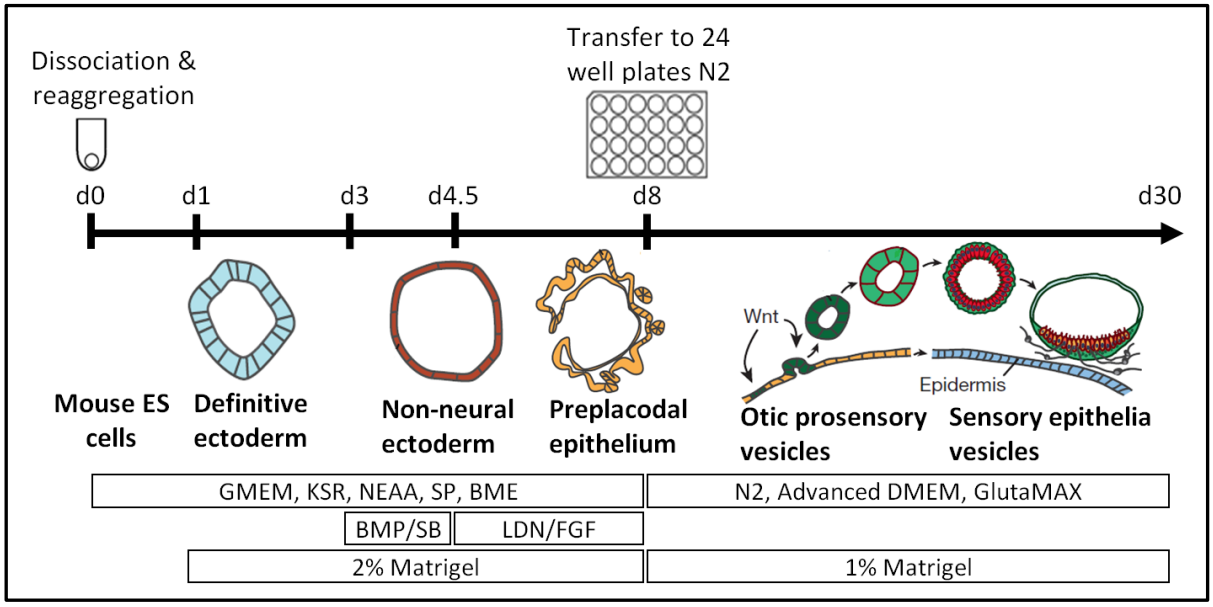

Figure 21 | Schematic drawing of the 30-day guidance protocol.

GMEM: Glasgow's Minimal Essential Medium, KOSR: Knockout Serum Replacement, NEAA: Nonessential Amino Acids, SP: Sodium Pyruvate, P/S: Penicillin/ Streptomycin, BME: 2-mercaptoethanol, Advanced DMEM/F12: Dulbecco's Modified Eagle Medium/Ham's F-12, BMP: Bone morphogenetic protein 4, SB: SB-431542, LDN: LDN-193189, FGF: Fibroblast growth factor 2. Reproduced from (Koehler et al., 2013)

This protocol is our model to establish a new protocol of stepwise inner ear cell differentiation using hPSCs, however, protocols which work well with mESCs often work less efficiently with human cells, so there is an unmet need to adopt such a 3D culture system for the production of cells specific to human auditory epithelia. To develop a precise protocol, we need to understand the architecture and developmental biology of the human auditory organs and the types of cells they comprise in parallel with the mouse system.

1.5.2. Restoration of auditory evoked responses by human ES-cell-derived otic progenitors

Chen and coworkers were the first to provide evidence that otic progenitors, sensory neurons, and hair-cell-like cells could be derived *in vitro* using hESCs (Chen et al., 2012). Initially, they used 3D culture method. To induce the formation of EBs, undifferentiated hESCs were dissociated into small clumps with collagenase IV and transferred into non-adherent bacterial petri dishes containing hESCs culture media. However, they focused on developing a method devoid of this initial cell aggregation step, which is prone to high variability. Unlike a monolayer culture method, cell number is a critical factor in 3D culture method, because EBs might receive various levels of signaling cues depending on their spatial regions within the EB. If they make the similar size of EBs such may be achieved using low attachment 96 well plates, it might be helpful to minimize the variability in 3D culture.

For the derivation of otic progenitors, they plated hESCs in a serum-free monolayer culture and treated with FGF3 and FGF10, which are the ligands involved in placode signaling in the mouse, for a period of 12 days. Although FGF signaling is necessary and sufficient for the induction *in vivo* of the otic placode, the timing of treatment is too early to induce otic progenitor cells considering the developmental time frame *in vivo*. Thus, it is unclear how FGF3 and FGF10 function to generate otic progenitors in this culture condition. It is conceivable that endogenous BMP signaling mediates the generation of non-neural cells or serum-free conditions might help to

generate cells of the neural lineage by default (Meyer et al., 2009b, Pankratz et al., 2007, Zhang et al., 2001).

Despite these mechanistic ambiguities, Chen et al. identified two morphologically distinct types of colonies that expressed PAX2, PAX8, FOXG1 SOX2, NESTIN, and SIX1, evidence of their otic progenitor-like characteristics. One cell population showed a flat phenotype, with large cytoplasm and formed epithelioid islands (otic epithelial progenitor cells (OEPs)), whereas the second was small, with denser chromatin, and presented cytoplasmic projections (otic neural progenitor cells (ONPs)). They found that OEPs produced hair-cell-like cells express ATOH1, BRN3C, and MYO7A. However, only less than 1% of cells had a rudimentary apical bundle expressing stereocilia specific marker ESPIN. Since the bundles did not have the typical cytoarchitecture as stereocilia on native hair cells, further characterization will be needed to determine the authenticity of these cells. Conversely, ONPs were committed to producing neurons. Under neuralizing conditions, almost all cells developed a bipolar morphology and were positive for BRN3A and TUBB3, as well as for TUBB3 and NF200.

So far, after transplantation of hair-cell-like cells or possible sensory neurons differentiated from mESCs, some cell types have shown engraftment, but none have shown evidence of functional recovery (Corrales et al., 2006, Hildebrand et al., 2005). Chen et al. for the first time showed when they transplant ONPs into an auditory neuropathy model, ONPs engraft, differentiate and significantly improve auditory evoked response thresholds. Notably, projections from the transplanted cells that reached the OC were targeting the hair cells, and fibres from the transplanted cells were visualized leaving the cochlea towards the brainstem. However, the number of projections detected in the brainstem was considerably lower than the number of transplanted cells bodies identified in the ganglion, so further exploration is needed to determine that path of the central innervations. Moreover, since the permanence of many forms of hearing loss is the result of the inner ear’s inability to replace lost sensory hair cells, transplantation of OEPs will be an interesting research as well.

1.5.3 Inner ear hair-cell-like cells from human embryonic stem cells

In 2014, Ronaghi and colleagues established a method for generating inner ear hair-cell-like cells from hESCs (Ronaghi et al., 2014). This method adopted the use of IGF1, which has been found to be integral to proper otic neurogenesis, from their previous mESC differentiation method described in (Oshima et al., 2010). Their strategy was to induce cells from ectoderm lineages by culturing them in serum-free condition together with selectively inhibiting mesoderm and endoderm cells. Despite this, *GATA6* which is an endoderm marker still expressed on day 15 and even further increased on day 42 of differentiation though they treated WNT inhibitor DKK-1 and TGFβ-signaling inhibitor SIS3 to suppress mesodermal and endodermal differentiation for first 15 days. As we discussed previously, early stage of mesoderm and endoderm cells secretes critical factors to induce otic lineages, but 100 times higher expression of *GATA6* comparing to undifferentiated hESCs might represent high proportions of endoderm-derived cells among the mixture of differentiated cells. Another point is that although treatment of DKK-1 might be useful to suppress meso- and endodermal lineages, it may prevent the development of otic placode as well. This is because WNT pathway is one of the most important pathways to establish otic placode. They added WNT activator with R-spondin1 between days 15 – 18, but it seems a bit late considering initiation of invagination to form otic vesicles at 3 WG *in vivo*.

They systematically tested the activation and inhibition of FGF-, BMP-, Notch-, and WNT-signaling pathways for the otic induction after generation of presumptive cranial ectoderm. To find optimal timing and guidance conditions for the early otic lineage, they used PAX2 expression as a standard. Although screening all otic lineage involved genes in various conditions is almost impossible, it is worth trying to think about PAX2 is the good marker to represent otic progenitor cells. To support their hypothesis they stained cells with PAX8, but PAX2 and PAX8 expression localize in the optic stalk, mid-hindbrain, and kidney as well as the otic vesicles.

Although this approach led to a heterogeneous mixture of cells, the researchers were able to identify a small population of hair-cell-like cells expressing a combination of marker proteins for sensory hair cells, including ATOH1, MYO7A, and ESPIN. This is a strong characterization because MYO7A is not a definite

marker for hair cells; however, they found a minority of MYO7A expressing cells co-expressed ESPIN. Multiple hair cell marker-positive cells were rare and in most cases, protrusions were splayed and did not closely resemble the typical morphology of sensory hair cell bundles. The lack of typical hair bundle morphology and no functional tests such as electrophysiological recordings suggest that human hair-cell-like cells are at a nascent stage of development and fail to fully mature in the conditions.

Lastly, Ronaghi and coworkers used a 3D-2D format, making easier to identify hair- cell-like cells amongst a monolayer of cells. During the first 15 days, they cultured EBs in serum-free medium to generate a presumptive non-neural/pre-placodal cell population, followed by otic induction period with the 2D method. The big advantage of using 3D methods is that cells can give and take signals by forming their own microenvironment helps to differentiation. However, in this study since they used different sizes of EBs, it might happen that each EB has their own direction of differentiation meaning that they might end up heterogeneous cell population.

1.5.4 Induction of differentiation of human embryonic stem cells into functional hair-cell-like cells in the absence of stromal cells

In 2016, Ding and coworkers introduced the two step-induction protocol for generating functional hair cell from hESCs (Ding et al., 2016). The differentiation of hESCs into the otic progenitors was the first induction step for first 12 days as described in (Chen et al., 2012), and the differentiation of OEPs separated form otic progenitors into hair-cell-like cells was the second induction step. For the hair cell differentiation, they used chicken utricle stromal cells or conditioned medium derived from these cells similar to previous methods described in (Oshima et al., 2010). The OEPs plated on a layer of mitotically inactivated chicken utricle supporting cells efficiently differentiated into mature-looking hair-cell-like cells, having a regular arrangement of stereocilia bundles. In order to avoid the interference from stromal cells, they cultured OEPs in the conditioned medium supplemented with epidermal growth factor (EGF) and RA. This promotes the organization of cells into epithelial

clusters displaying hair-cell-like cells with stereociliary bundles and these cells also displayed the expected electrophysiological properties. These results may indicate that cells in the chicken utricle provide an important signaling cue missing in the monolayer culture.

This study marked the first demonstration that functional hair cells having typical hair cell architecture could be derived from hESCs *in vitro*. Although useful for research purposes, these products are unsuitable for a therapeutic application because of exogenous cells. This method would also suggest that a 2D culture format without any exogenous supporting cells or conditioned medium might not be appropriate for proper hair cell differentiation. In support of this notion, recent studies on retinal differentiation suggest that complex epithelia with specialized cell types within them develop much more organized in a 3D culture environment (Eiraku et al., 2011, Nakano et al., 2012, Sasai et al., 2012). Considering the advantages of the 3D culture method, in this project, we will adopt an EB culture system to derive inner ear cells from hPSCs.

1.6 Project aims

The main reason for sensorineural hearing loss is damage to the hair cells in the cochlea. It is caused by genetics, injury from medicine or disease, tumor, or physical injury to the inner ear. Currently, the only treatment options for sensorineural hearing loss are hearing aids or cochlear implants (Russell et al., 2013), but these can't be applied in all cases so there are limitations. One of the great advantages of PSCs is that they can replicate *in vitro* many of the cell differentiation events occurring during embryonic development. Hair cell regeneration using stem cells and gene therapy is the most promising treatment for sensorineural hearing loss but, it is years or decades away from being clinically feasible (Parker, 2011). From this point of view, the primary objective of this work is to develop protocols for the differentiation of hPSCs into inner ear hair cells and other components of the auditory sensory epithelia such as the supporting epithelial cells or auditory neurons. We are going to test following 4 different protocols and find out which one is the best condition to generate cells of otic lineages by analysing these cells.

- mouse protocol (2.2.1): We take advantage of a published protocol with murine ESC which utilised 3D culture conditions and a stage-specific growth factor regime to generate otic EBs containing mechano-sensory hair cells (Koehler et al., 2013). Before optimization of a protocol for hESCs, we test the mouse protocol to hESCs to determine the applicability of this protocol in the human system.
- 2-mercaptoethanol high concentration protocol (2.2.2): We modify culture conditions by changing the base media from GMEM to DMEM/F12 and increasing the cell numbers.
- BME low concentration protocol (2.2.3): We test a 0.1mM 2-mercaptoethanol concentration which is widely used in hESC differentiation.
- KOSR high concentration protocol (2.2.4): We modify culture conditions by increasing the KOSR from 1.5% to 20%.

in vivo (WG)	In vitro (days)	Description
0 - 1	0	**hPSCs maintenance** Culture hESCs (line H9) and hiPSCs (line AD3) on mouse embryonic fibroblasts or on Matrigel-coated plates
3	0	**Initiation of ectodermal differentiation** Dissociate ES cells; distribute on U or V bottom 96-well plates in 4 different differentiation medium: the mouse protocol (2.2.1), 2-mercaptoethanol high concentration protocol (2.2.2), BME low concentration protocol (2.2.3) and KOSR high concentration protocol (2.2.4)
3	1	**Basement membrane formation** Add Matrigel
3	3	**Non-neural ectoderm induction** Add BMP4 and SB-431542
3	5	**Preplacodal ectoderm induction** Add FGF2 and LDN-193189
4	16 - 20	**Prosensory otic vesicle induction** Analyze EBs using Immunohistochemistry
7 - 9	60	**Maturing otic vesicles and neuronal cells** Analyze EBs using Immunohistochemistry and TEM

10 -	90	**Matured otic vesicles (hair cells and supporting cells) and neuronal cells** Analyze EBs using Immunohistochemistry, FM1-43 uptake assay, TEM and electrophysiological recordings

Table 1 | Specific aims for each differentiation stage

Chapter 2

Materials and Methods

Chapter 2. Materials and methods

2.1 Cell culture

In order to avoid bacterial and fungal contamination, cell culture was performed out using sterile technique in an IVF workstation N24 laminar flow hoods (K-SYSTEMS, www.k-systems.dk) with fitted dissection microscopes Nikon SMZ 1000 (Nikon, www.nikoninstruments.com). The facilities were sterilized by fumigation annually and all cells used in these facilities were tested for Mycoplasma every 2 – 4 weeks. To sustain stable tissue culture conditions, media were warmed to 37°C prior to use. Photographs were taken with a ZEISS AxioCam HRc (ZEISS, www.zeiss.com) connected to a Zeiss Axiovert 200M fluorescence microscope (ZEISS) using AxioVision software.

2.1.1 Mouse embryonic fibroblasts (MEFs) culture

Mouse embryonic fibroblasts (MEFs) were generated from Dr. Georgios Anyfantis consentingly. Swiss MF1 pregnant mice containing 12.5 - 13.5 day old embryos were sacrificed. After the embryos were released from the amniotic sacs, the limbs, heads, tails and all visible organs were removed from the embryos using fine dissection scissors or forceps. The remaining torsos were transferred to a petri dish containing 1% trypsin ethylene diaminetetraacetic acid (EDTA) (Lonza, www.lonza.com) for single cell dissociation. Fine scissors were used to mince the tissue for 1 minute at room temperature. The cells were then incubated in trypsin EDTA for 5 minutes at 37°C. Inactivation of the trypsin was achieved by the addition of twice the volume of MEF medium including 1X Dulbecco's Modified Eagle Medium (DMEM, Gibco; www.lifetechnologies.com), 10% Fetal Bovine Serum (FBS, Gibco), 1X Penicillin/Streptomycin (Gibco), 2 mM L-glutamine (Gibco), and 0.1mM Minimum Essential Medium Non-Essential Amino Acids (MEM NEAA, Gibco). The cell suspension was then gently passed through an 18 gauge needle once or twice to promote cell separation. The cells were then centrifuged at 300xg for 5 minutes. The supernatant was gently aspirated and the cell pellet was re-suspended in MEF medium. The cell suspension was distributed into T75cm^3 tissue culture flasks in

12ml of MEF medium. The cells were incubated at 37°C, 5% CO_2 and the medium was changed after 24 hours.

MEFs were passaged 1:3 when 90% confluent (maximum 5 passages). MEFs were passaged by washing with Phosphate Buffered Saline (PBS, Gibco) and incubated with 0.05% trypsin EDTA for 5 minutes in a humidified atmosphere with 5% CO_2 at 37°C. The trypsin was then inactivated using MEF medium and cell suspensions were collected by centrifugation at 200xg for 5 minutes. The supernatant was removed and cell pellets were suspended in MEF medium. Cells were plated into a flask at a density of 15,000 to 20,000 cells per cm^2. The tissue culture plastic used was pre-treated with a 0.1% gelatin from porcine skin (Sigma Aldrich) diluted in PBS for 1 - 2 hours at room temperature. MEF medium was changed every 2 days.

2.1.2 Freezing and thawing of MEFs

MEFs destined for freezing were harvested at the time of normal passage. The cell pellets were suspended in an ice-cold freezing medium (90% FBS, 10% dimethyl sulfoxide (DMSO; Sigma Aldrich) and quickly aliquoted into cryovials (Nunc, Roskilde, Thermo Fisher Scientific Germany, www.thermofisher.com) for storage. Cells were stored in a Mr. Frosty™ freezing container (Nalgene, www.thermofisher.com) containing isopropanol in a -80°C freezer overnight. The following day, the cryovials were transferred to cryogenic storage boxes for short term storage in a -80°C freezer or to a liquid nitrogen tank for long-term storage.

Thawing vials of frozen MEFs were taken from the 80°C freezer, thawed quickly at 37°C, transferred drop-wise into MEF media, and centrifuged at 200xg for 5 minutes. The pellet was then suspended in fresh MEF medium, before seeding in a $25cm^2$ flask (TPP, Switzerland, www.tpp.ch). The following day the MEF medium was changed to remove debris and any remaining cryoprotectant.

2.1.3 Mitotic inactivation of MEFs

Confluent T75 flasks of MEFs (passage 3 - 5) were inactivated by the irradiator (Faxitron CP-160 radiation machine) with the program 334 (160kV) and

were placed in the incubator to have recovery time for 20 minutes. The cells were washed with PBS and detached from the flasks with 0.05% trypsin EDTA, centrifuged at 200xg for 5 minutes and suspended in fresh MEF medium. After counting the remaining viable cells using Trypan Blue (Sigma Aldrich) in a hemocytometer, the MEFs were plated at a concentration of 18,500 cells /cm^2 on 0.1% gelatin-coated 6 well plates (TPP). The MEF plates were used within 3 - 4 days after plating.

2.1.4 Maintenance and passage of hESC and hiPSC on MEFs

hESC and hiPSC culture work were carried out inside laminar flow hoods with the 37°C heated panel. Undifferentiated hPSCs were maintained on a feeder layer of MEFs (mitotically inactivated by irradiation) in hESC medium (Knockout-Dulbecco's Modified Eagle's Medium (KO-DMEM; Gibco), 1 mM L- glutamine, 100 mM MEM NEAA, 20% Knockout Serum Replacement (KOSR, Gibco; www.lifetechnologies.com), 1% Penicillin-Streptomycin (Gibco) and 8 ng/ml bFGF (Invitrogen)). hESC medium was changed daily and cells were passaged every 4 - 5 days using 6 well plates at a ratio of 1:3 - 1:4 by incubation in 1 mg/ml collagenase IV. Before passage, spontaneously differentiated cells were removed using a 10 µl pipette tip and aspirated along with the old medium. Optimum time and ratio for subculture were determined by examination of colony size and morphology, the colonies ready for sub-culture usually contain roughly 1000 cells per colony. For the purpose of the studies, H9 which is one of the hESC lines (WiCell™, www.wicell.org) and AD3 (generated from Stembank consentingly) which is one of the hiPSC lines were used.

2.1.5 Feeder-free hESC and hiPSC culture

To avoid contamination with mouse feeder cells, hESCs and hiPSCs were plated on 6 well plates pre-coated with Matrigel hESC-qualified matrix (BD Biosciences, Oxford, UK, www.bdeurope.com; dilution in KO-DMEM followed by a description) prepared at least 2 hours prior to use. The cells were cultured in mTeSR1® medium (StemCell Technologies) and the medium was changed every day. To passage the cells, hESC and hiPSC colonies were treated with 0.02% EDTA (Lonza) for 3 minutes and EDTA was removed. 2ml of fresh medium was then added

to each well and cell colonies were picked out by mechanical disruption using a 1000µl pipette tip to give rise to small clumps. The detached cells were sub-cultured at a ratio of 1:4 or 1:6 on the Matrigel-coated plates in fresh mTeSR1® medium.

2.2 Differentiation protocols

Before induction of differentiation, the hESCs and hiPSCs on MEF plates were dissociated into small clumps using 1 ml of 1 mg/ml collagenase IV per each well of 6 well plates. The plate was incubated at 37°C for 20 minutes until edges of colonies start to detach. Then the collagenase IV was removed, 2 ml of fresh hESC medium including 10 μM Rho-associated protein kinase inhibitor (Rock-I) was added in each well. Cell colonies were then detached by using a 1000μl pipette tip. Cell clumps were transferred to 0.2% gelatin-coated 6 well plates and stored them in the 37°C incubator at least 1 hour to remove MEFs. All floating cells were collected 50 ml tubes and centrifuged at 900 rpm for 5 minutes. The supernatant was removed and the small clumps were further dissociated using 3 ml of Accutase (Gibco; www.lifetechnologies.com) at 37°C for 3 minutes. The Accutase digestion was terminated using 3 ml of hESC medium including 10 μM Rock-I, and the cell suspension was passed through a 100 μm cell strainer (Corning; www.corning.com). Cell counting was performed using a hemocytometer prior to replating of cells at the density 3000 - 12000 cells into one well of a 96 well low-cell-adhesion U-bottom plates (Lipidure Coat, NOF; www.nofamerica.com). Differentiation medium was Glasgow's MEM (G-MEM) (Life Tech; www.lifetechnologies.com) or DMEM/F12 (Life Tech) supplemented with 1.5% or 20% KOSR, 0.1 mM MEM NEAA, 1 mM sodium pyruvate, 1 mM penicillin-streptomycin and 0.1 - 1 mM 2-mercaptoethanol (Life Tech). IWR1e (Merck Millipore; www.merckmillipore.com) was added to final 3 μM for the high concentration of KOSR protocol. After seeding the cells, the 96 well plates were centrifuged at low speed (200xg for 3 minutes) to minimize the impact on the cells. On differentiation day 1, half of the medium in each well was exchanged for fresh differentiation medium containing Growth Factor Reduced Matrigel (2% (v/v) final concentration, BD; www.bd.com). On differentiation day 3, 25 μl of fresh differentiation media containing a 50 ng/ml bone morphogenetic protein (BMP) 4 (10 ng/ml final concentration, Gibco) and 5 μM SB- 431542 (1 μM final concentration, TOCRIS; www.tocris.com) was added to the pre-existing 100 μl of media in each well. On differentiation day 4.5 or 5, 25 μl of fresh differentiation media containing a 150 ng/ml FGF2 (25 ng/ml final concentration, Gibco) and 600 nM or 6 μM LDN-193189 (100 nM or 1 μM final concentration, STEMGENT; www.stemgent.com) was added to the pre-existing 125 μl of media in each well. The concentration of the Matrigel was maintained at 2% (v/v) throughout days 1 – 8. On differentiation day 8, EBs were

transferred to low attachment 6 or 12 or 24 well plates (Lipidure Coat, NOF) in N2 medium containing 1% (v/v) Matrigel. 24 well plates helped to avoid attaching EBs each other comparing the large size of plates such as 6 well plates. N2 medium contained Advanced DMEM/F12 (Gibco), 1X N2 Supplement (Life Tech), 1 mM penicillin/streptomycin or 50 µg/ml Normocin (InvivoGen; www.invivogen.com) and 1 mM GlutaMAX. Half of the medium was changed every day or every other day during long-term suspension culture for up to 32 - 161 days. Details can be found in each section of the protocol.

2.2.1 Differentiation protocol adapted from generation of inner ear sensory epithelia from mESCs in 3D culture (Koehler et al., 2013)

In brief, hESCs plated on Matrigel-coated plates were dissociated with 0.02% EDTA / hESCs on MEF plates were dissociated with 1 mg/ml collagenase IV, suspended in differentiation medium and plated at 3000 cells/well on 96 well low-cell-adhesion U-bottom plates. Differentiation medium was prepared as shown in Table 2.

Product Name	Final Concentration
GMEM	1X
KnockOut™ Serum Replacement	1.5%
MEM NEAA 10 mM (100X)	0.1 mM
Sodium Pyruvate 100 mM (100X)	1 mM
2-mercaptoethanol (55 mM)	1 mM
Penicillin/Streptomycin (100X)	1X

Table 2 │Composition of the differentiation medium on day 0.

On differentiation day 1, half of the medium in each well was exchanged for fresh differentiation medium containing growth factor reduced Matrigel (2% (v/v) final concentration). On differentiation day 3, 25 µl of fresh differentiation media containing a 50 ng/ml BMP 4 (10 ng/ml final concentration) and 5 µM SB- 431542 (1 µM final concentration) was added to the each well. On differentiation day 4.5, 25 µl of fresh differentiation media containing a 150 ng/ml FGF2 (25 ng/ml final concentration) and

600 nM LDN-193189 (100 nM final concentration) was added to the each well. On day 8 of differentiation, EBs were transferred to 24 well plates (4 - 8 EBs per well) in N2 medium containing 1% (v/v) Matrigel. The N2 medium contained Advanced DMEM/F12, 1X N2 Supplement, 1 mM penicillin/streptomycin and 1 mM GlutaMAX. Half of the medium was changed every day during long-term suspension culture for up to 35 days.

2.2.2 2-mercaptoethanol high concentration protocol

In brief, hESCs on MEF plates were dissociated with 1 mg/ml collagenase IV, suspended in differentiation medium and plated at 12000 cells/well on 96 well low-cell-adhesion U or V-bottom plates. Differentiation medium was prepared as shown in Table 3.

Product Name	Final Concentration
GMEM or DMEM/F12	1X
KnockOut™ Serum Replacement	1.5%
MEM NEAA 10 mM (100X)	0.1 mM
Sodium Pyruvate 100 mM (100X)	1 mM
2-mercaptoethanol (55 mM)	1 mM
Penicillin/Streptomycin (100X)	1X
Rock Inhibitor	20 µM

Table 3 │ Composition of the differentiation medium on day 0.

On differentiation day 1, half of the medium in each well was exchanged for fresh differentiation medium containing growth factor reduced Matrigel (2% (v/v) final concentration). On differentiation day 3, 25 µl of fresh differentiation media containing a 50 ng/ml BMP 4 (10 ng/ml final concentration) and 5 µM SB- 431542 (1 µM final concentration) was added to the each well. On differentiation day 5, 25 µl of fresh differentiation media containing a 150 ng/ml FGF2 (25 ng/ml final concentration) and 600 nM LDN-193189 (100 nM final concentration) was added to the each well. The concentration of Matrigel was maintained at 2% (v/v) throughout days 1 – 8. On differentiation day 8, EBs were transferred to 6 well plates (16 EBs per well) in N2 medium containing 1% (v/v) Matrigel. N2 medium contained Advanced DMEM/F12,

1X N2 Supplement, 1mM penicillin/streptomycin and 1mM GlutaMAX. Half of the medium was changed every day during long-term suspension culture for up to 32 days.

2.2.3 2-mercaptoethanol low concentration protocol

In brief, hESCs/hiPSCs on MEF plates were dissociated with 1 mg/ml collagenase IV, suspended in differentiation medium and plated at 9000 cells/well on 96-well low-cell-adhesion U-bottom plates. Differentiation medium was prepared as shown in Table 4.

Product Name	Final Concentration
GMEM	1X
KnockOut™ Serum Replacement	1.5%
MEM NEAA 10 mM (100X)	0.1 mM
Sodium Pyruvate 100 mM (100X)	1 mM
2-mercaptoethanol (55 mM)	0.1 mM
Penicillin/Streptomycin (100X)	1X
Rock Inhibitor	20 µM

Table 4 │ Composition of the differentiation medium on day 0.

On differentiation day 1, half of the medium in each well was exchanged for fresh differentiation medium containing growth factor reduced Matrigel (2% (v/v) final concentration). On differentiation day 3, 25 µl of fresh differentiation media containing a 50 ng/ml BMP 4 (10 ng/ml final concentration) and 5 µM SB- 431542 (1 µM final concentration) was added to the each well. On differentiation day 5, 25 µl of fresh differentiation media containing a 150 ng/ml FGF2 (25 ng/ml final concentration) and 6 µM LDN-193189 (1 µM final concentration) was added to the each well. The concentration of Matrigel was maintained at 2% (v/v) throughout days 1 – 8. On differentiation day 8, EBs were transferred to 12 well plates in N2 medium containing 1% (v/v) Matrigel. The N2 medium contained Advanced DMEM/F12, 1X N2 Supplement, 50 µg/ml Normocin and 1 mM GlutaMAX. After 48h the medium was changed completely with the new N2 medium. Beginning on day 10, half of the

medium was changed every other day during long-term suspension culture for up to 161 days.

2.2.4 KOSR high concentration protocol

In brief, hESCs on MEF plates were dissociated with 1mg/ml collagenase IV, suspended in differentiation medium and plated at 9000 cells/well on 96-well low-cell-adhesion U-bottom plates. Differentiation medium was prepared as shown in Table 5.

Product Name	Final Concentration
GMEM	1X
KnockOut™ Serum Replacement	20%
MEM NEAA 10 mM (100X)	0.1 mM
Sodium Pyruvate 100 mM (100X)	1 mM
2-mercaptoethanol (55 mM)	0.1 mM
Penicillin/Streptomycin (100X)	1X
IWR-1(25 mM)	3 µM
Rock Inhibitor	20 µM

Table 5 | Composition of the differentiation medium on day 0.

On differentiation day 1, half of the medium in each well was exchanged for fresh differentiation medium containing growth factor reduced Matrigel (2% (v/v) final concentration). On differentiation day 3, 25 µl of fresh differentiation media containing a 50 ng/ml BMP 4 (10 ng/ml final concentration) and 5 µM SB- 431542 (1 µM final concentration) was added to the each well. On differentiation day 5, 25 µl of fresh differentiation media containing a 150 ng/ml FGF2 (25 ng/ml final concentration) and 6 µM LDN-193189 (1 µM final concentration) was added to the each well. The concentration of Matrigel was maintained at 2% (v/v) throughout days 1 – 8. On differentiation day 8, EBs were transferred to 12 well plates in N2 medium containing 1% (v/v) Matrigel. The N2 medium contained Advanced DMEM/F12, 1X N2 Supplement, 50 µg/ml Normocin and 1 mM GlutaMAX. After 48h the medium was changed completely with the new N2 medium. Beginning on day 10, half of the medium was changed every other day during long-term suspension culture for up to 90 days.

2.3 Reverse transcription polymerase chain reaction (RT-PCR)

2.3.1 RNA isolation

ReliaPrep™ RNA Cell Miniprep System (Promega; https://www.promega.co.uk) was used for RNA isolation. Cells were washed with ice-cold, sterile 1X PBS and centrifuged at 300×g for 5 minutes to collect the cells. Then all supernatant was discarded carefully and cell pellets containing >2 × 10^6 to 5 × 10^6 were suspended in 500µl PL+TG buffer. Cells were lysed by vigorous vortexing. 170 µl volume of Isopropanol was added to the solution and shaken for 5 seconds. The lysate was then transferred to a ReliaPrep™ Minicolumn and centrifuged at 12,000×g for 30 seconds at room temperature. The liquid in the Collection Tube was discarded. 500µl of RNA Wash Solution was then added to the ReliaPrep™ Minicolumn and centrifuged at 12,000×g for 30 seconds. The Collection Tube was emptied and 30 µl of freshly prepared DNase I incubation mix was applied directly to the membrane inside the column. The solution was then allowed to incubate for 15 minutes at room temperature. 200 µl of Column Wash Solution was added and centrifuged at 12,000×g for 30 seconds. 500 µl of RNA Wash Solution was then added and centrifuged at 12,000×g for 30 seconds. The ReliaPrep™ Minicolumn was placed into a new Collection Tube and 300 µl of RNA Wash Solution was added then centrifuged at high speed for 2 minutes. The ReliaPrep™ Minicolumn was transferred from the Collection Tube to the Elution Tube and added 15 µl of Nuclease-Free Water to the membrane then centrifuged at 12,000 × g for 1 minute. The purified RNA was stored at -80°C.

2.3.2 cDNA synthesis

Total RNA samples were quantified using a Nanodrop 2000 spectrophotometer (Thermo Fisher Scientific) at 260nm and 280nm wavelengths. The 260:280 ratio was used to evaluate possible protein contamination. 1 µg of the RNA samples were reverse-transcribed using the GoScript Reverse Transcription System (Promega). 0.5 µg of random oligonucleotide primers or Oligo (dT) was added to RNA and the solution was heated to 70°C for 5 minutes to denature the

RNA and to resolve any secondary structure so that the primers can bind. Each reaction included 15 µl reverse transcription reaction mix (Table 6), 1 µl of reverse transcriptase primers and 4 µl of RNA sample. The samples were incubated at 25°C for 5 min, followed by 42°C for 1 hour, after this time the solution was heated to 70°C for 15 minutes to inactivate the reverse transcriptase enzyme.

Components	RT reaction mix per one reaction
5X Reaction Buffer	4 µl
MgCl2 (25mM)	1.5 µl
PCR Nucleotide Mix (10mM)	1 µl
Ribonuclease Inhibitor	0.5 µl
Reverse Transcriptase	1 µl
Nuclease Free Water	7 µl
Final Volume	15 µl

Table 6 | GoScript Reverse Transcription System reverse transcription reaction mix components.

2.3.3 Real-time quantitative polymerase chain reaction (qRT-PCR)

The qRT-PCR was performed with the GoTaq qPCR Master Mix (Promega) in a QuantStudio™ 7 Flex real-time PCR system (Life Technologies). Details of reaction composition are shown in Table 7.

Components	volume per one reaction	Final Concentration
GoTaq® qPCR Master Mix, 2X	5 µl	1X
Template DNA	1 µl	
CRX	0.1 µl	
Upstream PCR primer	0.2 µl	0.2µM
Downstream PCR primer	0.2 µl	0.2µM
Nuclease-Free Water	3.5 µl	
Final Volume	10 µl	

Table 7 | qRT-PCR reaction components.

The reaction parameters were as follows: 95°C for 2 minutes to denature the cDNA and primers, 50 cycles of 95°C for 15 seconds followed by annealing/extend 60°C for 60 seconds. A comparative Ct method was used to calculate the levels of relative expression, whereby the Ct was normalised to the endogenous control glyceraldehyde-3-phosphate dehydrogenase (GAPDH). This calculation gave the ΔCt value, which was then normalised to a reference sample (i.e. a positive control), giving the ΔΔCt. The fold change was calculated using the following formula: $2^{-\Delta\Delta Ct}$. A list of primers is given in Table 8.

Template cDNA	Forward primer (5' → 3'); Reverse primer (3' → 5')	Product size (bp)	Gene Bank
OCT4	AAGCCCTCATTTCACCAGG; CTTGGAAGCTTAGCCAGGTC	184	NM_002701.5
PAX6	GTCCATCTTTGCTTGGGAAA; TAGCCAGGTTGCGAAGAACT	110	NM_000280.4
SIX1	CTGGTTTAAGAACCGGAGGC; GGACTTTGGGGAGGTGAGAA	168	NM_005982.3
DLX5	GTCTTCAGCTACCGATTCTGAC; CTTTGCCATAGGAAGCCGAG	89	NM_005221.5
PAX8	CACTCCATTTGCTTGGCTCT; CTGCGATTCTGCCTTGTTCT	286	NM_013992.3
MYO7A	GAGTCAGGCTTCCTCAGCTT; GTGACCAGGGCCACAATCTC	194	XM_006718561.1
ATHO1	CCTTCCAGCAAACAGGTGAAT; TTGTTGAACGACGGGATAACAT	131	NM_005172.1
MYO6	GCCCTTTGACATTCGCACTG; GGTTTCAGCAATGACCTTGCC	103	NM_004999.3
ESPIN	CAGAGTGCAGGACAAAGACAA; GCAGCGTAGTGGATAGGCAG	153	NM_031475.2
SOX2	ATGGGTTCGGTGGTCAAGT; GGAGGAAGAGGTAACCACAGG	60	NM_003106.3
GAPDH	AGCCACATCGCTCAGACACC; GTACTCAGCGCCAGCATCG	302	NM_002046.4

Table 8 | List of primers used in this study.

2.4 Immunohistochemistry

EBs were washed with PBS and fixed with 4% paraformaldehyde (PFA, Sigma Aldrich) for 10 minutes at 37°C. The PFA was removed and the EBs were washed 3 times with PSB for 5 minutes. The fixed specimens were cryoprotected with a treatment of 30% sucrose (Sigma Aldrich) and then incubated at a 4°C freeze overnight. When the EBs settle down at the bottom of a tube, this solution was then removed and the EBs were embedded in tissue freezing medium OCT (Thermo Fisher Scientific). Frozen tissue blocks were sectioned into 12 µm cryosections. For immunostaining, tissue sectioned on Superfrost™ Plus Microscope Slides (Thermo Fisher Scientific) was washed with 3 times PBS for 3 minutes to remove embedding medium. Blocking buffer (PBS, 0.3% Triton-X (Sigma Aldrich), 5% normal goat serum) was added and the microscope slide was incubated for 1 hour at room temperature in a humidified camber. First antibody (Table 9) was diluted in antibody diluent (PBS, 1% bovine serum albumin (Sigma Aldrich), 0.3% Triton X), and then incubated overnight at 4°C in a humidified chamber. The microscope slide was gently washed with 3 times antibody diluent for 5 minutes. Secondary antibody diluted in antibody diluent was applied for 1 hour at room temperature in a humidified chamber. A fluorescein Isothiocyanate (FITC) AffiniPure fab fragment goat anti-rabbit IgG (H+L) (Jackson ImmunoResearch; www.jacksonimmuno.com) and Cy™3 AffiniPure Fab fragment goat anti-mouse IgG (H+L) (Jackson ImmunoResearch) were mainly used as secondary antibodies. The microscope slide was then gently washed with 3 times PBS for 5 minutes. A Hoechst stain was used to visualize cellular nuclei. The cover slip was mounted onto a microscope slide using anti-fade aqueous mounting medium (Vector Laboratories; http://vectorlabs.com/) and sealed with nail polish. Microscopy was performed on a Zeiss Axio Imager Z1 or Nikon Ti Eclipse confocal microscope.

Antigen	Primary antibody and dilution*	Secondary antibody and dilution*
OCT4	AB ab19857, 1:200	S T6778, 1:400
N-CADHERIN	SC sc-271386, 1:50	S F2012, 1:100
PAX6	AB ab5790, 1:100	S T6778, 1:400
SOX9	MI AB5535, 1:200	JI 111-097-003, 1:500
SOX2	RD MAB2018, 1:62.5	JI 115-166-003, 1:250
PAX2	TF 71-6000, 1:200	JI 111-097-003, 1:500
ECADHERIN	AB ab40772, 1:250	JI 111-097-003, 1:500
ECADHERIN	BD 562869, 1:200	JI 115-166-003, 1:250
ESPIN	NB NBP1-90588, 1:200	JI 111-097-003, 1:500
FACTIN	AB ab130935, 1:400	JI 115-166-003, 1:250
SYNAPTOPHYSIN	S S5768, 1:200	JI 115-166-003, 1:250
ATOH1	AB ab137534, 1:200	JI 111-097-003, 1:500
GLUTAMINE SYNTHETASE	MI MAB302, 1:200	JI 115-166-003, 1:250
BETA III TUBULIN	C MMS-435P, 1:500	JI 115-166-003, 1:250
MYO7A	AB ab3481, 1:500	JI 111-097-003, 1:500
MYO7A	SC sc-74516, 1:250	JI 115-166-003, 1:250
NEUROFILAMENT	IV 13-1300, 1:20	JI 115-166-003, 1:250
CB2	CC 101550, 1:50	JI 115-166-003, 1:250
OCM	NB NBP2-14568, 1:100	JI 111-097-003, 1:500
OTOP1	NB NBP1-86306, 1:50	JI 111-097-003, 1:500
PRESTIN	TF PA5-42533, 1:200	JI 111-097-003, 1:500
PARVALBUMIN	S P3088-.2ML, 1:2000	JI 115-166-003, 1:250

Table 9 │ List of antibodies used in this study

*MI, Millipore; RD, R&D system; TF, Thermo Fisher; AB, Abcam; BD, BD Biosciences; JI, Jackson Immunoresearch; S, Sigma Aldrich; C, Covance; SC, Santa Cruz Biotechnology; NB, Novus Biologicals; IV, Invitrogen; CC, Cayman Chemical.

2.5 Dye permeation experiment

2.5.1 Basic concepts of FM1-43

FM1-43, which is one of small styryl pyridinium dyes, is a fluorescent, nontoxic, and cationic dye (Betz et al., 1996). FM1-43 is basically non-fluorescent in an aqueous medium but is intensely fluorescent when it is inserted into the unit membrane (Meyers et al., 2003). FM1-43 fills the cytoplasm of hair cells in the inner ear, but labels only the plasma membrane in adjacent supporting cells, because it does not cross between the membrane (Betz et al., 1996). More precisely, FM1-43 rapidly enters hair cells by permeating directly through mechanically gated transduction channels at the tips of the stereocilia (Gale et al., 2001, Meyer et al., 2001, Meyers et al., 2003). For example, the experiment with mouse inner ear showed that 5 μM FM1-43 brightly and rapidly labelled the IHCs and OHCs (Figure 22) (Meyers et al., 2003). Fluorescence first appeared in the hair bundle and moved quickly into the apical cytoplasm. It spread to the level of the nucleus within 30 seconds, moved into the basal cytoplasm within 60 seconds, and accumulated as dye application continued. This labelling can be blocked by pharmacological or mechanical closing of the channels, but also inhibited by FM1-43 entry (Meyers et al., 2003). However, this phenomenon is not confined to hair cell transduction channels, because human embryonic kidney 293T cells expressing the vanilloid receptor (TRPV1) or a purinergic receptor ($P2X_2$) rapidly take up FM1-43 when those receptor channels are opened (Caterina et al., 1997). Except this, the pattern of FM1-43 labelling is specific to sensory cells; nonsensory cells and neurons remain unlabelled (Meyers et al., 2003). The labelling of the sensory neurons requires dye entry through the sensory terminal, consistent with passing through the sensory channels (Meyers et al., 2003).

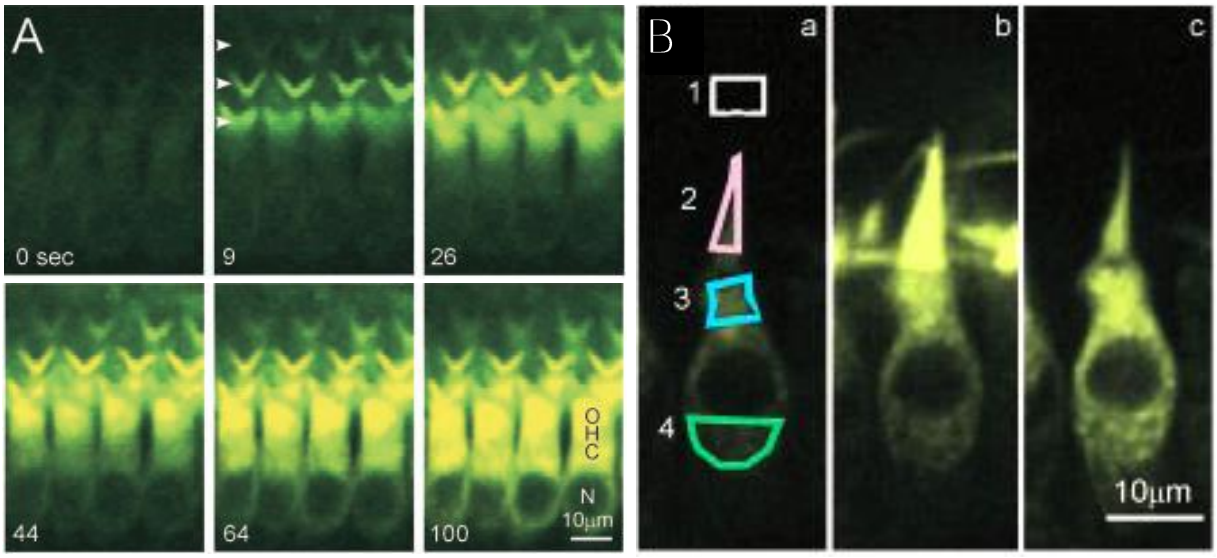

Figure 22 | FM1-43 rapidly fills the cytoplasm of mouse hair cells, entering from the tops and progressing to the bases of cells.

A, Confocal time series of FM1-43 labelling in cochlear OHCs removed from C3H/HeN mice. Dye spread through the cell within 60 seconds of application. Labelling begins with the hair bundles, three rows of which can be seen (arrowheads). Fluorescence then fills the cytoplasm of OHCs from the top down. B, Confocal images from a time series of FM1-43 libelling of mouse utricular hair cells, before FM1-43 (a), during FM1-43 staining (b), and during destaining (c). Regions indicate (1) medium, (2) hair bundle, (3) cell apex, (4) cell base. Reproduced from (Meyers et al., 2003).

2.5.2 FM1-43FX labelling protocol

The presence of functional mechanosensitive channels was confirmed using FM1 dye uptake assay. EBs were incubated in Advanced DMEM/F12 containing FM1 (5 μM final concentration; Invitrogen) for 1 min and then washed 3 times in Advanced DMEM-F12. EBs were dissociated to single cells by 40 minutes incubation in Accutase then added Advanced DMEM/F12 to inactivate Accutase. The cells were then plated onto slides by using the Cytopsin method. For nuclear staining Hoechst dye was used. The cells were imaged to confirm dye uptake and immediately fixed with 4% PFA. For some experiments, cells were fixed and stained with otic lineage associated antibodies as described in the section 2.4.1 to confirm the identity of hair

cells. Cells were examined using Nikon Ti Eclipse confocal microscope. Fields were chosen at random (n=5).

2.6 Electron microscopy

2.6.1 Basic concepts of Electron Microscopy

Electron microscopy (EM) is a type of microscope that uses a beam of electrons to create an image of the specimen. It allows a far higher resolution and has a greater resolving power than that obtained with a light microscope. The limit of resolution of a conventional light microscope is approximately 200 nm while that capable of EM is approximately 0.2 nm or less (Spence, 2013). The fundamental principle of EM is that electrons are used to illuminate the object and are focussed by electrostatic and electromagnetic lenses to form an image similar to how a light microscope uses glass lenses to focus light on or through a specimen to produce an image. (Spence, 2013). The greater resolution of EM over light microscopy occurs as a result of the electron having a much shorter wavelength than the light photon (Spence, 2013). There are mainly two different types of EM: scanning EM (SEM) and transmission EM (TEM).

2.6.2 Transmission electron microscopy (TEM) protocol

TEM was performed on day 36, 60, and 90 EBs fixed with 2% glutaraldehyde in 0.1M cacodylate buffer. Post fixation was performed at room temperature for 1 hour with 1% osmium and 1.5% potassium ferrocyanide. The samples were dehydrated in graded acetone and embedded in epoxy resin at 60°C. Half micron sections were stained with 1% toluidine blue and ultra-thin section were cut on Leica EM UC7 ultramicrotome and double stained with 1% uranyl acetate and lead citrate. The ultrastructual examination was performed with Philips CM 100 TEM at 100 kV. Digital images were recorded with an AMT40 CCD camera (Deben). TEM images were performed by Electron Microscope Labs at Newcastle University.

2.7 Flow cytometry

On day 90 of differentiation, the EBs stained with FM1 were dissociated after 40 minutes incubation in the Accutase solution, and the Accutase was inactivated using Advanced DMEM/F12 medium. Cell suspensions were then collected by centrifugation at 200xg for 5 minutes and washed with PBS. To make a single cell suspension in PBS, the cell mixture was passed through a 40 µm cell strainer (BD Biosciences), and incubated with 50 µg/ml propidium iodide (Sigma Aldrich) for dead cell labelling. Sorting was conducted with a BD FACS Aria IIu (BD Biosciences). Debris and cell clumps were excluded with two consecutive gating steps, followed by rejection of propidium iodide-positive cells. After sorting, cells were plated on coverslips in the N2 medium for electrophysiology recordings.

2.8 Electrophysiological recordings

2.8.1 Basic concepts of patch clamp techniques

The patch clamp technique was first introduced by Neher and Sakmann (Neher and Sakmann, 1976) to resolve currents through single acetylcholine-activated channels in cell-attached patches of membrane of frog skeletal muscle. Subsequent refinements of this method have led to techniques for high resolution recording of current in excised membrane patches in addition to those that remain cell-attached (Hamill et al., 1981). The patch-clamp recording technique (Figure 23) measures ionic currents under a voltage clamp and was designed to study small patches of membrane in which near-perfect control of the transmembrane voltage can be readily achieved (Langton, 2013). Today, this technique is most frequently used to characterize current flow through ionic channels, neurotransmitter receptors, and electrogenic transporters in cell types of virtually any origin (Langton, 2013).

Figure 23 │ The patch-clamp recording

The image shows the measurement of the OHC receptor potential with a patch-clamp capillary (from the left) due to stimulation of the hair bundle (capillary from the right). Figure adapted from http://www.imetum.tum.de/en/research-groups/bai/research/micromechanics/.

2.8.2 Electrophysiology recording protocol

On day 90 - 161 of differentiation, large lumen vesicles (about 600-mm diameter) were dissected from EBs. Two incisions were made using needles on the opposite side of the vesicle in order to expose and flatten the hair-cell-containing epithelium. The flattened epithelium was mounted onto round collagen-coated coverslips. The coverslips were transferred to the microscope chamber and immobilised using a nylon mesh fixed to a stainless steel ring. The chamber was continuously perfused with an extracellular solution containing (in mM): 135 NaCl, 5.8 KCl, 1.3 CaCl2, 0.9 MgCl2, 0.7 NaH2PO4, 5.6 D-glucose, 10 HEPES-NaOH, 2 Sodium pyruvate. MEM amino acids solution (50X), and MEM vitamins solution (100X) were added from concentrates (Fisher Scientific). The pH was adjusted to 7.48 (osmolality ~308 mmol kg 1). The cells were observed using an upright microscope (Leica DM LFSA) with Nomarski differential interference (DIC) contrast optics, using a 63X water-immersion objective. Whole-cell patch-clamp recordings were performed at room temperature using an Optopatch (Cairn Research) patch-clamp amplifier. Patch pipettes contained the following (in mM): 131 KCl, 3 MgCl2, 5 Na2ATP, 1 EGTA-KOH, 5 HEPES-KOH, 10 sodium phosphocreatine, pH 7.28 (osmolality ~295 mmol kg 1). For recording sodium currents in isolation, patch pipettes contained (in mM): 137 CsCl, 2.5 MgCl2, 1 EGTA-CsOH, 2.5 Na2ATP, 10 sodium phosphocreatine, 5 HEPES-CsOH, pH 7.3 (osmolality ~292 mOsmol kg 1). Patch pipettes were pulled to give a resistance in the range of 2-3 MΩ, and their tips were coated with surf wax (Mr. Zogs SexWax) to minimise the fast capacitive transient across the wall of the patch pipette. Immediately before recording, the series resistance (Rs) and the membrane capacitance (Cm) of the cell were noted.

Data were acquired through a CED Power 1401 data acquisition interface using Signal software (Cambridge Electronic Design) and stored on a computer for off-line analysis. Off-line analysis was performed using Origin (Origin Lab) data analysis software. For potassium current analysis, current amplitudes were measured from the steady-state current towards the end of the voltage step, before the tail currents emerged. For sodium current analysis, current amplitudes were measured at the peak of the sodium current. Electrophysiological recordings were performed by Professor Corne Kros's lab at Sussex University.

Chapter 3

Results

Differentiation of hESCs to otic lineages

Chapter 3. Differentiation of hESCs to otic lineages

To date, most attempts to derive inner ear hair cells and sensory neurons from hPSCs have resulted in inefficient or incomplete phenotypic and functional conversion of stem cells (Chen et al., 2012, Ronaghi et al., 2014). A key insight lacking from these previous studies is the importance of the 3D culture which may help to recapitulate *in vivo* development.

In this project, we used EB formation methods for otic lineage differentiation. Similar studies have shown that mouse inner ear sensory epithelia develop within EBs following *in vivo* developmental kinetics (Koehler et al., 2013). The generation of EBs used a serum-free media containing BMP4, TGF-β inhibitor, FGF2, and BMP inhibitor. In this chapter, we will discuss the stepwise differentiation of inner ear cells from hESCs in 3D culture under 4 different conditions: the mouse protocol (2.2.1), 2-mercaptoethanol high concentration protocol (2.2.2), 2-mercaptoethanol low concentration protocol (2.2.3) and KOSR high concentration protocol (2.2.4).

3.1 Differentiation of hESCs to inner ear cells using the mouse protocol

3.1.1 A timeline of mouse protocol

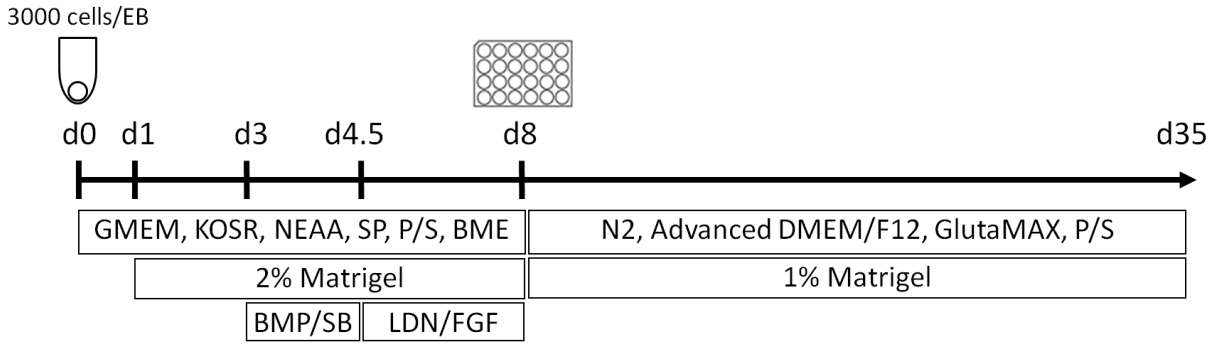

Figure 24 | Otic lineage guidance of hESCs using the mouse differentiation conditions published by Koehler et al (Koehler et al., 2013).

Schematic showing the different stages of the 35-day differentiation using the mouse protocol. GMEM: Glasgow's Minimal Essential Medium, KOSR: Knockout Serum Replacement, NEAA: Nonessential Amino Acids, SP: Sodium Pyruvate, P/S: Penicillin/ Streptomycin, BME: 2-mercaptoethanol, Advanced DMEM/F12: Dulbecco's Modified Eagle Medium/Ham's F-12, BMP: Bone morphogenetic protein 4, SB: SB-431542, LDN: LDN-193189, FGF: Fibroblast growth factor 2.

3.1.2 Analysis of differentiated hESCs under the mouse differentiation conditions

In 2013, Koehler et al. demonstrated that inner-ear sensory tissue is produced from mESCs under chemically defined conditions (Koehler et al., 2013). They showed that mESC EBs transform sequentially into non-neural ectoderm, preplacodal epithelium, otic-placode-like epithelia, otic sensory vesicles, and finally sensory epithelia vesicles containing functional hair cells. Before optimization of a protocol for hESCs, we applied the mouse protocol (Koehler and Hashino, 2014,

Koehler et al., 2013) to hESCs to determine the applicability of this protocol in the human system.

Initially, hESCs on Matrigel (a feeder-free system) were used to make EBs following the mouse protocol. In case of mESCs, there is no problem to survive as a single cell and they are easily aggregated as EBs within a few hours after seeding. However, unlike mESCs, hESCs did not form EBs and still stayed as dissociated single cells even 1 day after seeding on U bottom 96 well plates (results not shown). Moreover they usually formed hollow vesicles during the differentiation, and in that case it seemed like invagination which is important for otic vesicle formation was not occurring (Koehler and Hashino, 2014). To overcome these problems, we decided to use hESCs that were maintained on MEFs, because most of the published protocols about hESCs differentiation (Nakano et al., 2012, Ronaghi et al., 2014) used the cells cultured on MEFs. Using these cells, it was slightly more efficient to get healthy and aggregated EBs though these were morphologically different from mouse EBs. The complete role of these feeder cells is not known, but previous studies have showed that MEFs promote stem cell growth, including detoxifying the culture medium and secreting proteins that participate in cell growth (Lim and Bodnar, 2002). In our culture MEF especially somehow play an important role to improve connections between single hESCs although molecular mechanisms of MEF mediated hESC culture are still unsolved questions. Since culturing hESCs on MEF had advantages for EB aggregation and MEFs were easily removed by gelatin-coated plates before aggregating the hESCs, we decided to use this method for the rest of our studies.

The differentiation process was allowed to continue up to day 35 (Figure 24) that is 5 days longer than mESC differentiation considering different growth rate and differentiation rate between two species. It was difficult to culture the cells beyond day 35 because EBs were unstable and dissociated. To analyze differentiated cells, the samples were collected every 4 days. However, EBs were too small to get sufficient RNA for qRT-PCR and were too fragile to fix for immunohistochemistry. Even though we could not conclude anything about differentiated EBs on the basis of RNA and protein levels, one positive observation was that we observed otic vesicle-like structures similar to *in vivo* counterparts (Figure 7) in the EBs from around day 16 of differentiation (Figure 25D, G). Compared to the size of otic vesicles in 32 days human embryos (approximately 300 μm at their longest axis), the average size during hESC differentiation was approximately 15 times smaller. At days 16 - 24 of

differentiation, the average size of the vesicles was about 20 µm (Figure 25D - I) and at later times of differentiation sometimes we observed larger vesicles, up to about 40 µm (Figure 25J - L). In addition, the shape of the vesicles was also different from human embryos. *In vivo*, as soon as the otic pit is closed, otic vesicles start to elongate, however, the otic vesicle-like structure differentiated from hESCs were mostly spherical throughout the differentiation. Moreover, we failed to find other characteristics of otic lineage differentiation such as spiral ganglion cells which locate right near the otic vesicles during the development of the human embryo. From this, we concluded that the mouse protocol was not optimal for hESCs differentiation into inner ear cells.

To plan future experiments, differences between mouse and human had to be considered. Even though the protein-coding regions of the mouse and human genomes are 85% identical (Wasserman et al., 2000, Schwartz et al., 2003), there are still big differences between them that cannot be ignored such as developmental rates or signaling pathways. *In vitro*, one of the biggest differences between the mESCs and hESCs is the state of pluripotency. There are two phases of pluripotency: naive and primed (Nichols and Smith, 2009). Ground state naive pluripotency is established in the ICM and refers to ESCs *in vitro* (Nichols and Smith, 2009, Ying et al., 2008). Primed pluripotent cells are considered to be from the epiblast and can be differentiated into either the ectoderm, mesoderm, or endoderm lineages (Nichols and Smith, 2009). The main difference between the ESCs and epiblast stem cells (EpiSCs) is that EpiSCs are more readily differentiated by signaling cues than naive PSCs. Remarkably, hESCs are thought to retain a primed state of pluripotency and are thus analogous to mouse EpiSCs (Thomson and Marshall, 1998). So, hESCs differ significantly from mESCs in their culture requirements, morphology, clonogenicity, differentiation behavior, and molecular profile. Especially In this project, the gap in developmental timing is critical to understand the differences between the ways that mESCs and hESCs differentiate *in vitro*. In addition to differences of cell types, we realized that there are more factors that might have an effect on the differentiation of hESCs into otic lineages: shapes of plates (U or V bottom), basal medium (GMEM or DMEM/F12), cell numbers, the concentration of 2-mercaptoethanol and KOSR. Those factors were reflected to improve the protocols and these results will be introduced in the following sections.

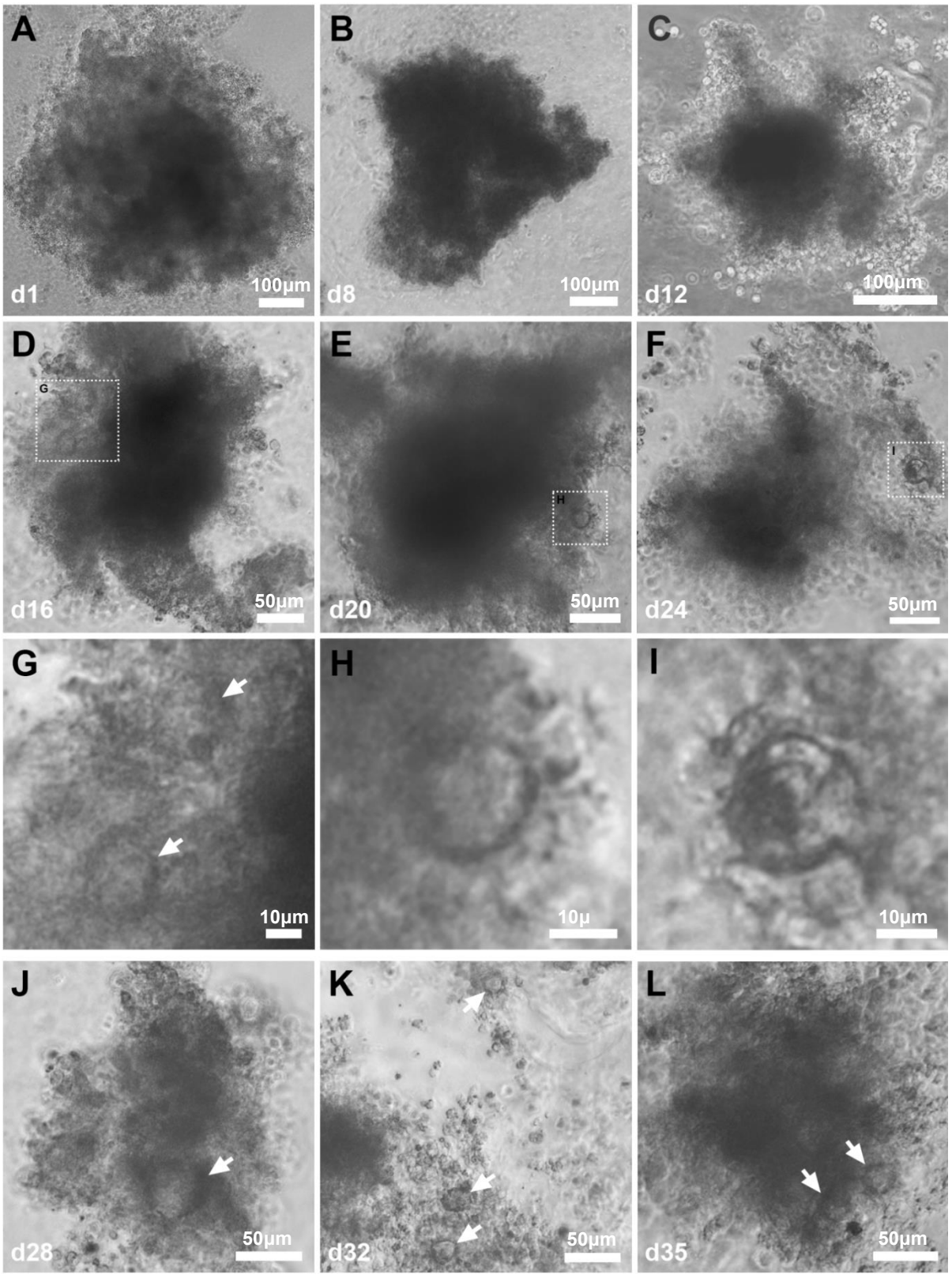

Figure 25 | Morphological changes during differentiation of hESCs under the mouse differentiation condition.

White arrowheads indicate possible otic vesicles. Picture shown are representative of at least 3 independent experiments (n=3).

3.1.3 Conclusions

- Unlike mESCs, hESCs do not form EBs well with protocols that use mouse medium.
- Even though otic vesicle-like structures are observed around day 16 of differentiation, EBs are fragile to be analyzed.
- To get better results, following factors should be considered: differences between cell types, shapes of plates (U or V bottom), basal medium (GMEM or DMEM/F12), cell numbers, the concentration of 2-mercaptoethanol and KOSR.

3.2 Differentiation of hESCs to inner ear cells using media with a high concentration of 2-mercaptoethanol

3.2.1. A timeline of high concentration of 2-mercaptoethanol protocol

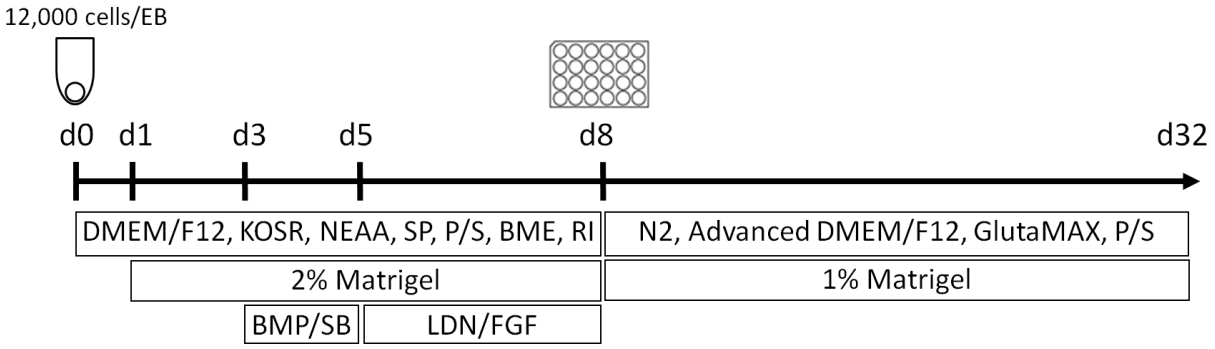

Figure 26 | Otic lineage guidance of hESCs under the high concentration of 2-mercaptoethanol condition.

Schematic showing the different stages of the 32-day differentiation using the high concentration of 2-mercaptoethanol protocol. DMEM/F12 Dulbecco's Modified Eagle Medium/Nutrient Mixture F-12, RI: Rock inhibitor.

3.2.2 Analysis of differentiated hESCs under the high concentration of 2-mercaptoethanol condition

To increase the survival rate of dissociated single hESCs and EB stability, Rock-I, Y-27632, was added to differentiation medium throughout days 0 – 8 (Watanabe et al., 2007, Krawetz et al., 2009). The effect of Rock-I was discovered by Yoshiki Sasai's team after examination of several caspase inhibitors, growth factors, trophic factors and kinase inhibitors (Watanabe et al., 2007). According to their data, dissociated hESCs treated with Rock-I are protected from apoptosis even in serum-free suspension culture and form floating EBs which we also observed. Unfortunately, even after treatment of Rock-I, most hESCs were still dissociated under the mouse differentiation medium (results not shown).

To solve those problems, we tried EB formation using differently shaped wells. Nakano et al. showed that the incomplete reaggregation of hESCs using a conventional U-bottomed well was solved by using a V-bottomed 96-well plate (Nakano et al., 2012). However, it was not completely helpful to aggregate the cells in our case. Instead, funnel-shaped V bottom plates helped by allowing pooling of all single hESCs using centrifugation. The day after spinning down the U-bottomed plates, cells were no longer splayed and formed sphere-like shapes. Despite improved physical aggregation, the resulting EB like structures were still different to those from mESC. It is possible that individual cells contacted each other, but perhaps the biological or chemical connection between them is less developed.

In view of this, we changed the basal medium from GMEM to DMEM/F12. Both GMEM and DMEM/F12 are serum-free, growth factor free basal media. Compared to GMEM, DMEM/F12 has a higher concentration of amino acids and vitamins. According to the manufacturer's description (Thermo Fisher Scientific), DMEM/F12 generally provides improved consistency in mammalian cell culture which results in better overall efficiency and more robust data, so DMEM/F12 is widely used for hESCs cultured on MEFs. However, it was unknown which basal medium was optimal for inducing otic lineages from hESCs, so it was worth trying to test both basal mediums. At the early stage of differentiation, cells looked healthier under the differentiation medium using DMEM/F12. Despite this, EBs were still fragile and disintegrated at later time points and were not useful to get sufficient RNA (results not shown).

For this reason, we increased cell numbers since higher cell density has been shown to correlate with EB stability during the differentiation of hESCs into optic cups (Nakano et al., 2012). Unlike a monolayer culture format, the number of aggregated cells is a critical factor in 3D culture, because EBs might receive various levels of signaling cues depending on their spatial region within the EB and the diffusion properties of molecules (Kinney et al., 2011). After increasing cell numbers, EBs were barely producing enough RNA for analysis though they were still not perfectly healthy like mouse EBs during the otic lineage differentiation. During the differentiation (Figure 26), the small numbers of otic vesicle-like structures appeared at days 12 - 16 (Figure 27A, B). Most of the vesicles formed on the surface of the EBs and each EB had at least one or two possible otic vesicles. Moreover the

average size of the vesicles were 60 – 80 μm which are larger than those under the mouse condition, but still 4 - 5 times smaller than human embryo counterparts.

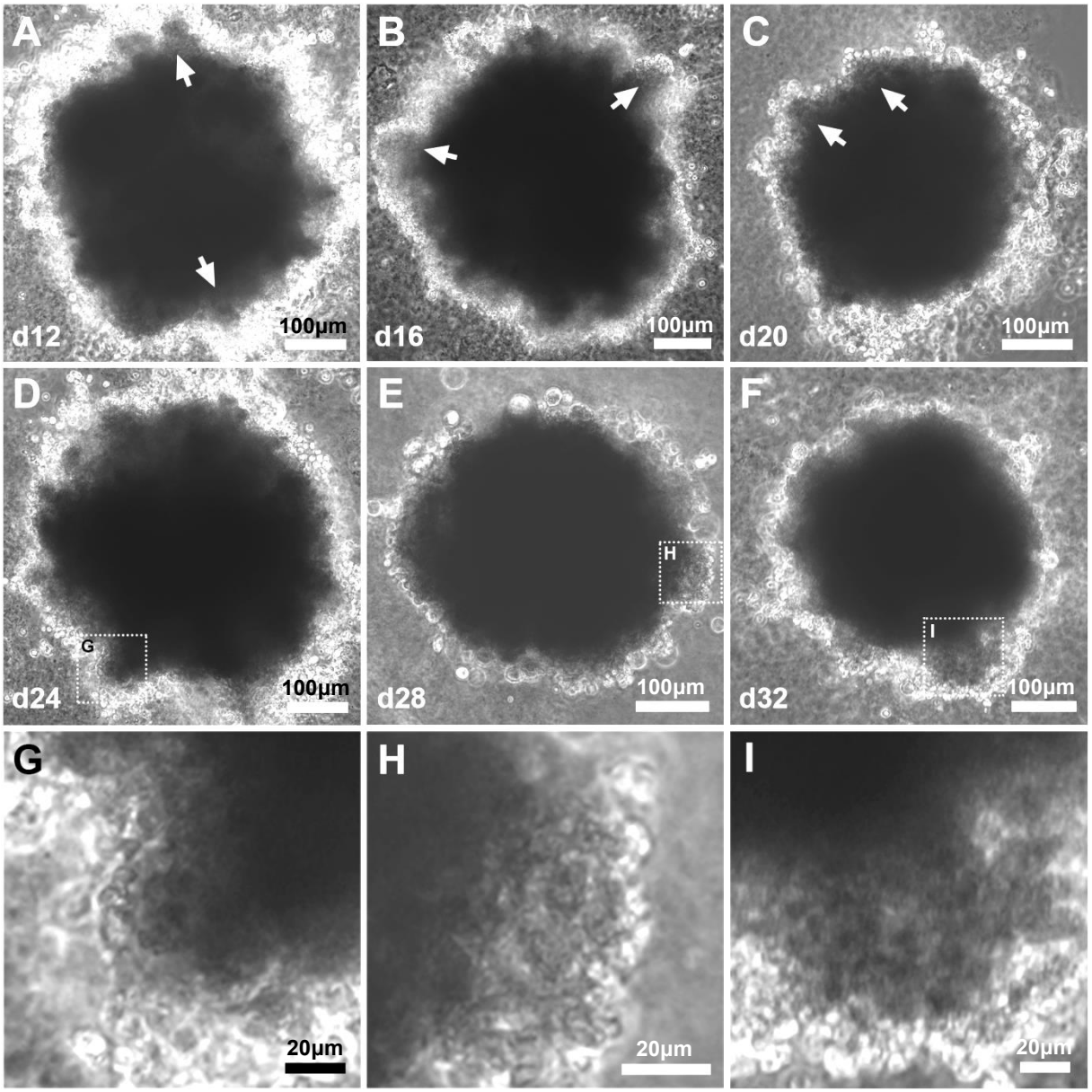

Figure 27 │ The inner ear cell induction of hESCs derived EBs under the high concentration of 2-mercaptoethanol condition.

Morphological changes during differentiation of hESCs. White arrowheads indicate possible otic vesicles. Picture shown are representative of at least 6 independent experiments (n=6).

Since it was difficult to isolate large quantities of RNA from the EBs, we have not been able to perform sufficient analysis; instead, we did the qRT-PCR analysis only for key genes involved in the otic differentiation process. Except *SIX1* which is one of the preplacodal ectoderm markers, all the other markers (preplacodal ectoderm marker (*DLX5*), anterior cranial placodes (*OTX2*), inner ear prosensory vesicles (*PAX8*), hair cells (*MYO7A, ATOH1, MYO6*), stereocilia bundles (*ESPIN*), and prosensory cells and supporting cells (*SOX2*)) were upregulated from day 16 or 20 (Figure 28). Upregulation of genes related to inner ear differentiation was exactly what we were seeking, but these data were not completely robust because of poor EBs.

Immunohistochemistry results also indicated some degree of otic differentiation as indicated by the presence of small numbers of putative MYO7A positive cells (Figure 29E, F). However we failed to find significant expression of other otic lineage markers: SOX2, PAX2, CCND1 (prosensory and supporting cells marker in mouse), JAG1 (prosensory and hair cell marker in mouse), BRN3C (a transcription factor required for hair cell survival and maturation in mouse), ESPIN, PAX8, and ATHO1 (Figure 29A, B, C, D, and G). The apparent lack of other otic lineage markers suggests that this protocol is not optimal for the differentiation of hESCs towards an otic lineage.

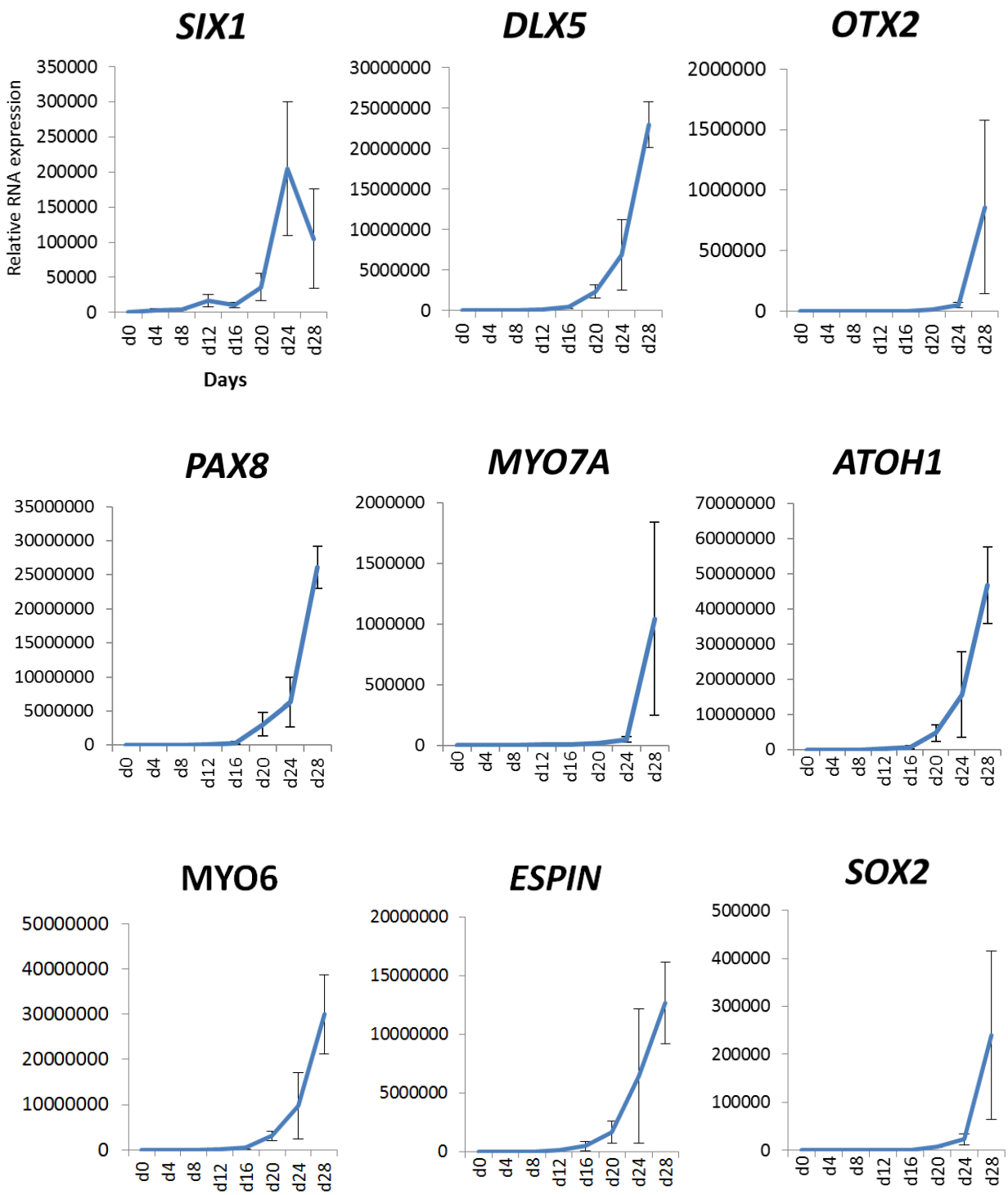

Figure 28 | qRT-PCR analysis.

qRT-PCR analysis of preplacodal ectoderm (*SIX1, DLX5*), anterior cranial placodes (*OTX2*), inner ear prosensory vesicles (*PAX8*), hair cells (*MYO7A, ATOH1, MYO6*), stereocilia bundles (*ESPIN*), and prosensory cells and supporting cells (*SOX2*) over the 28 days of differentiation (n=3; mean ±s.e.m).

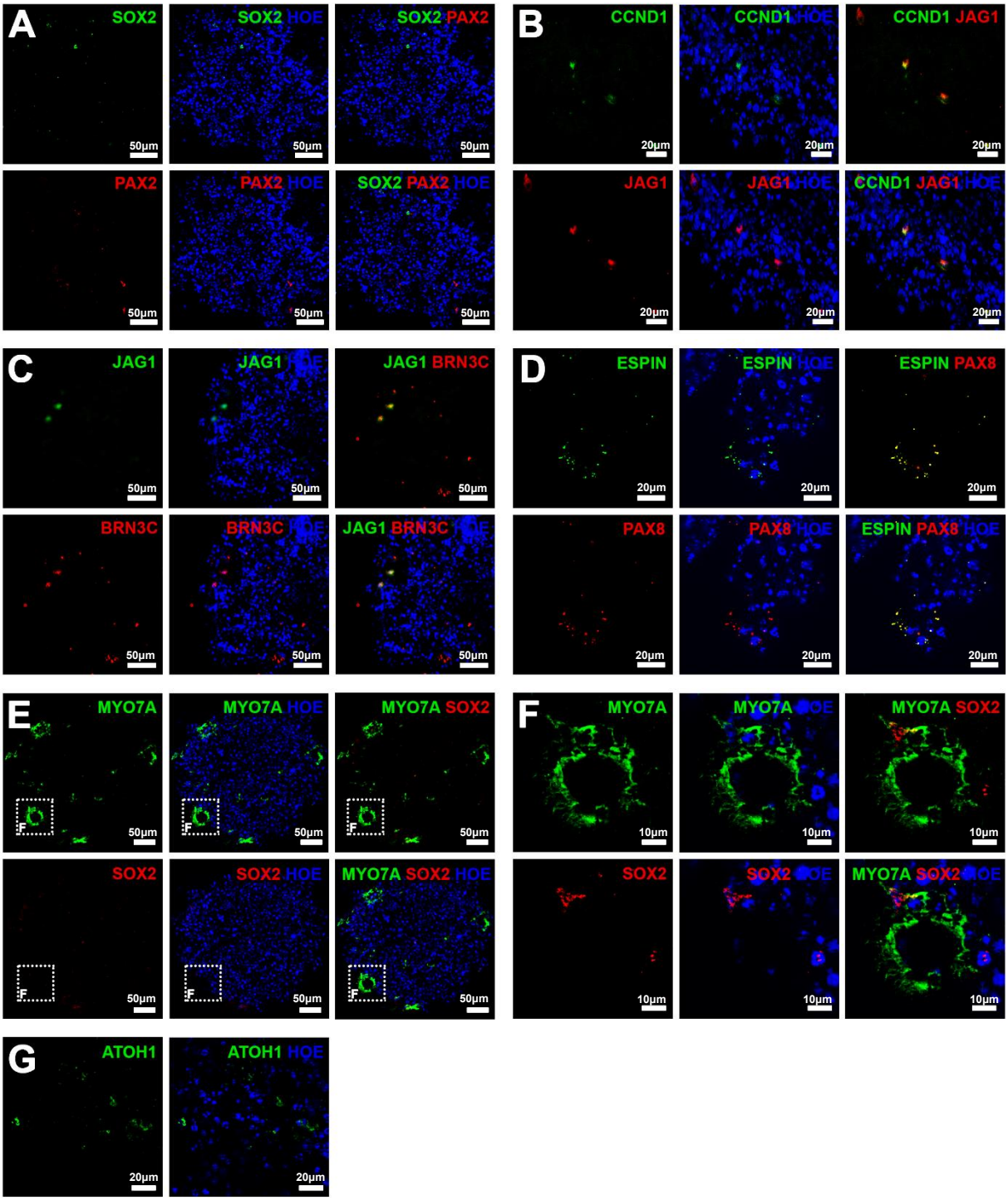

Figure 29 | Immunohistological analysis on day 32 under the high concentration of 2-mercaptoethanol condition.

MYO7A positive cells show the possible presence of hair cells (E, F), but most other otic lineage markers were negative or non-specific (A, B, C, D, G). Data are representative of 6 - 8 EBs from at least 3 separate experiments (n=3).

Among critical factors for otic differentiation as mentioned above, our analysis of the media composition used for differentiation of mouse ES cells indicated a possible problem with the concentration of 2-mercaptoethanol. The mouse protocol used more than 10 times higher concentration of this material compared with general human differentiation protocols (Nakano et al., 2012, Chen et al., 2012, Ronaghi et al., 2014). 2-mercaptoethanol has been known as a potent reducing agent used in cell culture medium to prevent toxic levels of oxygen radicals (Bevan et al., 1974). Since mouse cells are indeed very sensitive to oxidative metabolites 2-mercaptoethanol is principally used in culturing these cells (Bevan et al., 1974, Grill and Pixley, 1993). However, it was still unclear how variable concentrations of 2-mercaptoethanol affect the differentiation of hESCs which was a very important question because of side effects of excess 2-mercaptoethanol. Some proteins can be disrupted by 2-mercaptoethanol, which cleaves the disulfide bonds (S-S) that may form between thiol groups of cysteine residues (Hayakawa et al., 1996). So, in the case of excess 2-mercaptoethanol, both the tertiary structure and the quaternary structure of some proteins can be denatured by breaking the S-S bonds (Hayakawa et al., 1996). Because of its ability to disrupt the structure of proteins, it was used in the analysis of proteins to make sure that a protein solution contains monomeric protein molecules.

To find the appropriate 2-mercaptoethanol concentration for otic lineage differentiation from hESCs, we tested different concentration of 2-mercaptoethanol ranging from 0.1 mM to 1 mM. EBs did not compact well and looked fragile under high range 0.4 mM - 1 mM 2-mercaptoethanol condition (Figure 30). However, under the low concentration of it (0.1 - 0.2 mM), EBs were perfectly healthy and on day 16, they were at least 5 times bigger than those under the high concentration of 2-mercaptoethanol (Figure 30). Moreover, possible otic vesicles, comparable to human embryo counterparts (Figure 7), were observed under 0.1 and 0.2 mM 2-mercaptoethanol condition on day 24 and 32 of differentiation (Figure 30). Therefore, we have decided to analyze differentiated EBs using the low concentration of 2-mercaptoethanol protocol. Those analyzed data will be introduced in Chapter 3.3.

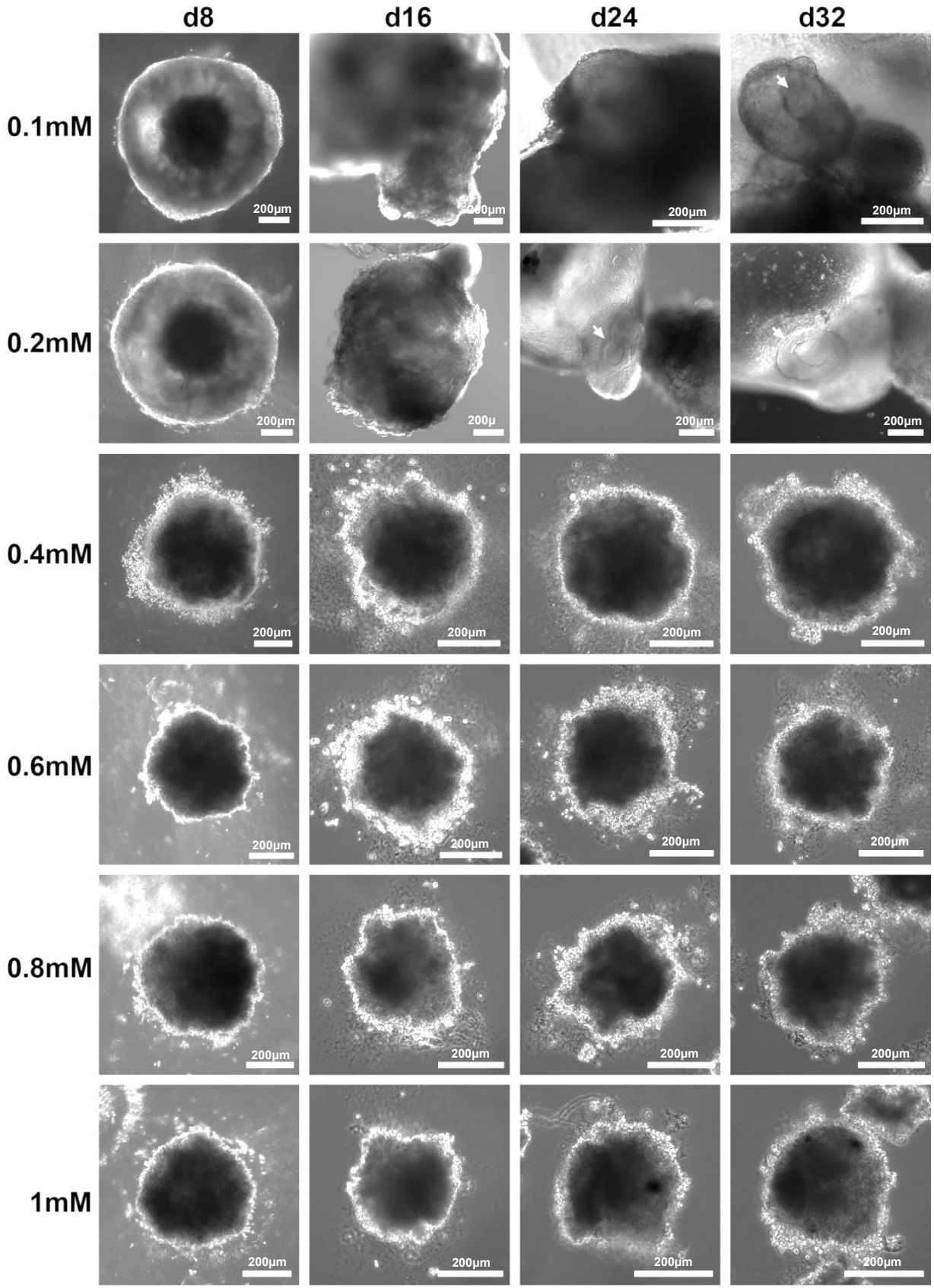

Figure 30 | Morphological changes at the various concentration of 2-mercaptoethanol condition.

White arrowheads indicate possible otic vesicles.

3.2.3 Conclusions

- Addition of Rock-I alone to defined culture media is not helpful for the EB stability.
- Centrifugation is helpful to form spherical shaped EBs.
- Changes of the basal medium from GMEM to DMEM/F12 only help at the early stage of differentiation to make healthy and compact EBs.
- Analysis of qRT-PCR and immunohistochemistry of differentiated EBs under high concentration of 2-mercaptoethanol condition shows this protocol is less likely optimal for the differentiation of hESCs towards an otic lineage.
- Among range from 0.1 mM to 1 mM 2-mercaptoethanol condition, EBs look fragile under high range 0.4 mM - 1 mM, but under low range 0.1 mM - 0.2 mM, hESCs are healthy and possible otic vesicles, comparable to human embryo counterparts, are observed on day 24, 32 of differentiation.

3.3 Differentiation of hESCs to inner ear cells using media with a low concentration of 2-mercaptoethanol

3.3.1. hESC differentiation protocol under low 2-mercaptoethanol concentration

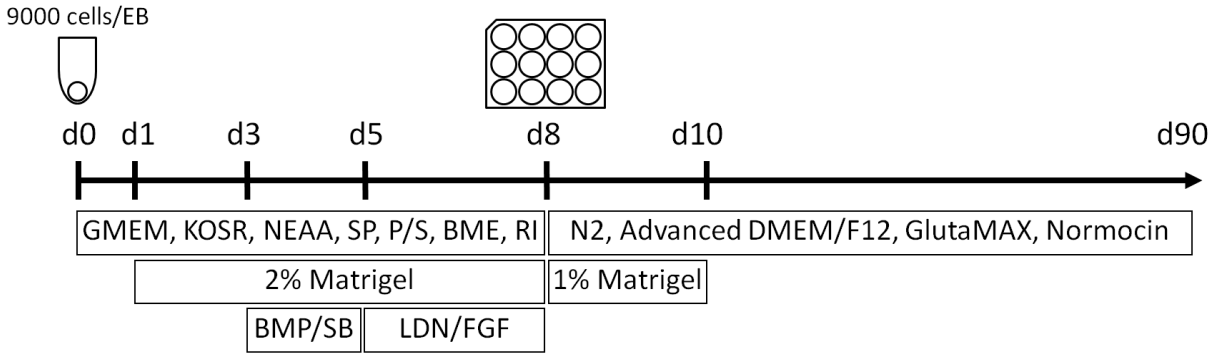

Figure 31 | Otic lineage guidance of hESCs under the low concentration of 2-mercaptoethanol condition.

Schematic showing the different stages of the 90-day differentiation using the low concentration of 2-mercaptoethanol protocol. In this protocol, Normocin was used instead of P/S from day 8 and 1% Matrigel lasts until day 10.

3.3.2. EB formation (d0 – d8)

Unlike EBs generated under the previous two conditions (the mouse protocol and high concentration of 2-mercaptoethanol protocol), there was no problem at all to aggregate cells and EBs were healthy under the low concentration of 2-mercaptoethanol condition. So, the EBs were induced towards otic lineage differentiation as described in the protocol (Figure 31). On day 1 of differentiation, half of the medium was removed from each well and fresh medium added including 2% growth factor reduced Matrigel, which promotes the development of epithelium on the surface of the EBs (Eiraku et al., 2011).

The cranial placodes including the otic placode are derived from the non-neural ectoderm. Suga et al. recently demonstrated that a non-neural ectoderm layer spontaneously arises on the outer most layer of the EBs by increasing the size of the mouse ESCs EB (10,000 cells per well or greater), leaving a neural layer underneath (Suga et al., 2011). Mimicking *in vivo* non-neural induction, their data suggested that endogenous BMP signaling probably mediates this process in 3D culture; however, the precise signaling mechanisms were unclear. Importantly, they also showed that treating smaller EBs with BMP4 induced non-neural markers. Therefore, on day 3 of differentiation, we treated BMP4 in EBs for induction of non-neural ectoderm. On the same day, we added SB-431542, which is a TGF-β inhibitor, for suppressing the mesendoderm lineage. It has been well known that TGF-β signaling plays a critical role in mesoderm induction, as well as previous studies show that TGF-β inhibition led to ectoderm differentiation from ES cells (James et al., 2005, Camus et al., 2006, Chambers et al., 2009). According to the recent study, subsequent BMP4 inhibition along with upregulation of FGF is necessary for non-neural cells to select a preplacodal ectoderm (Kwon and Riley, 2009, Kwon et al., 2010, Pieper et al., 2012). For this reason, we added BMP4 inhibitor LDN-193189 and FGF2 on day 5 for otic lineage induction. On day 8 of differentiation, EBs were transferred to a serum-free floating culture to allow self-guided differentiation. During this phase of culture, P/S had to be replaced with normocin, which does not contain aminoglycosides. Aminoglycosides such as streptomycin are toxic to inner ear hair cells and ampicillin would be another suitable alternative.

3.3.3. Prosensory vesicle formation (d8 – d20)

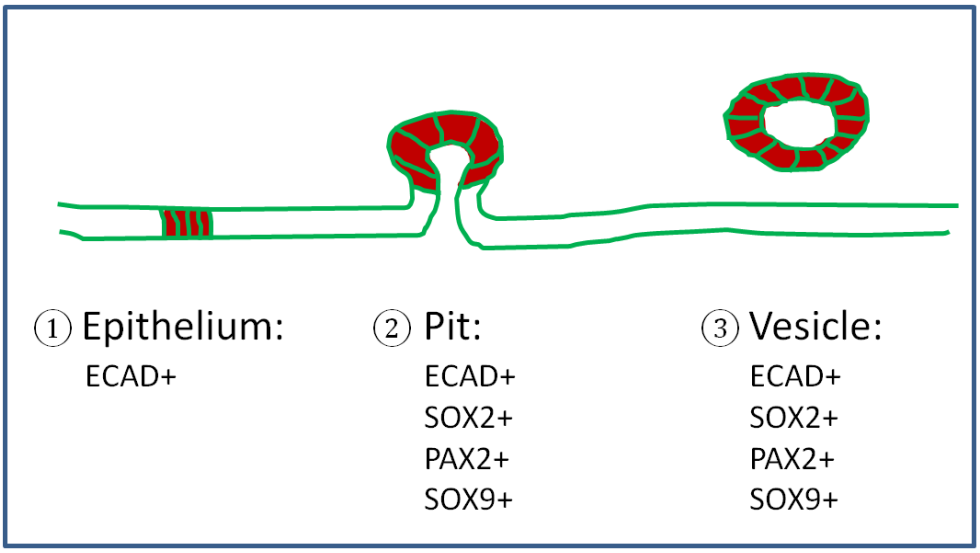

Figure 32 | Overview of otic vesicle formation and marker genes.

During days 16 – 20 of differentiation, we observed the unclosed otic pit like structures and closed vesicles as well (Figure 33A, E, and F). The average size of the vesicles on day 20 was 143.125 µm (Figure 36). During mESC differentiation towards inner ear sensory epithelia, co-expression of Pax2, Pax8, Ecad, and Sox2 indicates the 3 steps of vesicle formation: epithelium, pit, and vesicle (Koehler et al., 2013). Unfortunately, specific antibodies for early stages of fetal development of the human cochlea are missing. It has been only confirmed that, SOX2 expression is restricted to the human prosensory domain and all cells of the cochlear duct epithelium express SOX9 at 10 WG (Locher et al., 2013). So, most antibodies were selected based on the mouse data and deduced from expression patterns of fetal OC. Day 20 EBs were visualized the formation of possible otic vesicles by co-expression of ECAD/SOX2 (Figure 34A, E, and G), PAX2/ECAD (Figure 34B, H), SOX9/ECAD (Figure 34C, I), and SOX9/SOX2 (Figure 34D, F, and J). Unlike W10, SOX9 expression was relatively weak in possible otic pit and vesicles *in vitro* (Figure 34I, J). PAX2 expression was also observed in prosensory vesicles and near the vesicles as well (Figure 34H). We assume that those $PAX2^{+}$ cells not confined to the vesicles are progenitors of neurons. Collectively, we presumably concluded that each ECAD, SOX2, PAX2, and SOX9 alone is not perfect, but altogether those markers are good enough to show human otic vesicle formation.

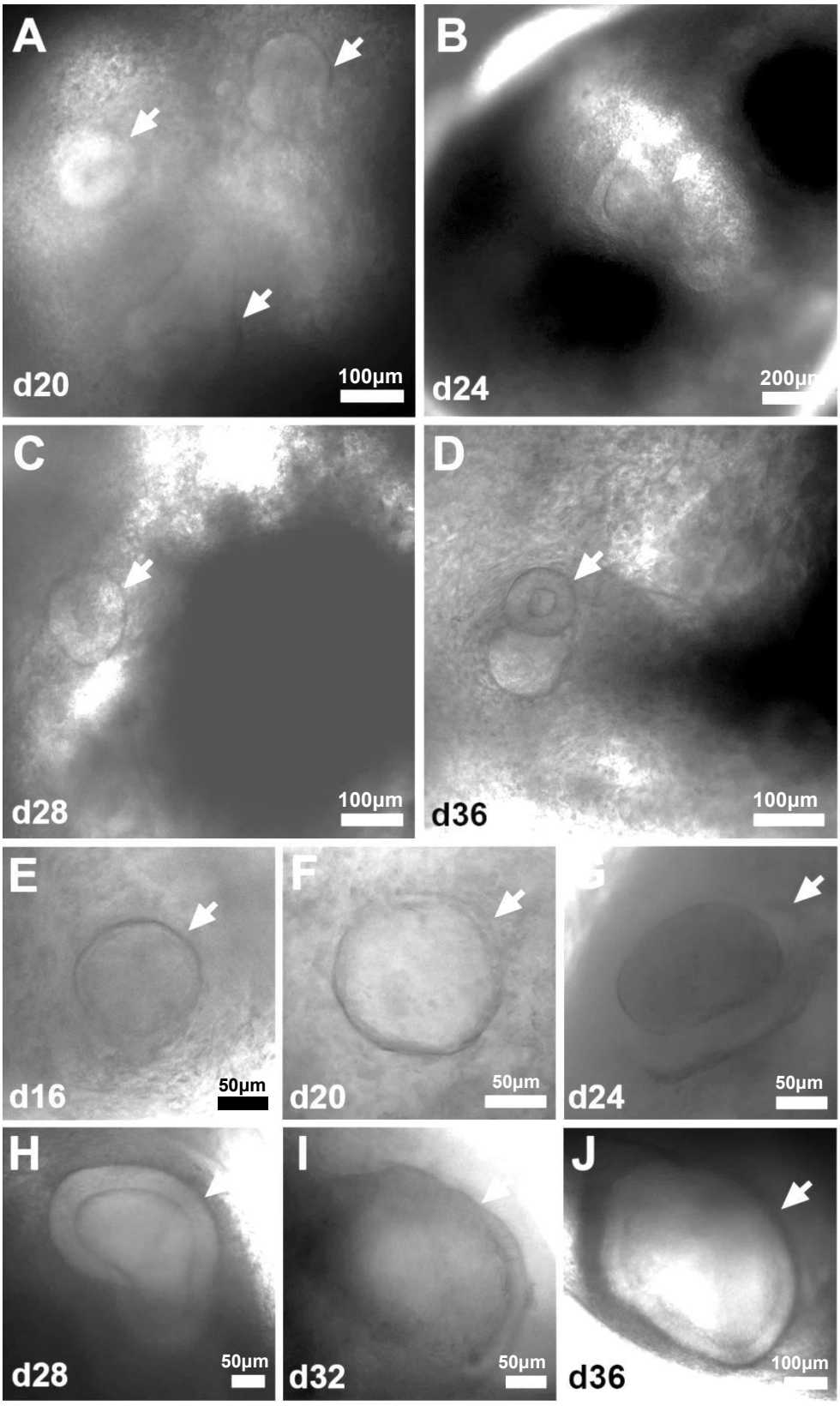

Figure 33 | Morphological changes during differentiation of hESCs.

White arrowheads indicate possible otic vesicles. Pictures shown are representative of at least 7 independent experiments (n=7).

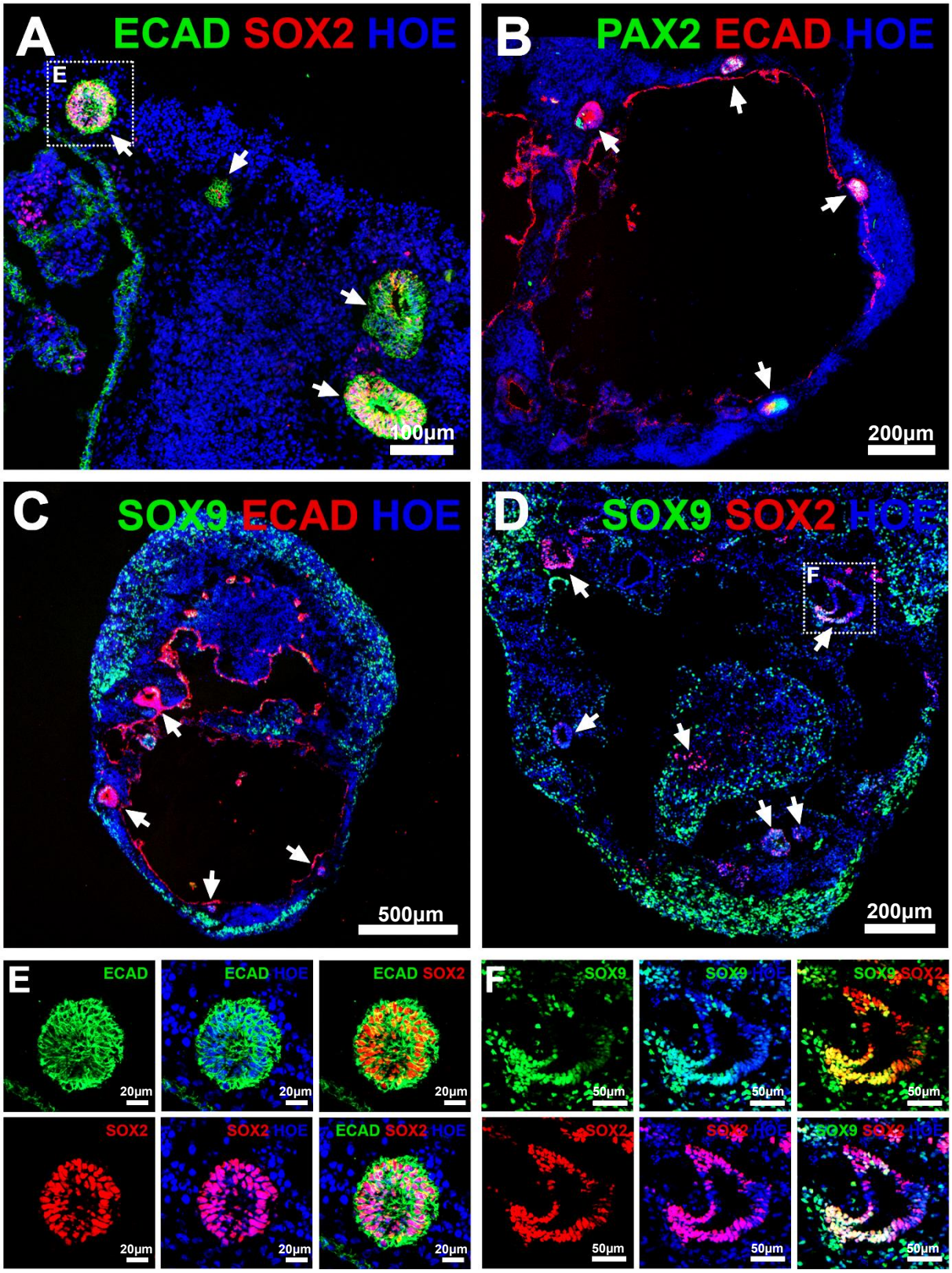
A
ECAD SOX2 HOE
E
100μm
B
PAX2 ECAD HOE
200μm
C
SOX9 ECAD HOE
500μm
D
SOX9 SOX2 HOE
F
200μm
E
ECAD
ECAD HOE
ECAD SOX2
SOX2
SOX2 HOE
ECAD SOX2 HOE
20μm
F
SOX9
SOX9 HOE
SOX9 SOX2
SOX2
SOX2 HOE
SOX9 SOX2 HOE
50μm

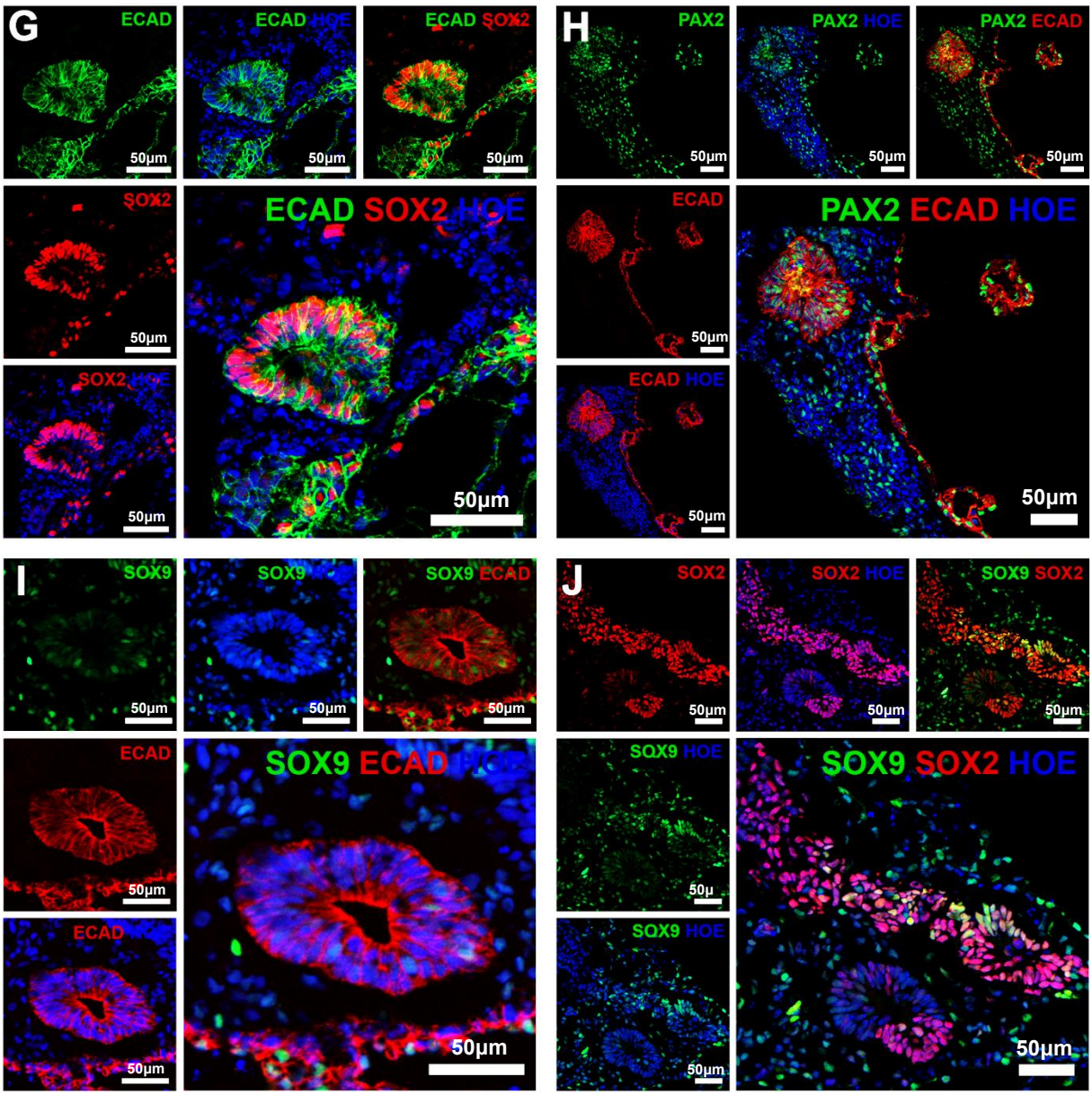

Figure 34 | Immunohistological analysis in the formation of possible otic vesicles (d20).

Co-staining with ECAD, PAX2, SOX9, and SOX2 shows the vesicle formation from the epithelium. White arrowheads indicate possible otic vesicles. Data are representative of 8 - 16 EBs from at least 4 separate experiments (n=4).

3.3.4. Prosensory otic vesicles (d36)

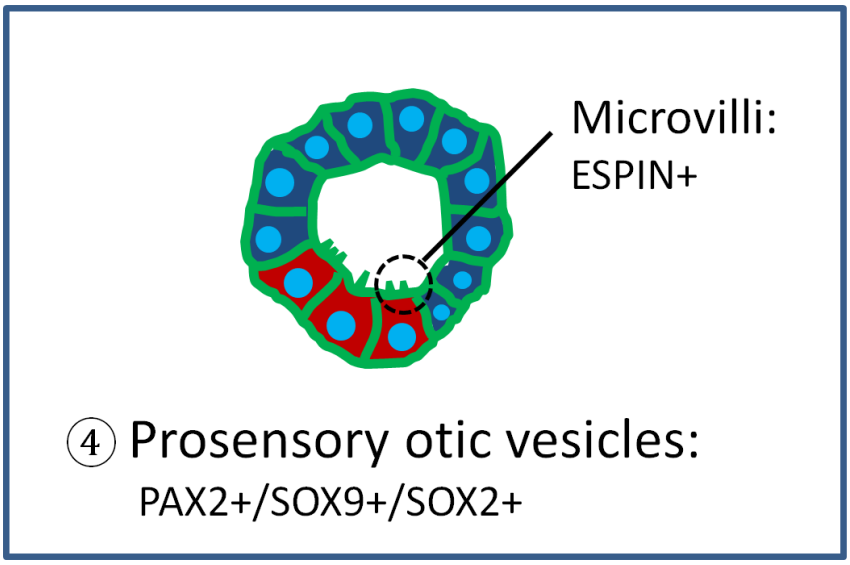

Figure 35 | Overview of prosensory otic vesicles and marker genes.

All inner ear cells, including the cochlear hair cells, supporting cells, and sensory neurons, arise from a common neurosensory domain within the otic vesicle (O'Rahilly, 1963, Moore and Linthicum, 2007). In the E9.5 mouse, prosensory otic vesicles are defined by the expression of Pax2, Pax8, Ecad, Sox2, Jag1, cD1, and Myo7a (Koehler et al., 2013). However, in humans, the neurosensory domain of the otic vesicle can be recognized very early in development by the expression of SOX2 (Kiernan et al., 2005). Also, it has been confirmed that W10 of developing cochlea express SOX9, SOX10, and PAX2 (Locher et al., 2013, Pechriggl et al., 2015). At this stage, there are no morphological signs of hair cell differentiation meaning no MYO7A positive cells yet. On day 36 of differentiation, we observed 404.167 µm size of otic vesicles like structures (Figure 33D, J and 36) which are slightly bigger than otic vesicles on day 32 embryo (Figure 7). Immunohistochemistry data show that those vesicles contain $PAX2^{+}/SOX2^{+}$ (Figure 37A) and $SOX9^{+}/SOX2^{+}$ cells (Figure 37B). Like *in vivo* study, there were no MYO7A positive hair cells yet at this stage (results not shown).

According to a recent paper about the anatomical development of the human inner ear, microvilli are observed before they are replaced by stereocilia at 9 - 11

WG (Lim and Brichta, 2016). On day 36 of differentiation relevant to stages before 9 WG, we found cells in the possible otic vesicles started to express EPSIN which is a stereocilia specific marker (Figure 37C, D). To test whether those are real microvilli, TEM was used. These TEM data will be introduced in chapter 5. For inducing more matured hair cells with stereocilia bundles, we decided to extend the time for culturing the cells.

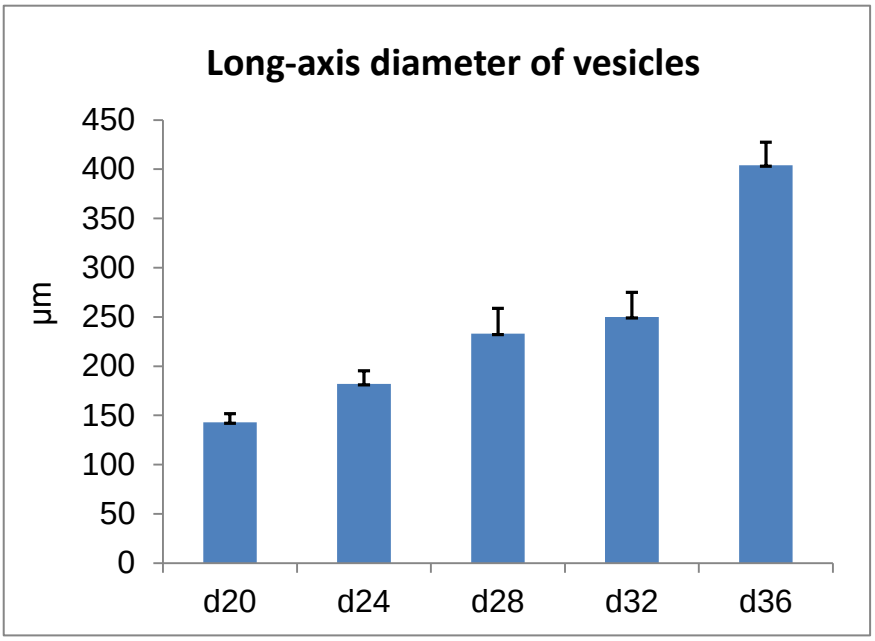

Figure 36 | Size of vesicles during differentiation of hESCs.

Long-axis diameters of the day 20, 24, 28, 32, and 36 otic vesicles derived from hESCs. Data are representative of 8 - 16 EBs from at least 3 separate experiments (n=3).

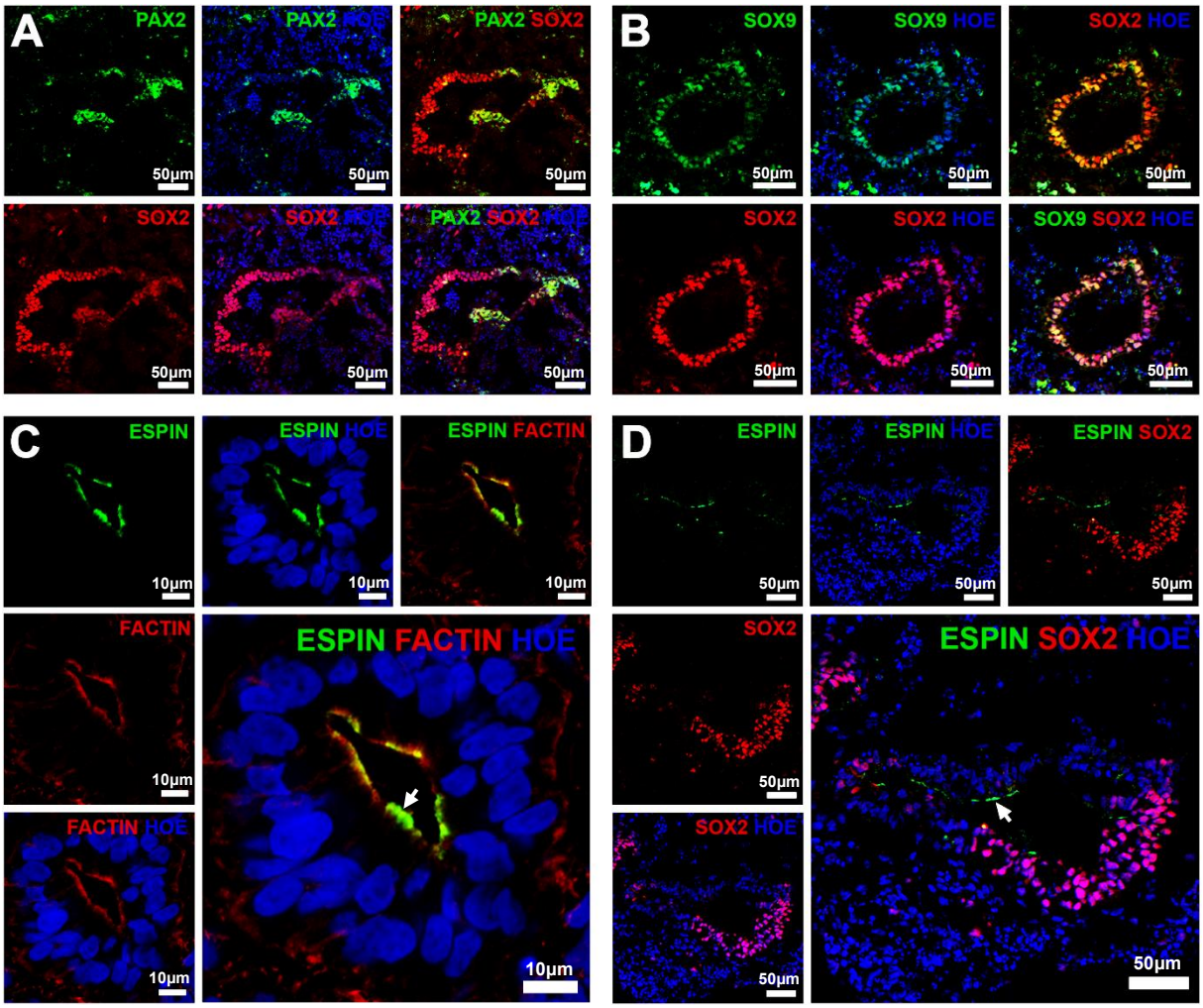

Figure 37 | Immunohistological analysis in the prosensory otic vesicle-like structures (d36).

A, B, At day 36 of differentiation, possible prosensory cells in the vesicles express PAX2, SOX9, and SOX2. C, D, Prosensory cells also start to express ESPIN which is a stereocilia (white arrows) specific marker. Data are representative of 8 - 16 EBs from at least 6 separate experiments (n=6).

3.3.5. Induction of early hair cells / supporting cells and auditory neurons (d60)

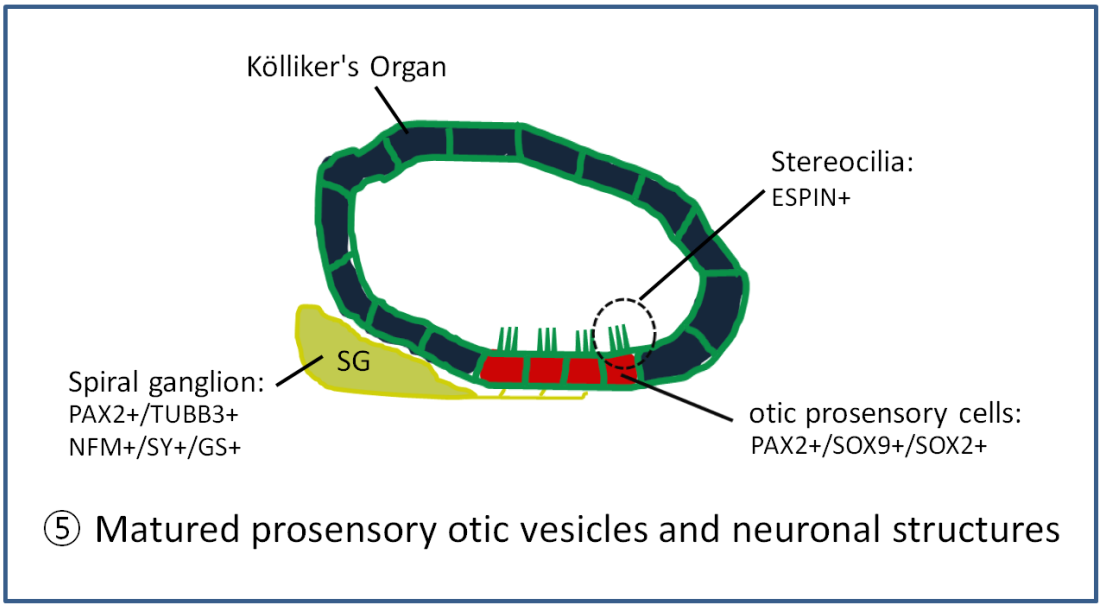

Figure 38 | Overview of matured prosensory otic vesicles and neuronal structures.

During mESC differentiation, maturing mouse prosensory otic vesicles (d16) express Jag1, Sox2 in both supporting cells and hair cells, while Myo7a, Brn3c and cD1 expression in confined to hair cells and supporting cells, respectively (Koehler et al., 2013). However, gene expression patterns are slightly different in human. During human development at 12 WG, the SOX2-positive prosensory domain is developing into the OC and cochlear hair cells are visible from basal to apex gradient (Locher et al., 2013). As maturation of hair cells, both IHCs and OHCs show specific downregulation of SOX2, SOX9, and SOX10, whereas the supporting cells underneath the hair cells remained positive for SOX2, SOX9, and SOX10 (Locher et al., 2013). Unlike SOX genes, PAX2, known as one of the earliest genes contributing to the inner ear development, is still positive in both IHCs and OHCs (Pechriggl et al., 2015). Lastly, MYO7A, which is the most specific marker of hair cells, confirms the otic lineage specification *in vivo* (Locher et al., 2013).

On day 60 of differentiation, matured otic vesicle-like structures expressed SOX2, SOX9, and PAX2 (Figure 39A, B, and 38B, C, K, O). Interestingly, the

innermost layers of some vesicles had a weak expression of SOX2 and SOX9, which are destined to be hair cells (Figure 39B). Whereas the outer layer still remained SOX2 and SOX9 expression and these cells will be supporting cells in the future mimicking *in vivo* development (Figure 39B). Co-staining of MYO7A and SOX2/SOX9 labelled hair cells and supporting cells, respectively (Figure 39C, E). Also, a cluster of otic vesicle-like structures was observed (Figure 39D). Those vesicles were visualized by ESPIN immunohistochemistry and $ESPIN^{+}$ stereocilia were protruding from the apical end into the lumen (Figure 39D).

In mouse, around E8.5, transient expression of Ngn1 occurs in cells which become inner ear neurons within the prosensory domain of the otic vesicles. Ngn1 promotes the expression of genes involved in inner ear neurogenesis, such as NeuroD, GATA3, Islet1, and Pou4f1 (Fritzsch, 2003, Ma et al., 2000, Raft et al., 2007). Then inner ear neuroblasts begin to divide into SGNs and VGNs promoted by GATA3 (Appler et al., 2013). In the case of human, from 8 weeks of development, precursors of SGNs delaminate from the ventral otic epithelium and are enveloped by peripheral glial cells (PGCs) after differentiation and maturation (Sher, 1971, Lawoko-Kerali et al., 2004). PGCs originate from the neural crest and migrate along nerve fibers to the spiral ganglion. Once they reach their target location, they differentiate via Schwann cell precursors into myelinating and nonmyelinating Schwann cells as well as satellite glial cells (Pechriggl et al., 2015).

As prosensory otic vesicles mature, cells of a neuronal lineage started to appear near the otic vesicles at day 60 of differentiation (Figure 40). SOX2 has been found to play a big role during early auditory neuron development in promoting otic epithelial cells into a proneurosensory lineage (Dabdoub et al., 2008, Puligilla et al., 2010). In addition to SOX2, PAX2, an early marker for hair cell differentiation, also participates in the establishment of the auditory neurons through upregulation of Neurogenin1 (Lawoko-Kerali et al., 2004). We found that differentiating neurons within the putative spiral ganglion exhibited a strong immune-positivity for PAX2 (Figure 40C, D, O, and P). To further evaluate the potential of hESCs to differentiate into the lineage of auditory neurons, the expression of a number of key genes (β-III-tubulin, Neurofilament, Synaptophysin and Glutamine synthetase) was analyzed. Detection of the neuron-specific marker, β-III-tubulin (TUBB3) in cells projecting toward the putative sensorineural epithelium (Fig 38A, B, and C) and also in the putative spiral ganglion (Figure 40D) suggests the possibility that neurons may be

“attempting” to establish a synaptic connection with cochlear hair cells. Similarly, positive staining for neurofilament (NFM) showed the presence of bipolar neurons (Figure 40E – H). Synaptophysin (SY), known as the major synaptic vesicle protein p38 in neuronal cells, was present in cells projecting into the greater epithelial ridge and reached the sensory epithelium (Figure 40I, J, and K). It was also highly expressed in possible spiral ganglion (Figure 40L). *In vivo*, glutamine synthetase (GS) is expressed by satellite glial cells (SGCs), which tightly envelope the SGNs. SGCs are responsible for micro-environmental and electrophysiological properties maintaining valid signal transmission (Hanani, 2005). We found strong expression of GS expressed in the sensory epithelium (Figure 40M, N, and O) together with the spiral ganglion (Figure 40P). Taken together, we observed precursors of neurons ($PAX2^+$ and $SOX2^+$ cells) and putative auditory neurons ($TUBB3^+$ and NFM^+ cells) at the same time on day 60 of differentiation. This may represent different neurosensory progenitor subpopulations or progenitors at different stages of differentiation, but for better understanding, further analysis is required. Nevertheless, these findings indicate that this protocol for the differentiation into cochlear hair cells is capable of differentiating hESCs toward a neurosensory lineage as well.

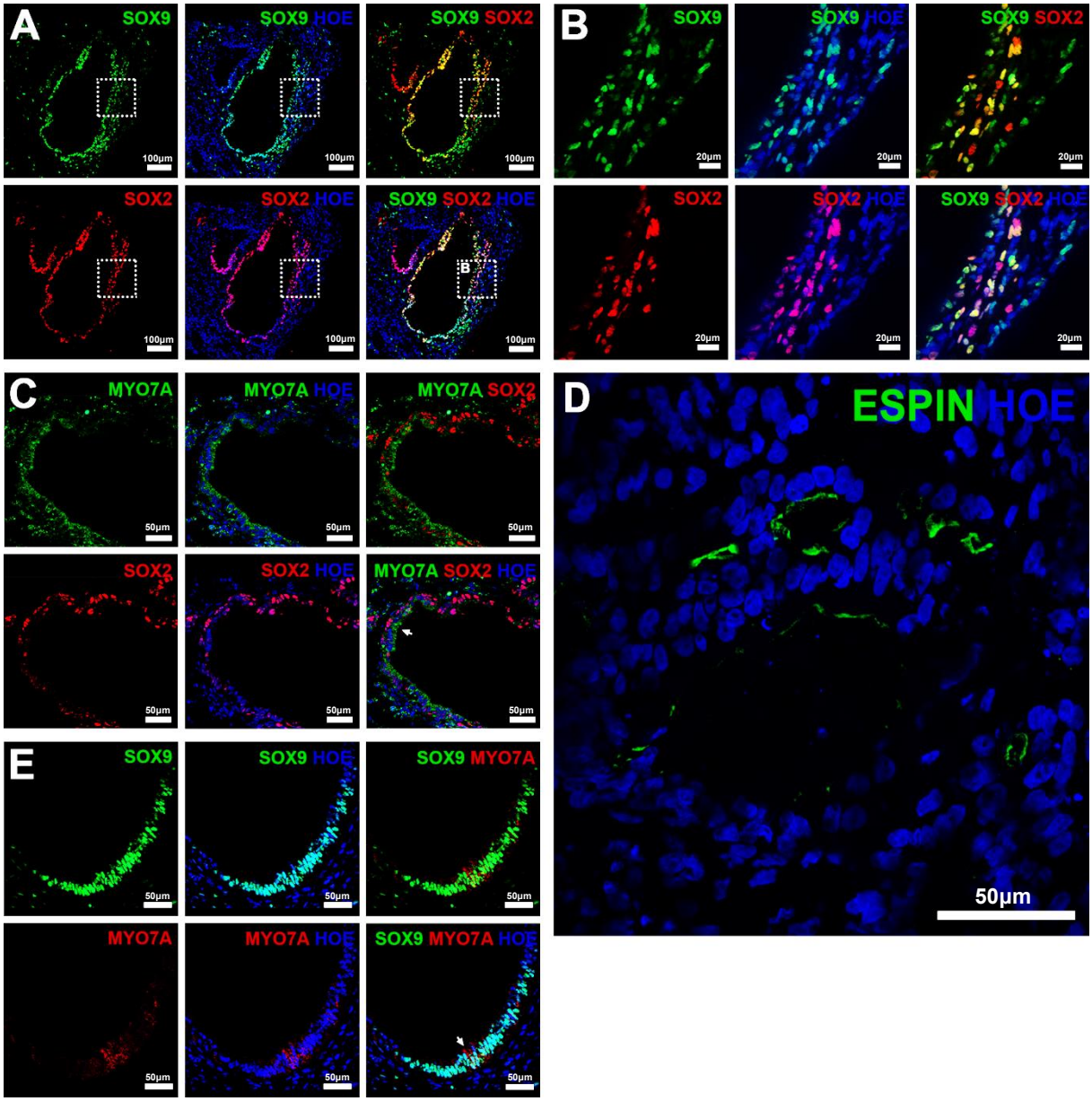

Figure 39 | Immunohistological analysis of the possible matured otic vesicles (d60).

A, B, Co-staining with SOX9 and SOX2 shows a precursor of possible hair cells and supporting cells. C, E, Maturing prosensory otic vesicles express MYO7A in putative hair cells, while expression of SOX2 and SOX9 is confined to possible supporting cells. D, Cluster of otic vesicles is visualized by expression of ESPIN. Data are representative of 8 - 16 EBs from at least 6 separate experiments (n=6).

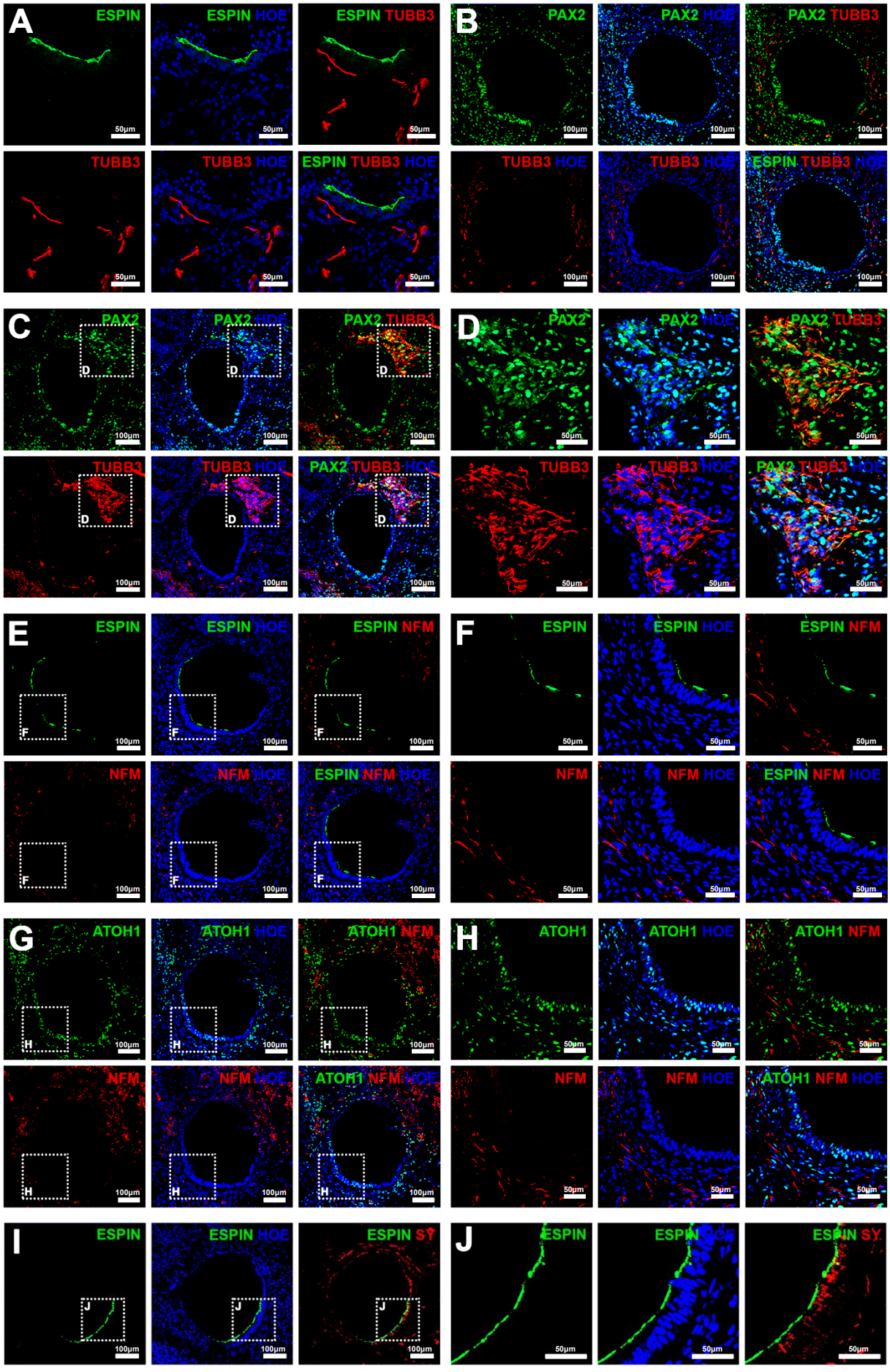
A
ESPIN
ESPIN HOE
ESPIN TUBB3
TUBB3
TUBB3 HOE
ESPIN TUBB3 HOE
B
PAX2
PAX2 HOE
PAX2 TUBB3
TUBB3
TUBB3 HOE
ESPIN TUBB3 HOE
C
PAX2
PAX2 HOE
PAX2 TUBB3
TUBB3
TUBB3 HOE
PAX2 TUBB3 HOE
D
PAX2
PAX2 HOE
PAX2 TUBB3
TUBB3
TUBB3 HOE
PAX2 TUBB3 HOE
E
ESPIN
ESPIN HOE
ESPIN NFM
NFM
NFM HOE
ESPIN NFM HOE
F
ESPIN
ESPIN HOE
ESPIN NFM
NFM
NFM HOE
ESPIN NFM HOE
G
ATOH1
ATOH1 HOE
ATOH1 NFM
NFM
NFM HOE
ATOH1 NFM HOE
H
ATOH1
ATOH1 HOE
ATOH1 NFM
NFM
NFM HOE
ATOH1 NFM HOE
I
ESPIN
ESPIN HOE
ESPIN SY
J
ESPIN
ESPIN HOE
ESPIN SY
100μm
50μm

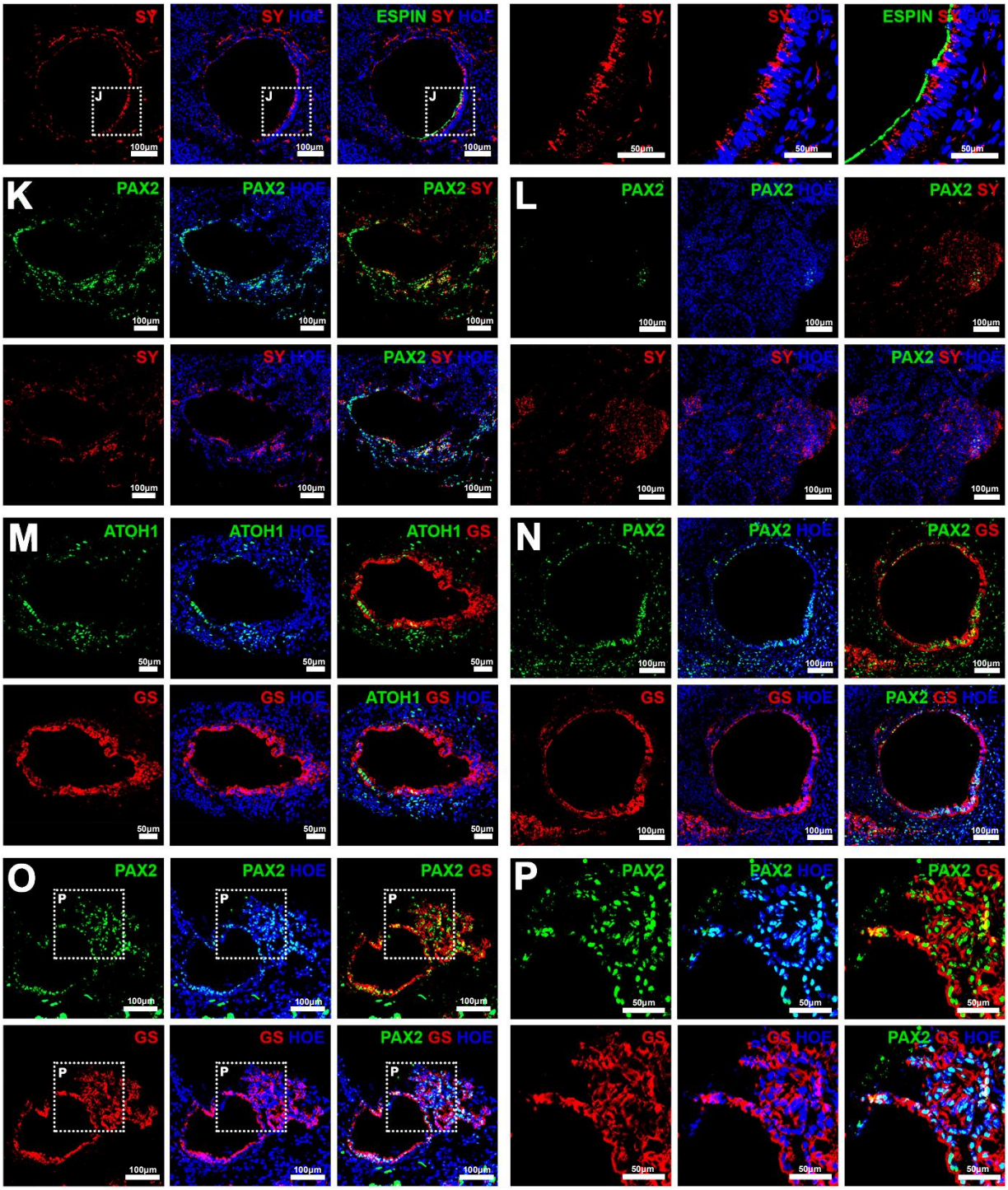

Figure 40 │ Immunohistological analysis in the possible auditory neurons (d60).

Expression of β-III-tubulin (TUBB3), neurofilament (NFM), synaptophysin (SY), glutamine synthetase (GS) and PAX2 in the cells of neuronal lineage on day 60 of differentiation. Data are representative of 8 - 16 EBs from at least 6 separate experiments (n=6).

3.3.6. Maturation of hair cells / supporting cells (d90)

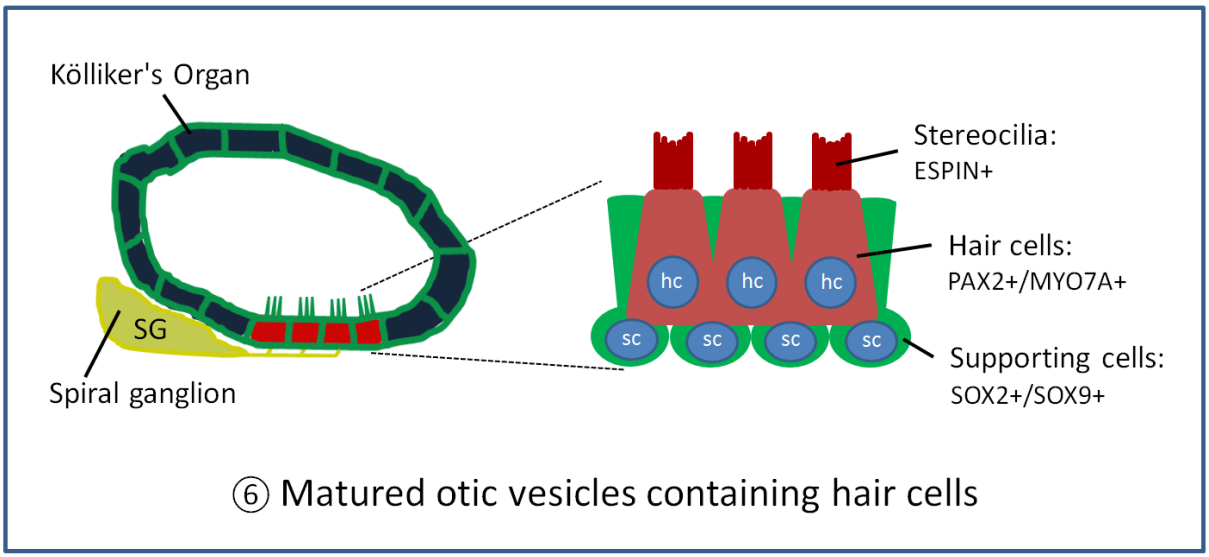

Figure 41 | Overview of matured otic vesicles containing hair cells and supporting cells

There are four distinct populations of hair cells in the inner ear; type I and type II in the vestibular organs and IHCs and OHCs in the cochlea. We wished to reveal which type of hair cells populated the hESC derived sensory epithelia. Previous studies have suggested that expression of Sox2 and Pax2 may distinguish vestibular from cochlear hair cells in mouse and chicken respectively (Oesterle et al., 2008, Warchol and Richardson, 2009). In our culture system, SOX2 expression was not detected in possible hair cells (Figure 42A). *In vivo*, oncomodulin (Ocm) was found in mouse type I vestibular hair cells and had a more diffuse subcellular localization throughout the hair cell body (Simmons et al., 2010). Immunoreactions to Ocm have been also detected in mouse OHCs, but it was localized preferentially to the basolateral outer hair cell membrane and to the base of the hair bundle (Simmons et al., 2010). Expression of OCM labelled possible stereocilia bundles of $MYO7A^{+}$ hair cells suggests the possibility of the presence of OHCs, though not all the cells expressed OCM (Figure 42B). Otopetrin1 (Otop1) has been known as specific to peripheral supporting cells of vestibular epithelia in mouse (Kim et al., 2010). However, it is not known whether, in humans, OTOP1 is specifically expressed in vestibular supporting cells, but it has been reported that OTOP1 is required for

normal formation of otoconia which is biomineral particles related to the process of detecting gravity and acceleration in the inner ear (Jang et al., 2006). In addition, it has been confirmed that expression of the calcium-binding protein calbindin2 (Cb2) uniquely labels type II hair cells in mouse (Koehler et al., 2013). The hESC derived hair-cell-like cells did not express both OTOP1 and CB2 (Figure 42C – E).

Compared to animal models, the protein expression to identify hair cell types has been less characterized in humans. Nevertheless, it has been reported that both IHCs and OHCs express PARVALBUMIN (PV) in the human cochlea (Rask-Andersen et al., 2009); however, whether PARVALBUMIN is localized to vestibular hair cells is unknown. Previous studies have also shown that expression of the PRESTIN uniquely labels human OHCs and not vestibular hair cells (Rask-Andersen et al., 2009). PRESTIN was predominantly expressed in the OHC basolateral plasma membrane and responsible for cell body contraction, increasing cochlear sensitivity and frequency resolution (Rask-Andersen et al., 2009). On day 90 of differentiation, nearly all hESC-derived $ESPIN^+$ hair-cell-like cells were PV^+ (Figure 42G) and some of the hair cells expressed PRESTIN suggesting a presence of OHCs again (Figure 42F). Moreover, at this stage of $MYO7A^+$ hair cells were innervated by $TUBB3^+$ neurons (Figure 42H).

It seems like expression pattern of transcription factors is evolutionally well conserved, but not all the data from animals apply to human. For example, unlike avian, PAX2 expression has been shown to persist in both vestibular and cochlear hair cells in human (Johnson Chacko et al., 2016, Locher et al., 2013). Therefore, further investigation will be needed to elucidate protein expression patterns of four types of hair cells in human. Despite this, the profile of current expression strongly suggests that the hESC derived EBs have adopted at least a cochlear OHC phenotype.

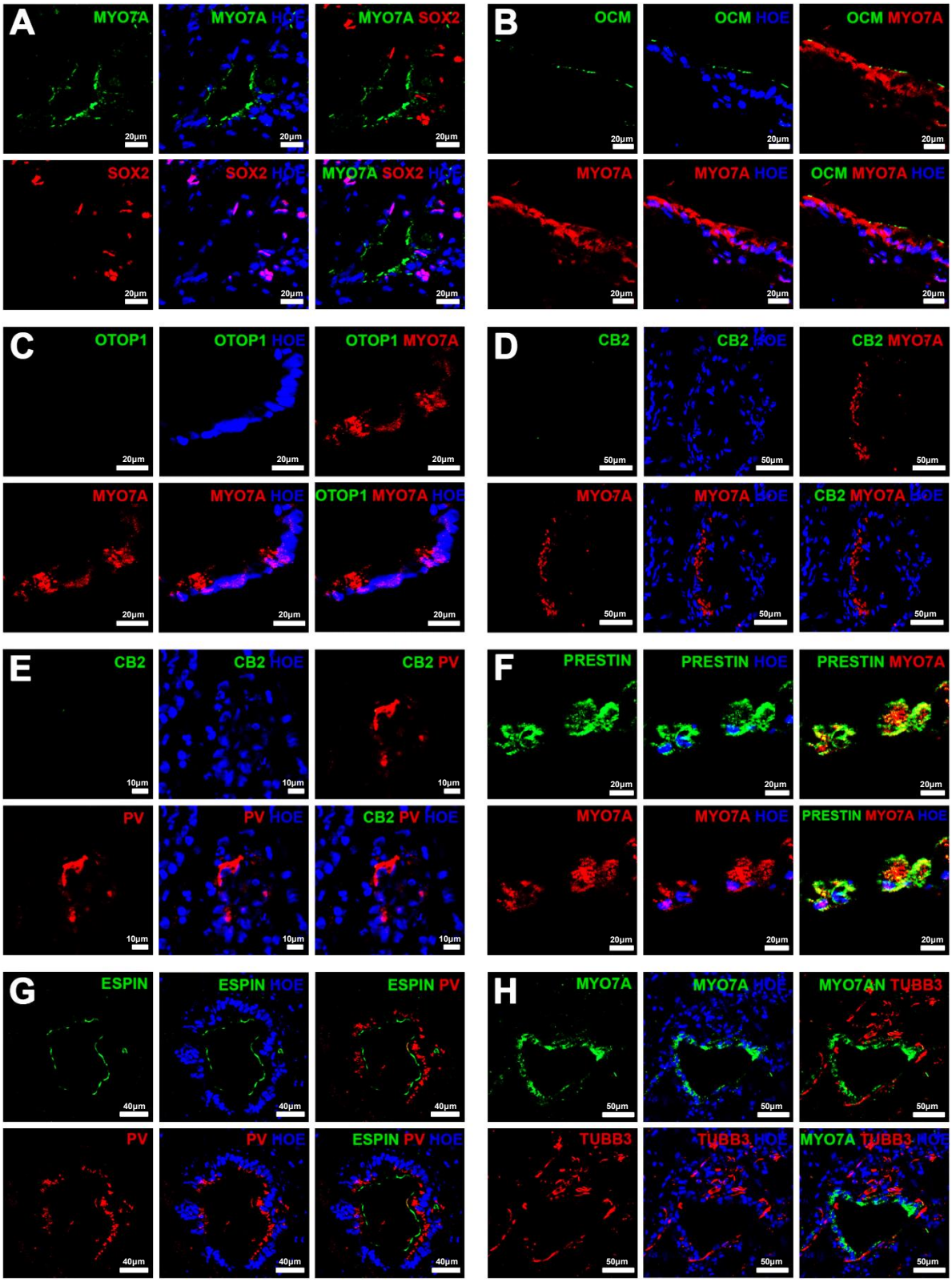

Figure 42 │ Immunohistological analysis to identify cell types (d90).

A – H, Expression of MYO7A, SOX2, OCM, OTOP1, CB2, ESPIN, PRESTIN, PV and TUBB3 in the matured otic vesicles on day 90 of differentiation. Data are representative of 16 EBs from at least 3 separate experiments (n=3).

3.3.7 Conclusions

- On day 20 of differentiation, the formation of possible otic vesicles is visualized by co-expression of ECAD, PAX2, SOX2, and SOX9.
- On day 36 of differentiation, microvilli ($ESPIN^+$) come out from the possible otic vesicles.
- On day 60 of differentiation, matured otic vesicle-like structures containing prosensory cells ($PAX2^+$, $SOX2^+$, and $SOX9^+$) and neuronal structures ($PAX2^+$, $TUBB3^+$, NFM^+, SY^+, and GS^+) are observed.
- From day 60 of differentiation, possible hair cells ($PAX2^+$, $MYO7A^+$) and supporting cells ($SOX2^+$, $SOX9^+$) start to appear.
- hESC derived EBs are likely to adopt a cochlear OHC phenotype.

3.4 Differentiation of hESCs to inner ear cells using media with a high concentration of KOSR

3.4.1. A timeline of high concentration of KOSR protocol

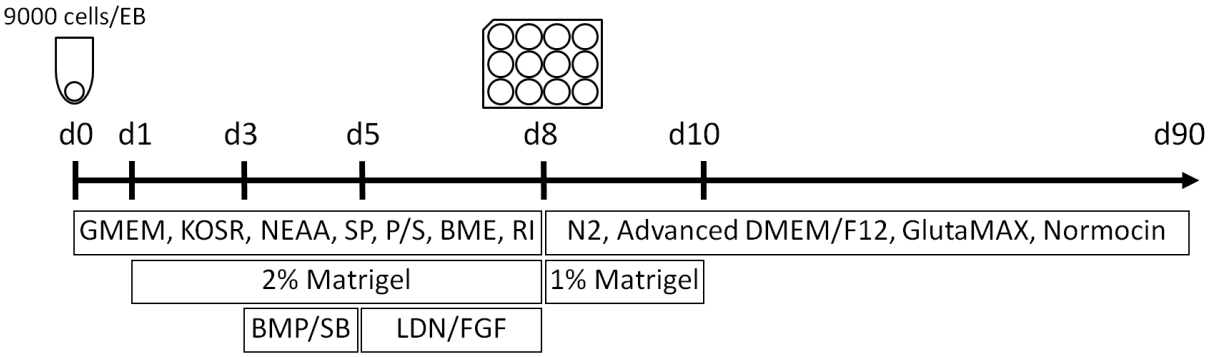

Figure 43 | Otic lineage guidance of hESCs under the high concentration of KOSR condition.

Schematic showing the different stages of the 90-day differentiation using the high concentration of KOSR protocol. In this protocol, 20% KOSR and Wnt inhibitor, IWR-1, were additionally used.

3.4.2. Analysis of differentiated hESCs under the high concentration of KOSR condition

Recent studies have demonstrated how optic cups and retina can be faithfully reconstituted *in vitro* by culturing hESCs (Nakano et al., 2012). In this paper, they showed hESCs efficiently formed retinal epithelium at high KOSR concentrations and addition of Wnt inhibitor to counteract the caudalizing activity of high KOSR (Lu et al., 2009). KOSR is a defined medium supplement that is optimized to grow PSCs and is suitable for replacing FBS. Before the development of KOSR, FBS was the only option for nutritive supplementation of ES media, but FBS contains many undefined and variable components which promote spontaneous differentiation, so each lot should be tested for its ability prior to use. Many different types of cells including

hESCs on MEF are usually more stable in the higher concentration serum supplemented medium than a low concentration of it. As inner ear shares a common precursor with retina (Nakano et al., 2012, Eiraku et al., 2011), the definitive ectoderm, and high concentration of KOSR improves cell viability, we also tested high concentration of KOSR (20% KOSR) condition parallel with low concentration of 2-mercaptoethanol condition introduced in the previous chapter.

Except for addition of IWR-1 and 20% KORS, this high concentration of KOSR protocol (Figure 43) is the same as the low concentration of 2-mercaptoethanol condition (Figure 31). Around day 20 of differentiation, otic like vesicles started to form (Figure 44A, E and F) showing an average size of 136.25 μm (Figure 45). From 12 days later, more EBs developed possible otic vesicles (Figure 44 C, D, I, and J) and their average size was 247.5 μm (Figure 45) comparable to otic vesicles on 32 days of human embryonic development (Figure 7). To test whether those vesicles develop into cells of the otic lineages, we examined differentiated EBs by using otic vesicle specific antibodies. On day 36 of differentiation, the emerging possible otic vesicles under the high concentration of KOSR condition expressed prosensory markers such as PAX2, SOX9, and SOX2 (Figure 46A, B). Notably, expression of the stereocilia marker ESPIN was found in possible otic vesicles (Figure 46C, D) and 3D confocal microscope images more clearly showed protruding individual microvilli from the possible otic vesicles (Figure 46E, F). Collectively, these data suggest that differentiation day 36 may represent a stage of maturing prosensory otic vesicles. On day 60 of differentiation, otic vesicle-like structures still expressed PAX2, SOX9, and SOX2 (Figure 47A, B, and E), but there were no MYO7A positive cells (Figure 47C, D). And we also failed to find low expression of SOX2 and SOX9 cells which are destined to be supporting cells (Figure 47A, B). These immature otic vesicles caused poor development of neural structures as well, because all inner ear cells including hair cells, supporting cells, and neuronal cells originate from a common neurosensory domain within the otic vesicle. Immunohistochemistry analyzed data showed some positive cells of neuronal markers such as GS, SY, and TUBB3, but most of them did not make a connection with sensory epithelium (Figure 47C – H).

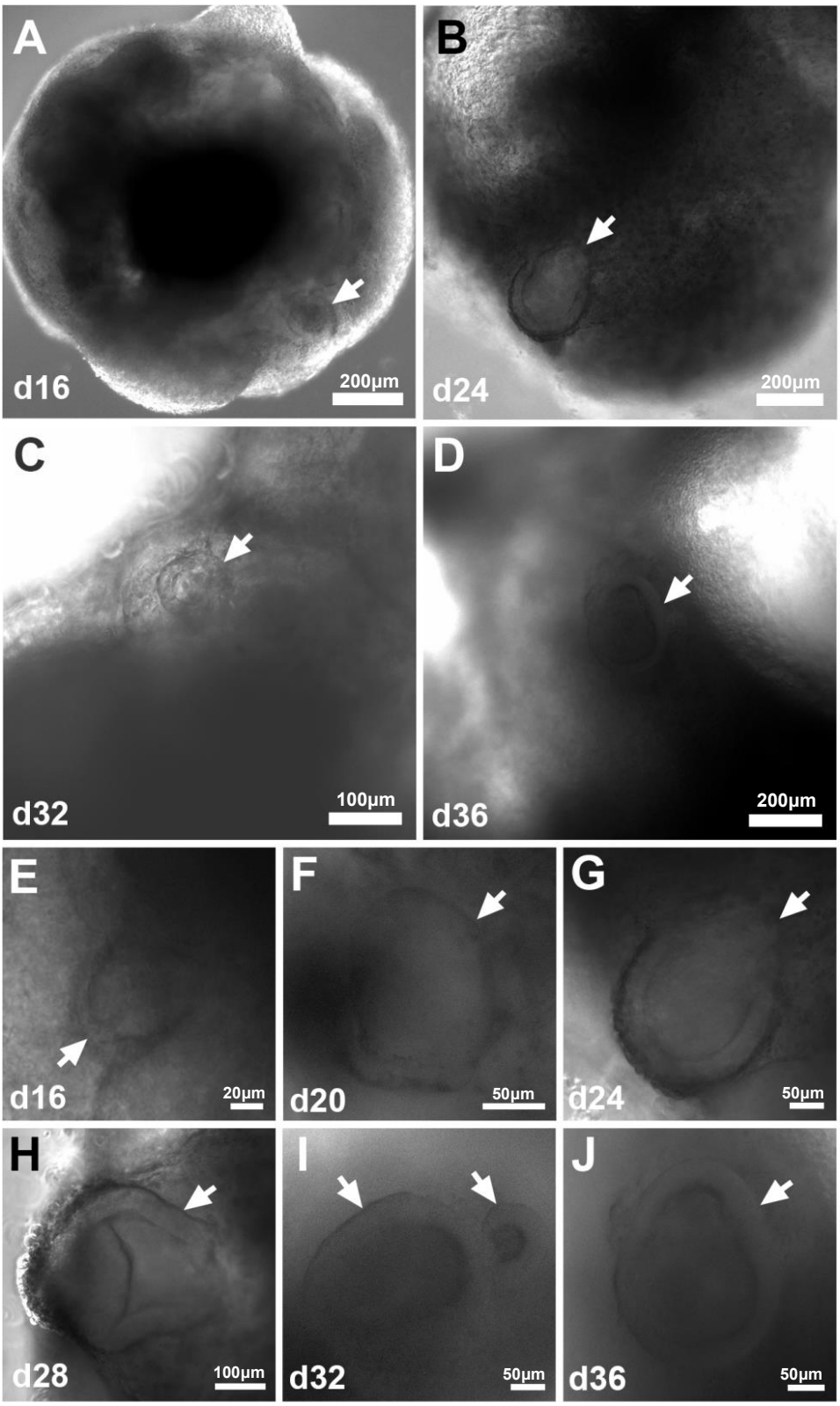

Figure 44 │ The inner ear cell induction of hESCs derived EBs.

Morphological changes during differentiation of hESCs. White arrowheads indicate possible otic vesicles. Pictures shown are representative of at least 8 independent experiments (n=8).

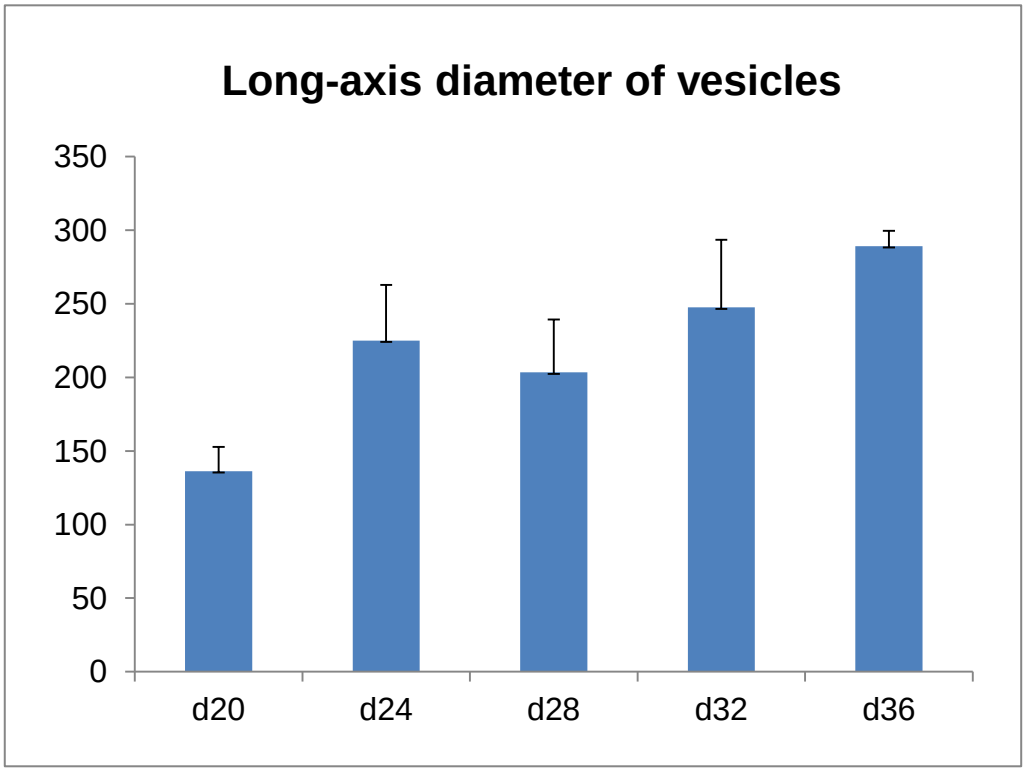

Figure 45 | Size of vesicles during differentiation of hESCs under the high concentration of KOSR condition.

Long-axis diameters of the day 20, 24, 28, 32, and 36 otic vesicles derived from hESCs using media with a high concentration of KOSR. Data are representative of 8 - 16 EBs from at least 3 separate experiments (n=3).

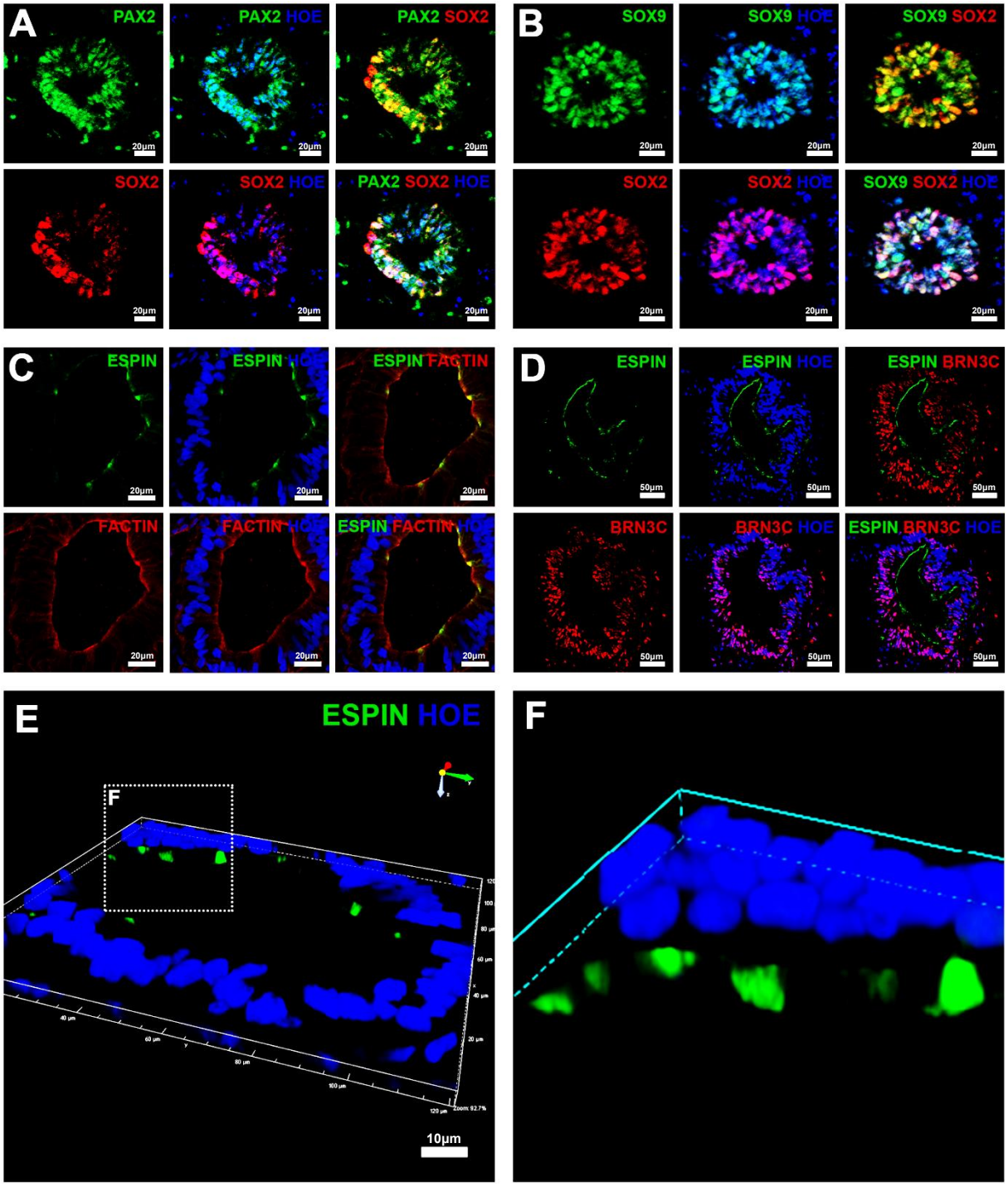

Figure 46 | Immunohistological analysis in the prosensory otic vesicle-like structures (d36).

A, B, At day 36 of differentiation, prosensory vesicles express PAX2, SOX9, and SOX2. C, D, Prosensory cells also start to express ESPIN which is stereocilia specific marker. E, 3-dimensional confocal microscope images show possible stereocilia bundles protruding from the vesicles. Data are representative of 8 - 16 EBs from at least 3 separate experiments (n=3).

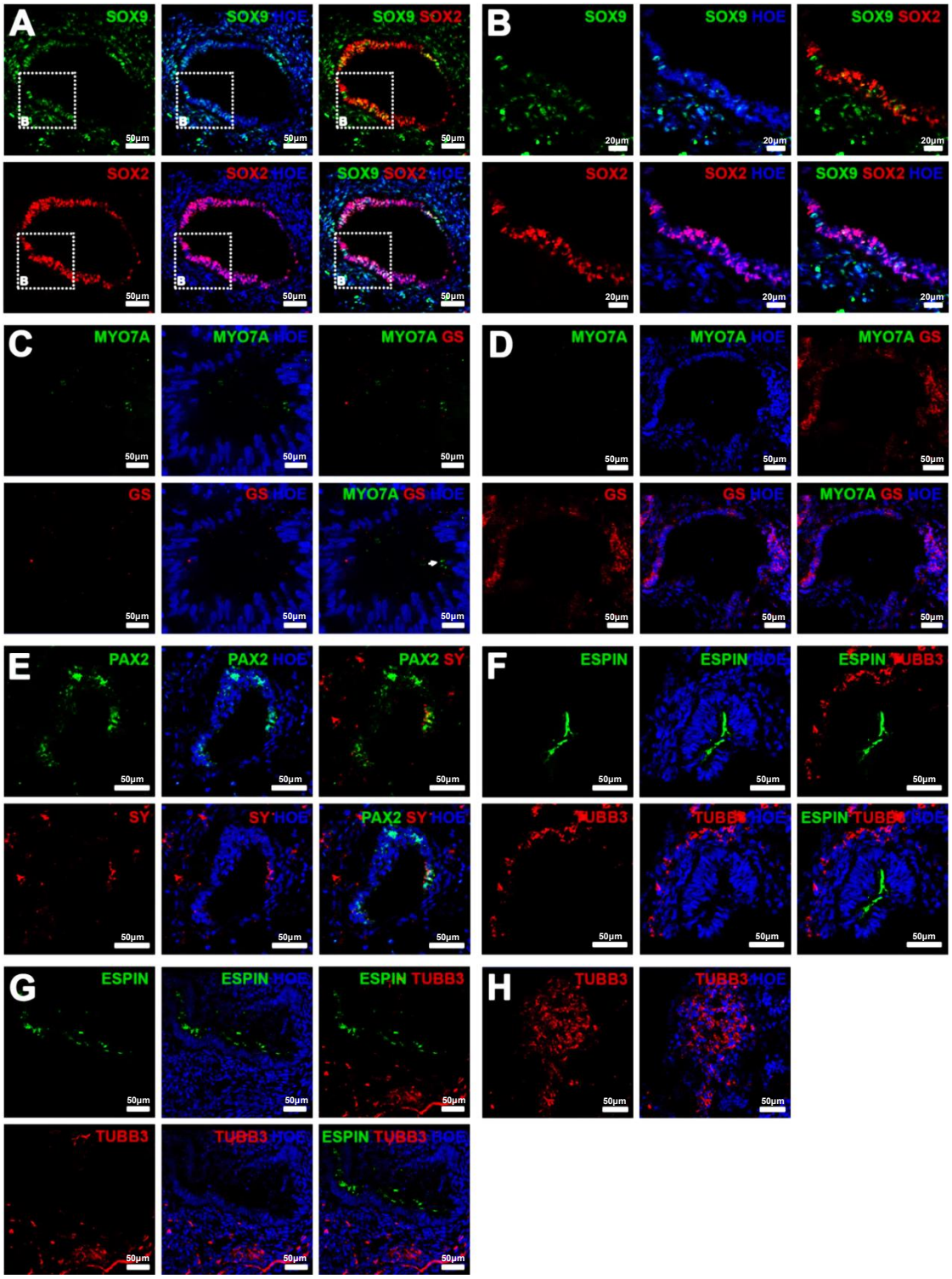

Figure 47 | Immunohistological analysis in possible otic vesicles and neuronal structures (d60).

A, B, Co-staining with SOX9 and SOX2 shows possible prosensory otic vesicles. C, D, There were no MYO7A positive cells. E – H, most of the neuronal positive cells (GS^+, SY^+, $TUBB3^+$) had a distance with possible prosensory cells. Data are representative of 8 - 16 EBs from at least 3 separate experiments (n=3).

The limitation of this protocol is that the efficiency of forming possible otic vesicles is low and these vesicles do not further develop into hair cells or supporting cells. During differentiation, observation of an outer layer of translucent epithelium seems to indicate the development of alternative lineage differentiation under these conditions. We also observed placodes which did not express otic specific markers. These may represent the development of other placode type structures such as adenohypophyseal, olfactory, lens, trigeminal, and epibranchial placodes. But we could not exclude the possibility that the vesicles are not mature enough to express otic lineage markers. In addition to non otic ectoderm tissues, we also observed possible contractile muscle cells which would originate from mesodermal differentiation. From this, we have concluded that high concentration of KOSR condition is not optimal for otic lineage differentiation.

There are two candidates for the reasons of failure to fully mature into inner ear cells: Wnt inhibitor and high concentration of KOSR. Multiple signaling pathways including Wnt, BMP, Notch, FGF, and Shh have been shown to play a big role in the development of the otic placode and further differentiation into the inner ear cells (Atkinson et al., 2015). Among these signaling pathways, the canonical Wnt signaling cascade is particularly important in the establishment of the otic placode *in vivo* (Jacques et al., 2012, Rakowiecki and Epstein, 2013, Munnamalai and Fekete, 2013b). Koehler et al. demonstrated that treating EBs with a potent Wnt inhibitor, XAV-939, abolishes otic vesicle formation in 3D culture (Koehler et al., 2013). With no additional treatments, cells in the epithelia of otic vesicles developed into hair cells and supporting cells. During our otic differentiation, EBs were exposed to Wnt inhibitor days 0 – 8 to counteract the caudalizing activity. Even though the Wnt signaling pathway probably only starts to play a critical role in establishment of the otic placode after day 8 after which time the medium was changed completely, there is still a possibility that a small amount of residual Wnt inhibitor could affect to otic lineage differentiation because we did not use Wnt agonist to counteract Wnt inhibitor added in the beginning of differentiation.

In addition, according to recent studies, many researchers have suggested a higher concentration of KOSR seems to prohibit proper epithelium development and decreasing concentration of it results in upregulation of genes indicative of hair cell differentiation (Ronaghi et al., 2014, Koehler and Hashino, 2014). The reasons for this are not clear, but most of the published protocols for otic lineage differentiation

used 1.5% of KOSR or attenuated concentrations from 20% to 5% throughout the otic lineage differentiation (Koehler and Hashino, 2014, Ronaghi et al., 2014). From this we concluded that high concentration KOSR condition is not good for inducing inner ear cells even it improves cell viability and hESCs efficiently formed retinal epithelium at high KOSR concentrations.

3.4.3 Conclusions

- On day 36 of differentiation, possible otic vesicles express prosensory markers and the stereocilia marker as well; however, we failed to fully mature them into hair cells, supporting cells, and auditory neurons.
- Possibly, Wnt inhibitor and high concentration of KOSR are the reasons for failure to induce inner ear cells.

Chapter 4

Results

Differentiation of hiPSCs to otic lineages

Chapter 4. Differentiation of hiPSCs to otic lineages

There are two types of hPSCs: hESCs and hiPSCs. hESCs are derived from ICM of the blastocyst stage embryo (Thomson et al., 1998). In contrast, hiPSCs have been reprogrammed from fully differentiated cells to an embryonic stem cell-like state (Takahashi et al., 2007). In general, hESCs and hiPSCs can be considered equivalent in developmental potential, though they have subtle differences in both their genomes and epigenome (Chin et al., 2010, Guenther et al., 2010).

From the clinical point of view, to avoid immune rejection, it is important that cells for replacing damaged inner ear cells can be patient-matched. Since hiPSCs are obtained from the adult cells, they offer an opportunity to generate patient-specific inner ear cells for transplantation. Therefore, successful differentiation of hiPSCs into otic lineage cells and neuronal cells is the first big step towards clinical translation. Here, we used a protocol which employs low concentrations of 2-mercaptoethanol, which is one of the best conditions for the differentiation of hESC into otic lineages, to induce inner ear cells from hiPSCs. Furthermore, these growth conditions were used in conjunction with a 3D culture system first developed for the generation of otic lineages from mESC since this has been shown to promote the formation of otic vesicle-like structures in suspension culture.

4.1 Differentiation of hiPSCs to inner ear cells using media with a low concentration of 2-mercaptoethanol

4.1.1 EB formation (d0 – d8)

For the differentiation of hiPSCs into inner ear cells, we employed growth media with a low concentration of 2-mercaptoethanol which proved to be the most successful protocol for the differentiation of hESCs to otic lineages (Figure 31). Also, we used 3D methods for hiPSCs for mimicking *in vivo* development. On day 1, fresh media containing 2% growth factor reduced Matrigel was added to enable development of epithelium on the surface of the EBs. On day 3 of differentiation, BMP4 and SB-431542 were added for induction of non-neural ectoderm and for suppressing mesendoderm lineage differentiation. On day 5, LDN-193189 and FGF2 were added for further otic lineage induction. On day 8 of differentiation, EBs were transferred to ultra-low-attachment 12 well plates. From this time point, the culture medium no longer contained serum, small molecules or recombinant proteins.

4.1.2 Prosensory vesicle formation (d8 – d20)

Similar to hESC differentiation (Chapter 3.3), around day 16 – 20 of differentiation, the otic placode gradually invaginated to first form an otic pit and then a closed, hollow otic vesicle (Figure 48A, B, E, and F). On day 20 of differentiation, the average size of possible otic vesicles was 206 µm (Figure 50), although it was noted that the resulting structures were often larger than so sometimes they were bigger than otic vesicles during hESCs differentiation (d20). *In vivo*, the otic epithelium starts to form the otic pit in the 3 WG in the human embryo, and further develops into otic vesicles at the end of the 4 WG. From this, we concluded that the developmental rate of otic vesicles was faster *in vitro* compared to *in vivo*.

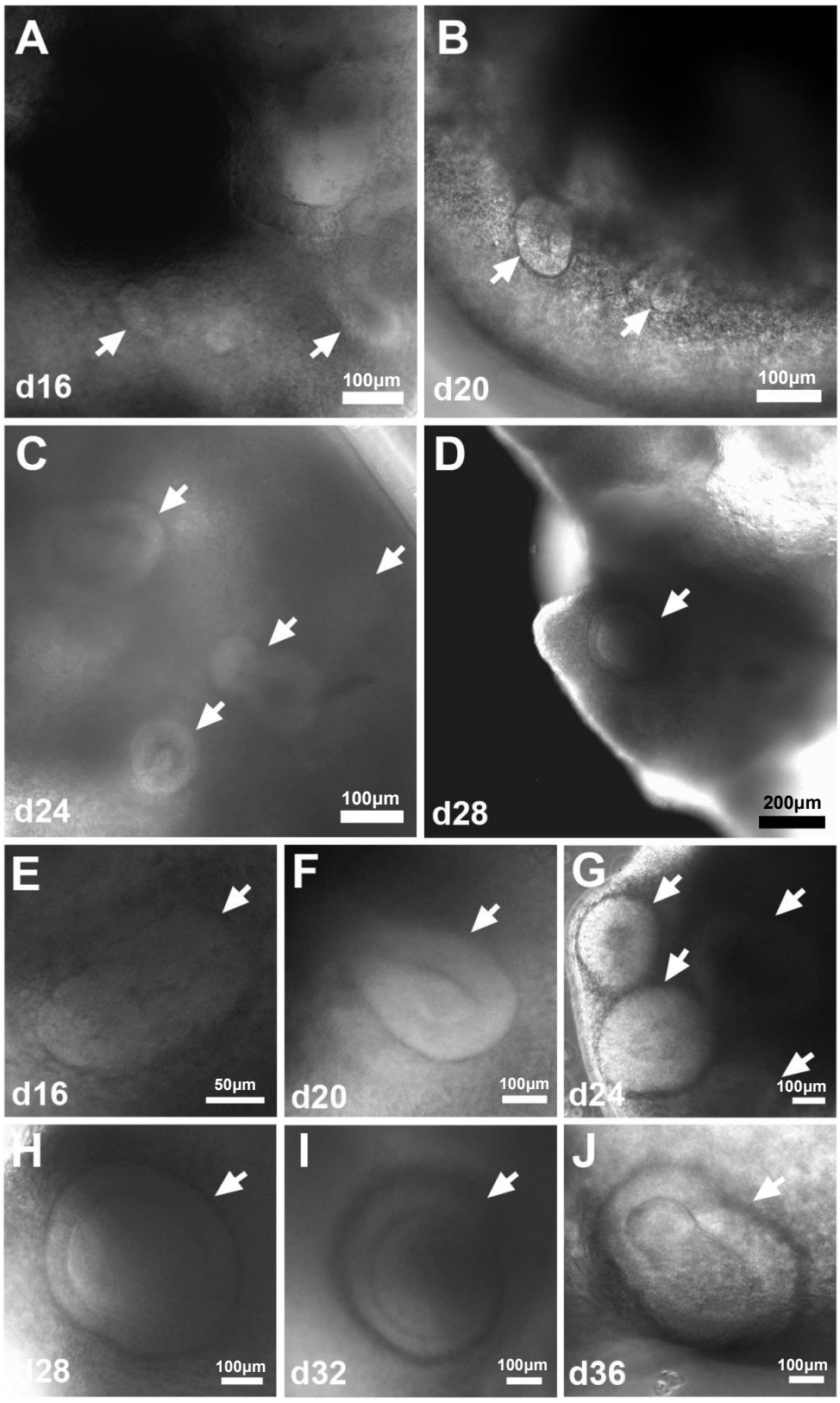

Figure 48 | Morphological changes during differentiation of hiPSCs.

A – J, White arrowheads indicate possible otic pit or vesicles. Picture shown representative of 8 EBs from at least 4 independent experiments (n=4).

Based on the immunohistochemistry data during hESCs differentiation using the low concentration of 2-mercaptoethanol containing media (Figure 34), we validated possible otic vesicle formation from iPSCs using the same antibodies. On day 20 of differentiation, co-expression of ECAD, PAX2, SOX9, and SOX2 indicated the 3 steps of possible otic vesicle formation: epithelium, pit, and otic vesicles (Figure 49). ECAD, an important marker for visualization of the vesicle formation was expressed on the surface of all the epithelial cells in EBs (Figure 49A, B, C, E, F, and G). Along with ECAD, nuclear SOX2 expression was observed indicating possible otic pit and otic vesicles (Figure 49A, D, E, and H). The SOX2 expression was not confined to the vesicles: additional expression was observed in the neural progenitor cells usually located near the otic vesicles (Figure 49A, D). Unlike ECAD and SOX2, SOX9 expression appeared everywhere in EBs (Figure 49C, D, G, and H). Sox9 plays several different functions during embryogenesis including male sexual development (De Santa Barbara et al., 1998) and pancreas development (Piper et al., 2002). During ectoderm lineage differentiation, Sox9 is a transcription factor that plays an important role in the development of the CNS and NC. In the CNS, Sox9 is essential for gliogenesis (Stolt et al., 2003, Stolt and Wegner, 2010) and the induction of embryonic and adult neural stem cells (Scott et al., 2010). During human ear development, at the 10.4 WG, SOX9 not only overlaps with SOX2 in the prosensory domain but shows uniform nuclear expression in all cells of the cochlear duct epithelium (Locher et al., 2013). SOX9 is also expressed in the Schwann cells of the adjacent spiral ganglion and in the cartilage cells of the otic capsule (Locher et al., 2013). During human development, PAX2 has a spatially restricted expression along the compartmental boundaries of the neural tube, and within developing eye, ear and kidneys as well (Terzic et al., 1998). For this reason, PAX2 expression was not only defined within the vesicles but also scattered outside of the vesicles (Figure 49B, F). However, those PAX2 positive cells not belonging to the vesicles were possibly neural progenitor cells considering immunohistochemistry data on day 60 (Figure 53A, E, and H). Taken together, even though single specific marker for the human otic vesicle formation has not been discovered yet, a combination of ECAD, SOX2, SOX9, and PAX2 is a good method to validate the process of the vesicle formation during differentiation of iPSCs into inner ear cells.

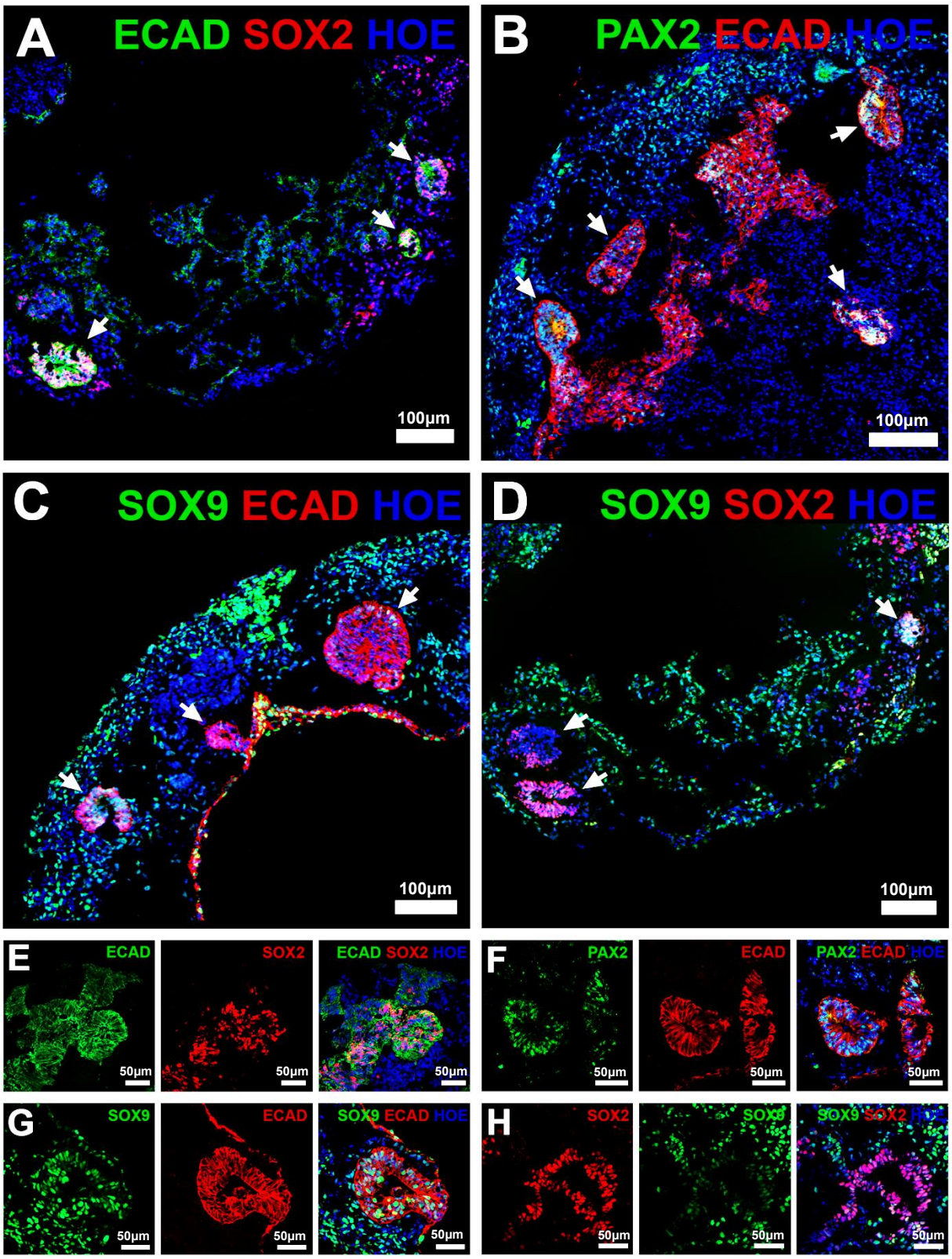

Figure 49 | Immunohistological analysis in the formation of otic vesicle-like structures (d20).

A – H, Co-staining with ECAD, PAX2, SOX9, and SOX2 shows the vesicle formation from the outer epithelium. Data are representative of 8 - 16 EBs from at least 4 separate experiments (n=4).

4.1.3 Prosensory otic vesicles (d36)

By day 36 of iPSC differentiation, the otic vesicles like structures had grown to 470 µm (Figure 48J and Figure 50). Their average size was bigger than their hESC derived counterparts (Figure 50), but the difference was not statistically significant (Figure 50). Analysis of immunohistochemistry data showed expression of markers for prosensory cells such as PAX2, SOX9, and SOX2 in otic vesicle-like structures (Figure 51A, B), similar to that described in the differentiating hESCs using the low concentration of 2-mercaptoethanol containing media (Figure 37). At this stage, the stereocilia specific marker ESPIN also started to appear in prosensory cells (Figure 51C, D). Interestingly, we sometimes found epithelial vesicles containing SOX2 negative cells with an ESPIN positive region which may be the precursors of hair cells (Figure 51D). During human cochlea development at 10.4 WG, a stage when the cochlear duct epithelium normally shows no clear morphological hair cell specification, the SOX2 expression is restricted to the human prosensory domain. No expression is visible in other regions of the cochlear duct, except for cytoplasmic SOX2 expression in the lateral wall of the cochlear duct epithelium (Locher et al., 2013). However, at 14 WG the SOX2 positive prosensory domain is developing into the OC and only supporting cells remain positive for SOX2. From this knowledge, we concluded that day 36 vesicles are maturing into cochlea cells or other types of inner ear cells. To investigate this further, we decided to culture them for a longer period.

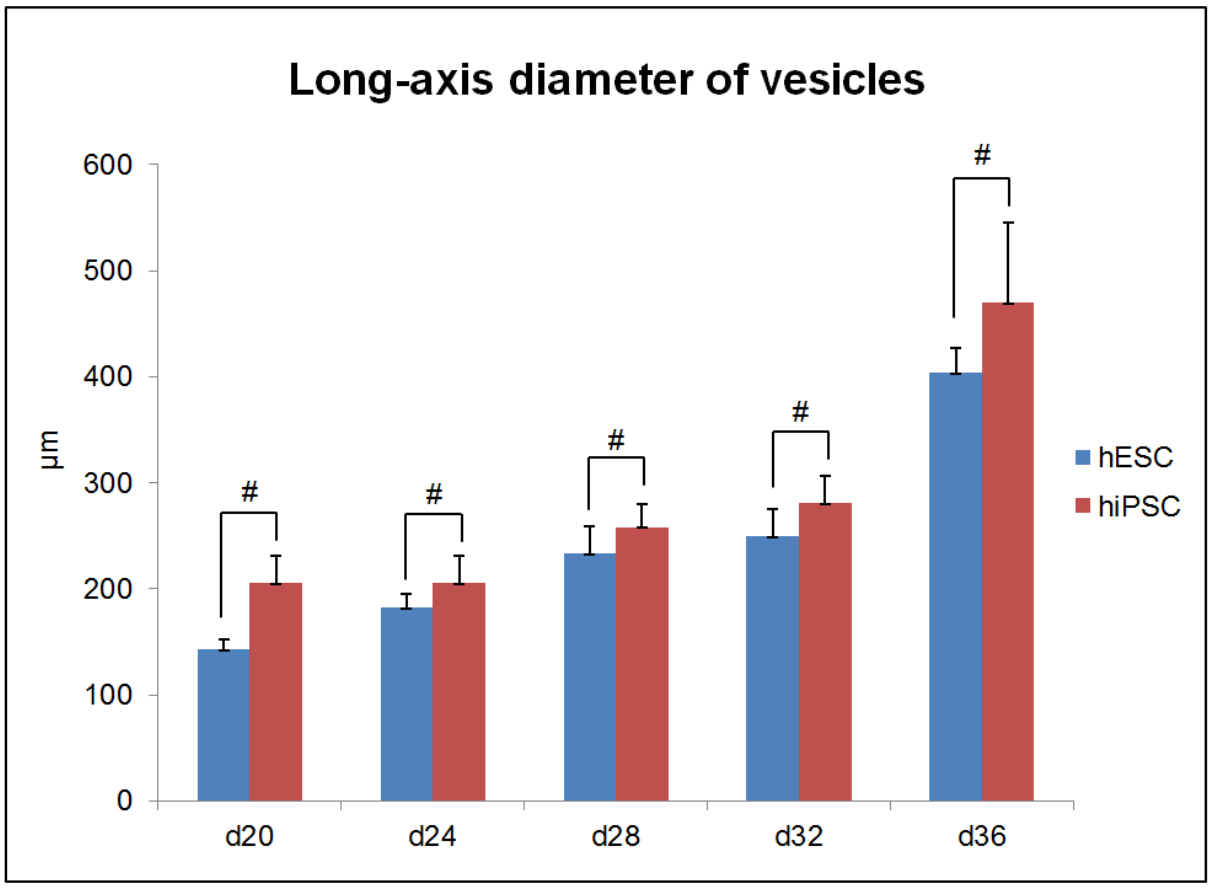

Figure 50 | Size of vesicles during differentiation

Long-axis diameters of the day 20, 24, 28, 32 and 36 otic vesicles derived from hESCs, compared with those of hiPSCs-derived. Data are representative of 8 - 16 EBs from at least 3 separate experiments (n=3). # $p > 0.05$, Student's t-test.

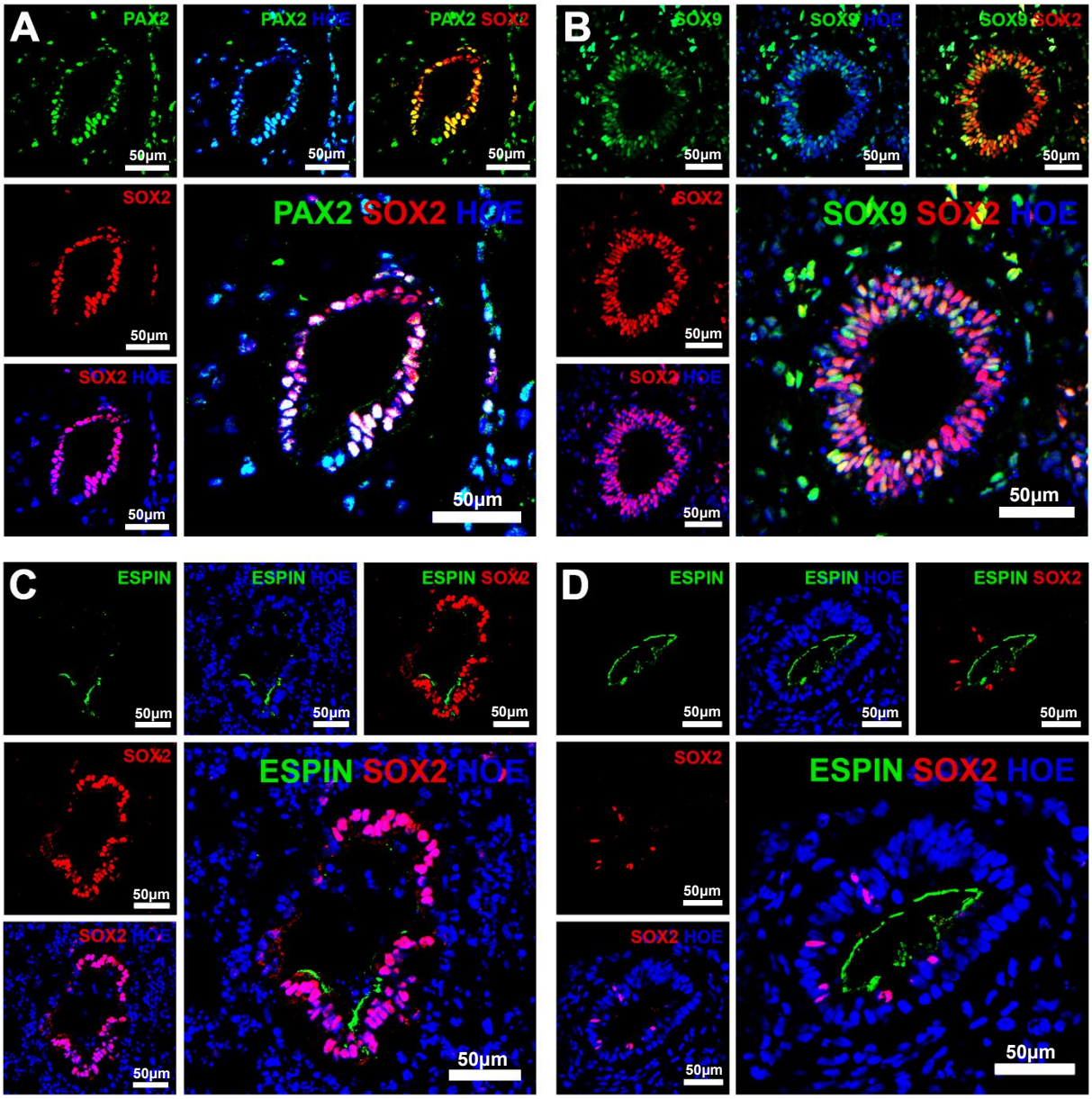

Figure 51 | Immunohistological analysis in the prosensory otic vesicle-like structures (d36).

A, B, At day 36 of differentiation, prosensory otic vesicle-like structures express PAX2, SOX9, and SOX2. C, D, Possible prosensory cells start to express ESPIN. Data are representative of 8 - 16 EBs from at least 4 separate experiments (n=4).

4.1.4 Induction of early hair cells and auditory neurons (d60)

On day 60 of iPSC differentiation, otic vesicle-like structures still expressed prosensory markers such as SOX2, SOX9, and PAX2 (Figure 52A, B, C, D and 53 A, E, H) and expression of the hair cell marker MYO7A started to appear from the tip (possible stereocilia bundles) of hair cell-like cells (Figure 52B, C, D). However, unlike the otic vesicles differentiated from hESCs, SOX2 or SOX9 was irregularly expressed and thus it was not easy to distinguish hair cells and supporting cells respectively (Figure 52B, C, D). Considering weak and partial expression of MYO7A in possible hair cells, those cells were in between prosensory cells and hair cells. Interestingly, we sometimes found possible otic vesicles containing only MYO7A positive cells without SOX2 expression at all (Figure 52E, F). Compared to the vesicles including MYO7A and SOX2 positive cells, the vesicles containing only MYO7A positive cells seemed like more matured hair cells because many of those cells expressed MYO7A protein in their cytoplasm as well as in the tips. Then we have to explain the following question; why do more matured otic vesicle-like structures not have SOX2 positive supporting cells? In the human cochlea, as prosensory cells ($SOX2^{+}$) mature, the cells destined to be hair cells start to lose SOX2 expression, whereas supporting cells still remain positive for SOX2 (Johnson Chacko et al., 2016). This is happening from 12 WG *in vivo* and SOX2 expression still remained in supporting cells at 19 WG (Johnson Chacko et al., 2016). Although expression of SOX2 after 19 WG in human cochlea has not been described, SOX2 expression continuing after birth in mouse cochlea has been already reported (Oesterle et al., 2008). Therefore, the possible explanation is that MYO7A positive cells without accompanying SOX2 positive supporting cells are simply cochlear hair cells without supporting cells or those are other types of hair cells (possibly vestibular cells).

In addition to hair cell markers, we also found some neuronal markers such as PAX2, TUBB3, NFM, GS, and SY in day 60 EBs (Figure 53). Compared to differentiated hESCs, the morphology of possible otic vesicles and spiral ganglion had less defined structures, but still we found some neuronal cells making a connection with possible hair cells (Figure 53A, B, C, G, H, and I). Collectively, the low concentration of 2-mercaptoethanol protocol worked moderately well with hiPSCs and overall hESCs and hiPSCs showed similar protein expression patterns during the otic differentiation.

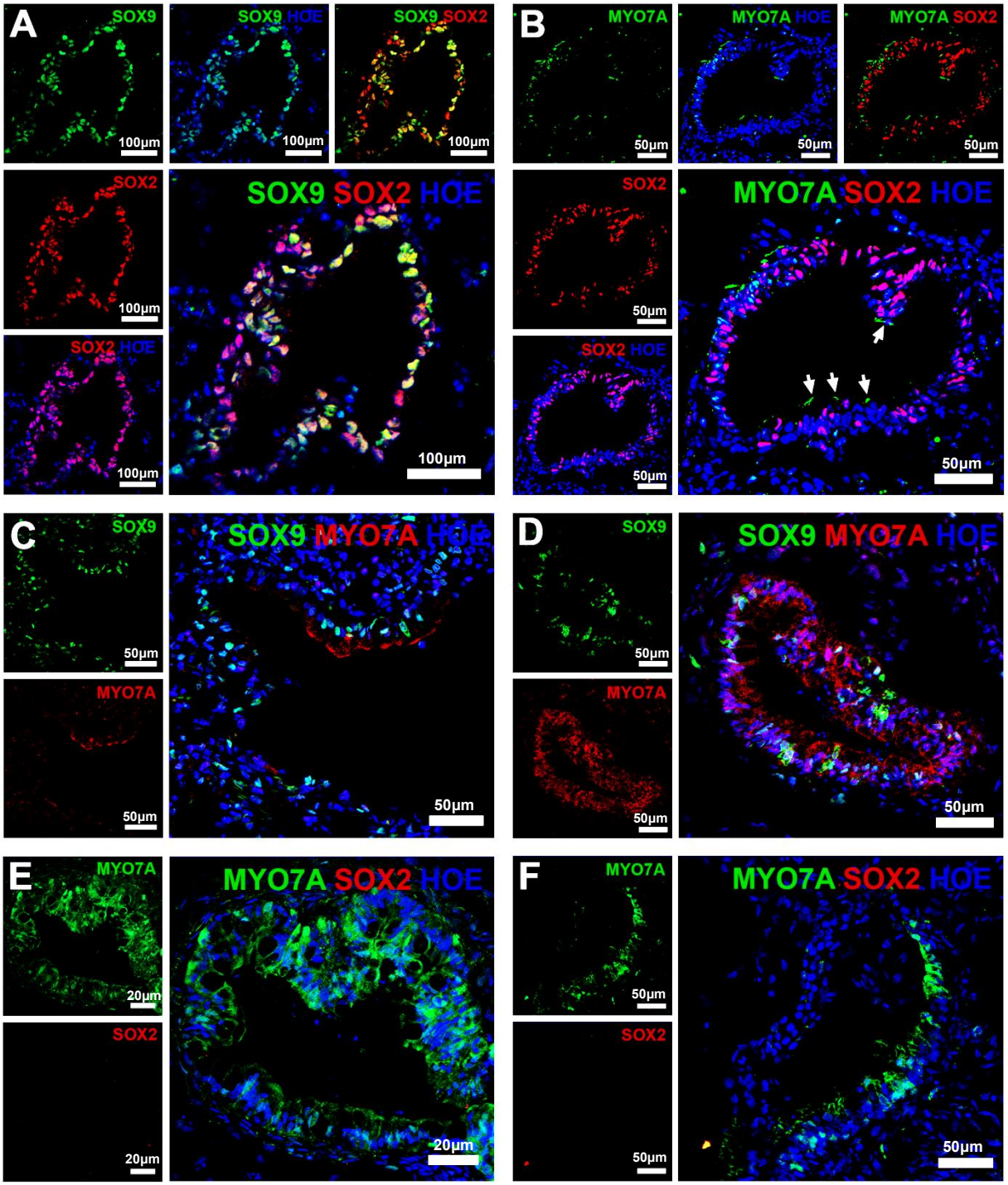

Figure 52 | Immunohistological analysis of the possible matured otic vesicles (d60).

A, Co-staining with SOX9 and SOX2 shows hiPSCs derived possible precursors of hair cells and supporting cells. B, C, D Maturing putative prosensory otic vesicles start to express MYO7A from the tip of hair cells. E, F, Sometimes otic vesicle-like structures contain only MYO7A positive cells without SOX2 positive cells. Data are representative of 8 - 16 EBs from at least 4 separate experiments (n=4).

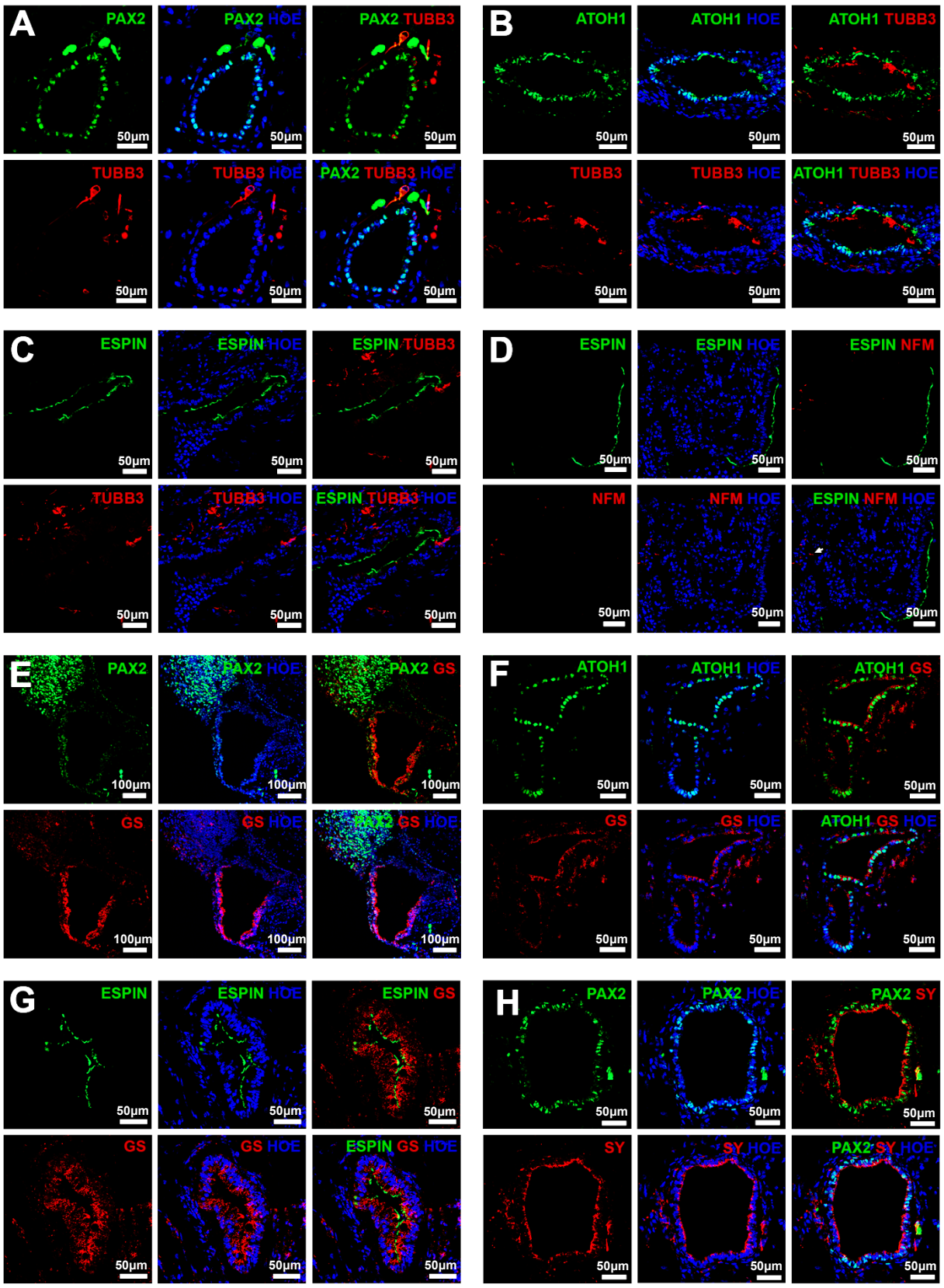
A
PAX2
PAX2 HOE
PAX2 TUBB3
TUBB3
TUBB3 HOE
PAX2 TUBB3 HOE
B
ATOH1
ATOH1 HOE
ATOH1 TUBB3
TUBB3
TUBB3 HOE
ATOH1 TUBB3 HOE
C
ESPIN
ESPIN HOE
ESPIN TUBB3
TUBB3
TUBB3 HOE
ESPIN TUBB3 HOE
D
ESPIN
ESPIN HOE
ESPIN NFM
NFM
NFM HOE
ESPIN NFM HOE
E
PAX2
PAX2 HOE
PAX2 GS
GS
GS HOE
PAX2 GS HOE
F
ATOH1
ATOH1 HOE
ATOH1 GS
GS
GS HOE
ATOH1 GS HOE
G
ESPIN
ESPIN HOE
ESPIN GS
GS
GS HOE
ESPIN GS HOE
H
PAX2
PAX2 HOE
PAX2 SY
SY
SY HOE
PAX2 SY HOE
50μm
100μm

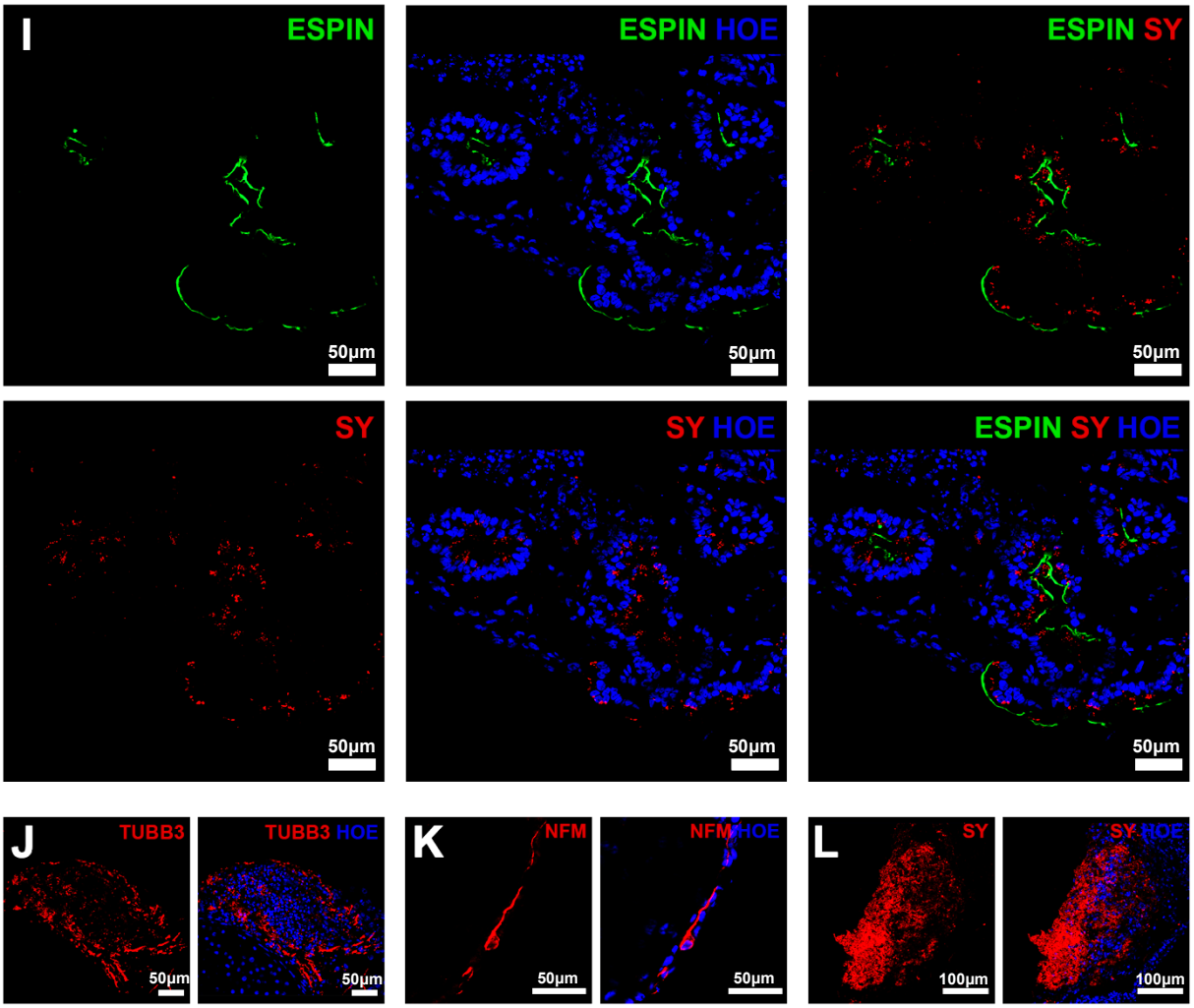

Figure 53 │ Immunohistological analysis in the possible neurons (d60).

A – L, Expression of β-III-tubulin (TUBB3), neurofilament (NFM), synaptophysin (SY), glutamine synthetase (GS) and PAX2 in the cells of neuronal lineage on day 60 of differentiation. Data are representative of 8 - 16 EBs from at least 4 separate experiments (n=4).

4.1.5 Induction of matured hair cells / supporting cells (d90)

To investigate whether hair-cell-like cells derived from hiPSCs assume a specialized fate, we labelled them with an antibody against PRESTIN and PV. Some MYO7A+ hair cells expressed PRESTIN which was most prominent in the lateral cell membrane with less expression in the cytosol of the cell (Figure 54A, B). Some of MYO7A+ and ESPIN+ hair cells also expressed PV (Figure 54C, D). This data suggests that the cell population derived from hiPSCs possibly induces OHCs. To test whether the differentiated hair-cell-like cells also have specific vestibular cell types, we stained for SOX2, CB2, OCM, and OTOP1. Mostly SOX2 expression was not observed in possible hair cells (Figure 54E), but some MOY7A+ hair cells still expressed SOX2 (Figure 54F). CB2, which is type II hair cell marker in mouse, expression was not detected in possible hair cells (Figure 54G). $MYO7A^+$ hair cells expressed OCM close to the base of the hair bundle (Figure 54H, I), but some $MYO7A^+$ cells did not label together with OCM (Figure 54J). Similarly, we found some expression of OTOP1 which was concentrated near the apical surface of the sensory epithelium (Figure 54K), but not all the otic vesicle-like structures containing MYO7A+ cells co-expressed with OTOP1 (Figure 54L). Lastly, TUBB3+ neurons were observed at the periphery of the nearly all otic vesicles and some of the hair cells made a connection with the neurons (Figure 54M, N). Taken together, expression of PRESTIN and PARVALBUMIN in hiPSC derived EBs strongly suggests that they include at least OHC like cell types and possibly IHCs as well as type I vestibular hair cells.

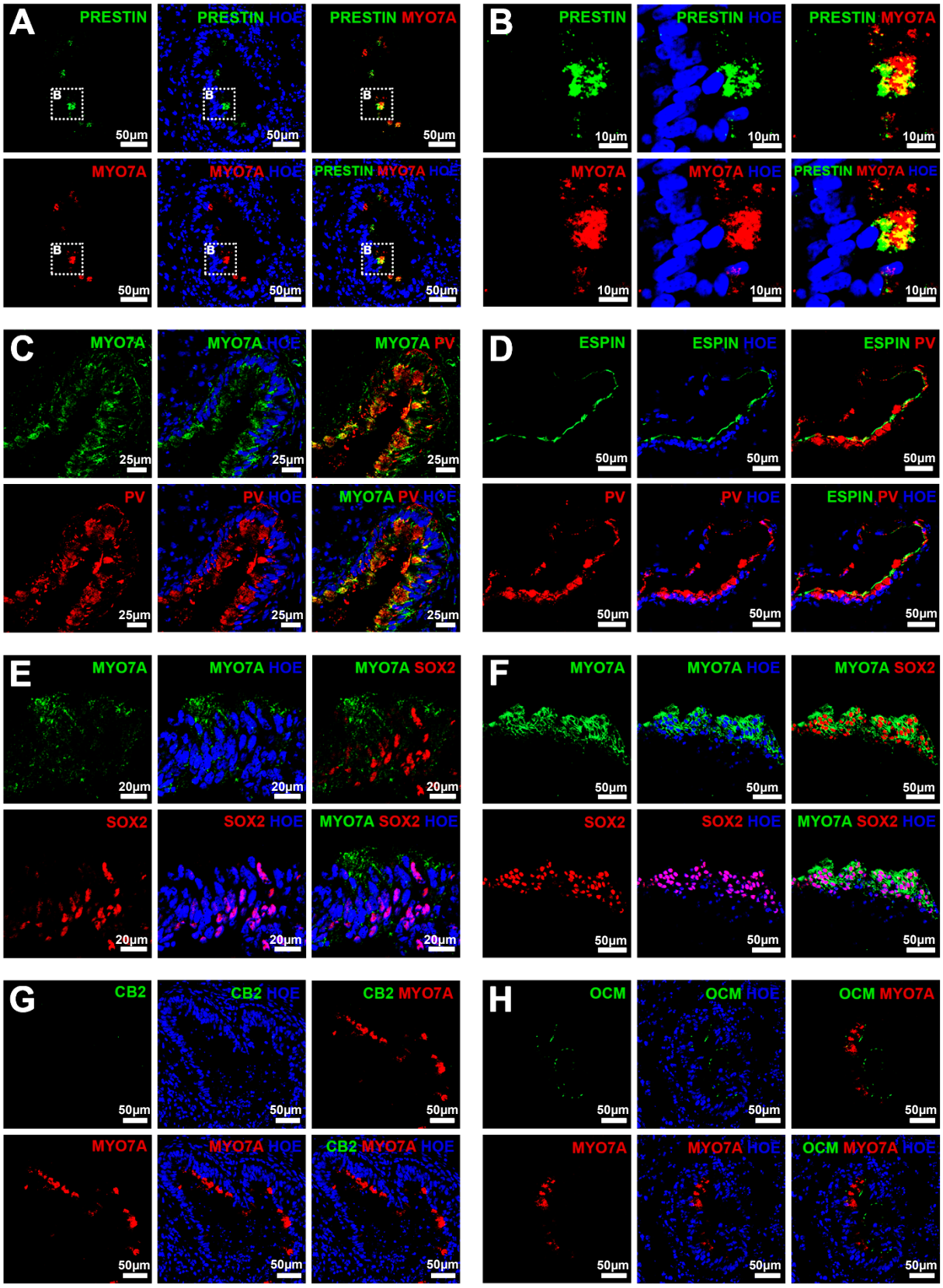
A
PRESTIN
PRESTIN HOE
PRESTIN MYO7A
MYO7A
MYO7A HOE
PRESTIN MYO7A HOE
B
B
PRESTIN
PRESTIN HOE
PRESTIN MYO7A
MYO7A
MYO7A HOE
PRESTIN MYO7A HOE
C
MYO7A
MYO7A HOE
MYO7A PV
PV
PV HOE
MYO7A PV HOE
D
ESPIN
ESPIN HOE
ESPIN PV
PV
PV HOE
ESPIN PV HOE
E
MYO7A
MYO7A HOE
MYO7A SOX2
SOX2
SOX2 HOE
MYO7A SOX2 HOE
F
MYO7A
MYO7A HOE
MYO7A SOX2
SOX2
SOX2 HOE
MYO7A SOX2 HOE
G
CB2
CB2 HOE
CB2 MYO7A
MYO7A
MYO7A HOE
CB2 MYO7A HOE
H
OCM
OCM HOE
OCM MYO7A
MYO7A
MYO7A HOE
OCM MYO7A HOE
10µm
20µm
25µm
50µm

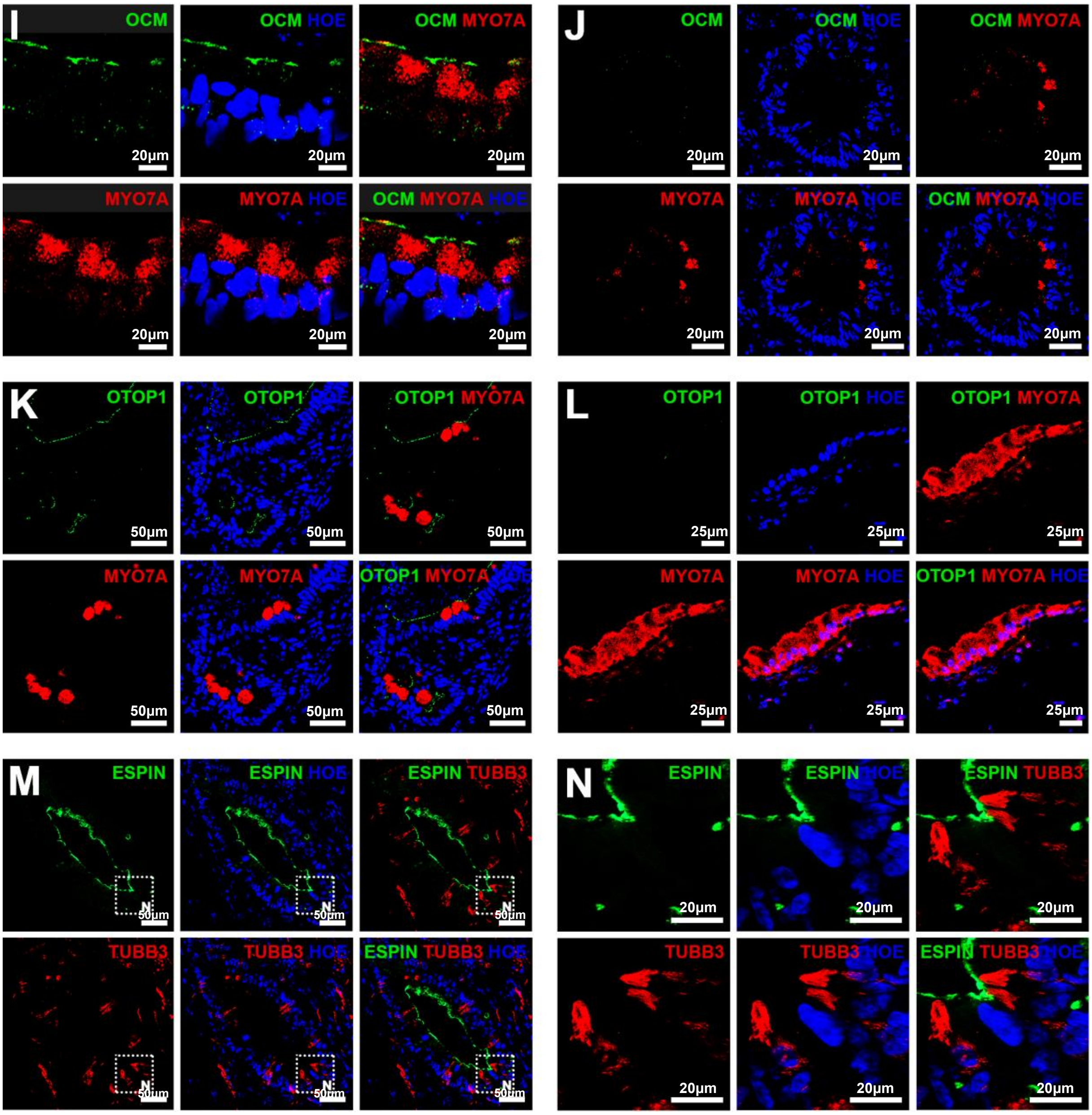

Figure 54 │ Immunohistological analysis to identify cell types (d90).

A – H, Expression of MYO7A, SOX2, CB2, OTOP1, ESPIN, PA, OCM, and PRESTIN in the matured otic vesicles on day 90 of differentiation. Data are representative of 16 EBs from at least 3 separate experiments (n=3).

4.2 Conclusions

- Similar to hESCs differentiation, possible sensory hair cells and neuronal cells are generated by hiPSCs using the low concentration of 2-mercaptoethanol method over 3 months.
- The average size of otic vesicles derived from hiPSCs during the differentiation is bigger than their hESC derived counterparts, but the differences are not statistically significant.
- Unlike hESCs differentiation, mixed populations of hair cells (possibly OHCs, IHCs, and type I vestibular hair cells) are observed.

Chapter 5

Results

TEM analysis and functional tests during otic lineage differentiation

Chapter 5. TEM analysis and functional tests during otic lineage differentiation

5.1 Differentiation of hESCs to inner ear cells using media with a low concentration of 2-mercaptoethanol

5.1.1. TEM analysis

One of the most important criteria to distinguish between otic progenitor cells and hair cells is cell morphology including the presence of stereocilia, kinocilium and synaptic specializations/innervation. For this reason, TEM was used to observe fine details of differentiated cells at a higher resolution. Especially in this project, the TEM was used to check whether ESPIN positive cells were real microvilli. Similar to immunohistochemistry analysis, TEM images indicated that possible microvilli appear along inside of the vesicles on differentiation day 36 (Figure 55A). Observing higher magnification, most of the sensory epithelial progenitors on day 36 showed one or two microvilli per cell (Figure 55). However, those microvilli were considered as having a potential to be stereocilia bundles because we observed several buds of microvilli (Figure 55L). The length of microvilli at this stage was variable as 300 nm - 3 µm.

TEM images on day 60 of differentiation strongly supported the assumption that the $ESPIN^{+}$ cells were stereocilia bundles (Figure 56A). The average heights of stereocilia were more than twice longer than the length of microvilli on day 36 and cross sections of stereocilia bundles were also visible (Figure 56B). Moreover, higher magnification of the otic vesicles revealed putative afferent nerve endings beneath the hair cells (Figure 56D). However, the more specialized kinocilia were not observed under this condition. Unlike mouse, human cochlear hair cells have relatively short kinocilium length. In addition, since kinocilia start to disappear at 24 WG and are not present in adult auditory hair cells, if differentiated cells are potential cochlear cells; there is less chance to detect kinocilium *in vitro*.

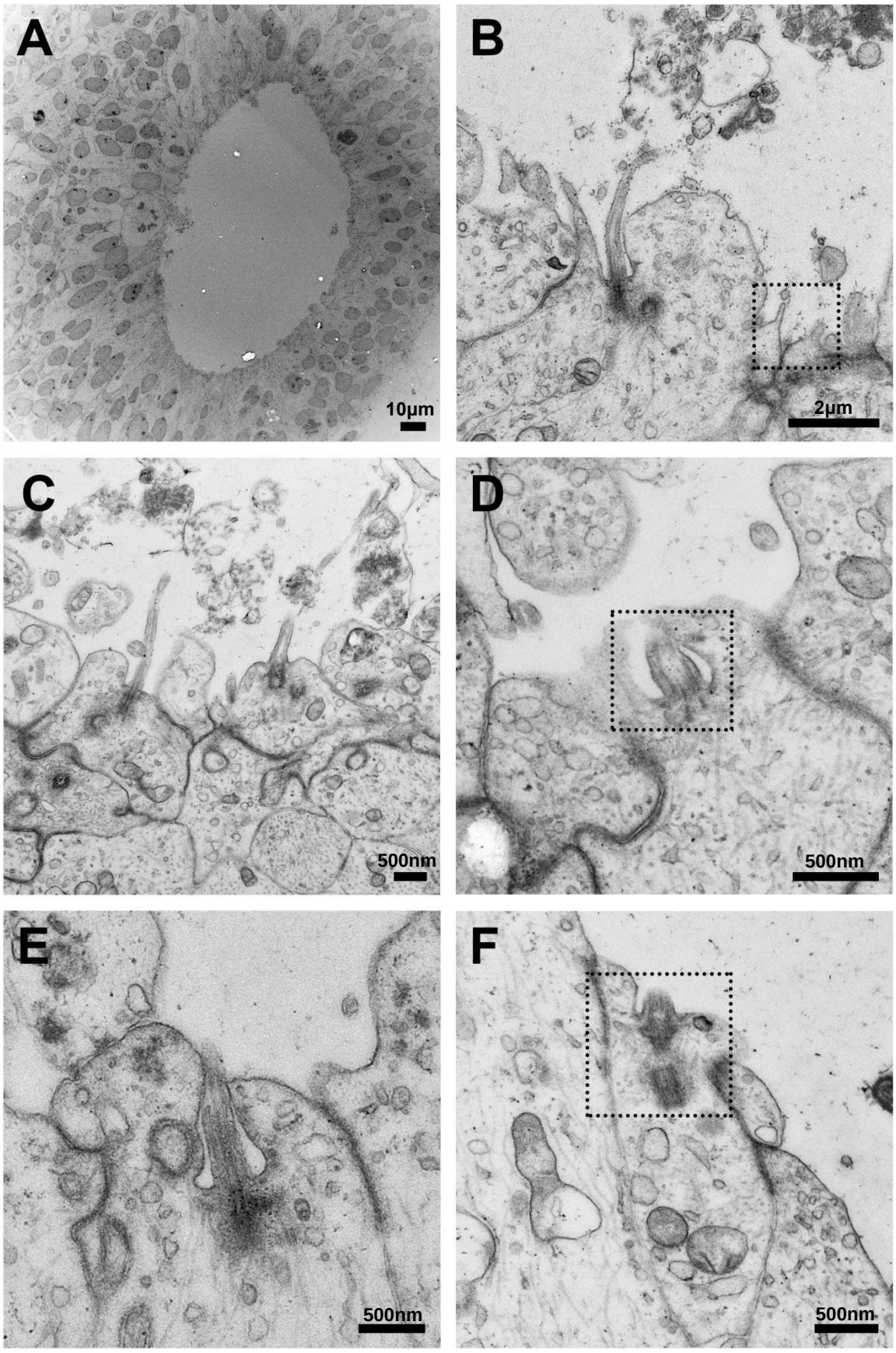
A
10µm
B
2µm
C
500nm
D
500nm
E
500nm
F
500nm

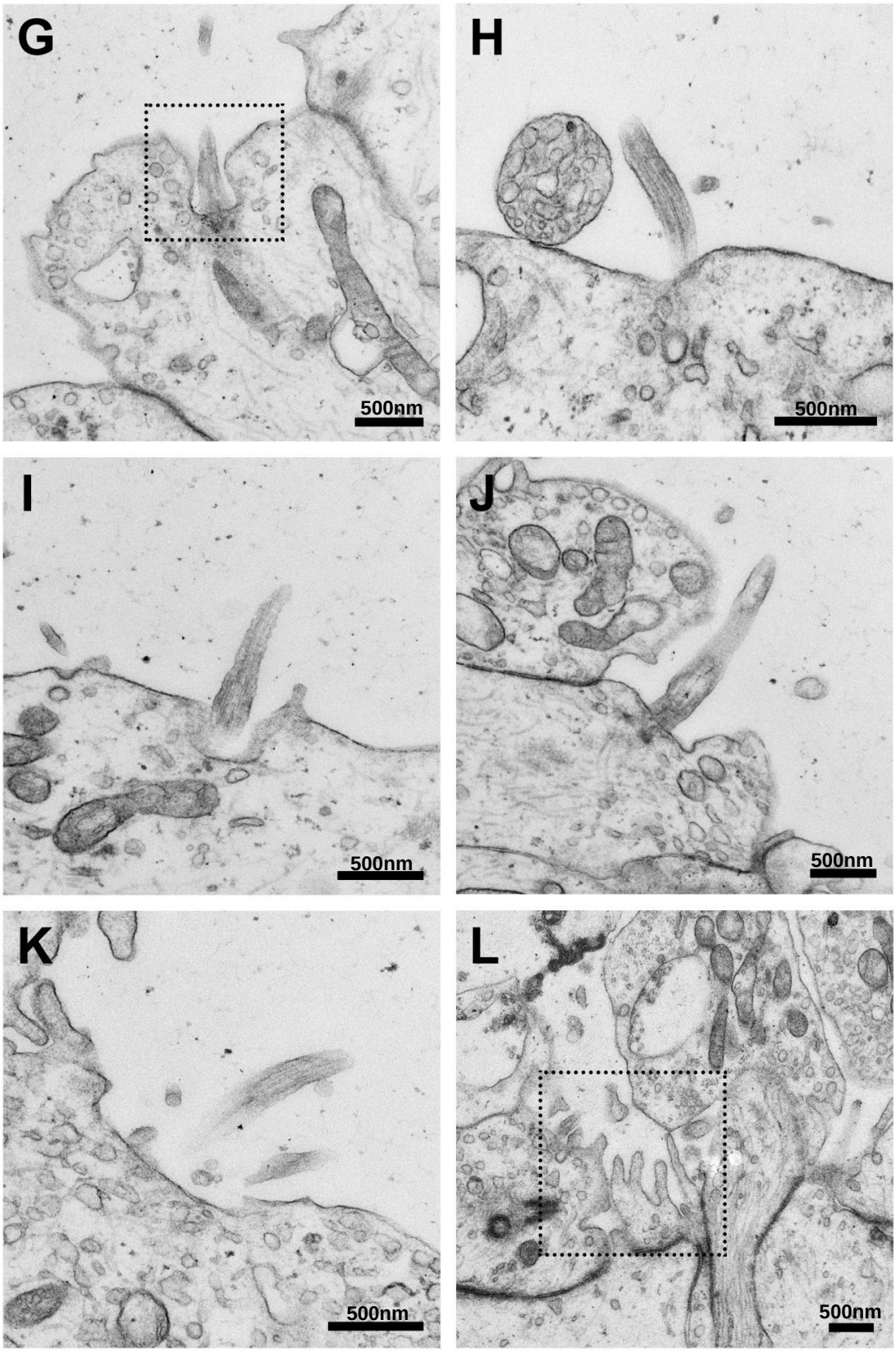

Figure 55 │ TEM images of possible microvilli or cilia (d36).

A, The typical shapes of possible otic vesicles. Generally, possible microvilli or cilia locate inside direction of the vesicles. B - L, Potential progenitors of hair cells have one or two microvilli or cilia per cell.

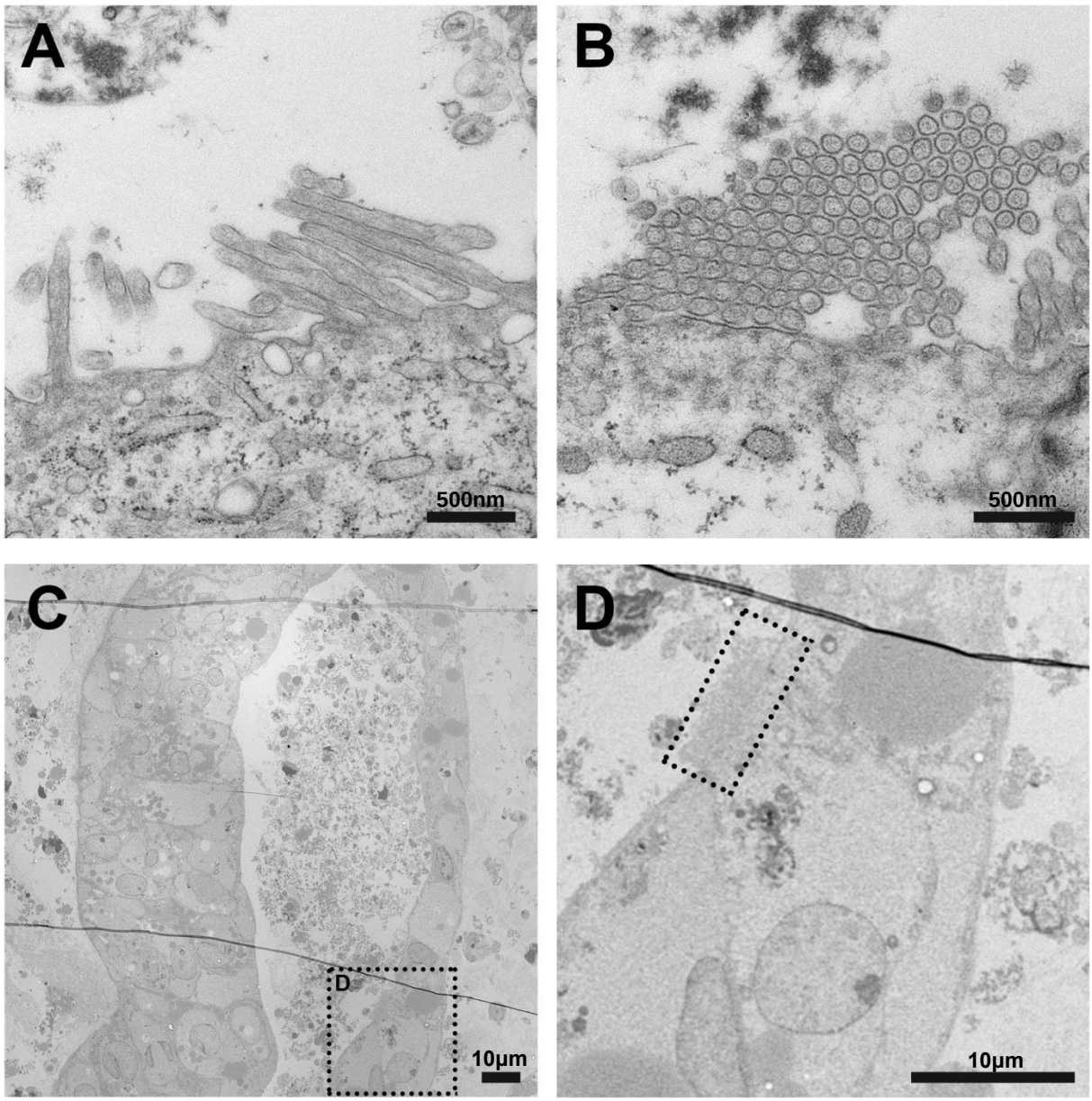

Figure 56 │ TEM images of possible stereocilia bundles (d60).

Possible stereocilia bundles (A) and cross sections of the stereocilia bundles (B) are observed on day 60 of differentiation. D, Higher magnifications of the otic vesicle-like structures (C). Black dotted square shows stereocilia bundles.

5.1.2. FM1-43FX uptake assay

To investigate whether differentiated cells derived from hESCs using media with a low concentration of 2-mercaptoethanol have functional mechanosensitive channels, we treated them with FM1 dye. The styryl pyridinium dye FM1 has been widely used to specifically label sensory hair cells and sensory neurons (Meyers et al., 2003). FM1 quickly fills the cytoplasm of sensory cells, but cannot penetrate plasma membrane in supporting cells (Meyers et al., 2003). The results showed that FM1 could rapidly penetrate into some of the sensory cells (Figure 57A, B). However, this labelling is not limited to sensory cells because 293T cells also take up FM1 (Meyers et al., 2003). For this reason, the immunostaining with otic lineage associated antibodies was performed after FM1 treatment to affirm the identity of sensory hair cells and sensory neurons. Nearly all MYO7A positive cells simultaneously stained with FM1 (Figure 57C), but there was no SOX2 (supporting cell marker) and FM1 double positive cells (Figure 57D). Most of the SOX2 labelled cells were still located near the FM1 positive hair cells same as in the 3D structure before dissociation of cells and the cytospin. In addition, some of FM1 positive cells were co-expressed with neuronal marker TUBB3 (Figure 57F), but most of the TUBB3 positive cells did not uptake FM1 (Figure 57E). TUBB3 is primarily expressed in neurons and a general marker of SGNs during ear development (Locher et al., 2014). Therefore, only FM1 and TUBB3 double positive cells are possibly sensory neurons while only TUBB3 positive cells are more likely to be non-sensory neurons.

Taken together, co-staining with FM1 and MYO7A/SOX2/TUBB3 showed hair cells like cells and possible sensory neurons have mechanosensitive ion channels. It suggests these FM1 positive cells are likely in response to mechanical stimulation. Thus, further examination especially electrophysiological recordings are needed to check true functional properties.

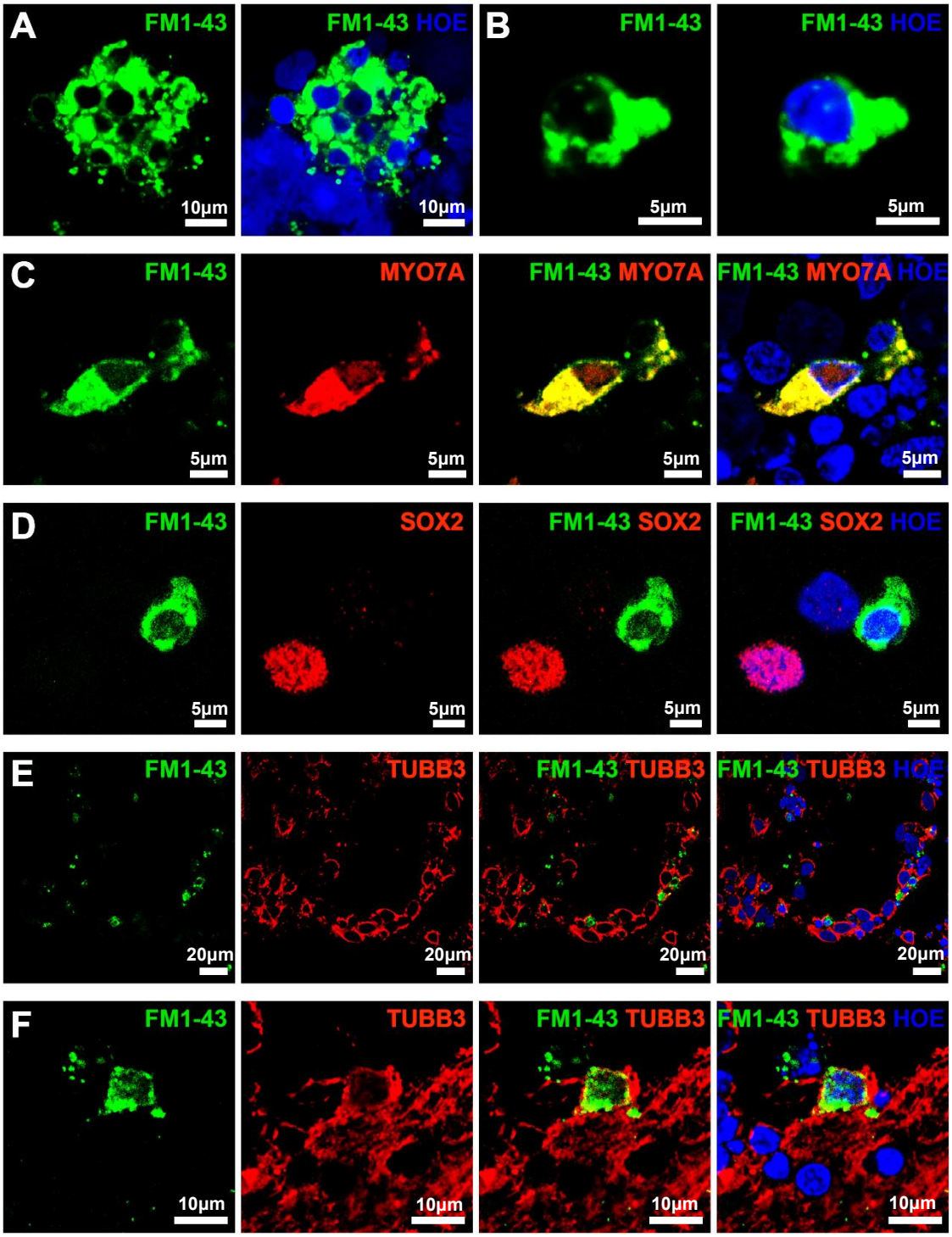

Figure 57 | Functional properties of hESCs-derived hair cells and neuronal cells using a FM1-43FX uptake assay.

Confocal images of dissociated d90 (A, B) EBs reveal FM1 labelled cells. FM1 labelled cells on d90 also express MYO7A (C), but not express SOX2 (D). Most TUBB3 positive cells do not uptake FM1 (E), but some cells co-express (F). Data are representative of 8 dissociated EBs from at least 3 independent experiments (n=3).

5.1.3. Electrophysiological recordings

Each cell type has certain distinctive membrane properties, and thus present unique electrophysiological recordings. *In vivo*, certain types of ion channels activate and inactivate much faster than others. Na^+ currents typically activate within 200 to 300 μs and inactivate completely within 2 to 5 ms, whereas K^+ currents take several milliseconds to activate, and often inactivate slowly (Walz, 2007). Simple current isolation can thus be accomplished by studying whole-cell currents at different time points following stimulation.

In this study, because of the fact that each EB has variable numbers of possible otic vesicles covered with non otic lineage cells, we isolated cysts (Figure 58A). These possible otocysts were then plated on collagen-coated coverslips for checking electrophysiological properties. 4 days after plating, neuronal-like cells appear at the periphery of the otic vesicles (Figure 58B). All cells examined in voltage-clamp displayed a fast-activating, rapidly inactivating inward current in response to increasing membrane depolarization. Rapid inward Na^+ currents are followed by slower outward K^+ currents (Figure 58C). Current-voltage (I-V) relationships are one of the most effective ways to summarize the behaviour of voltage- and ligand-activated ion channels. The peak I-V curve derived from the voltage-clamp recordings is predominantly determined by the inward Na^+ currents (Figure 58D), which activated positive to about 45 mV and reached a maximum size of 1.86 nA at 18 mV. A further three cells with similar morphology were tested with a Cs^+-based intracellular solution, which blocked the outward K^+ currents. In these cells (Cm 8.1 ± 1.1 pF), the peak inward Na+ currents averaged 1.35 ± 0.05 nA at 15.3 ± 1.8 mV (all means ± SEM). The expression profile of membrane currents in neuron-like cells closely resembled that found in primary auditory neurons of the rat cochlea (Jagger et al., 2000). The expression profile of membrane currents in neuron-like cells closely resembled that found in primary auditory neurons of the rat cochlea (Jagger et al., 2000).

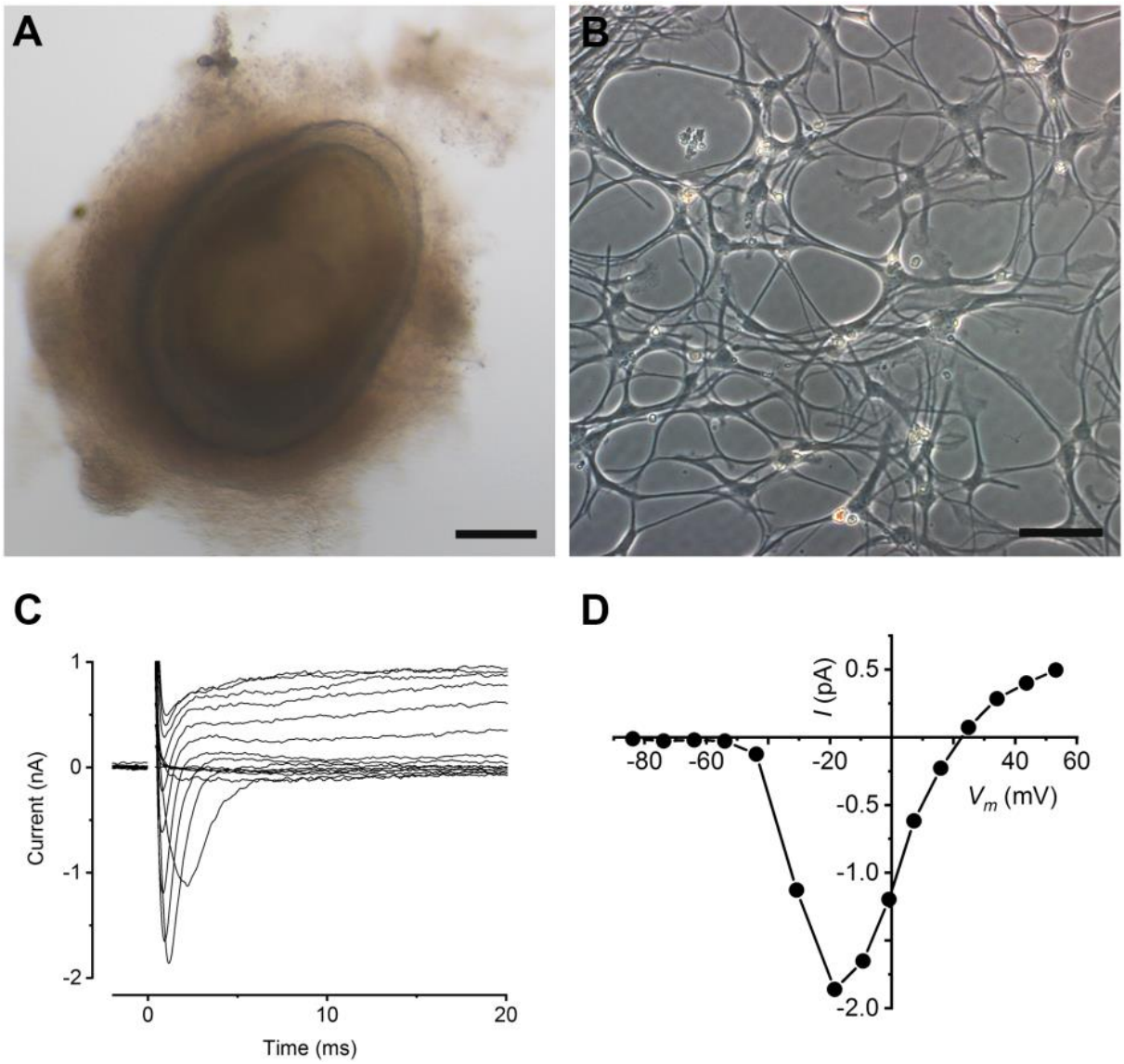

Figure 58 | Isolated possible otocysts and neuronal cells from EBs and electrophysiological recordings.

A, Possible otocysts isolated from EBs cultured for 161 days. B, Neuronal like cells appear at the periphery of the otic vesicles after the otocysts adhere to a collagen substrate. C, Membrane currents recorded from a bipolar neuron at the periphery of an otic placode. Rapid inward Na currents are followed by slower outward K currents. D, Peak I-V curve derived from C, predominantly determined by the inward Na currents. Currents, averaged from 3 repetitions of the stimulus protocol, were elicited from a -84 mV holding potential in nominal 10 mV steps. Recording conditions: Cm 6.6 pF; Rs 3.2 MΩ; gleak 3.2 nS; 22°C. Holding current of -48 pA was set to zero and leak currents were subtracted and membrane potentials were corrected for voltage drop across Rs.

5.2.4 Conclusions

- TEM images show possible stereocilia bundles and the possibility of innervation.
- Co-staining with FM1 and MYO7A/SOX2/TUBB3 show that hair-cell-like cells and possible sensory neurons have mechanosensitive ion channels.
- Whole-cell patch clamp recordings from bipolar neurons derived from hESCs display similar membrane currents in primary auditory neurons of the rat cochlea.

5.2 Differentiation of hiPSCs to inner ear cells using media with a low concentration of 2-mercaptoethanol

5.2.1. TEM analysis

TEM was used to examine fine details of the cells derived from hiPSCs cultured for 60 days (Figure 59). Most of the stereocilia on the possible hair cells gathered into a bundle (Figure 59E, F) and also mini-kinocilium like structures were observed (Figure 59A – D). TEM images on day 90 of differentiation showed typical kinocilium 9 × 2 + 2 structures (Figure 60F) and the stereocilia length were 2 – 3 fold increase compared to those on day 60 (Figure 60A – C). Some hair bundles had a rectilinear arrangement (Figure 60A) typical shape of stereocilia in adult IHCs (Lim and Brichta, 2016). In addition, stereocilia had rootlets that extended into the cell body (Figure 60C) and thin thread-like connections (Figure 60D, yellow dotted square) were observed. These cross-links between stereocilia would tend to make all the stereocilia of one row move together when some were deflected. However, it was not observed as tip-links which is a single, four-stranded link that connects the tip of one stereocilium to the side of the nearest taller stereocilium at this stage. It is generally believed that any tension imposed on these tip links during excitatory bundle displacement opens transducer channels located at or near the insertion of the links on the tips of the shorter stereocilia (Beurg et al., 2009). The previous study suggested that the earliest observation of these tip-links in human cochlear hair cells was 14 WG *in vivo* (Rhys Evans et al., 1985). Considering this information, day 90 EBs need more time to mature.

In addition to the structure of hair cell bundles, the TEM method also helped to elucidate shape of individual hair cells derived from hiPSCs. As mentioned in chapter 1, Type I hair cells are amphora-shaped with variability in the length of the constricted neck and type II hair cells are more club like (Oghalai et al., 1998). In contrast, OHCs have a cylindrical shape and IHCs have a more pear-shaped morphology (Oghalai et al., 1998, Pujol and Lavigne-Rebillard, 1985). Most of the possible hair cells show a long and cylindrical shape (Figure 60G, H) corresponding to the immunohistochemistry results in chapter 4 suggesting they may be OHCs.

Some of the hair cells, however, present a short length and a vase-shaped cell body (Figure 60J) typical type I hair cell morphology.

Moreover, similar to differentiated hESCs, possible otic vesicles revealed putative afferent nerve endings beneath the hair-cell-like cells. Enlargement from Figure 60K (red dot) shows a nerve ending filled with numerous and heterogeneous vesicles contacting with potential hair cells (Figure 60L). In addition to button-like nerve terminals, a calyx nerve terminal (enveloping cup-like) which contacts with type I hair cells was also observed (Figure 60N). Even though most of the putative nerve endings made a connection with hair cells (Figure 60L, M), it seemed to too an early stage to observe synaptogenesis.

Collectively, TEM images of possible hair cells on day 90 of differentiation showed some features which can be observed in the adult inner ear and these hair cells had typical shapes of OHCs and type I hair cells. Moreover, TEM images demonstrated that neurons derived from hiPSCs using a low concentration of 2-mercaptoethanol are capable of making a connection on developing hair cell-like cells *in vitro*.

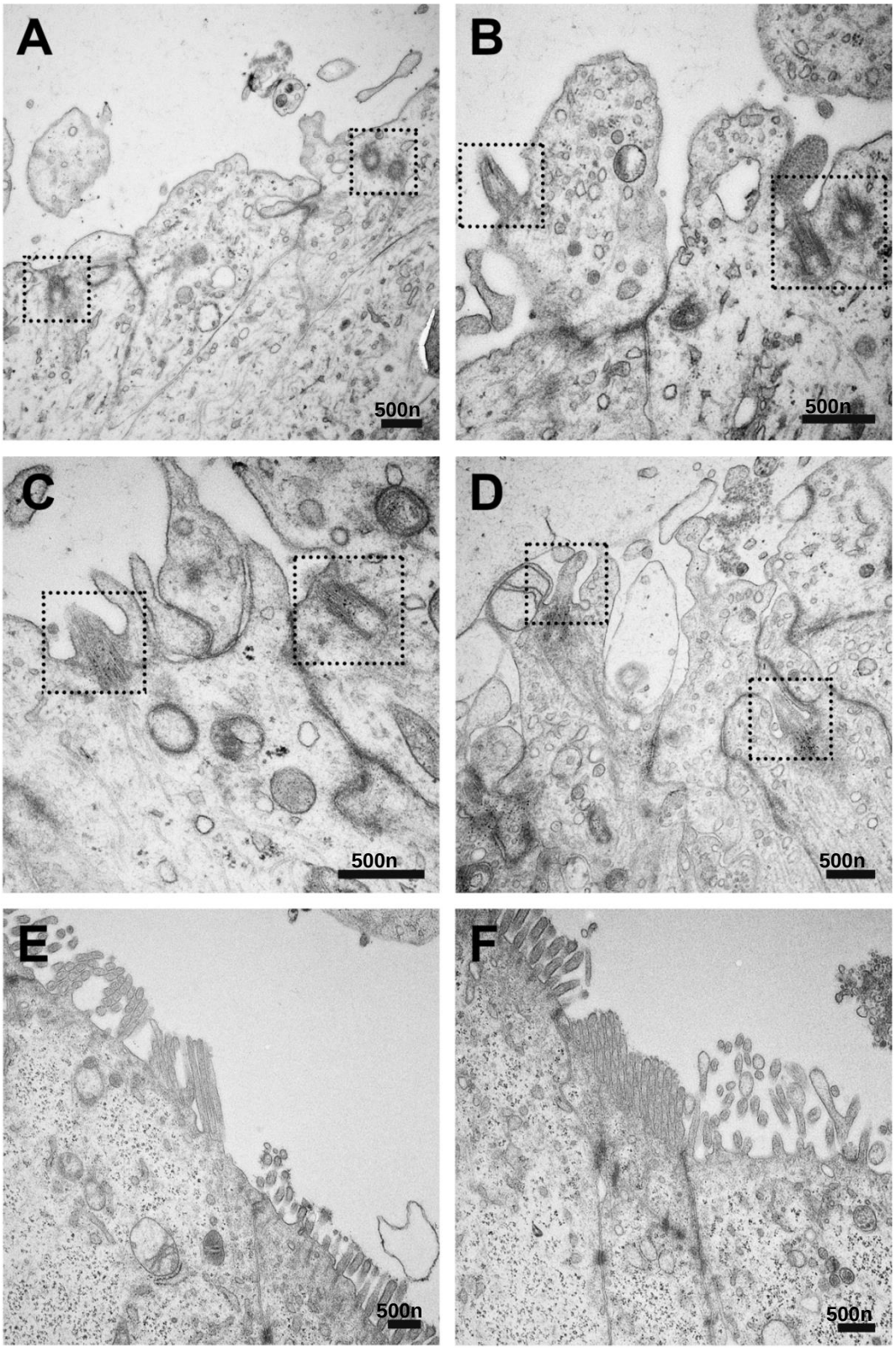

Figure 59 │ TEM images of possible stereocilia bundles (d60).

Potential mini-kinocilium (A – D, dotted squares) and stereocilia bundles (E and F) are observed on day 60 of differentiation.

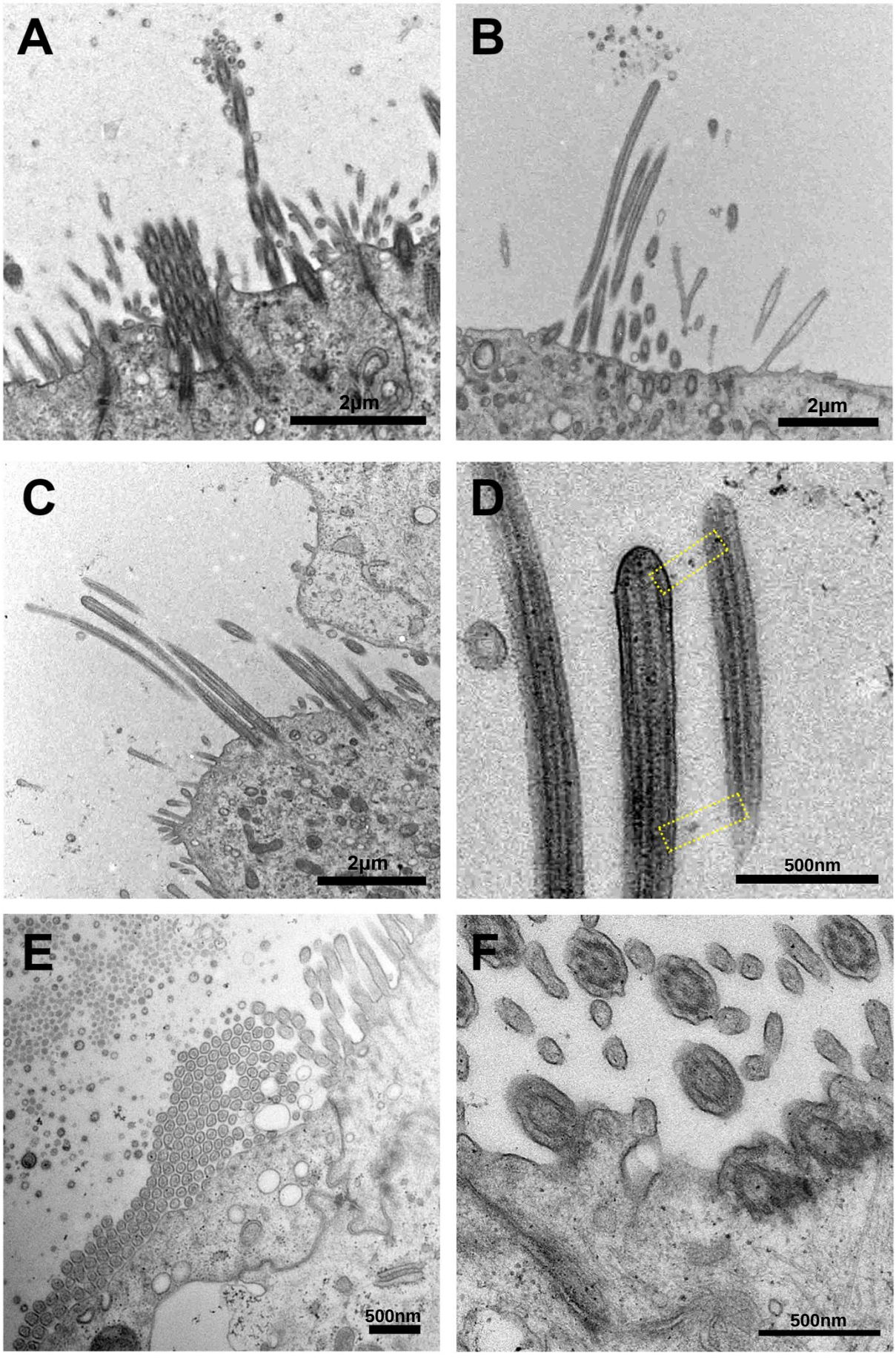
A
2µm
B
2µm
C
2µm
D
500nm
E
500nm
F
500nm

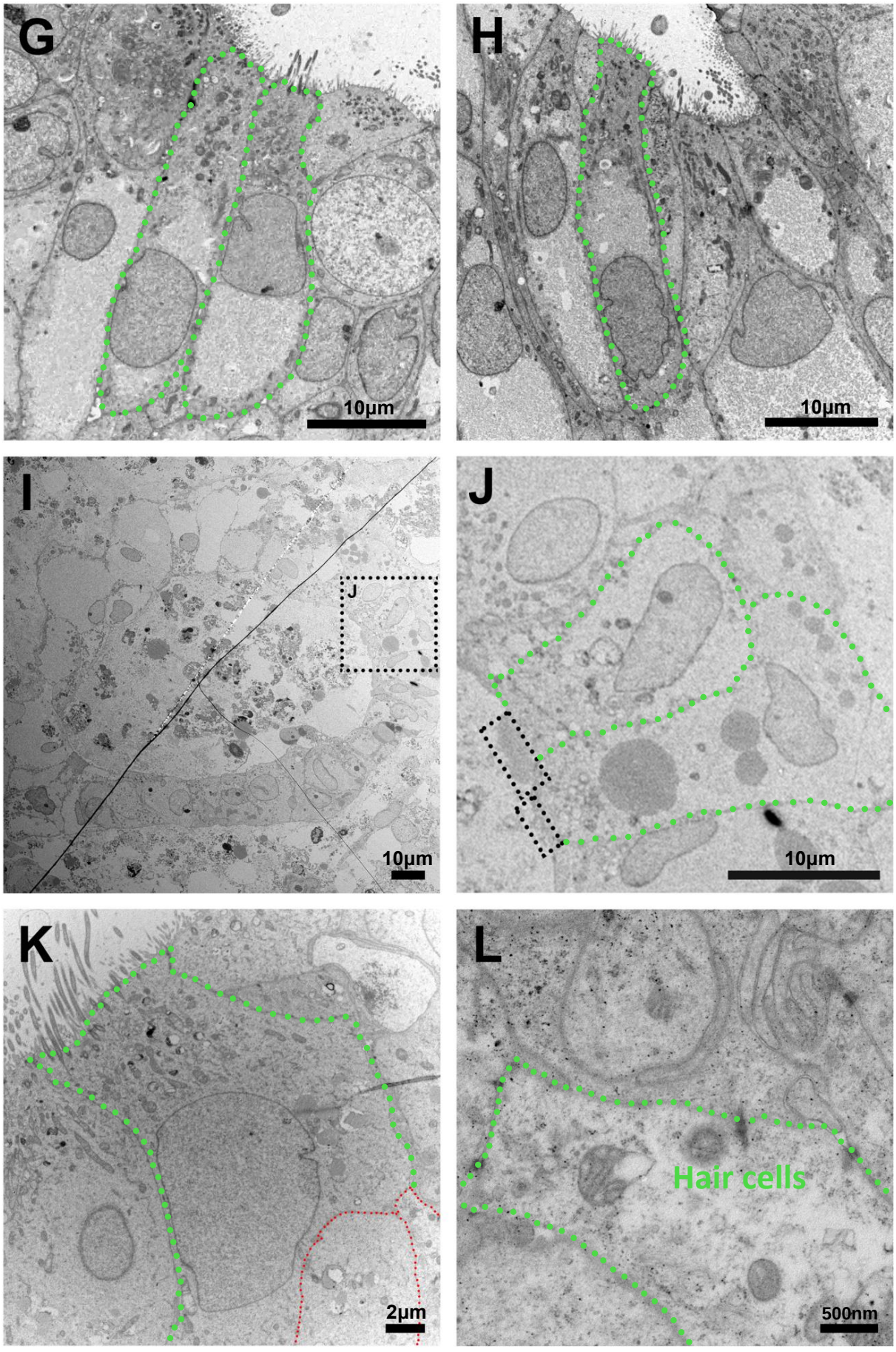
G
10μm
H
10μm
I
J
10μm
J
10μm
K
2μm
L
Hair cells
500nm

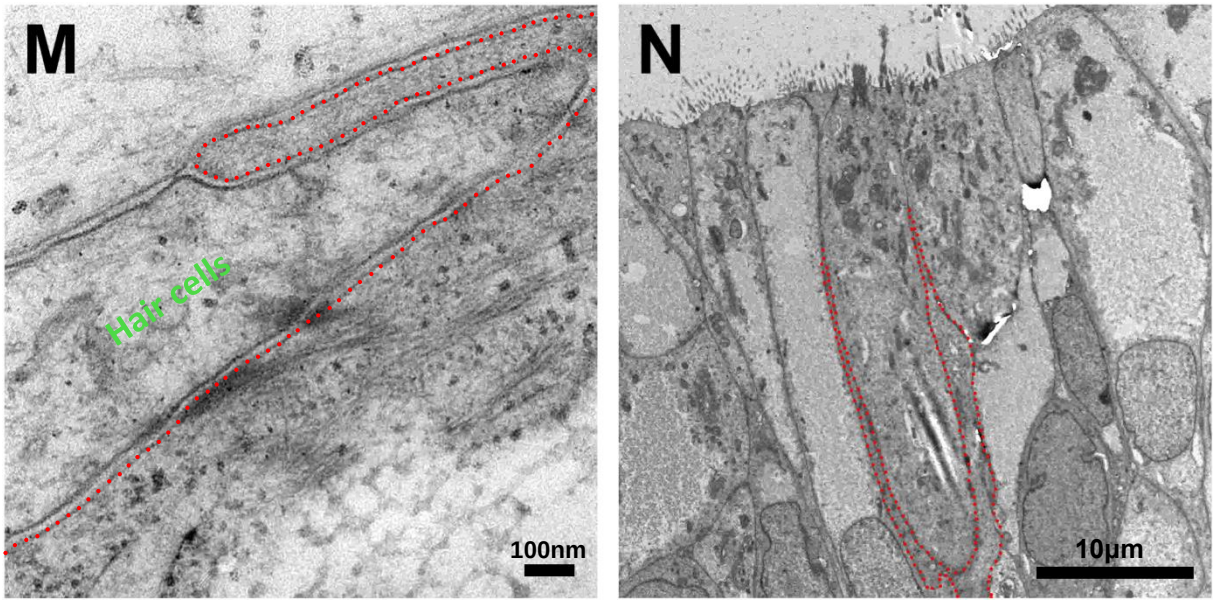

Figure 60 | TEM images of possible stereocilia bundles (d90).

Possible stereocilia bundles (A – D) and cross sections of the stereocilia bundles (E, F) are observed on day 90 of differentiation. The yellow dotted square indicates cross-links between stereocilia. G, H, Higher magnifications of the otic vesicle-like structures containing potential hair cells. Green dots and black dotted square show hair cells and stereocilia bundles, respectively. K – N, These hair cells make a connection with putative neurons (red dots). Data are representative of 8 EBs from at least 4 independent experiments (n=4).

5.2.2. FM1-43FX uptake assay

Functional properties of sensory cells including hair cells and sensory neurons generated by hiPSCs were also measured by staining with FM1. Similar to differentiated hESCs, dissociated EBs on day 90 derived from hiPSCs rapidly labelled with FM1 (Figure 61A, B). The immunostaining for MYO7A/SOX2/TUBB3 was performed after FM1 treatment to affirm the identity of hair cells and sensory neurons. More specifically, FM1 rapidly filled the cytoplasm of the MYO7A positive hair cell like cells (Figure 61C), but could not penetrate into the SOX2 positive supporting cells (Figure 61D). Once again some of FM1 labelled hair cells showed a vase shape like type I hair cell morphology (Figure 61C) and cylindrical OHC shapes (Figure 61D). Most of the TUBB3 positive cells did not uptake FM1 (Figure 61E), but some of them were double positive (Figure 61F) suggesting that only a minor population of cells are sensory neurons.

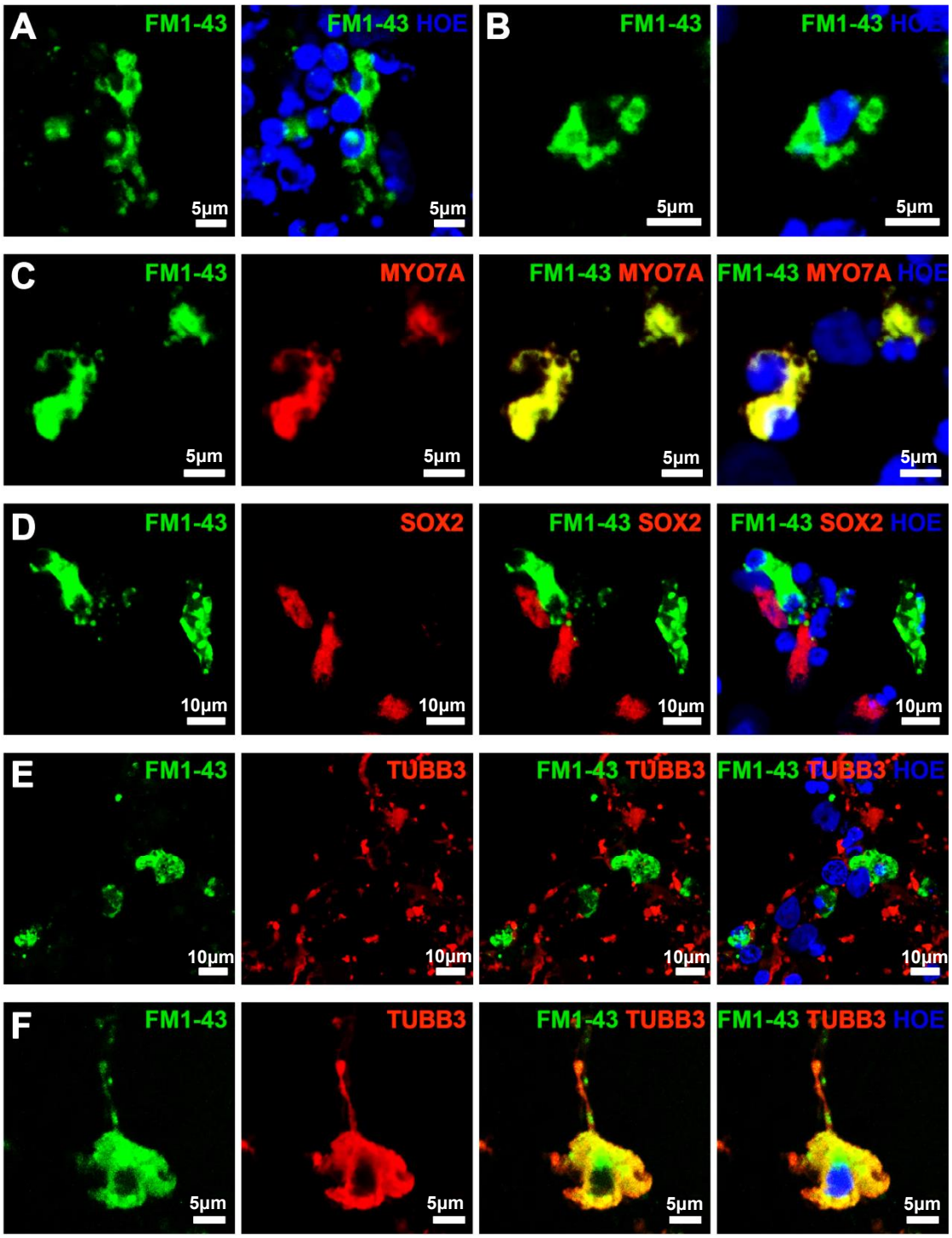

Figure 61 | Functional properties of hiPSCs-derived hair cells and neuronal cells using a FM1-43FX uptake assay.

Confocal images of dissociated d90 (A, B) EBs reveal FM1 labelled cells. FM1 labelled cells on d90 also express MYO7A (C), but not express SOX2 (D). Most of the TUBB3 positive cells are not uptake FM1 (E), but some cells co-express. Data are representative of 8 dissociated EBs from at least 3 independent experiments (n=3).

5.2.3. Electrophysiological recordings

Because of the density of cells in the 3D EBs and the thickness of the boundary layer, it proved difficult to patch clamp cells with a neuronal or hair cell morphology. For the easy access of sensory cells during electrophysiological recordings, we utilized specific uptake of FM1 dye for labelling of hair cells and sensory neurons, then enzymatic dissociation and flow cytometry was used to generate pure populations of sensory cells. After sorting flow cytometry most cells were dead or severely damaged. Some living cells were replated on the coverslips showed typical type I hair cell shape (Figure 62A) and bipolar neurons (Figure 62B). Despite isolating a pure population of hair cells and possible sensory neurons, we failed to measure patch-clamp recordings for the following reasons. In order for the sorter to function properly and to be able to deliver the proper results, the EBs were dissociated using Accutase, a gentle dissociation product for sensitive cells, and filtered through a 40 μm nylon mesh. To avoid sorting dead cells, a viability marker, Propidium iodide (PI), was added to the final suspension media. PI can enter cells with damaged membranes but not those with intact membranes and label the DNA brightly (Nicoletti et al., 1991) so that dead cells can then be excluded from the sort. Even though we used larger diameter nozzle tips and lower pressures to counter the viability effects of sorting, the viability of the sorted cells was low. One another reason that might affect cell viability is survival rate of epithelial cells decreases when they seed as a single cell. Despite all these problems, finally we got some healthy single hair cells (Figure 62A) and neuronal cells (Figure 62B), but unfortunately, it was not recorded any electrophysiological signals from them. We expect that proteolytic enzyme and physical pressure during filtration and sorting might destroy transduction channels on the cell surface. To lead successful recordings, we need to increase the efficiency of inducing hair cells or to engineer hPSC reporter cell line to label nascent hair cells with a fluorescent protein. More details would be discussed in chapter 6,

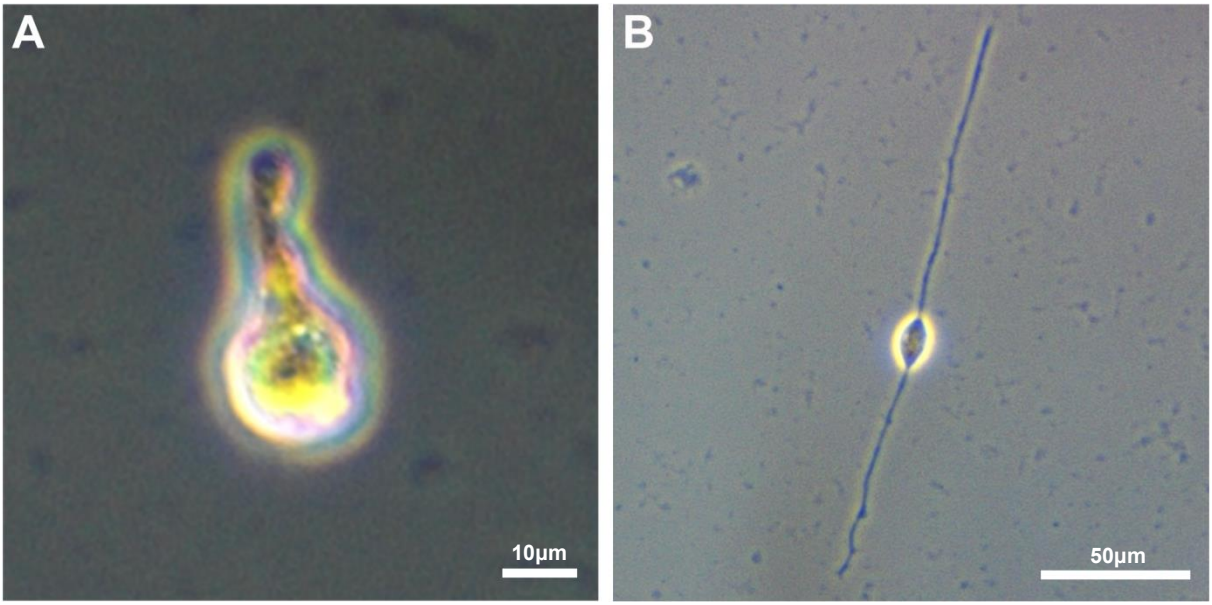

Figure 62 │ Possible hair cells and neuronal cells after sorting flow cytometry.

Isolated a single hair cell show a vase shape which is typical of type I vestibular hair cells (A), and possible a bipolar neuron (B) was sorted out using FM1 dye.

5.3.4 Conclusions

- TEM images of hair cells derived from hiPSCs using a low concentration of 2-mercaptoethanol show some of adult hair cell features *in vivo*, and these hair cells are attempting to make a connection with neurons.
- FM1 treatment together with Immunostaining using MYO7A/SOX2/TUBB3 antibodies demonstrates the presence of sensory hair cells and sensory neurons.
- For the easy access of sensory cells, EBs are sorted out using FM1, but this method is not good for the electrophysiological recordings.

Chapter 6

Discussion

Chapter 6. Discussion

6.1 Summary of findings

To summarize the *in vitro* otic lineage differentiation (Figure 63), on differentiation days 16 – 20, putative otic vesicles start to form from epithelium on the surface of the EB. Approximately 20 days later, ESPIN positive microvilli come out from the possible prosensory otic vesicles. As otic vesicles are getting mature, neuronal-like cells develop alongside otocysts containing primitive hair cells. From differentiation day 60, MYO7A positive hair-cell-like cells appear and thus could be observed possible hair cells and supporting cells separately.

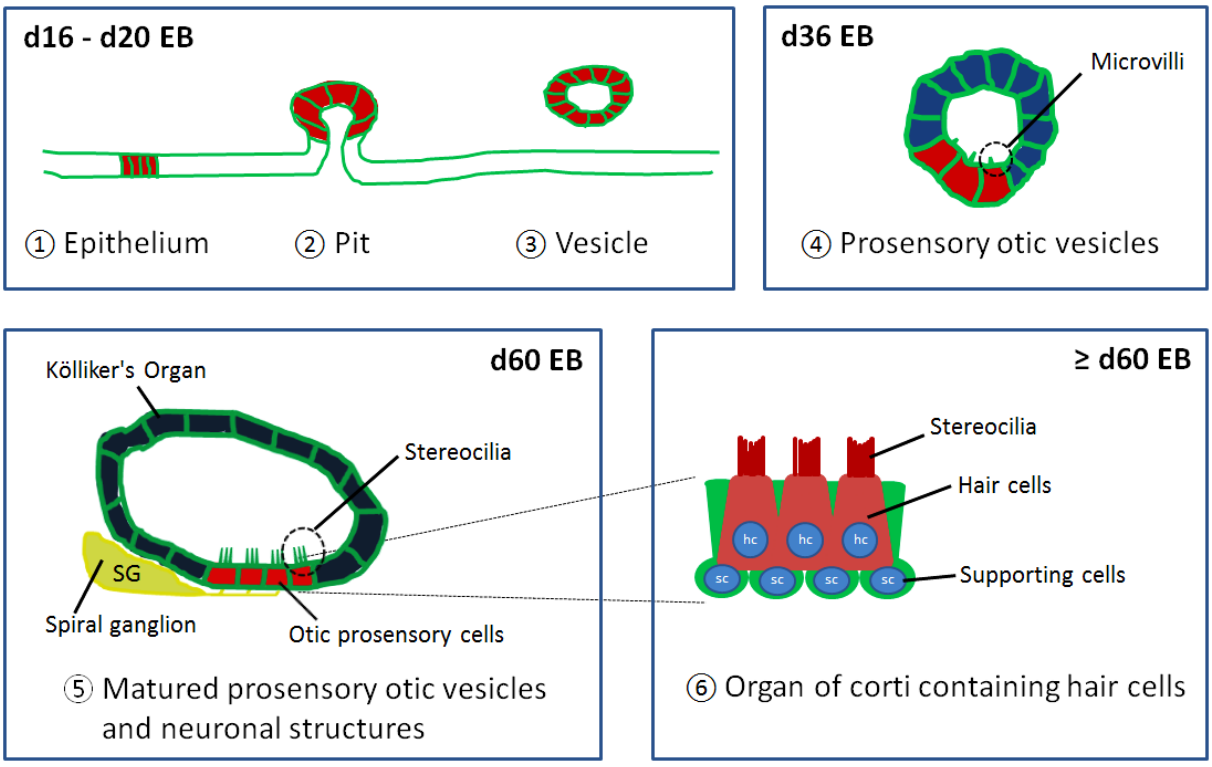

Figure 63 | Overview of an *in vitro* otic differentiation

Morphologically differentiated hair cells can be mainly classified by four criteria: 1) the expression of hair cell associated structure including the presence of stereocilia and kinocilium; 2) the presence of synaptic specialization – the pre and

post synaptic densities; 3) innervation – establishing appropriate nerve fiber connections; and 4) the expression of appropriate transcription factors (Lim and Brichta, 2016). The morphology of possible stereocilia bundles with innervation, the capability to take up FM1, and the electrophysiological properties of cells culture using media with a low concentration of 2-mercaptoethanol suggest that this culture condition is able to induce the differentiation of inner ear hair cells and functional neurons from hPSCs.

6.2 Importance of derivation of inner ear tissue from hPSCs

The inner ear is one of the few organs where biopsies cannot be easily taken because of its small size, complex architecture, and relative inaccessibility. For this reason, studying of the inner ear that enables insight into the molecular expression profiles involved in embryological development of the human fetal inner ear has been limited. It also makes difficult the evaluation of toxicity and monitoring pathological processes of auditory impairments in patients. Alternatively, genetically modified animal models have been used to study inner ear; however these animal models have a limitation to represent all of the phenotypes of human genetic disorder and probably will not be able to demonstrate certain properties unique to human sensation and behaviour. Therefore, the importance of establishing human model systems is reinforcement.

The inner ear sensory hair cells are mechanoreceptors of the auditory and vestibular systems and are essential for hearing and balance. Hair cells are easily damaged due to many reasons such as age-related dysfunction, high doses of ototoxic drugs, infectious diseases, genetic disorders, and exposure to high levels of noise (Bodmer, 2008, Cheng et al., 2005, Clark and Bohne, 1999, Fligor and Cox, 2004, Matsui and Cotanche, 2004, Suter and von Gierke, 1987). Unlike chick and zebrafish, in adult mammals, auditory hair cells and primary afferent neurons are unable to regenerate, and damage to these cells results in permanent hearing loss and balance disorders (Atkinson et al., 2015). Currently, the principal treatment for hearing loss is a cochlear implant. This device provides immense benefit to those with hearing loss by reinstating the transmission of sound information to the central auditory pathway, but it is imperfect cure deafness. Additionally, while the cochlear implant relies upon a functional population of primary auditory neurons that provide the critical link between the peripheral cochlea and the central auditory system, because electrical signals generated by the implant directly stimulate the cochlear nerve, causing it to send signals to the brain. For this reason, the cochlear implant can’t be applied in the case where the auditory neurons are damaged. Therefore, the stem cell based therapeutic strategy to regenerate inner ear cell has been suggested as a most powerful method for curing hearing loss. The protocol we developed in this project would enable human ear research such as *in vitro* studies of the mechanism of various disease processes within the human inner ear because 3D structural EBs follow *in vivo* developmental kinetics. Moreover, since the protocol we used in this

study works with hiPSCs and is free from cells of other species, it would perhaps be more applicable not only to modelling of sensorineural hearing loss disease but also for the generation of clinically useful sensory cells. The use of autologous cells would avoid the immunosuppression treatment and eliminate the complications associated with tissue rejection by transplanting sensory cells generated from the patient.

A number of studies have now demonstrated the potential of hPSCs to differentiate into inner ear mechanosensitive hair cells and neurosensory progenitors. However, so far, these attempts have resulted in the inefficient conversion of stem cells into inner-ear-like cells or only confined to vestibular like cells. In a paper published in 2012 by a group in Sheffield, a protocol to induce otic lineage differentiation from hESCs was presented, but the limitation of this method was that only less than 1% of cells had a hair bundle expressing ESPIN (Chen et al., 2012). Also, hair bundles rarely had a good arrangement as stereocilia on native hair cells (Chen et al., 2012). 2 years later, Stefan Heller's group in Stanford showed differentiated hair cell-like cells expressing multiple hair cell markers such as MYO7A and ESPIN (Ronaghi et al., 2014). However, they failed to fully mature into cells with typical hair cell cytoarchitecture. SEM images showed that potential hair bundle-like structures were mostly disorganized and splayed. A Chinese group also introduced methods to induce hair-cell-like cells from hESCs (Ding et al., 2016). Even though they successfully induced functional hair cell-like cells, the big disadvantage was that chicken utricle stromal cells or conditioned medium produced from such cells that were needed for differentiation. More recently, Koehler et al. reported a method for differentiating hPSCs to inner ear organoids using a developmentally faithful approach (Koehler et al., 2017). Intriguingly, the organoids harbored functional vestibular type II-like hair cells that are innervated by sensory neurons; however, further study is needed to fully understand which signalling mechanisms decide hair cell types. We may raise questions about whether the vestibular hair cell fate is perhaps the "default" hair cell fate because vestibular organs develop before auditory system such as the cochlea (Manley and Koppl, 1998, Fritzsch et al., 2013). Therefore it is possible that the preference for vestibular differentiation reflects this timescale in vitro but given that the 3D EBs from our study and others have been maintained for up to 150 days in culture, this seems a lesser possibility. Most likely there were signalling molecules missing in Koehler's method that contribute to cochlear specification. The literature pointed to Shh signalling as a critical inducer of

the cochlea (Bok et al., 2007, Riccomagno et al., 2002). *In vivo*, prior to hair cell differentiation in the developing mouse cochlea, Shh is expressed by spiral ganglia neurons, but it levels decrease from basal to the apex and this spatiotemporal pattern closely matches that of hair cell differentiation in the cochlear duct (Liu et al., 2010). Another paper reported that Fgf20 is expressed at the right time and place to mediate sensory cell specification (Hayashi et al., 2008). Remarkably, the vestibular epithelium was unaffected by deletion of Fgf20 suggesting that the role of Fgf20 in hair cell specification might be specific to the cochlea (Hayashi et al., 2008). Interestingly the pattern of Fgf20 expression paralleled Shh expression in the spiral ganglion and the excessive Shh signalling inhibited hair cell formation by upregulating Fgf20 suggesting that Fgf20 is downstream of Shh signalling (Tateya et al., 2013). These studies have shown the possibility that FGF/Shh signalling is involved in cochlea specification, but it remains to be seen whether these signalling mechanism translates to *in vitro* differentiation.

6.3 Ways to identify hair cell types *in vitro*

In the mammalian inner ear, there are four distinct types of hair cells. The sensory epithelia in the vestibule contain type I and II hair cells, whereas the organ of Corti in the cochlea contains IHCs and OHCs. In the animal, these hair cells can be readily distinguished by gross anatomical characteristics; however, to distinguish hair cell types derived from PSCs, *in vitro* genetic markers must be used. Compared to human, the protein expression in vestibular and cochlear hair cells relatively well studied in animal models. Therefore, the defining characteristics of different hair cell types from them can be used to identify hair cells *in vitro* (Table 10). It seems like expression pattern of transcription factors is evolutionally well conserved, but further investigation will be needed to further understanding of human.

	Vestibular		Cochlear	
Hair cell type	Type I	Type II	Inner	Outer
Shape				
Stereocilia				
Synapse				
MYO7A PAX2	h	h	h	h
PRESTIN				h
PARVALBUMIN*	m, r, g		h, g	h
OCM**	m			m
SOX2**	m	m		
CB2**		m		
OTOP1***	m	m		

Table 10 | Defining different hair cell types by morphology and protein markers.

Several criteria for identifying different types of hair cells derived *in vitro*. *PARVALBUMIN has been shown to be expressed in human cochlear hair cells (Rask-Andersen et al., 2009); however, whether PARVALBUMIN is localized to vestibular hair cells requires further investigation. In addition, expression of Parvalbumin was found in mouse, rat, and guinea pig type I hair cells (Dememes et al., 1993). **Selective expression has only been convincingly shown in the mouse and should be confirmed in the human inner ear. ***OTOP1 expression has been shown to persist in mouse vestibular supporting cells, not cochlear supporting cells (Kim et al., 2010). h; human, m; mouse, r; rat, g; guinea pig.

The single cell electrophysiological recording is another option to distinguish developing hair cell identities *in vitro*. Each type of hair cell should follow a stereotyped pattern of functional maturation characterized mainly by ion channels and synaptic proteins in the basolateral membrane (Geleoc and Holt, 2003, Geleoc et al., 2004). For example, during mouse embryonic stages of development all vestibular hair cells express a Na^+ current (I_{Na}), an inward rectifying K^+ current (I_{K1}), and a conventional delayed rectifying K^+ current (I_{Kv}) (Geleoc and Holt, 2003, Geleoc et al., 2004, Wooltorton et al., 2007). From E18, the voltage responses of these cells begin to diverge because of the acquisition of a negative activating K^+ current in type I hair cells (Geleoc et al., 2004). When mammalian cochlear hair cells begin to differentiate soon after terminal mitosis in mice, both IHCs and OHCs begin to express small outward delayed rectifier (I_K) and inward rectifier (I_{K1}) K^+ currents, so they are biophysically indistinguishable (Marcotti et al., 2003a, Helyer et al., 2005). The embryonic cochlear hair cells also express a Ca^{2+} current (I_{Ca}) and a sodium current (I_{Na}) (Marcotti et al., 2003b). From around P8, OHCs outward delayed rectifier I_K is down-regulated and the negatively activating K^+ current characteristic of adult cells begins to be expressed (Marcotti and Kros, 1999). In contrast to OHCs, all K^+ currents continue to increase in amplitude from birth up to about P10 - P12 in IHCs (Marcotti et al., 1999, Marcotti et al., 2003a, Marcotti et al., 2004). The properties of mechanotransduction and adaptation might also help distinguish between vestibular and cochlear hair cells, but there is a long way to go before we understand all the complexity of bio-physiological characteristics of four types of hair cells in human.

6.4 Limitations of the study and future directions

The studies in this project describe for the first time the differentiation of hESCs and hiPSCs to cochlear and vestibular hair cells and functional neurons. This provides a first step towards the refinement of protocols to generate human sensory hair cells and neurons for potential therapeutic purposes. However, several improvements to the technique need to be carried out before this therapeutic potential can be realised.

First, the next logical step would be engineering a hPSC reporter cell line to label nascent hair cells with a fluorescent protein. This transgenic line would be useful for guidance studies because stem cell-derived hair cell-like cells can be identified by expression of the fluorescent reaction. This technique has been widely used in the biomedical field including induction of otic lineages from PSCs to facilitate live-cell imaging and electrophysiological recordings. For example, Oshima and colleagues isolated mESC lines from Atoh1/nGFP blastocysts produced from the transgenic mouse strain Atoh1/nGFP express a nuclear variant of enhanced green fluorescent protein (nGFP) that is driven by an Atoh1 enhancer (Oshima et al., 2010). This cell line expressed typical mESC markers and interestingly expressed the nGFP reporter (Azuara et al., 2006). To generate iPSC lines, Atoh1/nGFP embryonic fibroblasts were infected with retroviruses expressing Oct4, Sox2, Klf4, and cMyc. It was observed that the Atoh1/nGFP reporter which was active in mESCs and miPSCs downregulated upon differentiation of the cells. 8 years later, the same group generated H9^{ATOH1}-nGFP hESCs using a murine Atoh1 enhancer to identify a limited number of hair cell-like cells. Although 20% of all differentiated cells expressed nGFP^{ATOH1}, cells that expressed multiple hair cell markers were also encountered in nGFP^{negative} cell populations. This could be explained by the fact that murine Atoh1 is downregulated as a hair cell mature or the proteins related to maturation of hair cells appear sequentially *in vivo*. However, the murine Atoh1 enhancer is activated in many additional Atoh1-dependent cell types, including developing cell populations in the nervous system in the spinal cord and cerebellum, Mercel cells, and secretory cells of the gut (Lumpkin et al., 2003). This suggests that Atoh1 is probably not an optimal reporter gene for human hair cell differentiation without additional markers. For these reasons, choosing the proper gene for transgenic cell line deserves careful consideration. Although it is highly unrealistic to find a specific gene only for the hair cell development, *MOY7A* and *ESPIN* would be good candidates. In addition, instead

of earlier methods used in previous two papers, the CRISPR-associated RNA-guided endonuclease Cas9, that can precisely target a genomic site to disrupt or repair a specific gene, would enable to generate fluorescent reporter cell line by editing genome more easily and quickly (Hsu et al., 2014). In this project, lack of the fluorescent cell lines made difficult to distinguish hair cells among mixed cell populations in EBs. Hair cell-like-cells were identified by morphology, so there was a limitation. Generation of transgenic cell line would be helpful to facilitate identification of developing hair cells in 3D culture.

The protocol developed in this project yields a variable quantity of vesicles containing hair cell-like cells. To improve the utility of our inner ear cell culture, we need to manipulate additional signalling molecules that could amplify the otic induction process. As stressed several times, the FGF signalling pathway plays an important role during the early inner ear development. More specifically, the FGF signalling pathway is required for induction of the otic placode, and the ligands involved in otic placode induction have been identified as FGF3 and FGF10 (Alvarez et al., 2003, Wright and Mansour, 2003). In our study, EBs were exposed to FGF on days 5 – 8 to promote otic lineage differentiation; however further studies should be undertaken such as optimization of FGF exposure time and inhibitor tests to identify how FGF signaling plays a role in our model. In addition to FGF, many studies have demonstrated that RA plays a role in controlling differentiation of location-specific aspects of hair cell phenotypes, such as luminal surface size, bundle height, stereocilia number and hair cell physiology (Najafzadeh et al., 2015, Sokolowski et al., 1999). Especially RA appears to regulate the stereocilia growth by upregulating the transcription of Espin and Fscn2, crosslinking proteins that regulate the elongation of the actin filled stereocilia (Thiede et al., 2014). In previous studies, Ding and colleagues showed the formation efficiency of ESPIN positive cells is significantly improved with treatment of RA during hESC differentiation into otic lineages (Ding et al., 2016). Lastly according to the recent paper, Wnt agonist CHIR99021 promotes inner ear development in 3D culture (DeJonge et al., 2016). Considering all these information, it is worth trying to elucidate FGF, RA, and Wnt signalling activity to improve induction of human otic tissues.

Although neural-like cells derived from hPSCs in this study showed typical current recordings of neurons *in vivo*, it remains to be determined whether those cells have an electrical phenotype capable of processing information in a similar manner

to the primary auditory neurons. In general, the glutamatergic primary auditory neurons have a large complement of ion channels that enable them to respond to complex signals with temporal precision (Needham et al., 2012). A key characteristic of this neural phenotype is the ability to reliably follow high-frequency stimulation since this is a hallmark of acoustic stimuli (Needham et al., 2012). Therefore, to verify the specific functional properties of hESC derived neuronal-like cells, it needs to examine the firing activity in response to pulse trains and to compare their responses to high-frequency stimulation with that of the primary auditory neuron population.

References

WHAT IS THE EVIDENCE FOR EVOLUTION? [Online]. Available: http://www.bio.miami.edu/dana/106/106F05_4.html.

AHMED, M., WONG, E. Y., SUN, J., XU, J., WANG, F. & XU, P. X. 2012. Eya1-Six1 interaction is sufficient to induce hair cell fate in the cochlea by activating Atoh1 expression in cooperation with Sox2. *Dev Cell,* 22**,** 377-90.

AHRENS, K. & SCHLOSSER, G. 2005. Tissues and signals involved in the induction of placodal Six1 expression in Xenopus laevis. *Dev Biol,* 288**,** 40-59.

ALVAREZ, I. S., MARTIN-PARTIDO, G., RODRIGUEZ-GALLARDO, L., GONZALEZ-RAMOS, C. & NAVASCUES, J. 1989. Cell proliferation during early development of the chick embryo otic anlage: quantitative comparison of migratory and nonmigratory regions of the otic epithelium. *J Comp Neurol,* 290**,** 278-88.

ALVAREZ, Y., ALONSO, M. T., VENDRELL, V., ZELARAYAN, L. C., CHAMERO, P., THEIL, T., BOSL, M. R., KATO, S., MACONOCHIE, M., RIETHMACHER, D. & SCHIMMANG, T. 2003. Requirements for FGF3 and FGF10 during inner ear formation. *Development,* 130**,** 6329-38.

AMIT, M. & ITSKOVITZ-ELDOR, J. 2012. *Atlas of human pluripotent stem cells : derivation and culturing,* New York, Humana Press.

APPLER, J. M., LU, C. C., DRUCKENBROD, N. R., YU, W. M., KOUNDAKJIAN, E. J. & GOODRICH, L. V. 2013. Gata3 is a critical regulator of cochlear wiring. *J Neurosci,* 33**,** 3679-91.

ATKINSON, P. J., HUARCAYA NAJARRO, E., SAYYID, Z. N. & CHENG, A. G. 2015. Sensory hair cell development and regeneration: similarities and differences. *Development,* 142**,** 1561-71.

AZUARA, V., PERRY, P., SAUER, S., SPIVAKOV, M., JORGENSEN, H. F., JOHN, R. M., GOUTI, M., CASANOVA, M., WARNES, G., MERKENSCHLAGER, M. & FISHER, A. G. 2006. Chromatin signatures of pluripotent cell lines. *Nat Cell Biol,* 8**,** 532-8.

BAHARVAND, H., MEHRJARDI, N. Z., HATAMI, M., KIANI, S., RAO, M. & HAGHIGHI, M. M. 2007. Neural differentiation from human embryonic stem cells in a defined adherent culture condition. *Int J Dev Biol,* 51**,** 371-8.

BAKER, B. M. & CHEN, C. S. 2012. Deconstructing the third dimension: how 3D culture microenvironments alter cellular cues. *J Cell Sci,* 125**,** 3015-24.

BAKER, C. V. & BRONNER-FRASER, M. 2001. Vertebrate cranial placodes I. Embryonic induction. *Dev Biol,* 232**,** 1-61.

BARTH, K. A., KISHIMOTO, Y., ROHR, K. B., SEYDLER, C., SCHULTE-MERKER, S. & WILSON, S. W. 1999. Bmp activity establishes a gradient of positional information throughout the entire neural plate. *Development,* 126**,** 4977-87.

BASCH, M. L., BROWN, R. M., 2ND, JEN, H. I. & GROVES, A. K. 2016. Where hearing starts: the development of the mammalian cochlea. *J Anat,* 228**,** 233-54.

BATTS, S. A., SHOEMAKER, C. R. & RAPHAEL, Y. 2009. Notch signaling and Hes labeling in the normal and drug-damaged organ of Corti. *Hear Res,* 249**,** 15-22.

BERMINGHAM-MCDONOGH, O., STONE, J. S., REH, T. A. & RUBEL, E. W. 2001. FGFR3 expression during development and regeneration of the chick inner ear sensory epithelia. *Dev Biol,* 238**,** 247-59.

BERMINGHAM, N. A., HASSAN, B. A., PRICE, S. D., VOLLRATH, M. A., BEN-ARIE, N., EATOCK, R. A., BELLEN, H. J., LYSAKOWSKI, A. & ZOGHBI, H. Y. 1999. Math1: an essential gene for the generation of inner ear hair cells. *Science,* 284**,** 1837-41.

BETZ, W. J., MAO, F. & SMITH, C. B. 1996. Imaging exocytosis and endocytosis. *Curr Opin Neurobiol,* 6**,** 365-71.

BEURG, M., FETTIPLACE, R., NAM, J. H. & RICCI, A. J. 2009. Localization of inner hair cell mechanotransducer channels using high-speed calcium imaging. *Nat Neurosci,* 12**,** 553-8.

BEVAN, M. J., EPSTEIN, R. & COHN, M. 1974. The effect of 2-mercaptoethanol on murine mixed lymphocyte cultures. *J Exp Med,* 139**,** 1025-30.

BODMER, D. 2008. Protection, regeneration and replacement of hair cells in the cochlea: implications for the future treatment of sensorineural hearing loss. *Swiss Med Wkly,* 138**,** 708-12.

BOK, J., BRONNER-FRASER, M. & WU, D. K. 2005. Role of the hindbrain in dorsoventral but not anteroposterior axial specification of the inner ear. *Development,* 132**,** 2115-24.

BOK, J., DOLSON, D. K., HILL, P., RUTHER, U., EPSTEIN, D. J. & WU, D. K. 2007. Opposing gradients of Gli repressor and activators mediate Shh signaling along the dorsoventral axis of the inner ear. *Development,* 134**,** 1713-22.

BRAUN, C. B. 1996. The sensory biology of the living jawless fishes: A phylogenetic assessment. *Brain Behavior and Evolution,* 48**,** 262-276.

BROOKER, R., HOZUMI, K. & LEWIS, J. 2006. Notch ligands with contrasting functions: Jagged1 and Delta1 in the mouse inner ear. *Development,* 133**,** 1277-86.

BROWN, S. T., WANG, J. M. & GROVES, A. K. 2005. Dlx gene expression during chick inner ear development. *Journal of Comparative Neurology,* 483**,** 48-65.

BROWNELL, W. E., BADER, C. R., BERTRAND, D. & DE RIBAUPIERRE, Y. 1985. Evoked mechanical responses of isolated cochlear outer hair cells. *Science,* 227**,** 194-6.

BRUGMANN, S. A. & MOODY, S. A. 2005. Induction and specification of the vertebrate ectodermal placodes: precursors of the cranial sensory organs. *Biology of the Cell,* 97**,** 303-319.

BRUGMANN, S. A., PANDUR, P. D., KENYON, K. L., PIGNONI, F. & MOODY, S. A. 2004. Six1 promotes a placodal fate within the lateral neurogenic ectoderm by functioning as both a transcriptional activator and repressor. *Development,* 131**,** 5871-81.

BRUSKA, M., ULATOWSKA-BLASZYK, K., WEGLOWSKI, M., WOZNIAK, W. & PIOTROWSKI, A. 2009. Differentiation of the facio-vestibulocochlear ganglionic complex in human embryos of developmental stages 13-15. *Folia Morphol (Warsz),* 68**,** 167-73.

CAI, T. & GROVES, A. K. 2015. The Role of Atonal Factors in Mechanosensory Cell Specification and Function. *Mol Neurobiol,* 52**,** 1315-29.

CAMUS, A., PEREA-GOMEZ, A., MOREAU, A. & COLLIGNON, J. 2006. Absence of Nodal signaling promotes precocious neural differentiation in the mouse embryo. *Dev Biol,* 295**,** 743-55.

CAREY, F. J., LINNEY, E. A. & PEDERSEN, R. A. 1995. Allocation of epiblast cells to germ layer derivatives during mouse gastrulation as studied with a retroviral vector. *Dev Genet,* 17**,** 29-37.

CARLSON, B. M. 2014. *Human embryology and developmental biology,* Philadelphia, PA, Elsevier/Saunders.

CATERINA, M. J., SCHUMACHER, M. A., TOMINAGA, M., ROSEN, T. A., LEVINE, J. D. & JULIUS, D. 1997. The capsaicin receptor: a heat-activated ion channel in the pain pathway. *Nature,* 389**,** 816-24.

CHAI, R., XIA, A., WANG, T., JAN, T. A., HAYASHI, T., BERMINGHAM-MCDONOGH, O. & CHENG, A. G. 2011. Dynamic expression of Lgr5, a Wnt target gene, in the developing and mature mouse cochlea. *J Assoc Res Otolaryngol,* 12**,** 455-69.

CHAMBERS, S. M., FASANO, C. A., PAPAPETROU, E. P., TOMISHIMA, M., SADELAIN, M. & STUDER, L. 2009. Highly efficient neural conversion of human ES and iPS cells by dual inhibition of SMAD signaling. *Nat Biotechnol,* 27**,** 275-80.

CHANDROSS KJ, M. E. 2001. Plasticity of adult bone marrow stem

cells. *Greenwich, CT: JAI Press*.

CHANG, W., BRIGANDE, J. V., FEKETE, D. M. & WU, D. K. 2004. The development of semicircular canals in the inner ear: role of FGFs in sensory cristae. *Development,* 131**,** 4201-11.

CHANG, W., LIN, Z., KULESSA, H., HEBERT, J., HOGAN, B. L. & WU, D. K. 2008. Bmp4 is essential for the formation of the vestibular apparatus that detects angular head movements. *PLoS Genet,* 4**,** e1000050.

CHEN, P., JOHNSON, J. E., ZOGHBI, H. Y. & SEGIL, N. 2002. The role of Math1 in inner ear development: Uncoupling the establishment of the sensory primordium from hair cell fate determination. *Development,* 129**,** 2495-505.

CHEN, W., JONGKAMONWIWAT, N., ABBAS, L., ESHTAN, S. J., JOHNSON, S. L., KUHN, S., MILO, M., THURLOW, J. K., ANDREWS, P. W., MARCOTTI, W., MOORE, H. D. & RIVOLTA, M. N. 2012. Restoration of auditory evoked responses by human ES-cell-derived otic progenitors. *Nature,* 490**,** 278-82.

CHENG, A. G., CUNNINGHAM, L. L. & RUBEL, E. W. 2005. Mechanisms of hair cell death and protection. *Curr Opin Otolaryngol Head Neck Surg,* 13**,** 343-8.

CHIN, M. H., PELLEGRINI, M., PLATH, K. & LOWRY, W. E. 2010. Molecular analyses of human induced pluripotent stem cells and embryonic stem cells. *Cell Stem Cell,* 7**,** 263-9.

CLARK, W. W. & BOHNE, B. A. 1999. Effects of noise on hearing. *JAMA,* 281**,** 1658-9.

COLAS, J. F. & SCHOENWOLF, G. C. 2001. Towards a cellular and molecular understanding of neurulation. *Dev Dyn,* 221**,** 117-45.

COLCLASURE, J. C. & HOLT, J. R. 2003. Transduction and adaptation in sensory hair cells of the mammalian vestibular system. *Gravit Space Biol Bull,* 16**,** 61-70.

COMIS, S. D., OSBORNE, M. P., O'CONNELL, J. & JOHNSON, A. P. 1990. The importance of early fixation in preservation of human cochlear and vestibular sensory hair bundles. *Acta Otolaryngol,* 109**,** 361-8.

CORRALES, C. E., PAN, L., LI, H., LIBERMAN, M. C., HELLER, S. & EDGE, A. S. 2006. Engraftment and differentiation of embryonic stem cell-derived neural progenitor cells in the cochlear nerve trunk: growth of processes into the organ of Corti. *J Neurobiol,* 66**,** 1489-500.

CORWIN, J. T. & COTANCHE, D. A. 1988. Regeneration of sensory hair cells after acoustic trauma. *Science,* 240**,** 1772-4.

COTANCHE, D. A. 1987. Regeneration of hair cell stereociliary bundles in the chick cochlea following severe acoustic trauma. *Hear Res,* 30**,** 181-95.

CRUZ, R. M., LAMBERT, P. R. & RUBEL, E. W. 1987. Light microscopic evidence of hair cell regeneration after gentamicin toxicity in chick cochlea. *Arch Otolaryngol Head Neck Surg,* 113**,** 1058-62.

DABDOUB, A., PULIGILLA, C., JONES, J. M., FRITZSCH, B., CHEAH, K. S., PEVNY, L. H. & KELLEY, M. W. 2008. Sox2 signaling in prosensory domain specification and subsequent hair cell differentiation in the developing cochlea. *Proc Natl Acad Sci U S A,* 105**,** 18396-401.

DALLOS, P., BILLONE, M. C., DURRANT, J. D., WANG, C. & RAYNOR, S. 1972. Cochlear inner and outer hair cells: functional differences. *Science,* 177**,** 356-8.

DAUDET, N., GIBSON, R., SHANG, J., BERNARD, A., LEWIS, J. & STONE, J. 2009. Notch regulation of progenitor cell behavior in quiescent and regenerating auditory epithelium of mature birds. *Dev Biol,* 326**,** 86-100.

DAYARATNE, M. W., VLAJKOVIC, S. M., LIPSKI, J. & THORNE, P. R. 2014. Kolliker's organ and the development of spontaneous activity in the auditory system: implications for hearing dysfunction. *Biomed Res Int,* 2014**,** 367939.

DE SANTA BARBARA, P., BONNEAUD, N., BOIZET, B., DESCLOZEAUX, M., MONIOT, B., SUDBECK, P., SCHERER, G., POULAT, F. & BERTA, P. 1998. Direct interaction of SRY-related protein SOX9 and steroidogenic factor 1 regulates transcription of the human anti-Mullerian hormone gene. *Mol Cell Biol,* 18**,** 6653-65.

DECHESNE, C. J. & SANS, A. 1985. Development of vestibular receptor surfaces in human fetuses. *Am J Otolaryngol,* 6**,** 378-87.

DEJONGE, R. E., LIU, X. P., DEIG, C. R., HELLER, S., KOEHLER, K. R. & HASHINO, E. 2016. Modulation of Wnt Signaling Enhances Inner Ear Organoid Development in 3D Culture. *PLoS One,* 11**,** e0162508.

DELMAGHANI, S., DEL CASTILLO, F. J., MICHEL, V., LEIBOVICI, M., AGHAIE, A., RON, U., VAN LAER, L., BEN-TAL, N., VAN CAMP, G., WEIL, D., LANGA, F., LATHROP, M., AVAN, P. & PETIT, C. 2006. Mutations in the gene encoding pejvakin, a newly identified protein of the afferent auditory pathway, cause DFNB59 auditory neuropathy. *Nat Genet,* 38**,** 770-8.

DEMEMES, D., EYBALIN, M. & RENARD, N. 1993. Cellular distribution of parvalbumin immunoreactivity in the peripheral vestibular system of three rodents. *Cell Tissue Res,* 274**,** 487-92.

DING, J., TANG, Z., CHEN, J., SHI, H., CHEN, J., WANG, C., ZHANG, C., LI, L., CHEN, P. & WANG, J. 2016. Induction of differentiation of human embryonic stem cells into functional hair-cell-like cells in the absence of stromal cells. *Int J Biochem Cell Biol,* 81**,** 208-222.

DOETSCHMAN, T. C., EISTETTER, H., KATZ, M., SCHMIDT, W. & KEMLER, R. 1985. The in vitro development of blastocyst-derived embryonic stem cell lines: formation of visceral yolk sac, blood islands and myocardium. *J Embryol Exp Morphol,* 87**,** 27-45.

DRAKE, R. L., VOGL, W., MITCHELL, A. W. M. & DRAKE, R. L. 2005. *Gray's anatomy for students flash cards,* New York, Churchill Livingstone.

EIRAKU, M., TAKATA, N., ISHIBASHI, H., KAWADA, M., SAKAKURA, E., OKUDA, S., SEKIGUCHI, K., ADACHI, T. & SASAI, Y. 2011. Self-organizing optic-cup morphogenesis in three-dimensional culture. *Nature,* 472**,** 51-6.

EIRAKU, M., WATANABE, K., MATSUO-TAKASAKI, M., KAWADA, M., YONEMURA, S., MATSUMURA, M., WATAYA, T., NISHIYAMA, A., MUGURUMA, K. & SASAI, Y. 2008. Self-organized formation of polarized cortical tissues from ESCs and its active manipulation by extrinsic signals. *Cell Stem Cell,* 3**,** 519-32.

ELZOUKI, A. Y. 2011. *Textbook of clinical pediatrics,* New York, Springer.

EVANS, M. J. & KAUFMAN, M. H. 1981. Establishment in culture of pluripotential cells from mouse embryos. *Nature,* 292**,** 154-6.

EVSEN, L., SUGAHARA, S., UCHIKAWA, M., KONDOH, H. & WU, D. K. 2013. Progression of neurogenesis in the inner ear requires inhibition of Sox2 transcription by neurogenin1 and neurod1. *J Neurosci,* 33**,** 3879-90.

FALK, N., LOSL, M., SCHRODER, N. & GIESSL, A. 2015. Specialized Cilia in Mammalian Sensory Systems. *Cells,* 4**,** 500-19.

FEKETE, D. M. 1999. Development of the vertebrate ear: insights from knockouts and mutants. *Trends Neurosci,* 22**,** 263-9.

FISH, J. L., DEHAY, C., KENNEDY, H. & HUTTNER, W. B. 2008. Making bigger brains-the evolution of neural-progenitor-cell division. *J Cell Sci,* 121**,** 2783-93.

FLIGOR, B. J. & COX, L. C. 2004. Output levels of commercially available portable compact disc players and the potential risk to hearing. *Ear Hear,* 25**,** 513-27.

FOSHAY, K. M., LOONEY, T. J., CHARI, S., MAO, F. F., LEE, J. H., ZHANG, L., FERNANDES, C. J., BAKER, S. W., CLIFT, K. L., GAETZ, J., DI, C. G., XIANG, A. P. & LAHN, B. T. 2012. Embryonic stem cells induce pluripotency in somatic cell fusion through biphasic reprogramming. *Mol Cell,* 46**,** 159-70.

FRETER, S., MUTA, Y., MAK, S. S., RINKWITZ, S. & LADHER, R. K. 2008. Progressive restriction of otic fate: the role of FGF and Wnt in resolving inner ear potential. *Development,* 135**,** 3415-24.

FRITZSCH, B. 2003. Development of inner ear afferent connections: forming primary neurons and connecting them to the developing sensory epithelia. *Brain Res Bull,* 60**,** 423-33.

FRITZSCH, B., PAN, N., JAHAN, I., DUNCAN, J. S., KOPECKY, B. J., ELLIOTT, K. L., KERSIGO, J. & YANG, T. 2013. Evolution and development of the tetrapod auditory system: an organ of Corti-centric perspective. *Evol Dev,* 15**,** 63-79.

FROLENKOV, G. I., BELYANTSEVA, I. A., FRIEDMAN, T. B. & GRIFFITH, A. J. 2004. Genetic insights into the morphogenesis of inner ear hair cells. *Nat Rev Genet,* 5**,** 489-98.

FUJIMOTO, S., YAMAMOTO, K., HAYABUCHI, I. & YOSHIZUKA, M. 1981. Scanning and transmission electron microscope studies on the organ of Corti and stria vascularis in human fetal cochlear ducts. *Arch Histol Jpn,* 44**,** 223-35.

GALE, J. E., MARCOTTI, W., KENNEDY, H. J., KROS, C. J. & RICHARDSON, G. P. 2001. FM1-43 dye behaves as a permeant blocker of the hair-cell mechanotransducer channel. *J Neurosci,* 21**,** 7013-25.

GELEOC, G. S. & HOLT, J. R. 2003. Developmental acquisition of sensory transduction in hair cells of the mouse inner ear. *Nat Neurosci,* 6**,** 1019-20.

GELEOC, G. S., RISNER, J. R. & HOLT, J. R. 2004. Developmental acquisition of voltage-dependent conductances and sensory signaling in hair cells of the embryonic mouse inner ear. *J Neurosci,* 24**,** 11148-59.

GEORGE, K. M., LEONARD, M. W., ROTH, M. E., LIEUW, K. H., KIOUSSIS, D., GROSVELD, F. & ENGEL, J. D. 1994. Embryonic Expression and Cloning of the Murine Gata-3 Gene. *Development,* 120**,** 2673-2686.

GERLACH, L. M., HUTSON, M. R., GERMILLER, J. A., NGUYEN-LUU, D., VICTOR, J. C. & BARALD, K. F. 2000. Addition of the BMP4 antagonist, noggin, disrupts avian inner ear development. *Development,* 127**,** 45-54.

GERMANGUZ, I., SEDAN, O., ZEEVI-LEVIN, N., SHTRICHMAN, R., BARAK, E., ZISKIND, A., ELIYAHU, S., MEIRY, G., AMIT, M., ITSKOVITZ-ELDOR, J. & BINAH, O. 2011. Molecular characterization and functional properties of cardiomyocytes derived from human inducible pluripotent stem cells. *J Cell Mol Med,* 15**,** 38-51.

GILBERT, S. F. 2010. *Developmental biology,* Sunderland, Mass., Sinauer Associates.

GILLESPIE, P. G. & MULLER, U. 2009. Mechanotransduction by hair cells: models, molecules, and mechanisms. *Cell,* 139**,** 33-44.

GLAVIC, A., HONORE, S. M., FEIJOO, C. G., BASTIDAS, F., ALLENDE, M. L. & MAYOR, R. 2004a. Role of BMP signaling and the homeoprotein iroquois in the specification of the cranial placodal field. *Developmental Biology,* 272**,** 89-103.

GLAVIC, A., MARIS HONORE, S., GLORIA FEIJOO, C., BASTIDAS, F., ALLENDE, M. L. & MAYOR, R. 2004b. Role of BMP signaling and the homeoprotein Iroquois in the specification of the cranial placodal field. *Dev Biol,* 272**,** 89-103.

GREEN, H., EASLEY, K. & IUCHI, S. 2003. Marker succession during the development of keratinocytes from cultured human embryonic stem cells. *Proc Natl Acad Sci U S A,* 100**,** 15625-30.

GRILL, R. J., JR. & PIXLEY, S. K. 1993. 2-Mercaptoethanol is a survival factor for olfactory, cortical and hippocampal neurons in short-term dissociated cell culture. *Brain Res,* 613**,** 168-72.

GRITSMAN, K., ZHANG, J. J., CHENG, S., HECKSCHER, E., TALBOT, W. S. & SCHIER, A. F. 1999. The EGF-CFC protein one-eyed pinhead is essential for nodal signaling. *Cell,* 97**,** 121-132.

GROVES, A. K. & BRONNER-FRASER, M. 2000. Competence, specification and commitment in otic placode induction. *Development,* 127**,** 3489-99.

GROVES, A. K. & FEKETE, D. M. 2012. Shaping sound in space: the regulation of inner ear patterning. *Development,* 139**,** 245-57.

GUENTHER, M. G., FRAMPTON, G. M., SOLDNER, F., HOCKEMEYER, D., MITALIPOVA, M., JAENISCH, R. & YOUNG, R. A. 2010. Chromatin structure and gene expression programs of human embryonic and induced pluripotent stem cells. *Cell Stem Cell,* 7**,** 249-57.

GUYTON, A. C. & HALL, J. E. 2006. *Textbook of medical physiology,* Philadelphia, Elsevier Saunders.

HADDON, C. & LEWIS, J. 1996. Early ear development in the embryo of the zebrafish, Danio rerio. *Journal of Comparative Neurology,* 365**,** 113-128.

HAMILL, O. P., MARTY, A., NEHER, E., SAKMANN, B. & SIGWORTH, F. J. 1981. Improved Patch-Clamp Techniques for High-Resolution Current Recording from Cells and Cell-Free Membrane Patches. *Pflugers Archiv-European Journal of Physiology,* 391**,** 85-100.

HANANI, M. 2005. Satellite glial cells in sensory ganglia: from form to function. *Brain Res Brain Res Rev,* 48**,** 457-76.

HARVEY, N. T., HUGHES, J. N., LONIC, A., YAP, C., LONG, C., RATHJEN, P. D. & RATHJEN, J. 2010. Response to BMP4 signalling during ES cell differentiation defines intermediates of the ectoderm lineage. *J Cell Sci,* 123**,** 1796-804.

HAYAKAWA, I., LINKO, Y. Y. & LINKO, P. 1996. Mechanism of high pressure denaturation of proteins. *Food Science and Technology-Lebensmittel-Wissenschaft & Technologie,* 29**,** 756-762.

HAYASHI, T., RAY, C. A. & BERMINGHAM-MCDONOGH, O. 2008. Fgf20 is required for sensory epithelial specification in the developing cochlea. *J Neurosci,* 28**,** 5991-9.

HEAD, J. R., GACIOCH, L., PENNISI, M. & MEYERS, J. R. 2013. Activation of canonical Wnt/beta-catenin signaling stimulates proliferation in neuromasts in the zebrafish posterior lateral line. *Dev Dyn,* 242**,** 832-46.

HELLER, N. & BRANDLI, A. W. 1999. Xenopus Pax-2/5/8 orthologues: novel insights into Pax gene evolution and identification of Pax-8 as the earliest marker for otic and pronephric cell lineages. *Dev Genet,* 24**,** 208-19.

HELYER, R. J., KENNEDY, H. J., DAVIES, D., HOLLEY, M. C. & KROS, C. J. 2005. Development of outward potassium currents in inner and outer hair cells from the embryonic mouse cochlea. *Audiol Neurootol,* 10**,** 22-34.

HEMMATI-BRIVANLOU, A. & MELTON, D. 1997. Vertebrate embryonic cells will become nerve cells unless told otherwise. *Cell,* 88**,** 13-7.

HERNANDEZ, P. P., OLIVARI, F. A., SARRAZIN, A. F., SANDOVAL, P. C. & ALLENDE, M. L. 2007. Regeneration in zebrafish lateral line neuromasts: expression of the neural progenitor cell marker sox2 and proliferation-dependent and-independent mechanisms of hair cell renewal. *Dev Neurobiol,* 67**,** 637-54.

HILDEBRAND, M. S., DAHL, H. H., HARDMAN, J., COLEMAN, B., SHEPHERD, R. K. & DE SILVA, M. G. 2005. Survival of partially differentiated mouse embryonic stem cells in the scala media of the guinea pig cochlea. *J Assoc Res Otolaryngol,* 6**,** 341-54.

HOSHINO, T. 1982. Scanning electron microscopic observation of the foetal labyrinthine vestibule. *Acta Otolaryngol,* 93**,** 349-54.

HSU, P. D., LANDER, E. S. & ZHANG, F. 2014. Development and applications of CRISPR-Cas9 for genome engineering. *Cell,* 157**,** 1262-78.

HUBNER, C. A. & JENTSCH, T. J. 2002. Ion channel diseases. *Hum Mol Genet,* 11**,** 2435-45.

HUDSPETH, A. J. & JACOBS, R. 1979. Stereocilia mediate transduction in vertebrate hair cells (auditory system/cilium/vestibular system). *Proc Natl Acad Sci U S A,* 76**,** 1506-9.

IGARASHI, Y. 1980a. Cochlea of the human fetus: a scanning electron microscope study. *Arch Histol Jpn,* 43**,** 195-209.

IGARASHI, Y. 1980b. Cochlea of the Human Fetus: A Scanning Electron Microscope Study. *Archivum histologicum japonicum,* 43**,** 195-209.

ITSKOVITZ-ELDOR, J., SCHULDINER, M., KARSENTI, D., EDEN, A., YANUKA, O., AMIT, M., SOREQ, H. & BENVENISTY, N. 2000. Differentiation of human embryonic stem cells into embryoid bodies compromising the three embryonic germ layers. *Mol Med,* 6**,** 88-95.

JACQUES, B. E., MONTGOMERY, W. H. T., URIBE, P. M., YATTEAU, A., ASUNCION, J. D., RESENDIZ, G., MATSUI, J. I. & DABDOUB, A. 2014. The role of Wnt/beta-catenin signaling in proliferation and regeneration of the developing basilar papilla and lateral line. *Dev Neurobiol,* 74**,** 438-56.

JACQUES, B. E., PULIGILLA, C., WEICHERT, R. M., FERRER-VAQUER, A., HADJANTONAKIS, A. K., KELLEY, M. W. & DABDOUB, A. 2012. A dual function for canonical Wnt/beta-catenin signaling in the developing mammalian cochlea. *Development,* 139**,** 4395-404.

JAGGER, D. J., ROBERTSON, D. & HOUSLEY, G. D. 2000. A technique for slicing the rat cochlea around the onset of hearing. *J Neurosci Methods,* 104**,** 77-86.

JAMES, D., LEVINE, A. J., BESSER, D. & HEMMATI-BRIVANLOU, A. 2005. TGFbeta/activin/nodal signaling is necessary for the maintenance of pluripotency in human embryonic stem cells. *Development,* 132**,** 1273-82.

JANG, Y. S., HWANG, C. H., SHIN, J. Y., BAE, W. Y. & KIM, L. S. 2006. Age-related changes on the morphology of the otoconia. *Laryngoscope,* 116**,** 996-1001.

JEFFERY, N. & SPOOR, F. 2004. Prenatal growth and development of the modern human labyrinth. *J Anat,* 204**,** 71-92.

JEON, S. J., FUJIOKA, M., KIM, S. C. & EDGE, A. S. 2011. Notch signaling alters sensory or neuronal cell fate specification of inner ear stem cells. *J Neurosci,* 31**,** 8351-8.

JIANG, L., ROMERO-CARVAJAL, A., HAUG, J. S., SEIDEL, C. W. & PIOTROWSKI, T. 2014. Gene-expression analysis of hair cell regeneration in the zebrafish lateral line. *Proc Natl Acad Sci U S A,* 111**,** E1383-92.

JOHNSON CHACKO, L., PECHRIGGL, E. J., FRITSCH, H., RASK-ANDERSEN, H., BLUMER, M. J., SCHROTT-FISCHER, A. & GLUECKERT, R. 2016. Neurosensory Differentiation and Innervation Patterning in the Human Fetal Vestibular End Organs between the Gestational Weeks 8-12. *Front Neuroanat,* 10**,** 111.

KAWAMOTO, K., IZUMIKAWA, M., BEYER, L. A., ATKIN, G. M. & RAPHAEL, Y. 2009. Spontaneous hair cell regeneration in the mouse utricle following gentamicin ototoxicity. *Hear Res,* 247**,** 17-26.

KEATS, B. J. & COREY, D. P. 1999. The usher syndromes. *Am J Med Genet,* 89**,** 158-66.

KEHAT, I., KENYAGIN-KARSENTI, D., SNIR, M., SEGEV, H., AMIT, M., GEPSTEIN, A., LIVNE, E., BINAH, O., ITSKOVITZ-ELDOR, J. & GEPSTEIN, L. 2001. Human embryonic stem cells can differentiate into myocytes with structural and functional properties of cardiomyocytes. *J Clin Invest,* 108**,** 407-14.

KELLEY, M. W. 2005. *Development of the inner ear,* New York, Springer.

KENDREW, J. C. & LAWRENCE, E. 1994. *The encyclopedia of molecular biology,* Oxford ; Cambridge, Mass., USA, Blackwell Science.

KHIMICH, D., NOUVIAN, R., PUJOL, R., TOM DIECK, S., EGNER, A., GUNDELFINGER, E. D. & MOSER, T. 2005. Hair cell synaptic ribbons are essential for synchronous auditory signalling. *Nature,* 434**,** 889-94.

KIERNAN, A. E., PELLING, A. L., LEUNG, K. K., TANG, A. S., BELL, D. M., TEASE, C., LOVELL-BADGE, R., STEEL, K. P. & CHEAH, K. S. 2005. Sox2 is required for sensory organ development in the mammalian inner ear. *Nature,* 434**,** 1031-5.

KIL, S. H., STREIT, A., BROWN, S. T., AGRAWAL, N., COLLAZO, A., ZILE, M. H. & GROVES, A. K. 2005. Distinct roles for hindbrain and paraxial mesoderm in the induction and patterning of the inner ear revealed by a study of vitamin-A-deficient quail. *Dev Biol,* 285**,** 252-71.

KIM, E., HYRC, K. L., SPECK, J., LUNDBERG, Y. W., SALLES, F. T., KACHAR, B., GOLDBERG, M. P., WARCHOL, M. E. & ORNITZ, D. M. 2010. Regulation of cellular calcium in vestibular supporting cells by otopetrin 1. *J Neurophysiol,* 104**,** 3439-50.

KIM, J. H., RODRIGUEZ-VAZQUEZ, J. F., VERDUGO-LOPEZ, S., CHO, K. H., MURAKAMI, G. & CHO, B. H. 2011. Early fetal development of the human cochlea. *Anat Rec (Hoboken),* 294**,** 996-1002.

KINNEY, M. A., SARGENT, C. Y. & MCDEVITT, T. C. 2011. The multiparametric effects of hydrodynamic environments on stem cell culture. *Tissue Eng Part B Rev,* 17**,** 249-62.

KISHIMOTO, Y., LEE, K. H., ZON, L., HAMMERSCHMIDT, M. & SCHULTE-MERKER, S. 1997. The molecular nature of zebrafish swirl: BMP2 function is essential during early dorsoventral patterning. *Development,* 124**,** 4457-66.

KOEHLER, K. R. & HASHINO, E. 2014. 3D mouse embryonic stem cell culture for generating inner ear organoids. *Nat Protoc,* 9**,** 1229-44.

KOEHLER, K. R., MIKOSZ, A. M., MOLOSH, A. I., PATEL, D. & HASHINO, E. 2013. Generation of inner ear sensory epithelia from pluripotent stem cells in 3D culture. *Nature,* 500**,** 217-21.

KOEHLER, K. R., NIE, J., LONGWORTH-MILLS, E., LIU, X. P., LEE, J., HOLT, J. R. & HASHINO, E. 2017. Generation of inner ear organoids containing functional hair cells from human pluripotent stem cells. *Nat Biotechnol*.

KORRAPATI, S., ROUX, I., GLOWATZKI, E. & DOETZLHOFER, A. 2013. Notch signaling limits supporting cell plasticity in the hair cell-damaged early postnatal murine cochlea. *PLoS One,* 8**,** e73276.

KOZLOWSKI, D. J., MURAKAMI, T., HO, R. K. & WEINBERG, E. S. 1997. Regional cell movement and tissue patterning in the zebrafish embryo revealed by fate mapping with caged fluorescein. *Biochem Cell Biol,* 75**,** 551-62.

KRAUSS, S., JOHANSEN, T., KORZH, V., MOENS, U., ERICSON, J. U. & FJOSE, A. 1991. Zebrafish Pax[Zf-a] - a Paired Box-Containing Gene Expressed in the Neural-Tube. *Embo Journal,* 10**,** 3609-3619.

KRAWETZ, R. J., LI, X. & RANCOURT, D. E. 2009. Human embryonic stem cells: caught between a ROCK inhibitor and a hard place. *Bioessays,* 31**,** 336-43.

KU, Y. C., RENAUD, N. A., VEILE, R. A., HELMS, C., VOELKER, C. C., WARCHOL, M. E. & LOVETT, M. 2014. The transcriptome of utricle hair cell regeneration in the avian inner ear. *J Neurosci,* 34**,** 3523-35.

KWAK, S. J., PHILLIPS, B. T., HECK, R. & RILEY, B. B. 2002. An expanded domain of fgf3 expression in the hindbrain of zebrafish valentino mutants results in mis-patterning of the otic vesicle. *Development,* 129**,** 5279-87.

KWON, H. J., BHAT, N., SWEET, E. M., CORNELL, R. A. & RILEY, B. B. 2010. Identification of early requirements for preplacodal ectoderm and sensory organ development. *PLoS Genet,* 6**,** e1001133.

KWON, H. J. & RILEY, B. B. 2009. Mesendodermal signals required for otic induction: Bmp-antagonists cooperate with Fgf and can facilitate formation of ectopic otic tissue. *Dev Dyn,* 238**,** 1582-94.

LADHER, R. K. 2016. Changing shape and shaping change: Inducing the inner ear. *Semin Cell Dev Biol*.

LANGTON, P. 2013. *Essential guide to reading biomedical papers : recognising and interpreting best practice,* Chichester, West Sussex England ; Hoboken, N.J., Wiley-Blackwell.

LAVIGNE-REBILLARD, M. & BAGGER-SJOBACK, D. 1992. Development of the human stria vascularis. *Hear Res,* 64**,** 39-51.

LAVIGNE-REBILLARD, M. & PUJOL, R. 1987. Surface aspects of the developing human organ of Corti. *Acta Otolaryngol Suppl,* 436**,** 43-50.

LAVIGNE-REBILLARD, M. & PUJOL, R. 1988. Hair cell innervation in the fetal human cochlea. *Acta Otolaryngol,* 105**,** 398-402.

LAWOKO-KERALI, G., RIVOLTA, M. N., LAWLOR, P., CACCIABUE-RIVOLTA, D. I., LANGTON-HEWER, C., VAN DOORNINCK, J. H. & HOLLEY, M. C. 2004. GATA3 and NeuroD distinguish auditory and vestibular neurons during development of the mammalian inner ear. *Mech Dev,* 121**,** 287-99.

LAWSON, K. A., MENESES, J. J. & PEDERSEN, R. A. 1991. Clonal analysis of epiblast fate during germ layer formation in the mouse embryo. *Development,* 113**,** 891-911.

LEGER, S. & BRAND, M. 2002. Fgf8 and Fgf3 are required for zebrafish ear placode induction, maintenance and inner ear patterning. *Mech Dev,* 119**,** 91-108.

LENZI, D., RUNYEON, J. W., CRUM, J., ELLISMAN, M. H. & ROBERTS, W. M. 1999. Synaptic vesicle populations in saccular hair cells reconstructed by electron tomography. *J Neurosci,* 19**,** 119-32.

LEUNG, A. W., KENT MOREST, D. & LI, J. Y. 2013. Differential BMP signaling controls formation and differentiation of multipotent preplacodal ectoderm progenitors from human embryonic stem cells. *Dev Biol,* 379**,** 208-20.

LI, H., LIU, H. & HELLER, S. 2003. Pluripotent stem cells from the adult mouse inner ear. *Nat Med,* 9**,** 1293-9.

LI, M., PEVNY, L., LOVELL-BADGE, R. & SMITH, A. 1998. Generation of purified neural precursors from embryonic stem cells by lineage selection. *Curr Biol,* 8**,** 971-4.

LI, X. J., DU, Z. W., ZARNOWSKA, E. D., PANKRATZ, M., HANSEN, L. O., PEARCE, R. A. & ZHANG, S. C. 2005. Specification of motoneurons from human embryonic stem cells. *Nat Biotechnol,* 23**,** 215-21.

LIM, J. W. & BODNAR, A. 2002. Proteome analysis of conditioned medium from mouse embryonic fibroblast feeder layers which support the growth of human embryonic stem cells. *Proteomics,* 2**,** 1187-203.

LIM, R. & BRICHTA, A. M. 2016. Anatomical and physiological development of the human inner ear. *Hear Res,* 338**,** 9-21.

LIM, R., DRURY, H. R., CAMP, A. J., TADROS, M. A., CALLISTER, R. J. & BRICHTA, A. M. 2014. Preliminary characterization of voltage-activated whole-cell currents in developing human vestibular hair cells and calyx afferent terminals. *J Assoc Res Otolaryngol,* 15**,** 755-66.

LIN, V., GOLUB, J. S., NGUYEN, T. B., HUME, C. R., OESTERLE, E. C. & STONE, J. S. 2011. Inhibition of Notch activity promotes nonmitotic regeneration of hair cells in the adult mouse utricles. *J Neurosci,* 31**,** 15329-39.

LITSIOU, A., HANSON, S. & STREIT, A. 2005. A balance of FGF, BMP and WNT signalling positions the future placode territory in the head. *Development,* 132**,** 4051-62.

LIU, A. M. & JOYNER, A. L. 2001. EN and GBX2 play essential roles downstream of FGF8 in patterning the mouse mid/hindbrain region. *Development,* 128**,** 181-191.

LIU, Z., OWEN, T., ZHANG, L. & ZUO, J. 2010. Dynamic expression pattern of Sonic hedgehog in developing cochlear spiral ganglion neurons. *Dev Dyn,* 239**,** 1674-83.

LOCHER, H., DE GROOT, J. C., VAN IPEREN, L., HUISMAN, M. A., FRIJNS, J. H. & CHUVA DE SOUSA LOPES, S. M. 2014. Distribution and development of peripheral glial cells in the human fetal cochlea. *PLoS One,* 9**,** e88066.

LOCHER, H., FRIJNS, J. H., VAN IPEREN, L., DE GROOT, J. C., HUISMAN, M. A. & CHUVA DE SOUSA LOPES, S. M. 2013. Neurosensory development and cell fate determination in the human cochlea. *Neural Dev,* 8**,** 20.

LU, J., MA, Z., HSIEH, J. C., FAN, C. W., CHEN, B., LONGGOOD, J. C., WILLIAMS, N. S., AMATRUDA, J. F., LUM, L. & CHEN, C. 2009. Structure-activity relationship studies of small-molecule inhibitors of Wnt response. *Bioorg Med Chem Lett,* 19**,** 3825-7.

LU, N., CHEN, Y., WANG, Z., CHEN, G., LIN, Q., CHEN, Z. Y. & LI, H. 2013. Sonic hedgehog initiates cochlear hair cell regeneration through downregulation of retinoblastoma protein. *Biochem Biophys Res Commun,* 430**,** 700-5.

LUMPKIN, E. A., COLLISSON, T., PARAB, P., OMER-ABDALLA, A., HAEBERLE, H., CHEN, P., DOETZLHOFER, A., WHITE, P., GROVES, A., SEGIL, N. & JOHNSON, J. E. 2003. Math1-driven GFP expression in the developing nervous system of transgenic mice. *Gene Expr Patterns,* 3**,** 389-95.

LYSAKOWSKI, A. & GOLDBERG, J. M. 1997. A regional ultrastructural analysis of the cellular and synaptic architecture in the chinchilla cristae ampullares. *J Comp Neurol,* 389**,** 419-43.

MA, E. Y., RUBEL, E. W. & RAIBLE, D. W. 2008. Notch signaling regulates the extent of hair cell regeneration in the zebrafish lateral line. *J Neurosci,* 28**,** 2261-73.

MA, Q., ANDERSON, D. J. & FRITZSCH, B. 2000. Neurogenin 1 null mutant ears develop fewer, morphologically normal hair cells in smaller sensory epithelia devoid of innervation. *J Assoc Res Otolaryngol,* 1**,** 129-43.

MA, W., FITZGERALD, W., LIU, Q. Y., O'SHAUGHNESSY, T. J., MARIC, D., LIN, H. J., ALKON, D. L. & BARKER, J. L. 2004. CNS stem and progenitor cell differentiation into functional neuronal circuits in three-dimensional collagen gels. *Exp Neurol,* 190**,** 276-88.

MAIER, E. C., SAXENA, A., ALSINA, B., BRONNER, M. E. & WHITFIELD, T. T. 2014. Sensational placodes: neurogenesis in the otic and olfactory systems. *Dev Biol,* 389**,** 50-67.

MAIER, E. C. & WHITFIELD, T. T. 2014. RA and FGF signalling are required in the zebrafish otic vesicle to pattern and maintain ventral otic identities. *PLoS Genet,* 10**,** e1004858.

MANCHAIAH, V. K., ZHAO, F., DANESH, A. A. & DUPREY, R. 2011. The genetic basis of auditory neuropathy spectrum disorder (ANSD). *Int J Pediatr Otorhinolaryngol,* 75**,** 151-8.

MANLEY, G. A. & KOPPL, C. 1998. Phylogenetic development of the cochlea and its innervation. *Curr Opin Neurobiol,* 8**,** 468-74.

MARCOTTI, W., GELEOC, G. S., LENNAN, G. W. & KROS, C. J. 1999. Transient expression of an inwardly rectifying potassium conductance in developing inner and outer hair cells along the mouse cochlea. *Pflugers Arch,* 439**,** 113-22.

MARCOTTI, W., JOHNSON, S. L., HOLLEY, M. C. & KROS, C. J. 2003a. Developmental changes in the expression of potassium currents of embryonic, neonatal and mature mouse inner hair cells. *J Physiol,* 548**,** 383-400.

MARCOTTI, W., JOHNSON, S. L. & KROS, C. J. 2004. A transiently expressed SK current sustains and modulates action potential activity in immature mouse inner hair cells. *J Physiol,* 560**,** 691-708.

MARCOTTI, W., JOHNSON, S. L., RUSCH, A. & KROS, C. J. 2003b. Sodium and calcium currents shape action potentials in immature mouse inner hair cells. *J Physiol,* 552**,** 743-61.

MARCOTTI, W. & KROS, C. J. 1999. Developmental expression of the potassium current IK,n contributes to maturation of mouse outer hair cells. *J Physiol,* 520 Pt 3**,** 653-60.

MAROON, H., WALSHE, J., MAHMOOD, R., KIEFER, P., DICKSON, C. & MASON, I. 2002. Fgf3 and Fgf8 are required together for formation of the otic placode and vesicle. *Development,* 129**,** 2099-108.

MARTIN, G. R. 1981. Isolation of a pluripotent cell line from early mouse embryos cultured in medium conditioned by teratocarcinoma stem cells. *Proc Natl Acad Sci U S A,* 78**,** 7634-8.

MARTIN, P. & PARKHURST, S. M. 2004. Parallels between tissue repair and embryo morphogenesis. *Development,* 131**,** 3021-34.

MARTIN, P. & SWANSON, G. J. 1993. Descriptive and experimental analysis of the epithelial remodellings that control semicircular canal formation in the developing mouse inner ear. *Dev Biol,* 159**,** 549-58.

MATHUR, P. & YANG, J. 2015. Usher syndrome: Hearing loss, retinal degeneration and associated abnormalities. *Biochim Biophys Acta,* 1852**,** 406-20.

MATSUI, J. I. & COTANCHE, D. A. 2004. Sensory hair cell death and regeneration: two halves of the same equation. *Curr Opin Otolaryngol Head Neck Surg,* 12**,** 418-25.

MEIER, S. 1978a. Development of the embryonic chick otic placode. I. Light microscopic analysis. *Anat Rec,* 191**,** 447-58.

MEIER, S. 1978b. Development of the embryonic chick otic placode. II. Electron microscopic analysis. *Anat Rec,* 191**,** 459-77.

METALLO, C. M., JI, L., DE PABLO, J. J. & PALECEK, S. P. 2008. Retinoic acid and bone morphogenetic protein signaling synergize to efficiently direct epithelial differentiation of human embryonic stem cells. *Stem Cells,* 26**,** 372-80.

MEYER, A. C., FRANK, T., KHIMICH, D., HOCH, G., RIEDEL, D., CHAPOCHNIKOV, N. M., YARIN, Y. M., HARKE, B., HELL, S. W., EGNER, A. & MOSER, T. 2009a. Tuning of synapse number, structure and function in the cochlea. *Nat Neurosci,* 12**,** 444-53.

MEYER, J., MACK, A. F. & GUMMER, A. W. 2001. Pronounced infracuticular endocytosis in mammalian outer hair cells. *Hear Res,* 161**,** 10-22.

MEYER, J. S., SHEARER, R. L., CAPOWSKI, E. E., WRIGHT, L. S., WALLACE, K. A., MCMILLAN, E. L., ZHANG, S. C. & GAMM, D. M. 2009b. Modeling early retinal development with human embryonic and induced pluripotent stem cells. *Proc Natl Acad Sci U S A,* 106**,** 16698-703.

MEYERS, J. R., MACDONALD, R. B., DUGGAN, A., LENZI, D., STANDAERT, D. G., CORWIN, J. T. & COREY, D. P. 2003. Lighting up the senses: FM1-43 loading of sensory cells through nonselective ion channels. *J Neurosci,* 23**,** 4054-65.

MIYAKE, T., VONHERBING, I. H. & HALL, B. K. 1997. Neural ectoderm, neural crest, and placodes: Contribution of the otic placode to the ectodermal lining of the embryonic opercular cavity in Atlantic cod (Teleostei). *Journal of Morphology,* 231**,** 231-252.

MIZUTARI, K., FUJIOKA, M., HOSOYA, M., BRAMHALL, N., OKANO, H. J., OKANO, H. & EDGE, A. S. 2013. Notch inhibition induces cochlear hair cell regeneration and recovery of hearing after acoustic trauma. *Neuron,* 77**,** 58-69.

MOORE, J. K. & LINTHICUM, F. H., JR. 2007. The human auditory system: a timeline of development. *Int J Audiol,* 46**,** 460-78.

MOSER, T., BRANDT, A. & LYSAKOWSKI, A. 2006. Hair cell ribbon synapses. *Cell Tissue Res,* 326**,** 347-59.

MSEKA, T., BAMBURG, J. R. & CRAMER, L. P. 2007. ADF/cofilin family proteins control formation of oriented actin-filament bundles in the cell body to trigger fibroblast polarization. *J Cell Sci,* 120**,** 4332-44.

MUGURUMA, K., NISHIYAMA, A., ONO, Y., MIYAWAKI, H., MIZUHARA, E., HORI, S., KAKIZUKA, A., OBATA, K., YANAGAWA, Y., HIRANO, T. & SASAI, Y. 2010. Ontogeny-recapitulating generation and tissue integration of ES cell-derived Purkinje cells. *Nat Neurosci,* 13**,** 1171-80.

MUNNAMALAI, V. & FEKETE, D. M. 2013a. Wnt signaling during cochlear development. *Semin Cell Dev Biol,* 24**,** 480-9.

MUNNAMALAI, V. & FEKETE, D. M. 2013b. Wnt signaling during cochlear development. *Seminars in Cell & Developmental Biology,* 24**,** 480-489.

MUNNAMALAI, V., HAYASHI, T. & BERMINGHAM-MCDONOGH, O. 2012. Notch prosensory effects in the Mammalian cochlea are partially mediated by Fgf20. *J Neurosci,* 32**,** 12876-84.

NAJAFZADEH, N., SAGHA, M., HEYDARI TAJADDOD, S., GOLMOHAMMADI, M. G., MASSAHI OSKOUI, N. & DELDADEH MOGHADDAM, M. 2015. In vitro neural differentiation of CD34 (+) stem cell populations in hair follicles by three different neural induction protocols. *In Vitro Cell Dev Biol Anim,* 51**,** 192-203.

NAKAJIMA, Y. 2015. Signaling regulating inner ear development: cell fate determination, patterning, morphogenesis, and defects. *Congenit Anom (Kyoto),* 55**,** 17-25.

NAKANO, T., ANDO, S., TAKATA, N., KAWADA, M., MUGURUMA, K., SEKIGUCHI, K., SAITO, K., YONEMURA, S., EIRAKU, M. & SASAI, Y. 2012. Self-formation of optic cups and storable stratified neural retina from human ESCs. *Cell Stem Cell,* 10**,** 771-85.

NASU, M., TAKATA, N., DANJO, T., SAKAGUCHI, H., KADOSHIMA, T., FUTAKI, S., SEKIGUCHI, K., EIRAKU, M. & SASAI, Y. 2012. Robust formation and maintenance of continuous stratified cortical neuroepithelium by laminin-containing matrix in mouse ES cell culture. *PLoS One,* 7**,** e53024.

NEAVE, B., HOLDER, N. & PATIENT, R. 1997. A graded response to BMP-4 spatially coordinates patterning of the mesoderm and ectoderm in the zebrafish. *Mech Dev,* 62**,** 183-95.

NEEDHAM, K., NAYAGAM, B. A., MINTER, R. L. & O'LEARY, S. J. 2012. Combined application of brain-derived neurotrophic factor and neurotrophin-3 and its impact on spiral ganglion neuron firing properties and hyperpolarization-activated currents. *Hear Res,* 291**,** 1-14.

NEHER, E. & SAKMANN, B. 1976. Single-channel currents recorded from membrane of denervated frog muscle fibres. *Nature,* 260**,** 799-802.

NEVES, J., UCHIKAWA, M., BIGAS, A. & GIRALDEZ, F. 2012. The prosensory function of Sox2 in the chicken inner ear relies on the direct regulation of Atoh1. *PLoS One,* 7**,** e30871.

NICHOLS, J. & SMITH, A. 2009. Naive and primed pluripotent states. *Cell Stem Cell,* 4**,** 487-92.

NICOLETTI, I., MIGLIORATI, G., PAGLIACCI, M. C., GRIGNANI, F. & RICCARDI, C. 1991. A rapid and simple method for measuring thymocyte apoptosis by propidium iodide staining and flow cytometry. *J Immunol Methods,* 139**,** 271-9.

NORNES, H. O., DRESSLER, G. R., KNAPIK, E. W., DEUTSCH, U. & GRUSS, P. 1990. Spatially and Temporally Restricted Expression of Pax2 during Murine Neurogenesis. *Development,* 109**,** 797-809.

O'RAHILLY, R. 1963. The Early Development of the Otic Vesicle in Staged Human Embryos. *J Embryol Exp Morphol,* 11**,** 741-55.

OESTERLE, E. C., CAMPBELL, S., TAYLOR, R. R., FORGE, A. & HUME, C. R. 2008. Sox2 and JAGGED1 expression in normal and drug-damaged adult mouse inner ear. *J Assoc Res Otolaryngol,* 9**,** 65-89.

OGHALAI, J. S., HOLT, J. R., NAKAGAWA, T., JUNG, T. M., COKER, N. J., JENKINS, H. A., EATOCK, R. A. & BROWNELL, W. E. 1998. Ionic currents and electromotility in inner ear hair cells from humans. *J Neurophysiol,* 79**,** 2235-9.

OHYAMA, T., BASCH, M. L., MISHINA, Y., LYONS, K. M., SEGIL, N. & GROVES, A. K. 2010. BMP signaling is necessary for patterning the sensory and nonsensory regions of the developing mammalian cochlea. *J Neurosci,* 30**,** 15044-51.

OHYAMA, T. & GROVES, A. K. 2004. Expression of mouse Foxi class genes in early craniofacial development. *Developmental Dynamics,* 231**,** 640-646.

OHYAMA, T., GROVES, A. K. & MARTIN, K. 2007. The first steps towards hearing: mechanisms of otic placode induction. *International Journal of Developmental Biology,* 51**,** 463-472.

OHYAMA, T., MOHAMED, O. A., TAKETO, M. M., DUFORT, D. & GROVES, A. K. 2006. Wnt signals mediate a fate decision between otic placode and epidermis. *Development,* 133**,** 865-75.

ORAHILLY, R. & MULLER, F. 1985. The Origin of the Ectodermal Ring in Staged Human-Embryos of the 1st 5 Weeks. *Acta Anatomica,* 122**,** 145-157.

OSHIMA, K., SHIN, K., DIENSTHUBER, M., PENG, A. W., RICCI, A. J. & HELLER, S. 2010. Mechanosensitive hair cell-like cells from embryonic and induced pluripotent stem cells. *Cell,* 141**,** 704-16.

OUJI, Y., ISHIZAKA, S., NAKAMURA-UCHIYAMA, F. & YOSHIKAWA, M. 2012. In vitro differentiation of mouse embryonic stem cells into inner ear hair cell-like cells using stromal cell conditioned medium. *Cell Death Dis,* 3**,** e314.

PAN, W., JIN, Y., CHEN, J., ROTTIER, R. J., STEEL, K. P. & KIERNAN, A. E. 2013. Ectopic expression of activated notch or SOX2 reveals similar and unique roles in the development of the sensory cell progenitors in the mammalian inner ear. *J Neurosci,* 33**,** 16146-57.

PANKRATZ, M. T., LI, X. J., LAVAUTE, T. M., LYONS, E. A., CHEN, X. & ZHANG, S. C. 2007. Directed neural differentiation of human embryonic stem cells via an obligated primitive anterior stage. *Stem Cells,* 25**,** 1511-20.

PARKER, M. A. 2011. Biotechnology in the treatment of sensorineural hearing loss: foundations and future of hair cell regeneration. *J Speech Lang Hear Res,* 54**,** 1709-31.

PATTHEY, C., EDLUND, T. & GUNHAGA, L. 2009. Wnt-regulated temporal control of BMP exposure directs the choice between neural plate border and epidermal fate. *Development,* 136**,** 73-83.

PECHRIGGL, E. J., BITSCHE, M., GLUECKERT, R., RASK-ANDERSEN, H., BLUMER, M. J., SCHROTT-FISCHER, A. & FRITSCH, H. 2015. Development of the innervation of the human inner ear. *Dev Neurobiol,* 75**,** 683-702.

PENZEL, R., OSCHWALD, R., CHEN, Y. L., TACKE, L. & GRUNZ, H. 1997. Characterization and early embryonic expression of a neural specific transcription factor xSOX3 in Xenopus laevis. *International Journal of Developmental Biology,* 41**,** 667-677.

PETROVIC, J., FORMOSA-JORDAN, P., LUNA-ESCALANTE, J. C., ABELLO, G., IBANES, M., NEVES, J. & GIRALDEZ, F. 2014. Ligand-dependent Notch signaling strength orchestrates lateral induction and lateral inhibition in the developing inner ear. *Development,* 141**,** 2313-24.

PEVNY, L. H., SOCKANATHAN, S., PLACZEK, M. & LOVELL-BADGE, R. 1998. A role for SOX1 in neural determination. *Development,* 125**,** 1967-78.

PFEFFER, P. L., GERSTER, T., LUN, K., BRAND, M. & BUSSLINGER, M. 1998. Characterization of three novel members of the zebrafish Pax2/5/8 family: dependency of Pax5 and Pax8 expression on the Pax2.1 (noi) function. *Development,* 125**,** 3063-74.

PHILLIPS, B. T., BOLDING, K. & RILEY, B. B. 2001. Zebrafish fgf3 and fgf8 encode redundant functions required for otic placode induction. *Dev Biol,* 235**,** 351-65.

PIEPER, M., AHRENS, K., RINK, E., PETER, A. & SCHLOSSER, G. 2012. Differential distribution of competence for panplacodal and neural crest induction to non-neural and neural ectoderm. *Development,* 139**,** 1175-87.

PIPER, K., BALL, S. G., KEELING, J. W., MANSOOR, S., WILSON, D. I. & HANLEY, N. A. 2002. Novel SOX9 expression during human pancreas development correlates to abnormalities in Campomelic dysplasia. *Mech Dev,* 116**,** 223-6.

PIRVOLA, U., CAO, Y., OELLIG, C., SUOQIANG, Z., PETTERSSON, R. F. & YLIKOSKI, J. 1995. The site of action of neuronal acidic fibroblast growth factor is the organ of Corti of the rat cochlea. *Proc Natl Acad Sci U S A,* 92**,** 9269-73.

POPPER, A. N. & FAY, R. R. 1992. *The Mammalian auditory pathway : neurophysiology,* New York, Springer-Verlag.

PUJOL, R. & LAVIGNE-REBILLARD, M. 1985. Early stages of innervation and sensory cell differentiation in the human fetal organ of Corti. *Acta Otolaryngol Suppl,* 423**,** 43-50.

PUJOL, R. & LAVIGNE-REBILLARD, M. 1995. Sensory and neural structures in the developing human cochlea. *Int J Pediatr Otorhinolaryngol,* 32 Suppl**,** S177-82.

PULIGILLA, C., DABDOUB, A., BRENOWITZ, S. D. & KELLEY, M. W. 2010. Sox2 induces neuronal formation in the developing mammalian cochlea. *J Neurosci,* 30**,** 714-22.

PYRGAKI, C., TRAINOR, P., HADJANTONAKIS, A. K. & NISWANDER, L. 2010. Dynamic imaging of mammalian neural tube closure. *Dev Biol,* 344**,** 941-7.

RAFT, S., KOUNDAKJIAN, E. J., QUINONES, H., JAYASENA, C. S., GOODRICH, L. V., JOHNSON, J. E., SEGIL, N. & GROVES, A. K. 2007. Cross-regulation of Ngn1 and Math1 coordinates the production of neurons and sensory hair cells during inner ear development. *Development,* 134**,** 4405-15.

RAKOWIECKI, S. & EPSTEIN, D. J. 2013. Divergent roles for Wnt/beta-catenin signaling in epithelial maintenance and breakdown during semicircular canal formation. *Development,* 140**,** 1730-9.

RASK-ANDERSEN, H., LIU, W. & BOSTRÖM, M. 2009. Immunolocalization of prestin in the human cochlea. *Audiological Medicine*.

RATHJEN, J., HAINES, B. P., HUDSON, K. M., NESCI, A., DUNN, S. & RATHJEN, P. D. 2002. Directed differentiation of pluripotent cells to neural lineages: homogeneous formation and differentiation of a neurectoderm population. *Development,* 129**,** 2649-61.

RAY, H. J. & NISWANDER, L. 2012. Mechanisms of tissue fusion during development. *Development,* 139**,** 1701-11.

REVERSADE, B. & DE ROBERTIS, E. M. 2005. Regulation of ADMP and BMP2/4/7 at opposite embryonic poles generates a self-regulating morphogenetic field. *Cell,* 123**,** 1147-60.

RHYS EVANS, P.H., C., S.D., O. & M.P., P., J.O., JEFFRIES, D.J., 1985. Crosslinks between stereocilia in the human organ of Corti. *J. Laryngol. Otol.*

RICCOMAGNO, M. M., MARTINU, L., MULHEISEN, M., WU, D. K. & EPSTEIN, D. J. 2002. Specification of the mammalian cochlea is dependent on Sonic hedgehog. *Genes Dev,* 16**,** 2365-78.

RICHARDSON, G. P., LUKASHKIN, A. N. & RUSSELL, I. J. 2008. The tectorial membrane: one slice of a complex cochlear sandwich. *Curr Opin Otolaryngol Head Neck Surg,* 16**,** 458-64.

RINKWITZBRANDT, S., JUSTUS, M., OLDENETTEL, I., ARNOLD, H. H. & BOBER, E. 1995. Distinct Temporal Expression of Mouse Nkx-5.1 and Nkx-5.2 Homeobox Genes during Brain and Ear Development. *Mechanisms of Development,* 52**,** 371-381.

RISS, D., ARNOLDNER, C., BAUMGARTNER, W. D., BLINEDER, M., FLAK, S., BACHNER, A., GSTOETTNER, W. & HAMZAVI, J. S. 2014. Indication criteria and outcomes with the Bonebridge transcutaneous bone-conduction implant. *Laryngoscope,* 124**,** 2802-6.

RONAGHI, M., NASR, M., EALY, M., DURRUTHY-DURRUTHY, R., WALDHAUS, J., DIAZ, G. H., JOUBERT, L. M., OSHIMA, K. & HELLER, S. 2014. Inner ear hair cell-like cells from human embryonic stem cells. *Stem Cells Dev,* 23**,** 1275-84.

ROSENHALL, U. 1972. Vestibular macular mapping in man. *Ann Otol Rhinol Laryngol,* 81**,** 339-51.

RUSSELL, J. L., PINE, H. S. & YOUNG, D. L. 2013. Pediatric cochlear implantation: expanding applications and outcomes. *Pediatr Clin North Am,* 60**,** 841-63.

RYALS, B. M. & RUBEL, E. W. 1988. Hair cell regeneration after acoustic trauma in adult Coturnix quail. *Science,* 240**,** 1774-6.

SAHLY, I., ANDERMANN, P. & PETIT, C. 1999. The zebrafish eya1 gene and its expression pattern during embryogenesis. *Dev Genes Evol,* 209**,** 399-410.

SAI, X. & LADHER, R. K. 2015. Early steps in inner ear development: induction and morphogenesis of the otic placode. *Front Pharmacol,* 6**,** 19.

SAI, X., YONEMURA, S. & LADHER, R. K. 2014. Junctionally restricted RhoA activity is necessary for apical constriction during phase 2 inner ear placode invagination. *Dev Biol,* 394**,** 206-16.

SANCHEZ-CALDERON, H., MARTIN-PARTIDO, G. & HIDALGO-SANCHEZ, M. 2002. Differential expression of Otx2, Gbx2, Pax2, and Fgf8 in the developing vestibular and auditory sensory organs. *Brain Research Bulletin,* 57**,** 321-323.

SANCHEZ FERNANDEZ, J. M., RIVERA, J. M. & MACIAS, J. A. 1983. Early aspects of human cochlea development and tectorial membrane histogenesis. *Acta Otolaryngol,* 95**,** 460-9.

SANS, A. & DECHESNE, C. 1985. Early development of vestibular receptors in human embryos. An electron microscopic study. *Acta Otolaryngol Suppl,* 423**,** 51-8.

SANS, A. & DECHESNE, C. J. 1987. Afferent nerve ending development and synaptogenesis in the vestibular epithelium of human fetuses. *Hear Res,* 28**,** 65-72.

SAPEDE, D., DYBALLA, S. & PUJADES, C. 2012. Cell lineage analysis reveals three different progenitor pools for neurosensory elements in the otic vesicle. *J Neurosci,* 32**,** 16424-34.

SASAI, Y., EIRAKU, M. & SUGA, H. 2012. In vitro organogenesis in three dimensions: self-organising stem cells. *Development,* 139**,** 4111-21.

SCHMAHL, W., KNOEDLSEDER, M., FAVOR, J. & DAVIDSON, D. 1993. Defects of neuronal migration and the pathogenesis of cortical malformations are associated with Small eye (Sey) in the mouse, a point mutation at the Pax-6-locus. *Acta Neuropathol,* 86**,** 126-35.

SCHOENWOLF, G. C., BLEYL, S. B., BRAUER, P. R. & FRANCIS-WEST, P. H. 2015. *Larsen's human embryology*.

SCHWARTZ, S., KENT, W. J., SMIT, A., ZHANG, Z., BAERTSCH, R., HARDISON, R. C., HAUSSLER, D. & MILLER, W. 2003. Human-mouse alignments with BLASTZ. *Genome Res,* 13**,** 103-7.

SCOTT, C. E., WYNN, S. L., SESAY, A., CRUZ, C., CHEUNG, M., GOMEZ GAVIRO, M. V., BOOTH, S., GAO, B., CHEAH, K. S., LOVELL-BADGE, R. & BRISCOE, J. 2010. SOX9 induces and maintains neural stem cells. *Nat Neurosci,* 13**,** 1181-9.

SEAL, R. P. & EDWARDS, R. H. 2006. The diverse roles of vesicular glutamate transporter 3. *Handb Exp Pharmacol***,** 137-50.

SHAMIM, H. & MASON, I. 1998. Expression of Gbx-2 during early development of the chick embryo. *Mechanisms of Development,* 76**,** 157-159.

SHEARER, A. E. & SMITH, R. J. H. 1993. OTOF-Related Deafness. *In:* PAGON, R. A., ADAM, M. P., ARDINGER, H. H., WALLACE, S. E., AMEMIYA, A., BEAN, L. J. H., BIRD, T. D., LEDBETTER, N., MEFFORD, H. C., SMITH, R. J. H. & STEPHENS, K. (eds.) *GeneReviews(R).* Seattle (WA).

SHENG, G. J. & STERN, C. D. 1999. Gata2 and Gata3: novel markers for early embryonic polarity and for nonneural ectoderm in the chick embryo. *Mechanisms of Development,* 87**,** 213-216.

SHER, A. E. 1971. The embryonic and postnatal development of the inner ear of the mouse. *Acta Otolaryngol Suppl,* 285**,** 1-77.

SHI, F., HU, L. & EDGE, A. S. 2013. Generation of hair cells in neonatal mice by beta-catenin overexpression in Lgr5-positive cochlear progenitors. *Proc Natl Acad Sci U S A,* 110**,** 13851-6.

SHIN, S., MITALIPOVA, M., NOGGLE, S., TIBBITTS, D., VENABLE, A., RAO, R. & STICE, S. L. 2006. Long-term proliferation of human embryonic stem cell-derived neuroepithelial cells using defined adherent culture conditions. *Stem Cells,* 24**,** 125-38.

SHNERSON, A., DEVIGNE, C. & PUJOL, R. 1981. Age-related changes in the C57BL/6J mouse cochlea. II. Ultrastructural findings. *Brain Res,* 254**,** 77-88.

SIMMONS, D. D., TONG, B., SCHRADER, A. D. & HORNAK, A. J. 2010. Oncomodulin identifies different hair cell types in the mammalian inner ear. *J Comp Neurol,* 518**,** 3785-802.

SOBKOWICZ, H. M., ROSE, J. E., SCOTT, G. E. & SLAPNICK, S. M. 1982. Ribbon synapses in the developing intact and cultured organ of Corti in the mouse. *J Neurosci,* 2**,** 942-57.

SOKOLOWSKI, B. H., CSUS, J., HAFEZ, O. I. & HAGGERTY, H. S. 1999. Neurotrophic factors modulate hair cells and their potassium currents in chick otocyst explants. *Eur J Neurosci,* 11**,** 682-90.

SOLLOWAY, M. J. & ROBERTSON, E. J. 1999. Early embryonic lethality in Bmp5;Bmp7 double mutant mice suggests functional redundancy within the 60A subgroup. *Development,* 126**,** 1753-1768.

SPEAR, P. C. & ERICKSON, C. A. 2012. Interkinetic nuclear migration: a mysterious process in search of a function. *Dev Growth Differ,* 54**,** 306-16.

SPENCE, J. C. H. 2013. *High-resolution electron microscopy*.

SPICER, S. S., SALVI, R. J. & SCHULTE, B. A. 1999. Ablation of inner hair cells by carboplatin alters cells in the medial K(+) flow route and disrupts tectorial membrane. *Hear Res,* 136**,** 139-50.

STOLT, C. C., LOMMES, P., SOCK, E., CHABOISSIER, M. C., SCHEDL, A. & WEGNER, M. 2003. The Sox9 transcription factor determines glial fate choice in the developing spinal cord. *Genes Dev,* 17**,** 1677-89.

STOLT, C. C. & WEGNER, M. 2010. SoxE function in vertebrate nervous system development. *Int J Biochem Cell Biol,* 42**,** 437-40.

STONE, J. S. & COTANCHE, D. A. 2007. Hair cell regeneration in the avian auditory epithelium. *Int J Dev Biol,* 51**,** 633-47.

STONE, J. S. & RUBEL, E. W. 1999. Delta1 expression during avian hair cell regeneration. *Development,* 126**,** 961-73.

STREETER, G. L. 1905. On the Development of the Membranous Labyrinth and the Acoustic and Facial Nerves in the Human Embryo. *Amer. J Anat,* 6**,** 139-165.

STREIT, A. 2002. Extensive cell movements accompany formation of the otic placode. *Developmental Biology,* 249**,** 237-254.

STREIT, A. 2004. Early development of the cranial sensory nervous system: from a common field to individual placodes. *Developmental Biology,* 276**,** 1-15.

SUGA, H., KADOSHIMA, T., MINAGUCHI, M., OHGUSHI, M., SOEN, M., NAKANO, T., TAKATA, N., WATAYA, T., MUGURUMA, K., MIYOSHI, H., YONEMURA, S., OISO, Y. & SASAI, Y. 2011. Self-formation of functional adenohypophysis in three-dimensional culture. *Nature,* 480**,** 57-62.

SUTER, A. H. & VON GIERKE, H. E. 1987. Noise and public policy. *Ear Hear,* 8**,** 188-91.

SUTER, D. M., TIREFORT, D., JULIEN, S. & KRAUSE, K. H. 2009. A Sox1 to Pax6 switch drives neuroectoderm to radial glia progression during differentiation of mouse embryonic stem cells. *Stem Cells,* 27**,** 49-58.

TAKAHASHI, K., TANABE, K., OHNUKI, M., NARITA, M., ICHISAKA, T., TOMODA, K. & YAMANAKA, S. 2007. Induction of pluripotent stem cells from adult human fibroblasts by defined factors. *Cell,* 131**,** 861-72.

TAKAHASHI, K. & YAMANAKA, S. 2006. Induction of pluripotent stem cells from mouse embryonic and adult fibroblast cultures by defined factors. *Cell,* 126**,** 663-76.

TATEYA, T., IMAYOSHI, I., TATEYA, I., HAMAGUCHI, K., TORII, H., ITO, J. & KAGEYAMA, R. 2013. Hedgehog signaling regulates prosensory cell properties during the basal-to-apical wave of hair cell differentiation in the mammalian cochlea. *Development,* 140**,** 3848-57.

TERZIC, J., MULLER, C., GAJOVIC, S. & SARAGA-BABIC, M. 1998. Expression of PAX2 gene during human development. *Int J Dev Biol,* 42**,** 701-7.

THIEDE, B. R., MANN, Z. F., CHANG, W., KU, Y. C., SON, Y. K., LOVETT, M., KELLEY, M. W. & CORWIN, J. T. 2014. Retinoic acid signalling regulates the development of tonotopically patterned hair cells in the chicken cochlea. *Nat Commun,* 5**,** 3840.

THOMSON, J. A., ITSKOVITZ-ELDOR, J., SHAPIRO, S. S., WAKNITZ, M. A., SWIERGIEL, J. J., MARSHALL, V. S. & JONES, J. M. 1998. Embryonic stem cell lines derived from human blastocysts. *Science,* 282**,** 1145-7.

THOMSON, J. A. & MARSHALL, V. S. 1998. Primate embryonic stem cells. *Curr Top Dev Biol,* 38**,** 133-65.

TORRES, M. & GIRALDEZ, F. 1998. The development of the vertebrate inner ear. *Mech Dev,* 71**,** 5-21.

WALTHER, C. & GRUSS, P. 1991. Pax-6, a murine paired box gene, is expressed in the developing CNS. *Development,* 113**,** 1435-49.

WALZ, W. 2007. *Patch-clamp analysis : advanced techniques,* Totowa, N.J., Humana Press.

WANG, G. P., CHATTERJEE, I., BATTS, S. A., WONG, H. T., GONG, T. W., GONG, S. S. & RAPHAEL, Y. 2010. Notch signaling and Atoh1 expression during hair cell regeneration in the mouse utricle. *Hear Res,* 267**,** 61-70.

WANG, T., CHAI, R., KIM, G. S., PHAM, N., JANSSON, L., NGUYEN, D. H., KUO, B., MAY, L. A., ZUO, J., CUNNINGHAM, L. L. & CHENG, A. G. 2015. Lgr5+ cells regenerate hair cells via proliferation and direct transdifferentiation in damaged neonatal mouse utricle. *Nat Commun,* 6**,** 6613.

WARCHOL, M. E. & CORWIN, J. T. 1996. Regenerative proliferation in organ cultures of the avian cochlea: identification of the initial progenitors and determination of the latency of the proliferative response. *J Neurosci,* 16**,** 5466-77.

WARCHOL, M. E. & RICHARDSON, G. P. 2009. Expression of the Pax2 transcription factor is associated with vestibular phenotype in the avian inner ear. *Dev Neurobiol,* 69**,** 191-202.

WASKIEWICZ, A. J., RIKHOF, H. A. & MOENS, C. B. 2002. Eliminating zebrafish pbx proteins reveals a hindbrain ground state. *Dev Cell,* 3**,** 723-33.

WASSERMAN, W. W., PALUMBO, M., THOMPSON, W., FICKETT, J. W. & LAWRENCE, C. E. 2000. Human-mouse genome comparisons to locate regulatory sites. *Nat Genet,* 26**,** 225-8.

WATANABE, K., UENO, M., KAMIYA, D., NISHIYAMA, A., MATSUMURA, M., WATAYA, T., TAKAHASHI, J. B., NISHIKAWA, S., NISHIKAWA, S., MUGURUMA, K. & SASAI, Y. 2007. A ROCK inhibitor permits survival of dissociated human embryonic stem cells. *Nat Biotechnol,* 25**,** 681-6.

WHITE, P. M., DOETZLHOFER, A., LEE, Y. S., GROVES, A. K. & SEGIL, N. 2006. Mammalian cochlear supporting cells can divide and trans-differentiate into hair cells. *Nature,* 441**,** 984-7.

WHITE, P. M., STONE, J. S., GROVES, A. K. & SEGIL, N. 2012. EGFR signaling is required for regenerative proliferation in the cochlea: conservation in birds and mammals. *Dev Biol,* 363**,** 191-200.

WHITFIELD, T. T. 2015. Development of the inner ear. *Curr Opin Genet Dev,* 32**,** 112-8.

WILSON, P. A. & HEMMATI-BRIVANLOU, A. 1995. Induction of epidermis and inhibition of neural fate by Bmp-4. *Nature,* 376**,** 331-3.

WILSON, P. A., LAGNA, G., SUZUKI, A. & HEMMATI-BRIVANLOU, A. 1997. Concentration-dependent patterning of the Xenopus ectoderm by BMP4 and its signal transducer Smad1. *Development,* 124**,** 3177-84.

WOOD, H. B. & EPISKOPOU, V. 1999. Comparative expression of the mouse Sox1, Sox2 and Sox3 genes from pre-gastrulation to early somite stages. *Mechanisms of Development,* 86**,** 197-201.

WOOLTORTON, J. R., GABOYARD, S., HURLEY, K. M., PRICE, S. D., GARCIA, J. L., ZHONG, M., LYSAKOWSKI, A. & EATOCK, R. A. 2007. Developmental changes in two voltage-dependent sodium currents in utricular hair cells. *J Neurophysiol,* 97**,** 1684-704.

WRIGHT, E., HARGRAVE, M. R., CHRISTIANSEN, J., COOPER, L., KUN, J., EVANS, T., GANGADHARAN, U., GREENFIELD, A. & KOOPMAN, P. 1995. The Sry-Related Gene Sox9 Is Expressed during Chondrogenesis in Mouse Embryos. *Nature Genetics,* 9**,** 15-20.

WRIGHT, T. J. & MANSOUR, S. L. 2003. Fgf3 and Fgf10 are required for mouse otic placode induction. *Development,* 130**,** 3379-90.

WU, D. K. & KELLEY, M. W. 2012. Molecular mechanisms of inner ear development. *Cold Spring Harb Perspect Biol,* 4**,** a008409.

XU, P. X., ADAMS, J., PETERS, H., BROWN, M. C., HEANEY, S. & MAAS, R. 1999. Eya1-deficient mice lack ears and kidneys and show abnormal apoptosis of organ primordia. *Nature Genetics,* 23**,** 113-117.

YAMADA, M., JOHANNESSON, B., SAGI, I., BURNETT, L. C., KORT, D. H., PROSSER, R. W., PAULL, D., NESTOR, M. W., FREEBY, M., GREENBERG, E., GOLAND, R. S., LEIBEL, R. L., SOLOMON, S. L., BENVENISTY, N., SAUER, M. V. & EGLI, D. 2014. Human oocytes reprogram adult somatic nuclei of a type 1 diabetic to diploid pluripotent stem cells. *Nature,* 510**,** 533-6.

YANG, C., YANG, Y., BRENNAN, L., BOUHASSIRA, E. E., KANTOROW, M. & CVEKL, A. 2010. Efficient generation of lens progenitor cells and lentoid bodies from human embryonic stem cells in chemically defined conditions. *FASEB J,* 24**,** 3274-83.

YASUDA, M., YAMADA, S., UWABE, C., SHIOTA, K. & YASUDA, Y. 2007. Three-dimensional analysis of inner ear development in human embryos. *Anat Sci Int,* 82**,** 156-63.

YING, Q. L., STAVRIDIS, M., GRIFFITHS, D., LI, M. & SMITH, A. 2003. Conversion of embryonic stem cells into neuroectodermal precursors in adherent monoculture. *Nat Biotechnol,* 21**,** 183-6.

YING, Q. L., WRAY, J., NICHOLS, J., BATLLE-MORERA, L., DOBLE, B., WOODGETT, J., COHEN, P. & SMITH, A. 2008. The ground state of embryonic stem cell self-renewal. *Nature,* 453**,** 519-23.

ZHANG, J. J., TALBOT, W. S. & SCHIER, A. F. 1998. Positional cloning identifies zebrafish one-eyed pinhead as a permissive EGF-related ligand required during gastrulation. *Cell,* 92**,** 241-251.

ZHANG, K. D. & COATE, T. M. 2016. Recent advances in the development and function of type II spiral ganglion neurons in the mammalian inner ear. *Semin Cell Dev Biol*.

ZHANG, S. C., WERNIG, M., DUNCAN, I. D., BRUSTLE, O. & THOMSON, J. A. 2001. In vitro differentiation of transplantable neural precursors from human embryonic stem cells. *Nat Biotechnol,* 19**,** 1129-33.

ZINE, A. & DE RIBAUPIERRE, F. 1998. Replacement of mammalian auditory hair cells. *Neuroreport,* 9**,** 263-8.